Universiteit
Leiden
The Netherlands

Forever young: how AHL15 delays developmental phase transitions to prevent ageing in plants

Luden, T.

Citation
Luden, T. (2025, May 28). *Forever young: how AHL15 delays developmental phase transitions to prevent ageing in plants*. Retrieved from https://hdl.handle.net/1887/4247279

Version:	Publisher's Version
License:	Licence agreement concerning inclusion of doctoral thesis in the Institutional Repository of the University of Leiden
Downloaded from:	https://hdl.handle.net/1887/4247279

Note: To cite this publication please use the final published version (if applicable).

Forever Young:
How AHL15 delays developmental phase transitions to prevent ageing in plants

Thalia Luden

© 2025 Thalia Luden, Leiden, the Netherlands.

This work was supported by the Green Top Sectors grant nr. GSGT.2019.024 which was financed by the Dutch Research Council (NWO).

Front cover: Arabidopsis thaliana plant in the adult vegetative state, drawing by Thalia Luden. Mirrored plot of average enrichment profile of AHL15 and H2A variants scaled over Arabidopsis genes.

Cover design: Thalia & Urit Luden

Printed and bound by: Gildeprint

ISBN/EAN: 978-94-6496-402-8

Forever Young:
How AHL15 delays developmental phase transitions to prevent ageing in plants

Proefschrift

ter verkrijging van
de graad van doctor aan de Universiteit Leiden,
op gezag van rector magnificus prof.dr.ir. H. Bijl,
volgens besluit van het college voor promoties
te verdedigen op woensdag 28 mei 2025
klokke 14:30 uur

door

Thalia Luden
geboren te Amsterdam
in 1993

Promotores:
Prof. dr. R Offringa
Dr. S. Balazadeh

Promotiecommissie:
Prof. Dr. A. H. Meijer
Prof. Dr. J. Memelink
Dr. K. Spaninks
Prof. Dr. M. E. Schranz, Wageningen University & Research
Dr. M. E. Stam, University of Amsterdam

Contents

Chapter 1 7

Regulation of the life history of flowering plants (Introduction)

Chapter 2 47

Insights into polycarpic plant development through natural variation in the aerial rosette phenotype in *Arabidopsis thaliana*

Chapter 3 87

GreenLeafVI: An ImageJ plugin for high-throughput analysis of leaf chlorophyll content

Chapter 4 107

The plant longevity gene AHL15 inhibits leaf senescence by repressing *ORESARA1* and cytokinin degradation

Chapter 5 141

AHL15 modulates gene expression independently of chromatin accessibility and histone modifications

Summary 179

Samenvatting 187

Curriculum Vitae 195

Chapter 1

Regulation of the life history of flowering plants

(Introduction)

Thalia Luden[1] and Remko Offringa[1]

[1] Plant Developmental Genetics, Institute of Biology Leiden, Leiden University, Sylviusweg 72, 2333 BE Leiden, the Netherlands

Summary

The life history strategy of plants can vary strongly between different plant species. Some annuals, such as the model plant *Arabidopsis thaliana* (Arabidopsis) germinate, grow, flower, set seed and die within a period of a few months, whereas woody perennials grow and flower every year and are among the longest lived organisms on this earth. The majority of our knowledge on longevity-associated traits in plants is based on research in Arabidopsis, which following germination undergoes four developmental phases from juvenile vegetative through adult vegetative and reproductive to the senescence phase. Here we will review the regulation of life history traits, with a focus on the juvenile-to-adult transition, called Vegetative Phase Change (VPC), the transition from vegetative to reproductive growth also called the floral transition, leaf senescence, and the maintenance of vegetative development during the reproductive stage in the context of life history strategy. We will also discuss how the protein AHL15 plays a role in each of these processes, and elaborate on the current knowledge of how AHL proteins function.

Keywords: *Arabidopsis thaliana,* vegetative phase change, phyllotaxis, flowering, floral transition, vernalization, inflorescence architecture, senescence, life history strategy, polycarpy, monocarpy, global proliferative arrest, AHL15, AHLs

Life cycle of flowering plants

The life cycle of the model plant *Arabidopsis thaliana* (Arabidopsis) and other seed plants begins with the germination of the seed. Seeds contain a dormant embryo, and germination is initiated when water is available (imbibition) and can be accelerated by other factors such as prior exposure to cold (stratification) (Iwasaki et al., 2022). Imbibed seeds will rapidly produce a radicle, an outgrowth of the embryonic root, followed by the expansion of the hypocotyl, which is a stem-like structure between the developing root and one or two embryonic leaves called cotyledons (Boyes et al., 2001) (Figure 1). Hypocotyl growth is responsive to light, and the hypocotyl will elongate when kept in dark or low-light conditions to ensure that the cotyledon(s) can emerge from the soil. The hypocotyl initially emerges with an apical hook in which the top of the hypocotyl is curved at an 180° angle, resulting in a downward position of the cotyledons and the stem cell zone called the shoot apical meristem (SAM), which helps to protect them when the shoot moves through the soil to reach the light. Upon exposure to light, the apical hook is resolved allowing the cotyledons to open, expand and produce chlorophyll to start photosynthesis (Abbas et al., 2013; Krahmer and Fankhauser, 2024). The primary root elongates by division and differentiation of cells in the root apical meristem, and lateral roots are produced by a specific stem cell zone in the root called the pericycle (Beeckman and De Smet, 2014). The aboveground tissues of the developing plant will be formed by the SAM as it produces new aerial organs. In Arabidopsis, the first pair of true leaves emerges simultaneously from the SAM after about one week, and subsequent leaves are formed one by one in a radial pattern. Leaves produced early on in the plant's life cycle are typically in a juvenile state, and over time the plant will gradually transition into an adult state, a process that is called vegetative phase change (VPC) (Poethig, 2013; Poethig and Fouracre, 2024). Before flowering, Arabidopsis plants grow as a rosette, meaning that leaves are produced from the SAM directly after one another without elongation of the stem in between. In addition to the SAM, axillary meristems (AMs) are located in leaf axils, which can either produce additional organs or remain dormant (Tian et al., 2014; Tian et al., 2019; Zhu and Wagner, 2020).

The floral transition is initiated during the plant's adult stage and its timing is strongly influenced by environmental conditions such as day length and temperature (Kinoshita and Richter, 2020). In Arabidopsis, flowering is promoted in long days and is repressed in short days, but this can be different in other species such as tomato whose floral transition is insensitive to day length (Lifschitz and Eshed, 2006), or chrysanthemum in which flowering is promoted

by short days (SharathKumar et al., 2021). In Arabidopsis, the flowering process starts with the formation of a primary inflorescence stem that emerges from the SAM in a process called bolting, and grows upwards to form flowers in a raceme: an indeterminate inflorescence from which new flowers emerge at the sides of the SAM, with the oldest flowers at the bottom and the youngest flowers at the top (Figure 1). Additional inflorescences can emerge from AMs in the rosette, which usually develop after the primary inflorescence has started elongating. The inflorescences also produce inflorescence AMs that can form secondary branches, resulting in a branched inflorescence architecture (Zhu and Wagner, 2020).

Arabidopsis is a self-pollinating plant, and upon fertilization, embryogenesis and seed formation occur in an elongated gynoecium, which develops into a silique that ripens as the rest of the plant undergoes senescence. The inflorescences continue to produce new flowers until the inflorescence meristem stops producing new stem cells and arrests its production of new flowers (Thomas, 2013; Balanzà et al., 2019). The life cycle of Arabidopsis is concluded when the whole plant has senesced and the siliques and seeds are ripened, resulting in the death of the plant and the release of seeds for a new generation (Figure 1).

Vegetative Phase Change

Plants generally undergo a juvenile and an adult growth phase during their vegetative state. The juvenile-to-adult transition during which plants shift from producing juvenile leaves to adult leaves and acquire the competence to flower is referred to as vegetative phase change (VPC). Juvenile Arabidopsis leaves are typically round in shape with smooth margins and lacking abaxial trichomes, whereas adult leaves are typically oblong or oval-shaped with serrated margins at the base and have trichomes on both sides of the leaf (Telfer et al., 1997; Rahimi et al., 2022a). This difference in phenotype between juvenile and adult leaves is called heteroblasty, and can be seen in many but not all plant species. Although heteroblasty is conserved, the specific traits associated with juvenile and adult leaves can differ widely between genotypes and species (Huijser and Schmid, 2011; Doody et al., 2022; this thesis).

VPC has generally been considered as a necessary transition in the plant to gain competence to flower (Huijser and Schmid, 2011; Hyun et al., 2017). However, recent findings have challenged the idea that VPC is a necessary step for the initiation of the flowering process. For example, growth in monochromatic blue light accelerates flowering time while the VPC is only

weakly affected (Spaninks et al., 2020). In addition, the timing of VPC also does not always correlate with the timing of the floral transition, indicating that these two processes are regulated independently (Hyun et al., 2017; Spaninks et al., 2020; Doody et al., 2022; this thesis).

The molecular pathway controlling VPC has been studied in detail in Arabidopsis, and is regulated primarily by the microRNAs *miR156* and *miR157*, and members of the SQUAMOSA PROMOTER BINDING PROTEIN-LIKE (SPL)

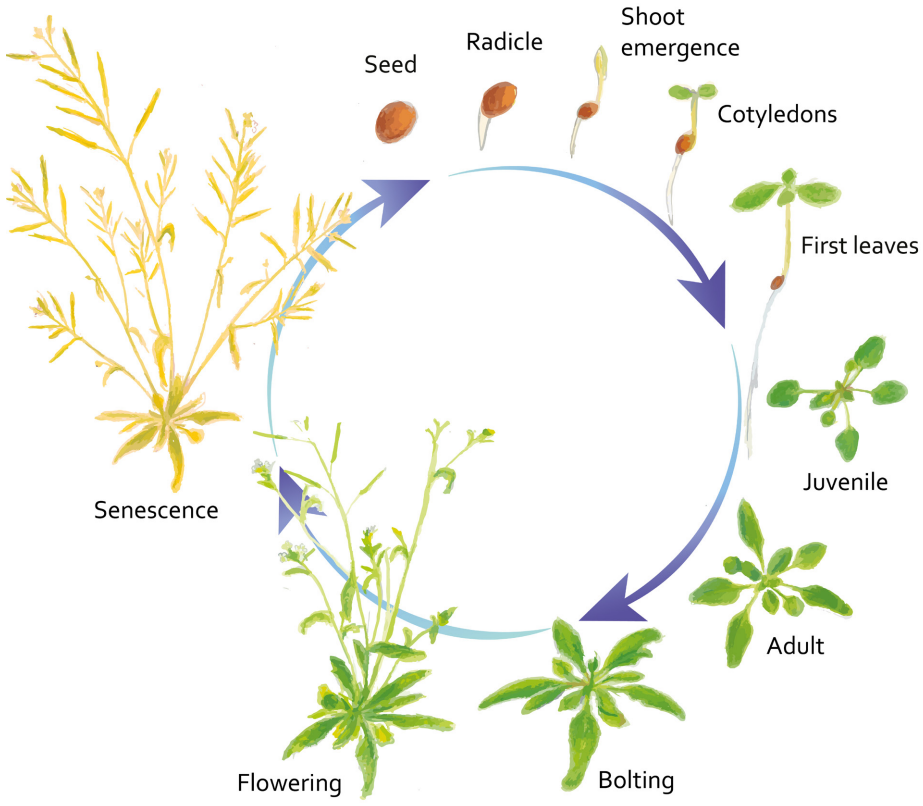

Figure 1: Life cycle of *Arabidopsis thaliana*. Germination of the seed starts with the emergence of the embryonic root (radicle), followed by the emergence of the shoot with an apical hook from which the two cotyledons will angle upwards and unfold once in the light. The first true leaves emerge symmetrically in a pair from the shoot apical meristem, and subsequent leaves are formed in a radial pattern. Juvenile leaves are rounded in shape with a long petiole, whereas adult leaves are more oblong with shorter petioles. The flowering process is induced in adult plants and starts with the formation of a bolt (the emerging primary inflorescence), and additional inflorescences are produced from axillary meristems in the rosette. Inflorescences form flowers in a raceme, an inflorescence type in which the oldest flowers are produced at the bottom and new flowers emerge from the top. After pollination, seeds are produced inside a silique. Upon flowering the senescence of the rosette is initiated, followed by senescence of the inflorescence tissues resulting in whole-plant death.

transcription factor (TF) family. Juvenile plants strongly express *miR156* and *miR157*, and their abundance decreases gradually over developmental time in a process that is controlled by the rate of cell division in the SAM (Cheng et al., 2021). The sequence of *miR156* and *miR157* is highly complementary to the mRNA sequence of many *SPL* genes, and causes post-transcriptional silencing of these genes via the RNAi pathway (Wang et al., 2009a). As miR156 abundance decreases over time, the post-transcriptional silencing of *SPLs* is reduced, resulting in a gradual increase of SPL protein levels (Wang et al., 2009a; Wu et al., 2009; Xu et al., 2016). SPLs regulate expression of several genes involved in leaf shape, trichome production, and flowering. For example, SPLs promote the expression of miR172, which targets the transcripts of a number of APETALA2 (AP2)-like genes that inhibit flowering and abaxial trichome formation, and thereby promote flowering and adult traits (Wu et al., 2009).

Perturbations in the miR156/SPL pathway can dramatically change the phenotype of the plant, resulting in a prolonged and ectopic juvenile state or an accelerated transition to the adult state depending on which part of the pathway is affected. For example, constitutive overexpression of *miR156* delays both the VPC and flowering time (Wu et al., 2009; Xu et al., 2016), and inflorescences of these plants produce rosette-like leaves from the inflorescence AMs that are called aerial rosettes (ARs) (Rahimi et al., 2022a). A similar phenotype can be seen in higher-order *spl* mutants, but this effect is less pronounced than in *MIR156* overexpressing plants. This can be explained by the fact that miR156 regulates as many as ten *SPL* genes, whereas only five *SPLs* were mutated in the highest-order *spl* knockout (Xu et al., 2016). On the other hand, plants overexpressing SPLs or those expressing miR156-insensitive *SPL* alleles (*rSPL)* show an accelerated VPC and flower early (Wang et al., 2009a; Wu et al., 2009; Xu et al., 2016).

Leaf development and rosette architecture

As the plant grows, new above-ground organs including leaves are produced from the pool of totipotent cells at the SAM. The pattern in which new leaves are formed is referred to as phyllotaxis, and the phyllotactic pattern varies between plant species. In Arabidopsis, phyllotaxis occurs in a radial pattern following Fibonacci's "golden angle", where each new leaf emerges at an angle of circa 137° relative to the one produced before (Kuhlemeier, 2017). Many other plant species show the same phyllotactic pattern: sunflower heads, pinecones, and pineapples all follow the same golden angle, although other phyllotactic patterns such as bilateral or fourfold symmetry or alternating

leaves are common as well.

Leaves develop from primordia in the periphery of the SAM, and the position of these primordia relative to one another determines the phyllotactic pattern. Primordia consist of groups of differentiating cells, and the central zone of the SAM contains totipotent cells (Kuhlemeier, 2017). Both the primordia and the cells in the SAM central zone continuously divide, resulting in an outward push of cells from the central zone to the periphery, and concomitant growth of the primordia. This results in in a pattern where the oldest, and largest, primordia are the most distant from the SAM, and new primordia arise closer to the SAM centre (Yin, 2021). In Arabidopsis and other plants with radial phyllotaxis, new primordia arise at the location that is most distant from previous primordia as a result of strong differences in local concentrations of the hormone auxin. Auxin promotes the division and differentiation of cells by activating specific target genes, and new primordia arise at local auxin maxima (Yin, 2021). This is demonstrated by the fact that primordium formation can be artificially induced by exogenous application of auxin (Reinhardt et al., 2000; Reinhardt et al., 2003).

The position of auxin maxima is determined by polar auxin transport which is regulated by auxin efflux carriers of the PIN-FORMED (PIN) family (Reinhardt et al., 2003). PIN proteins are predominantly located on the plasma membrane, where they are distributed asymmetrically (i.e. on one side of the cell). This asymmetric distribution establishes a directional auxin flow between cells (Okada et al., 1991). The position of PIN1, the most important PIN protein involved in phyllotaxis, is regulated by auxin in a positive feedback loop where a high local concentration of auxin stimulates efflux of auxin against the auxin gradient, resulting in local auxin hyperaccumulation (Reinhardt et al., 2003; Galvan-Ampudia et al., 2020). The high concentration of auxin then stimulates the formation of a primordium, whereas the vicinity is depleted of auxin, inhibiting the formation of other primordia. Together with the continuous division of cells in the SAM central zone, this results in a divergence angle of approximately 137° between subsequent leaves (Galvan-Ampudia et al., 2020). Disruptions in the transport of or response to auxin cause differences in phyllotaxis, and the absence of local auxin maxima in, for example, the *pin1* mutant or by inhibition of polar auxin transport abolishes the formation of primordia altogether (Reinhardt et al., 2000; Reinhardt et al., 2003).

In addition to the position and maintenance of local auxin maxima in the SAM, the size and number of cells in the SAM central zone also affects the phyllotactic pattern (Giulini et al., 2004; Yin, 2021). The SAM size is strongly

affected by the hormone cytokinin (CK), which promotes cell division in the SAM central zone (Leibfried et al., 2005). In parallel to the induction of primordium development by auxin, repression of CK signalling contributes to the phyllotactic pattern (Giulini et al., 2004; Besnard et al., 2014a; Besnard et al., 2014b). Knockout mutants of genes that negatively regulate the CK response show altered phyllotactic patterns as a result of the enhanced SAM size (Giulini et al., 2004), and the enhanced CK response results in the simultaneous initiation of multiple primordia (Giulini et al., 2004; Besnard et al., 2014a). This implies that CK promotes the outgrowth of newly arising primordia, and that repression of the CK response in developing primordia helps to time their outgrowth. The timing of primordium development is an important contributor to plant architecture, as this determines whether leaves are produced sequentially or in groups. Sequential initiation of primordia results in spiral or alternate phyllotaxis, whereas simultaneous initiation of primordia gives rise to opposing pairs or whorls of leaves. Finally, mechanical forces caused by cell expansion as well as stem torsion influence the phyllotactic pattern by affecting PIN polarity (Heisler et al., 2010; Yin, 2021).

The floral transition

Several factors can influence the floral transition, a process during which the plant undergoes several developmental changes that result in the production of an inflorescence and flowers (Figure 2A). In the absence of environmental stimuli, the developmental age of the plant will initiate the flowering process under influence of SPLTFs, most importantly SPL9 and SPL15 (Hyun et al., 2016; Xu et al., 2016). As the miR156 levels decrease with age and plants transition to the adult state, a threshold is reached in which the floral promoters overrule the floral inhibitors and flowering is initiated in a process called the age-dependent flowering pathway (Wang, 2014; Hyun et al., 2017).

Flowering cues are integrated by so-called floral integrators, such as SUPPRESSOR OF OVEREXPRESSION OF CONSTANS 1 (SOC1) and FLOWERING LOCUS T (FT). Together with SPL15, SOC1 promotes the expression of *miR172* and *FRUITFULL (FUL)* in the SAM (Hyun et al., 2016). FT is a mobile protein that is unable to directly bind DNA but promotes the expression of several flowering genes including *SOC1* when interacting with the DNA-binding TF FLOWERING LOCUS D (FD) in the SAM (Abe et al., 2005; Zhu et al., 2020). The genes targeted by SOC1 and the FT-FD complex promote differentiation of the SAM into an inflorescence meristem (IM) that produces bracts and flowers instead of leaves.

Growth in long-day conditions can accelerate the induction of flowering in long-day plants due to the activation of *FT* expression in leaves. *FT* transcription is controlled by the diurnally regulated TF CONSTANS (CO), whose stability is day-length dependent. In Arabidopsis, CO levels are low in short days, and sufficiently high levels to initiate *FT* transcription are only reached in long-day conditions (>12h light) (An et al., 2004; Valverde et al., 2004; Maple et al., 2024). The FT protein is expressed in the leaf vasculature and from there it enters the phloem and moves to different locations where it regulates the expression of its target genes. In the SAM, it interacts with FD to promote the expression of flowering genes, but FT can also regulate branch outgrowth and sugar transport (Fichtner et al., 2021). The daylength-dependent expression of *FT* is responsible for the rapid flowering of Arabidopsis under long day, but the daytime-dependent (diurnal) regulation of CO stability and subsequent *FT* expression varies between species and differs in species that, for example, flower under short days.

In addition to developmental age and day length, environmental temperature also plays an important role in controlling flowering time. For example, most *Brassica* species require vernalization, a prolonged exposure to cold conditions, to flower. This cold requirement is conveyed by *FLOWERING LOCUS C (FLC),* a floral repressor that is expressed in the whole plant upon germination and targets the flowering-promoting genes *SOC1, FT,* and *SPL15* and represses their expression (Deng et al., 2011). *FLC* expression is gradually silenced upon cold exposure, and becomes permanently silenced in Arabidopsis after a threshold period of cold exposure is reached (Michaels and Amasino, 1999; Shindo et al., 2006; Duncan et al., 2015). *FLC* expression is promoted by the TF FRIGIDA (FRI) (Michaels and Amasino, 1999; Johanson et al., 2000), and cold conditions cause a perturbation in the FRI transcriptional complex (Hu et al., 2014), reducing *FLC* expression immediately. More importantly, vernalization induces a gradual silencing of the *FLC* gene during extended cold exposure by recruiting the Polycomb Repressive Complex2 (PRC2) that trimethylates the Lysine 29 of histone 3 (H3K29me3; a repressive epigenetic mark) (De Lucia et al., 2008; Angel et al., 2011). The FLC pathway helps to prevent precocious flowering during winter, and the mechanism with which *FLC* is silenced during vernalization is an ongoing subject of study and is a widely used model to study epigenetic silencing mechanisms.

Inflorescence architecture and flower production

In Arabidopsis, the inflorescence phyllotaxis is regulated similarly to the

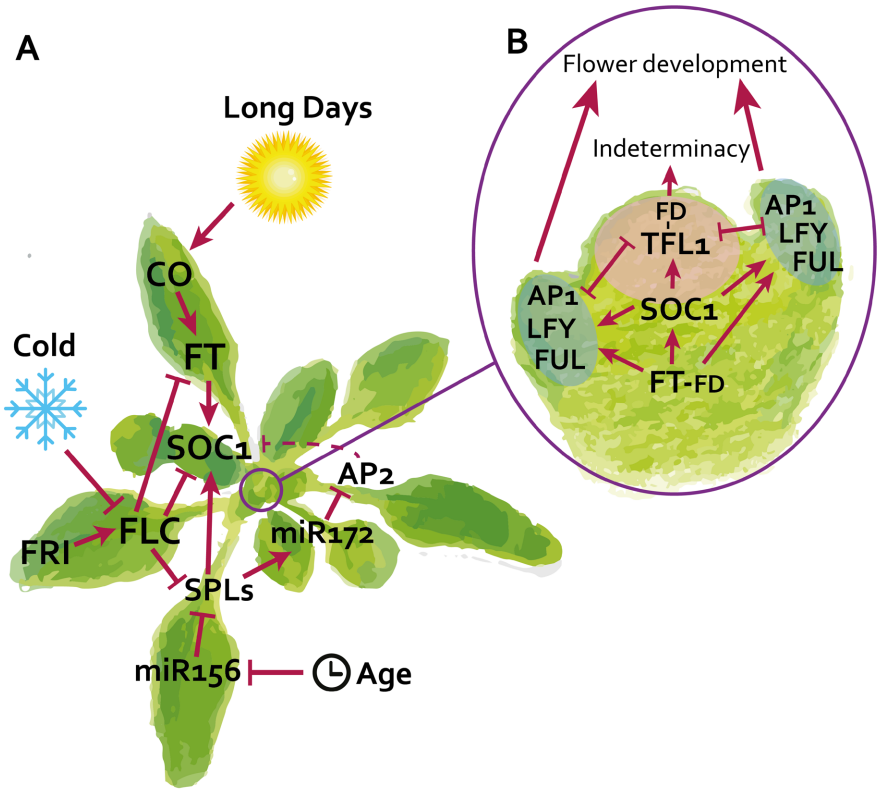

Figure 2: Induction of flowering in Arabidopsis. **A:** Long days promote the stability of the TF CONSTANS (CO) in leaves, which promotes transcription of *FLOWERING LOCUS T* (*FT*). The mobile FT signal travels to the SAM, where it binds to FD. This complex promotes flowering by inducing expression of *SUPPRESSOR OF OVEREXPRESSION OF CO 1* (*SOC1*). SOC1 activates the expression of several other TFs, such as *APETALA1* (*AP1*), *LEAFY* (*LFY*), and *FRUITFULL* (*FUL*), that promote the transition from a vegetative to a reproductive meristem and the subsequent formation of flowers. Flowering is suppressed by FLOWERING LOCUS C (FLC), whose expression is promoted by FRIGIDA (FRI) and is suppressed by prolonged cold exposure (vernalization). In addition, flowering is repressed in young plants by high levels of miR156, which post-transcriptionally repress the *SQUAMOSA PROMOTER BINDING-LIKE* (*SPL*) genes. Age reduces the expression of *miR156*, relieving the suppression of *SPL* genes and thereby increasing the expression of the flowering-promoting genes *SOC1* and *miR172*. miR172 targets the flowering-repressing gene *APETALA2* (*AP2*) and several of its family members.
B: Regulation of indeterminacy and inflorescence architecture in the SAM (area encircled in purple). FT binds FD in the SAM and promotes the expression of several flowering-promoting genes. TERMINAL FLOWER 1 (TFL1) competes with FT to bind FD. The TFL1-FD complex represses the expression of several flower-specifying genes (*AP1, LFY* and *FUL*) in the central zone of the IM to ensure its indeterminacy (area colored pink). On the other hand, in the peripheral zone of the IM the TFs AP1, LFY, and FUL initiate the flower developmental program by promoting the differentiation into a floral meristem that subsequently produces a flower (area colored blue).

rosette architecture: both tissue types are arranged in a spiral pattern. In order to produce flowers, primordia separate from the SAM and undergo a transition from the inflorescence identity of the IM to a floral identity, thereby becoming a floral meristem (FM). Each flower in the Arabidopsis inflorescence is produced by an individual FM that splits off from the IM, resulting in a raceme architecture in which the oldest flowers are produced at the bottom and new flowers are continuously produced near the SAM. The transition of IM- to FM identity is regulated by floral identity TFs, and in the SAM the balance between expression of TFs that convey either the IM or FM identity determines the architecture of the inflorescence (Prusinkiewicz et al., 2007; Azpeitia et al., 2021). IM-promoting TFs ensure indeterminacy of the SAM, whereas FMs are determinate and produce a single flower. To produce a raceme, TFs promoting the IM identity are generally expressed in the center of the SAM whereas TFs promoting floral identity are expressed in the primordia in the peripheral zone of the SAM, resulting in flowers that split off from the side and an indeterminate SAM in the center (Prusinkiewicz et al., 2007; Azpeitia et al., 2021).

Retaining at least some IM cells in the SAM is required for making an inflorescence that contains multiple flowers, because the complete transition of the IM to an FM would result in the production of a single flower. This can be seen in the *terminal flower 1* mutant, which does not express the *TERMINAL FLOWER 1 (TFL1)* gene that plays a role in preventing the transition of the IM to the FM fate. As its name suggests, the *tfl1* mutant produces only a single flower from each inflorescence (Alvarez et al., 1992; Bowman et al., 1993). TFL1 blocks the expression of floral identity genes in the center of the SAM and thereby ensures indeterminacy. This effect is achieved because TFL1 competes with FT to bind FD in the SAM. FT and TFL1 have opposite effects on FD target genes, resulting in a flowering-promoting effect by FT and a flowering-delaying effect by TFL1 (Zhu et al., 2020). *TFL1* expression is controlled in part by SOC1 and other flowering-inducing genes that restrict its expression to the center of the SAM, where TFL1 represses the transition to FM identity (Ratcliffe et al., 1999; Liu et al., 2013; Azpeitia et al., 2021).

FM identity is conveyed by TFs such as FUL, LEAFY (LFY), and APETALA1 (AP1) (Bowman et al., 1993; Liu et al., 2013; Azpeitia et al., 2021). Their expression is initially promoted by SOC1, the FT-FD complex, SPL3, and other flowering-promoting TFs (Xu et al., 2016; Zhu et al., 2020; Azpeitia et al., 2021). *LFY* is the first to be expressed, and acts as a pioneer TF to promote expression of *AP1* and other target genes (Jin et al., 2021). AP1 promotes the expression of flower-specific genes and blocks the expression of *TFL1*, which

enforces the FM identity in domains in which AP1 is expressed (Ratcliffe et al., 1999; Prusinkiewicz et al., 2007; Azpeitia et al., 2021). Knockout of FM-specific genes usually results in defects in the flower architecture: *lfy* mutants produce indeterminate branches with many bracts instead of flowers, and when flowers are eventually made they are subtended by many additional bracts (Schultz and Haughn, 1991; Weigel and Nilsson, 1995). *ap1* loss-of-function plants produce flowers with defective petals or no petals at all (Alejandra Mandel et al., 1992), and double mutants of *ap1* and its close homolog *cauliflower (cal)* produce an enlarged, cauliflower-like IM with many FMs that do not develop into flowers (Bowman et al., 1993). The proper control of IM and FM boundaries is required to ensure functional inflorescence and flower architectures, and changes in their expression patterns explain the variation in inflorescence architectures that have evolved (Harder and Prusinkiewicz, 2013). In addition, human selection for mutations in IM- and FM identity genes have resulted in the various *Brassicaceae*- and other vegetables that are cultivated worldwide: cauliflower, for example, is a *Brassica oleraceae* variety with mutations in its *ap1* and *cal* orthologs (Azpeitia et al., 2021). Thus, knowledge of the TFs shaping the inflorescence architecture is of fundamental as well as agricultural interest.

Leaf senescence

Soon after bolting and the formation of the first flowers, Arabidopsis plants will gradually start to relocate their nutrients from the rosette leaves to the developing flowers and seeds through a process called senescence. Senescence is a developmental process during which the chlorophyll (Chl) and other components of a plant organ (primarily leaves) are systematically degraded and transported for reuse to other, newly developing parts of the plant, and can contribute to a plant's health and reproductive success (Lim et al., 2007a; Schippers et al., 2015). Proper regulation and a timely onset of senescence is important for the plant's ability to cope with a sudden change in nutrient availability and for securing sufficient nutrients for their offspring (Schippers et al., 2015). For example, it was shown that seed protein content correlates with early leaf senescence in wheat and barley, indicating that senescence positively impacts the seed quality (Uauy et al., 2006; Jukanti and Fischer, 2008). On the other hand, delayed leaf senescence can increase the photosynthetic capacity of those leaves and thereby increase the final seed yield, even if the quality and protein content of the individual seeds is somewhat reduced (Guo et al., 2021). Delayed senescence can also be a valuable trait for commercially cultivated food- and ornamental crops, as the yield and shelf life of leafy crops

and the shelf life of cut flowers is increased when senescence is delayed (Zhou and Yang, 2023). Senescence is therefore an agriculturally important trait and improved control of plant senescence can help to increase the fitness of plants in nutrient-limited conditions, improve nutritional qualities, and improve the marketability of crops and reduce food waste.

The most commonly studied and most visible type of senescence is leaf senescence, which can be induced via several processes: sequential, induced, reproductive, and post-harvest senescence. Sequential or age-dependent senescence is the process during which older leaves are degraded and their nutrients are relocated to newly developing leaves. This process is induced primarily by developmental age and is unaffected by reproduction or other developmental processes (Zentgraf et al., 2004; Schippers et al., 2015). The timing of sequential senescence has been proposed to be regulated by the metabolic rate and the accumulation of oxidative stress over a leaf's life time, and mutants with reduced photosynthetic efficiency show a delayed senescence phenotype (Lim et al., 2007a). Senescence can also be induced by several external factors, such as treatment with plant hormones, dark incubation, salt- or drought stress, environmental temperature, or pathogen infection (Guo and Gan, 2005; Bresson et al., 2018). Reproductive senescence is induced upon flower- and seed production. It ensures that the plant's resources are relocated from the leaves to the newly developing seeds, providing the maximum amount of resources to the next generation, and can be delayed in some species by removal of the reproductive structures (Schippers et al., 2015). Finally, post-harvest senescence is the process in which senescence is induced when a plant is cut from its roots or when leaves are removed from the plant. In all cases, the expression of a large set of senescence-associated genes is induced, which eventually results in the degradation of Chl and other macronutrients.

Leaf senescence is regulated by several plant hormones, most notably ethylene. Ethylene promotes fruit ripening, etiolation (stem elongation in dark conditions), and plays a central role in promoting leaf senescence (e.g. Guo et al., 2021). Other hormones that can induce senescence are strigolactones, abscisic acid (ABA), jasmonic acid (JA), and salicylic acid (SA), whereas CK and auxin have been shown to delay the onset of leaf senescence (Guo and Gan, 2005; Ueda and Kusaba, 2015). Interestingly, ethylene-induced senescence can only occur when a leaf has reached a certain age, as ethylene application could only induce senescence in Arabidopsis leaves that were at least 25 days old (Jing et al., 2005). In addition to hormone treatment, senescence

can be externally induced by placing plants or detached leaves in the dark. This adaptive trait helps a plant relocate its nutrients away from leaves that do not catch sufficient sunlight for photosynthesis to new leaves (Schippers et al., 2015). Ethylene treatment and dark incubation are two commonly used methods to induce leaf senescence in an experimental setup to investigate

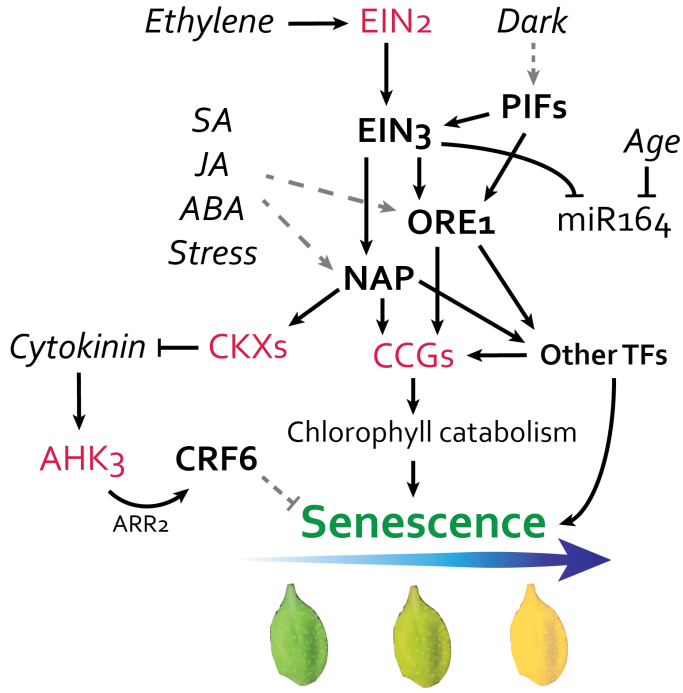

Figure 3: A simplified overview of regulation of leaf senescence in *Arabidopsis thaliana*. Senescence can be induced by ethylene, which is perceived by receptors such as ETHYLENE RESISTANT1 (ETR1) and via ETHYLENE INSENSITIVE2 (EIN2) activates the TF ETHYLENE INSENSITIVE3 (EIN3). EIN3 promotes the transcription of several TF-encoding genes, of which the most important are *ORESARA1* (*ORE1*) and *NAC-LIKE ACTIVATED BY AP3/PI* (*NAP*). NAP and ORE1 then promote the expression of several Chlorophyll Catabolic Genes (*CCGs*) either directly or indirectly via other TFs. *ORE1* mRNA is targeted by miR164, whose transcription is repressed by EIN3 and decreases with age, thereby regulating the age-dependent senescence pathway. Senescence can be induced by several other hormones (e.g. JA, SA, ABA) or external stressors that promote the expression of the senescence-inducing TFs *NAP* and *ORE1* in an ethylene-independent manner. Dark treatment activates PHYTOCHROME INTERACTING FACTOR (PIF) 4 and PIF5, which promote senescence by inducing the transcription of *EIN3* and *ORE1*. Finally, cytokinin represses senescence via its receptor ARABIDOPSIS HISTIDINE KINASE 3 (AHK3), which phosphorylates ARABIDOPSIS RESPONSE REGULATOR 2 (ARR2). Phosphorylated ARR2 promotes transcription of the TF *CYTOKININ RESPONSE FACTOR 6* (*CRF6*), which inhibits senescence by an unknown mechanism. During the senescence process, NAP also induces expression of the *CYTOKININ OXIDASE/DEHYDROGENASE* (*CKX*) proteins, which degrade cytokinin and thereby relieve CK-mediated suppression of senescence. TFs are in indicated in green, other types of protein are indicated in lack, and hormones and other factors affecting senescence are italicized.

senescence under controlled conditions (Bresson et al., 2018).

Induction of senescence triggers the expression of a set of genes that are involved in the catabolism of Chl and other macromolecules. Their expression can be induced via several regulatory pathways depending on the method of senescence induction. Chl degradation occurs in several steps, and involves the activity of the genes *NON-YELLOW COLORING1 (NYC1), NON-YELLOW COLORING-LIKE (NOL)* to convert Chl-*b* to Chl-*a*, which is then further degraded to pheophytin by genes in the *NON-YELLOWING (NYE)* class. The PHEOPHYTINASE (PPH) enzyme is responsible for hydrolyzing pheophytin into pheophorbide *a* and phytol, and pheophorbide *a* is subsequently catabolized by PHEOPHORBIDE A OXYGENASE (PAO), resulting in a loss of green color (reviewed by Hörtensteiner and Kräutler, 2011). Knockout of any of these catabolic genes results in a stay-green or delayed senescence phenotype, and loss-of-function of TFs that promote their expression directly or indirectly has a similar effect. On the other hand, genes that negatively regulate senescence have a stay-green phenotype when overexpressed, and may also show accelerated senescence when knocked out.

Several central regulators of senescence have been identified, and cross-talk between different senescence-inducing pathways is common (Figure 3). One central regulator of senescence is the TF ETHYLENE INSENSITIVE 3 (EIN3), which is activated by EIN2, a key regulator of ethylene perception that itself is activated by ethylene receptors such as ETHYLENE RESISTANT 1 (ETR1) (Alonso et al., 1999). EIN3 promotes transcription of the NAC-family TFs *ORESARA1 (ORE1)* and *NAC-LIKE ACTIVATED BY AP3/PI (NAP)*, which promote transcription of several Chl catabolic genes and of other TFs involved in senescence (Qiu et al., 2015). In addition, *ORE1* transcripts are targeted by miR164, whose expression is decreased over plant age and thereby conveys an age-dependent regulation of senescence (Kim et al., 2009). Expression of *miR164* is repressed by EIN3, resulting in a release of post-transcriptional silencing of *ORE1* in addition to the direct activation of *ORE1* transcription by EIN3 (Li et al., 2013). *EIN3* activation and *ORE1* transcription can also be induced by PHYTOCHROME INTERACTING FACTORS (PIF) 4 and 5, which are induced by dark treatment (Song et al., 2014). *ORE1* transcription is also induced indirectly by salt stress and ABA, and the transcription of several ORE1 targets including Chl catabolic genes can be induced by other hormones like JA and SA and by salt stress (Balazadeh et al., 2010; Woo et al., 2019). Because of the complex interaction between several TFs that regulate senescence, there is a large overlap between different senescence pathways, which makes it difficult

to identify at what level a stay-green mutant is affected.

Unlike the senescence-promoting hormones ethylene, JA, SA, and ABA, CKs repress the progression of leaf senescence. Although much remains to be understood about the role of CK in repressing senescence, it has been shown that it depends specifically on the CK receptor ARABIDOPSIS HISTIDINE KINASE 3 (AHK3) which causes phosphorylation of the ARABIDOPSIS RESPONSE REGULATOR 2 (ARR2) upon CK perception (Kim et al., 2006). Phosphorylated ARR2 then promotes the expression of cytokinin-responsive genes and indirectly represses expression of Chl catabolic genes (Kim et al., 2006). AHK3 also induces the expression of CYTOKININ RESPONSE FACTOR 6 (CRF6), which is partially responsible for the repressive effect of CK on senescence (Zwack et al., 2013). In contrast, the expression of the CK-degrading *CYTOKININ OXIDASE/DEHYDROGENASE* (*CKX*) genes is upregulated during senescence by NAP and possibly also by other factors, resulting in decreased CK levels and subsequent release of senescence inhibition (Hu et al., 2021; this thesis). Application of exogenous CK delays senescence, and transgenic plants expressing a plant- or *Agrobacterium*-derived *ISOPENTENYL TRANSERASE* (*IPT*) CK biosynthesis gene under a senescence-specific promoter are significantly longer-lived than wild-type plants (Jordi et al., 2000; McCabe et al., 2001; Guo et al., 2021). Progression of senescence thus not only requires the activation of a regulatory pathway that induces the expression of Chl catabolic genes, but also requires the active down-regulation of CK levels in order to lift the repressive effects of CK on senescence.

Life history strategies of higher plants

The life cycle of Arabidopsis is that of a typical monocarpic plant: reproductive senescence ensures that all resources are reallocated from the senescent tissue to the ripening seeds, followed by the senescence and death of the aboveground meristems in a process that is called general proliferative arrest (GPA) (Balanzà et al., 2018; Wang et al., 2023). In monocarpic plants, reproductive senescence and GPA result in the death of the whole plant upon seed maturation. In contrast, polycarpic plants are able to maintain vegetative growth independently of flowering, which allows for a longer life span in which several, often seasonal flowering cycles can be attained (Thomas, 2013; Kiefer et al., 2019; Figure 4). In addition to the ability to flower repeatedly, the formation of a cambium ring in the stem producing wood (secondary growth) and the production of a more complex root network are traits typically associated with polycarpic species (Glover et al., 2010).

The terms "annual" and "perennial" are often used interchangeably with the terms "monocarpic" and "polycarpic", but these terms are misleading because the life span of a plant is not necessarily reflective of its life history. For example, some monocarpic plants can live for decades before initiating the flowering program, but are unable to return to their vegetative stage upon flowering. This process is also known as a "death bloom" and can be observed in several species, although it is not always clear whether these species are truly monocarpic or whether they can regenerate from below-ground rhizomes (Simcha, 2017). On the other hand, the capability to maintain vegetative growth during and after flowering in polycarpic plants does not always imply a long

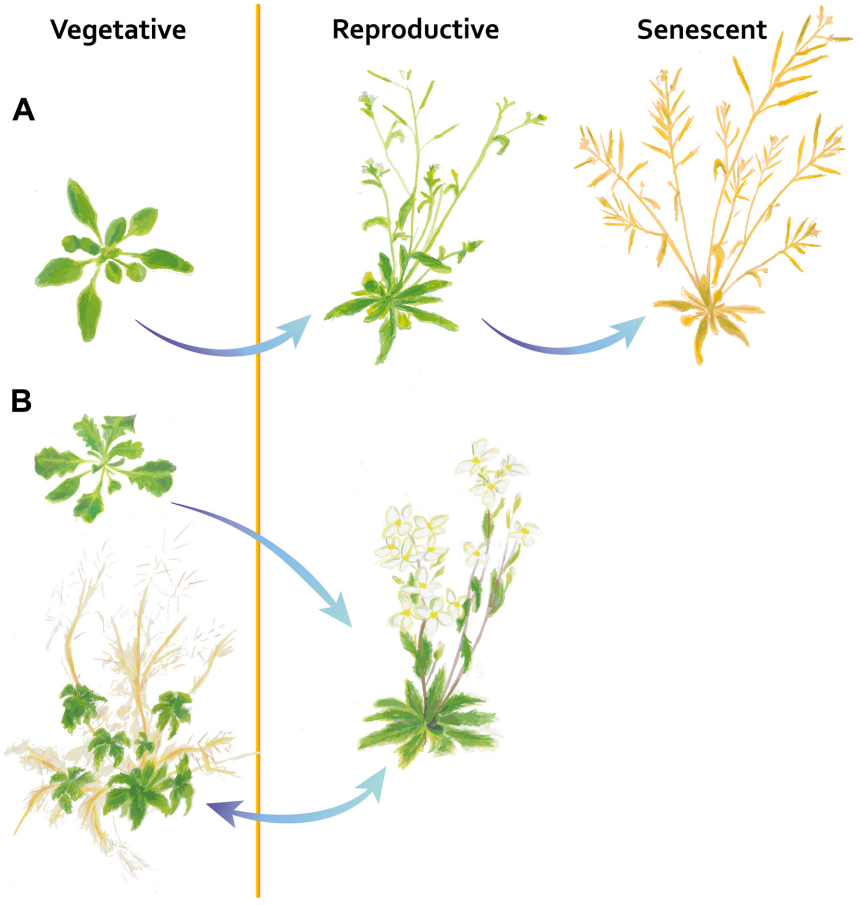

Figure 4: Schematic representation of the monocarpic and polycarpic life history strategy. **A:** Monocarpic plants like *Arabidopsis thaliana* transition from a vegetative to a reproductive phase in which flowers and seeds are produced, followed by a general proliferative arrest of the meristems, whole-plant senescence and death. **B:** Polycarpic plants like *Arabis alpina* transition between the vegetative and reproductive phase and back. During flowering, some meristems retain their vegetative identify and stay alive while reproductive structures arrest, senesce and die.

life span, because their survival might be affected by other factors than their capacity to maintain vegetative growth. For example, species such as the ornamental plant Petunia (*Petunia hybrida)* are commercially referred to as "annual" but are actually (sub)tropical polycarps that cannot survive the cold winter temperatures of the (Northern) countries in which they are cultivated (Vandenbussche et al., 2016). In addition to temperature, limited nutrient availability and exposure to pathogens or herbivores can be factors that limit the life span of polycarpic species. Finally, many species including those of the *Brassicaceae* family of which Arabidopsis is a member are often referred to as "winter annuals" or "biannuals": these species require vernalization (i.e. winter cold) to flower, but die soon after seed set. These are in fact monocarpic species that germinate in spring, but will survive over the winter because the repression of flowering has not yet been relieved (Schiessl et al., 2019). The terms "monocarpic" and "polycarpic" are therefore preferred over other terms, because they refer to the plant's developmental traits rather than its expected life span.

Monocarps and polycarps are both common in nature, and species vary widely in their lifespan and the overall biomass that can be achieved. The polycarpic life history strategy underlies the largest and longest-living organisms in the world, such as the giant redwood trees (*Sequoiadendron giganteum*) and clonally growing poplar groves (*Populus tremuloides*) that can reach ages of over 1000 years (Thomas, 2013). On the other hand, the monocarpic life history strategy is inherent to, or has been selected for in many economically important crops such as the *Brassicaceae* (cabbage and mustard family), pulses, and grains such as maize, rice, and wheat (Thomas, 2013). A likely cause for this is that monocarps relocate the maximum amount of resources to their fruits or seeds, which improves the yield of monocarpic plants compared to polycarpic plants in the same season (Jukanti and Fischer, 2008). In addition, many polycarpic species require a longer time period to achieve the competence to flower and thereby are slower to form fruits than monocarpic species (Kiefer et al., 2019). It is also possible that polycarpic species have not performed better than monocarps in cultivation systems where crops are completely harvested at the end of each season, resulting in inadvertent selection for monocarpy. Finally, some polycarpic crops are cultivated as monocarps and are harvested yearly, despite being able to renew their vegetative cycle. However, despite the apparent preference for monocarpy, polycarpic traits can also be beneficial to agricultural systems, and recent efforts have been made to reintroduce polycarpic traits to monocarpic grain species

(Glover et al., 2010; Zhang et al., 2023). The increased complexity and depth of a polycarp's root system compared to that of a monocarp, for example, can result in a more efficient uptake of nutrients and water in the soil, reducing the demand for fertilizer and irrigation (Glover et al., 2010). In addition, the annual plowing and replanting of a field is a major contributor to soil erosion and salinification, and cultivating crops over multiple years can reduce this issue. Finally, established plants are often more resilient to competition from weeds and pathogen attack than seedlings, reducing the losses due to disease and the need for herbicide and pesticide application (Glover et al., 2010).

Regulation of monocarpic and polycarpic traits on a molecular level

The maintenance of vegetative development in polycarpic species relies on repression of floral identity in some of the AMs of the plant during the flowering process. In monocarpic plants all meristems transition into an inflorescence- or floral fate or become dormant upon flowering, whereas polycarpic plants can prevent this transition in some of their AMs and can reactivate dormant buds (Ponraj and Theres, 2020; Vayssières et al., 2020). Although this process is not entirely understood, a few players have been identified in this process by comparing Arabidopsis with *Arabis alpina,* a polycarpic relative in the *Brassicaceae* family. In this section, we will discuss which genes have been shown to play a role in the maintenance of vegetative identity and other traits associated with life history in plants.

The aforementioned floral repressor FLC is one of the best-studied genes involved in maintenance of vegetative identity. In addition to a global repression of the flowering program, it was shown that FLC can repress flowering genes locally in AMs of flowering *Arabis alpina* (Lazaro et al., 2018). In vernalization-sensitive Arabidopsis, *FLC* expression can be permanently silenced by prolonged cold exposure, resulting in flowering followed by reproductive senescence and GPA (Michaels and Amasino, 1999). In contrast, vernalization causes only a temporary silencing of the *FLC* homolog *PERPETUAL FLOWERING 1 (PEP1)* in *A. alpina*, and *PEP1* expression is restored upon return to ambient temperatures. This causes a transition to the flowering state in some meristems during vernalization while in others PEP1 represses this transition and thereby helps retain the vegetative identity (Wang et al., 2009b; Hyun et al., 2019; Vayssières et al., 2020). In addition, *A. alpina pep1* knockout mutants do not require vernalization and lose most of their polycarpic traits (Wang et al., 2009b). It was shown that in contrast to *A. alpina, FLC* expression

is not reinitiated after flowering in Arabidopsis or in the monocarpic *Arabis montbretiana* (Kiefer et al., 2017). Recently, this differential regulation of *FLC* expression between mono- and polycarpic species was confirmed by crossing sets of mono- and polycarpic species from two *Brassicaceae* genera (Zhai et al., 2024). Moreover, transgenic Arabidopsis plants expressing polycarpic *FLC* homologs under their native polycarpic promoter gained a polycarpic phenotype, indicating that *FLC* expression after flowering is sufficient to induce a polycarpic life history strategy (Zhai et al., 2024).

Although differences in the cis-regulatory elements in the *FLC* loci of mono- and polycarpic species largely explain life history, it is not yet fully known which other genes are involved and which genes act upstream of *FLC* to reset its expression. Some additional regulators have been identified in *A. alpina:* for example, reactivation of *PEP1* expression in AMs after vernalization is regulated in part by the *A. alpina* AP2 homolog PEP2 (Lazaro et al., 2019). In addition, the *A. alpina* homolog of *TFL1* is expressed more highly in the SAM of young plants and in AMs, and AaTFL1 blocks the transition to flowering in these tissues in parallel to PEP1 (Wang et al., 2011). Interestingly, TFL1 homologues appear to be more important for the life history strategy of *Rosaceae* species than FLC, indicating that polycarpic life history can be achieved in multiple ways (Kurokura et al., 2013). Overall, it is clear that the maintenance of vegetative AMs contributes to the polycarpic life history strategy by ensuring the plant's capability to produce new organs during and after flowering.

Wood formation is another trait associated with polycarpy, and recent findings have indicated that the regulation of flowering and wood formation are at least partially linked. The floral integrator *SOC1* and the floral identity gene *FUL* have been shown to act as important moderators of wood formation and other polycarpic traits (Melzer et al., 2008). In addition to a significantly delayed flowering time and polycarpic traits, the *soc1 ful* double mutant showed a strongly enhanced secondary growth in the inflorescence stems, indicating that these two genes act together to repress wood formation. In addition, the AMs on the inflorescences of *soc1* single- and *soc1 ful* double mutants produced many rosette-like leaves in ARs, indicating that these axillary meristems have a (partially) vegetative identity similar to what occurs in polycarpic plants (Melzer et al., 2008; Dorca-Fornell et al., 2011). The development of the *soc1 ful* double mutant strongly resembles that of polycarpic species, because the overall longevity and biomass of these plants was also increased to more than 14 months (Melzer et al., 2008). The phenotype of this double mutant strongly implies that SOC1 and FUL play an important role in repressing longevity and

are required for the monocarpic life history strategy of Arabidopsis.

An important component of the monocarpic life history strategy is the ability to stop flower development before nutrient availability is too low to support the production of new fruits (Thomas, 2013; Wang et al., 2023). This can be achieved by proper timing of GPA. GPA timing is regulated by several processes, in which the TFs FUL and AP2 play important roles. In addition to its roles in promoting flower production and repressing wood formation, FUL is also an important regulator of GPA (Balanzà et al., 2018; Balanzà et al., 2019). In Arabidopsis, the single knockout of *ful* delays GPA by 3-4 weeks resulting in a longer life span and higher seed yield (Balanzà et al., 2018). *FUL* is expressed in the IM and restricts its proliferative capacity by indirect repression of *WUSCHEL (WUS),* a gene involved in maintenance of the stem cell pool in meristems. By restricting *WUS* expression, the proliferation of the meristem is also restricted, which limits the number of flowers and fruits that can be produced from a single inflorescence meristem (Balanzà et al., 2018). The floral inhibitor AP2, on the other hand, promotes stem cell proliferation by promoting *WUS* expression directly and indirectly, and its induction prolongs the proliferation of IMs (Martínez-Fernández et al., 2020). Merelo et al. (2022) showed that IM arrest is initiated around three weeks after bolting in Arabidopsis as a result of decreased meristem size and decreased cell division. This is caused by a decrease in the levels of CKs that promote cell division, and a subsequent decrease in *WUS* expression (Merelo et al., 2022). At five weeks after bolting, the IM stops producing new flowers in WT plants, but *ful* mutants proceed to produce flowers at a low rate, due to a higher CK concentration in the IM at this time point. AP2, on the other hand, promotes CK biosynthesis and downregulates genes associated with bud dormancy (Martínez-Fernández et al., 2020). Earlier research has indicated that FUL represses *AP2* expression and promotes the expression of the CK-degrading *CKX3* and *CKX5* genes, thereby reducing CK levels in the IM (Balanzà et al., 2014; Bemer et al., 2017). Taken together, IM longevity is stimulated by AP2-induced CK production and cell division, and limited by the repressive action of FUL on these processes.

Proliferative arrest of IMs is also accelerated by the fruits it has produced. An arrested IM can be reinitiated by pruning the siliques on that inflorescence (Hensel et al., 1994; Balanzà et al., 2019; Ware et al., 2020; Merelo et al., 2022), and IM proliferation is not arrested in male-sterile plants that are unable to produce seeds (Hensel et al., 1994). This indicates that seeds or fruits produce a mobile signal that represses IM proliferation, and it was shown that auxin acts as such a mobile signal (Ware *et al.*, 2020). Auxin represses the IM proliferation

when its levels are high, and Ware et al. (2020) showed that fertilized siliques export auxin into the polar auxin transport system that transports auxin from the SAM to the rest of the plant. High auxin export from the fruits interferes with auxin export from the SAM, resulting in its accumulation at the SAM and subsequent inflorescence arrest, similar to how auxin prevents the formation of new leaf primordia during the vegetative stage. This effect is achieved only by fruits in close proximity to the apical IM, as removal of proximal fruits could delay IM arrest whereas removal of distal fruits had no effect on the SAM. In addition, local silique- or flower removal does not affect the development of other inflorescences on the same plant, showing that the auxin-induced SAM arrest is a local process (Ware et al., 2020). Together these data indicate that reproductive senescence in monocarpic plants is not necessarily linked to IM arrest, which explains why polycarpic plants can produce inflorescences that senesce while other tissues are unaffected.

AHL15 as a regulator of vegetative development

Recently, the AT-HOOK MOTIF NUCLEAR LOCALIZED (AHL) family protein AHL15 was shown to negatively regulate various longevity phenotypes (Karami et al., 2020; Rahimi et al., 2022a; Rahimi et al., 2022b). The *AHL* gene family is conserved in all land plants and contains 29 members in Arabidopsis (Zhao et al., 2014). Knockout mutants of *ahl15* and other single *ahl* mutants show few or mild developmental- or other phenotypic defects, indicating that these genes act redundantly (Zhao et al., 2013; Karami et al., 2020). Knowledge on AHL function is therefore based initially on the comparison of mutants that overexpress *AHL* genes to wild-type plants.

AHL15 and several closely related *AHLs* have been shown to delay several developmental processes when overexpressed. For example, overexpression of *AHL22, AHL27* or *AHL29* inhibits hypocotyl elongation (Street et al., 2008; Xiao et al., 2009; Zhou et al., 2013; Favero et al., 2016), *AHL15* overexpression delays VPC (Rahimi et al., 2022a), and several *AHL* genes delay flowering when overexpressed (Lim et al., 2007b; Street et al., 2008; Yun et al., 2012; Karami et al., 2020; Tayengwa et al., 2020). Leaf senescence can be delayed by overexpression of *AHL27* (Lim et al., 2007b) and *AHL15* (this thesis). Finally, *AHL15* overexpressing plants show a delayed proliferative arrest and whole-plant senescence, indicating that this gene may be involved in regulating life history strategy (Karami et al., 2020).

AHL15 and developmental phase transitions

AHL15 is expressed abundantly in the early embryo, the seed, and juvenile plants, and as the plant matures its expression is gradually limited to the AMs in the rosette and on the inflorescence (Zhao et al., 2013; Karami et al., 2020). This expression indicates that AHL15's primary function is in embryonic and juvenile development. The phenotypes caused by *AHL15* overexpression also suggest that AHL15 represses ageing and the transition to an adult state: Overexpression of *AHL15* in immature zygotic embryos results in the formation of somatic embryos (Karami et al., 2021), and *AHL15* overexpression was shown to delay the VPC by indirectly repressing several *SPL* genes independent of *miR156* (Rahimi et al., 2022a). Expression of *AHL15* in the IM results in leafy inflorescences with ARs (Karami et al., 2020; Rahimi et al., 2022a), and induction of a fusion protein of AHL15 and the glucocorticoid receptor (AHL15-GR) in inflorescences by dexamethasone treatment causes a similar phenotype (Karami et al., 2020). It was shown that *AHL15* expression in the AMs is repressed by SOC1 and FUL and that the AR phenotype of the *soc1 ful* double mutant is alleviated when crossed with *ahl15*, indicating that AHL15 is involved in repressing the reproductive state of inflorescence AMs (Karami et al., 2020). Finally, the inflorescence stems of *soc1 ful* and *AHL15* overexpressing plants show increased radial growth and enhanced xylem production, whereas *ahl15* loss-of-function results in a relative reduction of this trait in both wild-type and *soc1 ful* mutant background, again indicating that AHL15 acts antagonistically to SOC1 and FUL (Rahimi et al., 2022b). Taken together, these phenotypes show that AHL15 acts as a positive regulator of vegetative growth in several developmental stages, but its precise targets and mode of action remain unknown.

Molecular mechanism of AHL proteins

Like all AHL proteins, AHL15 contains two characteristic domains: the AT-hook domain that can bind the minor groove of AT-rich DNA, and the Plant-Prokaryote Conserved (PPC) domain that facilitates protein-protein interactions (Zhao et al., 2013; Zhao et al., 2014). Within the *AHL* gene family, two types of AT-hook domains (type I and II) and two types of PPC domains (type A and B) have evolved (Zhao et al., 2014). The AHL family can be divided into two subclades based on the type and number of AT-hook and PPC domains: clade A AHL proteins contain one type-I AT-hook as well as a type-A PPC domain, whereas clade B AHLs contain a type-B PPC domain and one type-II AT-hook that is sometimes

accompanied by a type-I AT-hook (Zhao et al., 2014). Clade-A AHLs have been shown to aggregate into complexes of dimers and trimers with themselves and with other AHL proteins (Zhao et al., 2013). Generally, members of clade A have been studied in more detail than clade B AHLs, although in recent years increasing attention has been dedicated to clade B AHLs.

The discovery of mutant alleles with structural modifications in the AT-hook and PPC domains has helped to understand the function of AHL proteins. Mutations in either of the two characteristic AHL domains can give rise to dominant-negative alleles. These are mutations that alter the protein structure resulting in stronger phenotypic changes than loss-of-function mutations where the gene is no longer expressed (Zhao et al., 2013; Karami et al., 2020). Mutation or removal of the AT-hook domain causes a loss of DNA binding ability, as was seen when a spontaneous mutation in the activation-tagged *AHL29* gene resulted in dominant-negative phenotypes in Arabidopsis (Street et al., 2008). This dominant-negative *ahl29* mutant lacked a functional AT-hook domain and produced longer hypocotyls than both wild type and *ahl29* loss-of-function mutants. A similar mutant lacking the core of the PPC domain also showed a dominant-negative phenotype, indicating that both domains are crucial for AHLs to function properly (Zhao et al., 2013).

Interaction with both AHL and non-AHL proteins is facilitated by the PPC domain. Yeast-2-Hybrid (Y2H) experiments have shown that AHLs can dimerize via their PPC domain, and it is thought that AHLs bind DNA as multimers (Zhao et al., 2013; Seo and Lee, 2021). Within the PPC domain, a conserved GRFEIL motif called the G motif is crucial for the interaction with non-AHL proteins and for transcriptional activation by AHLs, and deletion of this motif also causes dominant-negative phenotypes (Zhao et al., 2013; Karami et al., 2020). One such dominant-negative mutant that lacks the G motif is the *ahl15ΔG* mutant described by Karami et al. (2020), where introgression of an allele with a mutated G-motif into a heterozygous background (*ahl15-/+*) causes dominant-negative phenotypes similar to the removal of the AT-hook domain in *ahl29* (Figure 5). A similar effect was obtained by fusion of the large reporter protein GUS to AHL15, indicating that the fused GUS protein interfered with the PPC domain. This loss of the G-motif had such a strong impact on AHL15 functioning that plants carrying this allele were only viable if at least a single copy of the wild-type *AHL15* allele was present, showing that dominant-negative mutations can have severe phenotypic effects and highlighting the importance of AHLs during embryogenesis.

Although both types of dominant-negative alleles cause strong phenotypic

defects, they appear to cause these defects in different ways. Mutation or removal of the AT-hook domain prevents the resulting protein from binding DNA, but not from interacting with other proteins, and may act in a dominant-negative manner by reducing the DNA-binding ability of the AHL complex it is incorporated into (Zhao et al., 2013). On the other hand, deletion of the G motif might reduce transcriptional activation by AHLs by inhibiting interaction of the AHL with non-AHL proteins such as TFs or chromatin remodellers (Zhao et al., 2013). This impaired interaction likely reduces access to the DNA for these interactors, causing changes in transcriptional regulation. Thus, both types of mutations prevent the proper functioning of the AHL complex, but the nature of this disruption differs between the two types of mutant alleles.

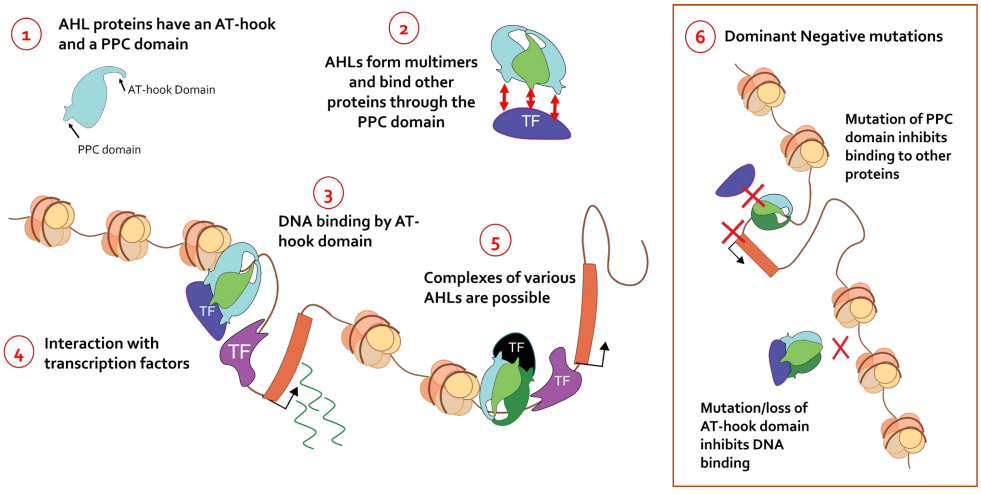

Figure 5: Overview of AT-HOOK MOTIF NUCLEAR LOCALISED (AHL) protein function. AHL proteins have two functional domains: the DNA-binding AT-hook domain and the PPC protein-interaction domain (**1**). AHLs can form multimers comprised of different AHL types (indicated in green and blue) and interact with other classes of proteins, such as TFs, via the PPC domain (**2**). AHL complexes bind the minor groove of AT-rich DNA via their AT-hook domains (**3**).
AHLs can form (heterotrimeric) complexes with other AHL proteins, and the interaction with other proteins might depend on the composition of the AHL complex (different types of TFs are colored dark blue, purple, or black). AHL-TF complexes can either promote transcription (**4;** arrow indicates transcription start site and wavy lines represent RNA transcripts) or repress transcription (**5**), depending on the composition of the complex. Finally, mutating either the AT-hook or PPC domain can result in dominant-negative effects (**6**). Without an AT-hook domain, AHLs lose the ability to bind DNA, whereas disruption of the PPC domain by mutation or by fusion with a large protein like GUS interferes with their ability to interact with other proteins. Both situations are likely to reduce the ability of the complex to regulate transcription, resulting in an altered transcription of AHL-bound genes.

Several studies have investigated the proteins with which AHLs can interact. Y2H and co-immunoprecipitation followed by mass spectrometry (coIP-MS) experiments using AHLs as bait have consistently identified a range of other AHL proteins as interactors, but other types of proteins have also been found. Among these, TFs of the TCP (TEOSINTE BRANCHED 1, CYCLOIDEA, PROLIFERATING CELL FACTOR) family have been identified in Y2H (Zhao et al., 2013; Yin et al., 2018), but most interactors are non-TF nuclear proteins. Interestingly, multiple studies have shown that AHLs can interact with proteins that form part of chromatin remodelling complexes. For example, Lee and Seo (2017) showed that AHL29 interacts with Actin-related Protein 4 (ARP4), a protein in the SWI2/SNF2-RELATED 1 (SWR1) complex that facilitates exchange of HISTONE 2A (H2A) for its variant H2A.Z, and that AHL29 recruits this complex to the *YUCCA9* (*YUC9*) locus, thereby repressing *YUC9* expression (Lee and Seo, 2017). Xu et al. (2013) showed that AHL16 is involved in silencing transposable elements (TEs) by interacting with MULTICOPY SUPPRESSOR OF IRA1 4 (MSI4) and MSI5, both of which are subunits of a complex that mediates HISTONE 3 (H3) deacetylation (Xu et al., 2013). AHL22 interacts with multiple HISTONE DEACETYLASE (HDA) proteins (Yun et al., 2012), and it was recently shown that it also interacts with the transcriptional repressors FAR1-RELATED SEQUENCE (FRS) 6 and 12 at matrix attachment regions (MARs) that anchor the DNA to the nuclear matrix (Xu et al., 2024). It was shown that the presence of a MAR in the *ETTIN/ARF3* locus was required for its silencing by AHL21, and that AHL29 promotes H3K9me2 deposition at this locus (Ng et al., 2009). H3K9me2 is a repressive chromatin modification that is involved in, among others, heterochromatin silencing (Xu and Jiang, 2020). Multiple chromatin immunoprecipitation (ChIP) experiments have shown that *AHL* overexpression can lead to increased levels of the repressive mark H3K9me2 and depletion of the permissive mark H3Ac, implying that AHLs are involved primarily in depositing modifications that are considered as silencing marks (Ng et al., 2009; Yun et al., 2012; Xu et al., 2013; Xiong et al., 2020). In addition to the evidence showing that AHLs are directly involved in silencing TEs, *FT, YUC9,* and *ETTIN,* RNA-seq data also show that the majority of differentially expressed genes in *AHL* overexpressing lines are downregulated (Favero et al., 2020; Karami et al., 2022, this thesis), further supporting the notion that AHLs play a role in supressing gene expression. Considering that various AHL interactors are subunits of chromatin remodelling complexes, it is most likely that AHLs affect gene expression by recruiting or facilitating the activity of chromatin remodelling complexes that remove the active mark H3Ac and promote the

deposition of repressive marks, especially H3K9me2. However, the precise role that AHL proteins play in this process remains to be investigated.

Thesis outline

This thesis focuses on the effects of AHL15 on various aspects of plant longevity. In **chapter 2**, we investigated the natural variation in life history strategy in the monocarpic plant Arabidopsis using AR formation as longevity phenotype, and show that profound differences in life history strategy are tightly linked to the expression of the floral repressor *FLC*. We also show that the expression of the floral integrator *SOC1* is negatively correlated with the AR phenotype. Expression of *AHL20*, a closely related homolog of *AHL15,* also correlated with the AR phenotype, indicating that this gene may play a role similar to AHL15 in polycarpy. Silencing of *FLC* by vernalization removed the AR phenotype, indicating that *FLC* acts upstream of all other genes tested in this chapter.

The longevity of leaves can be determined by measuring their Chl content. In order to measure leaf Chl content in a rapid and non-destructive manner, we developed an ImageJ plugin to quantify Chl based on digital images. This plugin, which is described in **chapter 3**, provides a non-invasive method to measure leaf Chl content and can be applied in a high-throughput, low-tech and low-cost experimental setup, e.g. for senescence measurements but also for other applications in which Chl content is a relevant parameter.

In **chapter 4**, we show that the longevity in Arabidopsis leaves can be significantly extended by overexpressing *AHL15.* We show that the expression of several senescence marker genes and the genes encoding the cytokinin-degrading CKX2, CKX3 and CKX5 enzymes is upregulated in dark-incubated detached leaves, but that their expression is delayed or inhibited upon activation of AHL15 in these leaves. Together, these data show that the delayed senescence phenotype seen in *AHL15* overexpressing plants relies on a reduced degradation of the phytohormone cytokinin.

In **chapter 5**, we dive into the molecular mechanism of AHL15 and describe its DNA binding sites and its effect on DNA structure and transcription in order to better understand how it can induce such dramatic changes in plant development. We show that AHL15 has profound effects on transcription and development when activated in seedlings, but that these changes do not rely on changes in chromatin accessibility. Our results indicate that AHL15 binding is enhanced near their transcription start- and end sites of genes that are differentially expressed upon AHL15 induction, and that AHL15 binding near the transcription start site is strongest near upregulated genes, whereas AHL15

binding to the transcription end site is strongest for downregulated genes. In addition, we compared the genome-wide binding sites of AHL15 to those of various epigenetic marks, and show that they do not coincide at the same location and that AHL15 is found predominantly at the borders of regions marked by epigenetic modifications. Finally, we show that AHL15 binds similar target regions as the AT-hook containing HMGA-family protein GH1-HMGA2/HON5, which suggests that AHL15 could have a similar function as this protein in regulating gene loop formation.

Literature

Abbas M., Alabadí D., Blázquez M.A. (2013). Differential growth at the apical hook: All roads lead to auxin. Front Plant Sci **4**: 64424.

Abe M., Kobayashi Y., Yamamoto S., Daimon Y., Yamaguchi A., Ikeda Y., Ichinoki H., Notaguchi M., Goto K., Araki T. (2005). FD, a bZIP protein mediating signals from the floral pathway integrator FT at the shoot apex. Science (1979) **309**: 1052–1056.

Alejandra Mandel M., Gustafson-Brown C., Savidge B., Yanofsky M.F. (1992). Molecular characterization of the Arabidopsis floral homeotic gene *APETALA1*. Nature **360**: 273–277.

Alonso J.M., Hirayama T., Roman G., Nourizadeh S., Ecker J.R. (1999). EIN2, a bifunctional transducer of ethylene and stress responses in Arabidopsis. Science (1979) **284**: 2148–2152.

Alvarez J., Guli C.L., Yu X. H., Smyth D.R. (1992). terminal flower: a gene affecting inflorescence development in *Arabidopsis thaliana*. Plant J **2**: 103–116.

An H., Roussot C., Suárez-López P., Corbesier L., Vincent C., Piñeiro M., Hepworth S., Mouradov A., Justin S., Turnbull C., et al (2004). CONSTANS acts in the phloem to regulate a systemic signal that induces photoperiodic flowering of Arabidopsis. Development **131**: 3615–3626.

Angel A., Song J., Dean C., Howard M. (2011). A Polycomb-based switch underlying quantitative epigenetic memory. Nature **476**: 105–108.

Azpeitia E., Tichtinsky G., Le Masson M., Serrano-Mislata A., Lucas J., Gregis V., Gimenez C., Prunet N., Farcot E., Kater M.M., et al (2021). Cauliflower fractal forms arise from perturbations of floral gene networks. Science (1979). doi: 10.1126/science.abg5999

Balanzà V., Martínez-Fernández I., Ferrándiz C. (2014). Sequential action of FRUITFULL as a modulator of the activity of the floral regulators SVP and SOC1. J EXP BOT **65**: 1193–1203.

Balanzà V., Martínez-Fernández I., Sato S., Yanofsky M.F., Ferrándiz C. (2019). Inflorescence Meristem Fate Is Dependent on Seed Development and FRUITFULL in *Arabidopsis thaliana*. Front Plant Sci **10**: 1622.

Balanzà V., Martínez-Fernández I., Sato S., Yanofsky M.F., Kaufmann K., Angenent G.C., Bemer M., Ferrándiz C. (2018). Genetic control of meristem arrest and life span in Arabidopsis by a FRUITFULL-APETALA2 pathway. Nat Commun **9**: 565.

Balazadeh S., Siddiqui H., Allu A.D., Matallana-Ramirez L.P., Caldana C., Mehrnia M., Zanor M.I., Köhler B., Mueller-Roeber B. (2010). A gene regulatory network controlled by the NAC transcription factor ANAC092/AtNAC2/ORE1 during salt-promoted senescence. Plant J **62**: 250–264.

Beeckman T., De Smet I. (2014). Pericycle. Curr Biol **24**: R378–R379.

Bemer M., Van Mourik H., Muiño J.M., Ferrándiz C., Kaufmann K., Angenent

G.C. (2017). FRUITFULL controls *SAUR10* expression and regulates Arabidopsis growth and architecture. J EXP BOT **68**: 3391.

Besnard F., Refahi Y., Morin V., Marteaux B., Brunoud G., Chambrier P., Rozier F., Mirabet V., Legrand J., Lainé S., et al (2013). Cytokinin signalling inhibitory fields provide robustness to phyllotaxis. Nature **505**: 417–421.

Besnard F., Rozier F., Vernoux T. (2014). The AHP6 cytokinin signaling inhibitor mediates an auxin-cytokinin crosstalk that regulates the timing of organ initiation at the shoot apical meristem. Plant Signal Behav **9**: e28788.

Bowman J.L., Alvarez J., Weigel D., Meyerowitz E.M., Smyth D.R. (1993). Control of flower development in *Arabidopsis thaliana* by APETALA1 and interacting genes. Development **119**: 721–743.

Boyes D.C., Zayed A.M., Ascenzi R., Mccaskill A.J., Hoffman N.E., Davis K.R., Görlach J. (2001). Growth stage-based phenotypic analysis of Arabidopsis: A model for high throughput functional genomics in plants. Plant Cell **13**: 1499–1510.

Bresson J., Bieker S., Riester L., Doll J., Zentgraf U. (2018). A guideline for leaf senescence analyses: from quantification to physiological and molecular investigations. J EXP BOT **69**: 769–786.

Cheng Y.J., Shang G.D., Xu Z.G., Yu S., Wu L.Y., Zhai D., Tian S.L., Gao J., Wang L., Wang J.W. (2021). Cell division in the shoot apical meristem is a trigger for miR156 decline and vegetative phase transition in Arabidopsis. PNAS **118**: e2115667118.

Deng W., Ying H., Helliwell C.A., Taylor J.M., Peacock W.J., Dennis E.S. (2011). FLOWERING LOCUS C (FLC) regulates development pathways throughout the life cycle of Arabidopsis. PNAS **108**: 6680–6685.

Doody E., Zha Y., He J., Poethig S. (2022). The genetic basis of natural variation in the timing of vegetative phase change *in Arabidopsis thaliana*. Development **149**: dev200321.

Dorca-Fornell C., Gregis V., Grandi V., Coupland G., Colombo L., Kater M.M. (2011). The Arabidopsis *SOC1*-like genes *AGL42, AGL71* and *AGL72* promote flowering in the shoot apical and axillary meristems. Plant J **67**: 1006–1017.

Duncan S., Holm S., Questa J., Irwin J., Grant A., Dean C. (2015). Seasonal shift in timing of vernalization as an adaptation to extreme winter. Elife **4**: e06620.

Favero D.S., Jacques C.N., Iwase A., Le K.N., Zhao J., Sugimoto K., Neff M.M. (2016). Suppressor Of phytochrome B4-#3 represses genes associated with auxin signaling to modulate hypocotyl growth. Plant Physiol **171**: 2701–2716.

Favero D.S., Kawamura A., Shibata M., Takebayashi A., Jung J.H., Suzuki T., Jaeger K.E., Ishida T., Iwase A., Wigge P.A., et al (2020). AT-Hook transcription factors restrict petiole growth by antagonizing PIFs. Curr Biol **30**: 1454–1466.

Fichtner F., Barbier F.F., Annunziata M.G., Feil R., Olas J.J., Mueller-Roeber B.,

Stitt M., Beveridge C.A., Lunn J.E. (2021). Regulation of shoot branching in Arabidopsis by trehalose 6-phosphate. New Phytol **229**: 2135–2151.

Galvan-Ampudia C.S., Cerutti G., Legrand J., Brunoud G., Martin-Arevalillo R., Azais R., Bayle V., Moussu S., Wenzl C., Jaillais Y., et al (2020). Temporal integration of auxin information for the regulation of patterning. Elife **9**: 1–65.

Giulini A., Wang J., Jackson D. (2004). Control of phyllotaxy by the cytokinin-inducible response regulator homologue ABPHYL1. Nature **430**: 1031–1034.

Glover J.D., Reganold J.P., Bell L.W., Borevitz J., Brummer E.C., Buckler E.S., Cox C.M., Cox T.S., Crews T.E., Culman S.W., et al (2010). Increased Food and Ecosystem Security via Perennial Grains. Science (1979) **328**: 1638–1640.

Guo Y., Gan S. (2005). Leaf Senescence: Signals, Execution, and Regulation. Curr Top Dev Biol **71**: 83–112.

Guo Y., Ren G., Zhang K., Li Z., Miao Y., Guo H. (2021). Leaf senescence: progression, regulation, and application. Mol Hortic **1**: 1–25.

Harder L.D., Prusinkiewicz P. (2013). The interplay between inflorescence development and function as the crucible of architectural diversity. Ann Bot **112**: 1477–1493.

Heisler M.G., Hamant O., Krupinski P., Uyttewaal M., Ohno C., Jönsson H., Traas J., Meyerowitz E.M. (2010). Alignment between PIN1 polarity and microtubule orientation in the shoot apical meristem reveals a tight coupling between morphogenesis and auxin transport. PLOS Biol **8**: e1000516.

Hensel L.L., Nelson M.A., Richmond T.A., Bleecker A.B. (1994). The fate of inflorescence meristems is controlled by developing fruits in Arabidopsis. Plant Physiol **106**: 863–876.

Hörtensteiner S., Kräutler B. (2011). Chlorophyll breakdown in higher plants. BBA **1807**: 977–988.

Hu X., Kong X., Wang C., Ma L., Zhao J., Wei J., Zhang X., Loake G.J., Zhang T., Huang J., et al (2014). Proteasome-Mediated Degradation of FRIGIDA Modulates Flowering Time in Arabidopsis during Vernalization. Plant Cell **26**: 4763–4781.

Hu Y., Liu B., Ren H., Chen L., Watkins C.B., Gan S.S. (2021). The leaf senescence-promoting transcription factor AtNAP activates its direct target gene *CYTOKININ OXIDASE 3* to facilitate senescence processes by degrading cytokinins. Mol Hortic **1**: 1–12.

Huijser P., Schmid M. (2011). The control of developmental phase transitions in plants. Development **138**: 4117–4129.

Hyun Y., Richter R., Coupland G. (2017). Competence to Flower: Age-Controlled Sensitivity to Environmental Cues. Plant Physiol **173**: 36–46.

Hyun Y., Richter R., Vincent C., Martinez-Gallegos R., Porri A., Coupland G. (2016). Multi-layered regulation of SPL15 and cooperation with SOC1 integrate

endogenous flowering pathways at the Arabidopsis shoot meristem. Dev Cell **37**: 254–266.

Hyun Y., Vincent C., Tilmes V., Bergonzi S., Kiefer C., Richter R., Martinez-Gallegos R., Severing E., Coupland G. (2019). A regulatory circuit conferring varied flowering response to cold in annual and perennial plants. Science (1979) **363**: 409–412.

Iwasaki M., Penfield S., Lopez-Molina L. (2022). Parental and Environmental Control of Seed Dormancy in *Arabidopsis thaliana*. Annu Rev Plant Biol **73**: 355–378.

Jin R., Klasfeld S., Zhu Y., Garcia M.F., Xiao J., Han S.-K., Konkol A., Wagner D. (2021). LEAFY is a pioneer transcription factor and licenses cell reprogramming to floral fate. Nat Commun **12**: 1–14.

Jing H.C., Schippers J.H.M., Hille J., Dijkwel P.P. (2005). Ethylene-induced leaf senescence depends on age-related changes and OLD genes in Arabidopsis. J EXP BOT **56**: 2915–2923.

Johanson U., West J., Lister C., Michaels S., Amasino R., Dean C. (2000). Molecular analysis of *FRIGIDA*, a major determinant of natural variation in Arabidopsis flowering time. Science (1979) **290**: 344–347.

Jordi W., Schapendonk A., Davelaar E., Stoopen G.M., Pot C.S., De Visser R., Van Rhijn J.A., Gan S., Amasino R.M. (2000). Increased cytokinin levels in transgenic *PSAG12–IPT* tobacco plants have large direct and indirect effects on leaf senescence, photosynthesis and N partitioning. Plant Cell Environ **23**: 279–289.

Jukanti A.K., Fischer A.M. (2008). A high-grain protein content locus on barley (Hordeum vulgare) chromosome 6 is associated with increased flag leaf proteolysis and nitrogen remobilization. Physiol Plant **132**: 426–439.

Karami O., Henkel C., Offringa R. (2022). The effect of short-term activation of AHL15 on long-term plant developmental change and transcriptome profile. bioRxiv 2022.09.05.506087.

Karami O., Rahimi A., Khan M., Bemer M., Hazarika R.R., Mak P., Compier M., van Noort V., Offringa R. (2020). A suppressor of axillary meristem maturation promotes longevity in flowering plants. Nat Plants **6**: 368–376.

Karami O., Rahimi A., Mak P., Horstman A., Boutilier K., Compier M., van der Zaal B., Offringa R. (2021). An Arabidopsis AT-hook motif nuclear protein mediates somatic embryogenesis and coinciding genome duplication. Nat Commun **12**: 2508.

Kiefer C., Bergonzi S., Brand L., Wötzel S., Koch M.A. (2019). Contrasting life history traits in monocarpic versus polycarpic plants from a molecular-evolutionary point of view. Annu Plant Rev **2**: 479–504.

Kiefer C., Severing E., Karl R., Bergonzi S., Koch M., Tresch A., Coupland G. (2017). Divergence of annual and perennial species in the *Brassicaceae* and the contribution of cis-acting variation at *FLC* orthologues. Mol Ecol **26**: 3437–3457.

Kim H.J., Ryu H., Hong S.H., Woo H.R., Lim P.O., Lee I.C., Sheen J., Nam H.G., Hwang I. (2006). Cytokinin-mediated control of leaf longevity by AHK3 through phosphorylation of ARR2 in Arabidopsis. PNAS **103**: 814–819.

Kim J.H., Woo H.R., Kim J., Lim P.O., Lee In Chul, Choi S.H., Hwang D., Hong G.N. (2009). Trifurcate feed-forward regulation of age-dependent cell death involving miR164 in Arabidopsis. Science (1979) **323**: 1053–1057.

Kinoshita A., Richter R. (2020). Genetic and molecular basis of floral induction in *Arabidopsis thaliana*. J EXP BOT **71**: 2490–2504.

Krahmer J., Fankhauser C. (2024). Environmental control of hypocotyl elongation. Annu Rev Plant Biol **75**: 489–519.

Kuhlemeier C. (2017). Phyllotaxis. Curr Biol **27**: 882–887.

Kurokura T., Mimida N., Battey N.H., Hytönen T. (2013). The regulation of seasonal flowering in the *Rosaceae*. J EXP BOT **64**: 4131–4141.

Lazaro A., Obeng-Hinneh E., Albani M.C. (2018). Extended vernalization regulates inflorescence fate in *Arabis alpina* by stably silencing *PERPETUAL FLOWERING*. Plant Physiol **176**: 2819–2883.

Lazaro A., Zhou Y., Giesguth M., Nawaz K., Bergonzi S., Pecinka A., Coupland G., Albani M.C. (2019). PERPETUAL FLOWERING2 coordinates the vernalization response and perennial flowering in *Arabis alpina*. J EXP BOT **70**: 949–961.

Lee K., Seo P.J. (2017). Coordination of matrix attachment and ATP-dependent chromatin remodeling regulate auxin biosynthesis and Arabidopsis hypocotyl elongation. PLoS One **12**: 1–19.

Leibfried A., To J.P.C., Busch W., Stehling S., Kehle A., Demar M., Kieber J.J., Lohmann J.U. (2005). WUSCHEL controls meristem function by direct regulation of cytokinin-inducible response regulators. Nature **438**: 1172–1175.

Li Z., Peng J., Wen X., Guo H. (2013). *ETHYLENE-INSENSITIVE3* Is a Senescence-Associated Gene That Accelerates Age-Dependent Leaf Senescence by Directly Repressing miR164 Transcription in Arabidopsis. Plant Cell **25**: 3311.

Lifschitz E., Eshed Y. (2006). Universal florigenic signals triggered by FT homologues regulate growth and flowering cycles in perennial day-neutral tomato. J EXP BOT **57**: 3405–3414.

Lim P.O., Kim H.J., Nam H.G. (2007a). Leaf Senescence. Annu Rev Plant Biol **58**: 115–136.

Lim P.O., Kim Y., Breeze E., Koo J.C., Woo H.R., Ryu J.S., Park D.H., Beynon J., Tabrett A., Buchanan-Wollaston V., et al (2007b). Overexpression of a chromatin architecture-controlling AT-hook protein extends leaf longevity and increases the post-harvest storage life of plants. Plant J **52**: 1140–1153.

Liu C., Wei Z., Teo N., Bi Y., Song S., Xi W., Yang X., Yin Z., Yu H. (2013). A Conserved Genetic Pathway Determines Inflorescence Architecture in Arabidopsis and Rice. Dev Cell **24**: 612–622.

De Lucia F., Crevillen P., Jones A.M.E., Greb T., Dean C. (2008). A PHD-polycomb repressive complex 2 triggers the epigenetic silencing of *FLC* during vernalization. PNAS **105**: 16831–16836.

Maple R., Zhu P., Hepworth J., Wang J.-W., Dean C. (2024). Flowering time: From physiology, through genetics to mechanism. Plant Physiol **195**: 190–202.

Martínez-Fernández I., de Moura S.M., Alves-Ferreira M., Ferrándiz C., Balanzà V. (2020). Identification of players controlling meristem arrest downstream of the FRUITFULL-APETALA2 pathway. Plant Physiol **184**: 945–959.

McCabe M.S., Garratt L.C., Schepers F., Jordi W.J.R.M., Stoopen G.M., Davelaar E., Van Rhijn J.H.A., Power J.B., Davey M.R. (2001). Effects of PSAG12-IPT gene expression on development and senescence in transgenic lettuce. Plant Physiol **127**: 505–516.

Melzer S., Lens F., Gennen J., Vanneste S., Rohde A., Beeckman T. (2008). Flowering-time genes modulate meristem determinacy and growth form in *Arabidopsis thaliana*. Nat Genet **40**: 1489–1492.

Merelo P., González-Cuadra I., Ferrándiz C. (2022). A cellular analysis of meristem activity at the end of flowering points to cytokinin as a major regulator of proliferative arrest in Arabidopsis. Curr Biol **32**: 749-762.e3.

Michaels S.D., Amasino R.M. (1999). *FLOWERING LOCUS C* encodes a novel MADS domain protein that acts as a repressor of flowering. Plant Cell **11**: 949–956.

Ng K.H., Yu H., Ito T. (2009). AGAMOUS controls GIANT KILLER, a multifunctional chromatin modifier in reproductive organ patterning and differentiation. PLoS Biol **7**: e1000251.

Okada K., Ueda J., Komaki M.K., Bell C.J., Shimura Y. (1991). Requirement of the auxin polar transport system in early stages of Arabidopsis floral bud formation. Plant Cell **3**: 677–684.

Poethig R.S. (2013). Vegetative phase change and shoot maturation in plants. Curr Top Dev Biol **105**: 125–152.

Poethig R.S., Fouracre J. (2024). Temporal regulation of vegetative phase change in plants. Dev Cell **59**: 4–19.

Ponraj U., Theres K. (2020). Keep a distance to be different: axillary buds initiating at a distance from the shoot apical meristem are crucial for the perennial lifestyle of *Arabis alpina*. New Phytol **227**: 116–131.

Prusinkiewicz P., Erasmus Y., Lane B., Harder L.D., Coen E. (2007). Evolution and development of inflorescence architectures. Science (1979) **316**: 1452–1456.

Qiu K., Li Z., Yang Z., Chen J., Wu S., Zhu X., Gao S., Gao J., Ren G., Kuai B., et al (2015). EIN3 and ORE1 Accelerate Degreening during Ethylene-Mediated Leaf Senescence by Directly Activating Chlorophyll Catabolic Genes in Arabidopsis. PLoS Genet **11**: e1005399.

Rahimi A., Karami O., Balazadeh S., Offringa R. (2022a). miR156 -independent repression of the ageing pathway by longevity-promoting AHL proteins in

Arabidopsis. New Phytol **235**: 2424–2438.

Rahimi A., Karami O., Lestari A.D., de Werk T., Amakorová P., Shi D., Novák O., Greb T., Offringa R. (2022b). Control of cambium initiation and activity in Arabidopsis by the transcriptional regulator AHL15. Curr Biol **32**: 1764–1775.

Ratcliffe O.J., Bradley D.J., Coen E.S. (1999). Separation of shoot and floral identity in Arabidopsis. Development **126**: 1109–1120.

Reinhardt D., Mandel T., Kuhlemeier C. (2000). Auxin regulates the initiation and radial position of plant lateral organs. Plant Cell **12**: 507–518.

Reinhardt D., Pesce E.R., Stieger P., Mandel T., Baltensperger K., Bennett M., Traas J., Friml J., Kuhlemeier C. (2003). Regulation of phyllotaxis by polar auxin transport. Nature **426**: 255–260.

Schiessl S. V., Quezada-Martinez D., Tebartz E., Snowdon R.J., Qian L. (2019). The vernalisation regulator *FLOWERING LOCUS C* is differentially expressed in biennial and annual *Brassica napus*. Sci Rep **9**: 1–15.

Schippers J.H.M., Schmidt R., Wagstaff C., Jing H.C. (2015). Living to die and dying to live: The survival strategy behind leaf senescence. Plant Physiol **169**: 914–930.

Schultz E.A., Haughn G.W. (1991). LEAFY, a homeotic gene that regulates inflorescence fevelopment in Arabidopsis. Plant Cell **3**: 771.

Seo M., Lee J.-Y. (2021). Dissection of Functional Modules of AT-HOOK MOTIF NUCLEAR LOCALIZED PROTEIN 4 in the Development of the Root Xylem. Front Plant Sci **12**: 632078.

SharathKumar M., Heuvelink E., Marcelis L.F.M., van Ieperen W. (2021). Floral Induction in the Short-Day Plant Chrysanthemum Under Blue and Red Extended Long-Days. Front Plant Sci. doi: 10.3389/fpls.2020.610041

Shindo C., Lister C., Crevillen P., Nordborg M., Dean C. (2006). Variation in the epigenetic silencing of *FLC* contributes to natural variation in Arabidopsis vernalization response. Genes Dev **20**: 3079–3083.

Simcha L.Y. (2017). How monocarpic is Agave? Flora **230**: 12–13.

Song Y., Yang C., Gao S., Zhang W., Li L., Kuai B. (2014). Age-Triggered and Dark-Induced Leaf Senescence Require the bHLH Transcription Factors PIF3, 4, and 5. Mol Plant **7**: 1776–1787.

Spaninks K., van Lieshout J., van Ieperen W., Offringa R. (2020). Regulation of Early Plant Development by Red and Blue Light: A Comparative Analysis Between *Arabidopsis thaliana* and *Solanum lycopersicum*. Front Plant Sci **11**: 2109.

Street I.H., Shah P.K., Smith A.M., Avery N., Neff M.M. (2008). The AT-hook-containing proteins SOB3/AHL29 and ESC/AHL27 are negative modulators of hypocotyl growth in Arabidopsis. Plant Journal **54**: 1–14.

Tayengwa R., Sharma Koirala P., Pierce C.F., Werner B.E., Neff M.M. (2020).

Overexpression of AtAHL20 causes delayed flowering in Arabidopsis via repression of FT expression. BMC Plant Biol **20**: 559.

Telfer A., Bollman K.M., Poethig R.S. (1997). Phase change and the regulation of trichome distribution in *Arabidopsis thaliana*. Development **124**: 645–654.

Thomas H. (2013). Senescence, ageing and death of the whole plant. New Phytol **197**: 696–711.

Tian C., Wang Y., Yu H., He J., Wang J., Shi B., Du Q., Provart N.J., Meyerowitz E.M., Jiao Y. (2019). A gene expression map of shoot domains reveals regulatory mechanisms. Nat Commun **10**: 1–12.

Tian C., Zhang X., He J., Yu H., Wang Y., Shi B., Han Y., Wang G., Feng X., Zhang C., et al (2014). An organ boundary-enriched gene regulatory network uncovers regulatory hierarchies underlying axillary meristem initiation. MOL SYST BIOL **10**: 755.

Uauy C., Distelfeld A., Fahima T., Blechl A., Dubcovsky J. (2006). A NAC gene regulating senescence improves grain protein, zinc, and iron content in wheat. Science (1979) **314**: 1298–1301.

Ueda H., Kusaba M. (2015). Strigolactone Regulates Leaf Senescence in Concert with Ethylene in Arabidopsis. Plant Physiol **169**: 138–147.

Valverde F., Mouradov A., Soppe W., Ravenscroft D., Samach A., Coupland G. (2004). Photoreceptor Regulation of CONSTANS Protein in Photoperiodic Flowering. Science (1979) **303**: 1003–1006.

Vandenbussche M., Chambrier P., Rodrigues Bento S., Morel P. (2016). Petunia, Your Next Supermodel? Front Plant Sci **7**: 1–11.

Vayssières A., Mishra P., Roggen A., Neumann U., Ljung K., Albani M.C. (2020). Vernalization shapes shoot architecture and ensures the maintenance of dormant buds in the perennial *Arabis alpina*. New Phytol **227**: 99–115.

Wang J.-W. (2014). Regulation of flowering time by the miR156-mediated age pathway. J EXP BOT **65**: 4723–4730.

Wang J.-W., Czech B., Weigel D. (2009a). miR156-Regulated SPL Transcription Factors Define an Endogenous Flowering Pathway in *Arabidopsis thaliana*. Cell **138**: 738–749.

Wang R., Albani M.C., Vincent C., Bergonzi S., Luan M., Bai Y., Kiefer C., Castillo R., Coupland G. (2011). Aa TFL1 confers an age-dependent response to vernalization in perennial *Arabis alpina*. Plant Cell **23**: 1307–1321.

Wang R., Farrona S., Vincent C., Joecker A., Schoof H., Turck F., Alonso-Blanco C., Coupland G., Albani M.C. (2009b). PEP1 regulates perennial flowering in *Arabis alpina*. Nature **459**: 423–427.

Wang Y., Shirakawa M., Ito T. (2023). Arrest, Senescence and Death of Shoot Apical Stem Cells in *Arabidopsis thaliana*. Plant Cell Phys **64**: 284–290.

Ware A., Walker C.H., Šimura J., González-Suárez P., Ljung K., Bishopp A.,

Wilson Z.A., Bennett T. (2020). Auxin export from proximal fruits drives arrest in temporally competent inflorescences. Nat Plants **6**: 699–707.

Weigel D., Nilsson O. (1995). A developmental switch sufficient for flower initiation in diverse plants. Nature **377**: 495–500.

Woo H.R., Kim H.J., Lim P.O., Nam H.G. (2019). Leaf Senescence: Systems and Dynamics Aspects. Annu Rev Plant Biol **70**: 347–376.

Wu G., Park M.Y., Conway S.R., Wang J.W., Weigel D., Poethig R.S. (2009). The Sequential Action of miR156 and miR172 Regulates Developmental Timing in Arabidopsis. Cell **138**: 750–759.

Xiao C., Chen F., Yu X., Lin C., Fu Y.F. (2009). Over-expression of an AT-hook gene, AHL22, delays flowering and inhibits the elongation of the hypocotyl in Arabidopsis thaliana. Plant Mol Biol **71**: 39–50.

Xiong S.X., Zeng Q.Y., Hou J.Q., Hou L.L., Zhu J., Yang M., Yang Z.N., Lou Y. (2020). The temporal regulation of TEK contributes to pollen wall exine patterning. PLoS Genet **16**: e1008807.

Xu L., Jiang H. (2020). Writing and Reading Histone H3 Lysine 9 Methylation in Arabidopsis. Front Plant Sci. doi: 10.3389/fpls.2020.00452

Xu L., Zheng S., Witzel K., Van De Slijke E., Baekelandt A., Mylle E., Van Damme D., Cheng J., De Jaeger G., Inzé D., et al (2024). Chromatin attachment to the nuclear matrix represses hypocotyl elongation in *Arabidopsis thaliana*. Nat Commun **15**: 1286.

Xu M., Hu T., Zhao J., Park M.-Y., Earley K.W., Wu G., Yang L., Poethig R.S. (2016). Developmental functions of miR156-Regulated SQUAMOSA PROMOTER BINDING PROTEIN-LIKE (SPL) genes in *Arabidopsis thaliana*. PLOS Genet **12**: e1006263.

Xu Y., Wang Y., Stroud H., Gu X., Sun B., Gan E.S., Ng K.H., Jacobsen S.E., He Y., Ito T. (2013). A matrix protein silences transposons and repeats through interaction with retinoblastoma-associated proteins. Curr Biol **23**: 345–350.

Yin D., Liu X., Shi Z., Li D., Zhu L. (2018). An AT-hook protein DEPRESSED PALEA1 physically interacts with the TCP Family transcription factor RETARDED PALEA1 in rice. Biochem Biophys Res Commun **495**: 487–492.

Yin X. (2021). Phyllotaxis: from classical knowledge to molecular genetics. J Plant Res **134**: 373–401.

Yun J., Kim Y.-S., Jung J.-H., Seo P.J., Park C.-M. (2012). The AT-hook Motif-containing Protein AHL22 Regulates Flowering Initiation by Modifying *FLOWERING LOCUS T* Chromatin in Arabidopsis. J Biol Chem **287**: 15307–15316.

Zentgraf U., Jobst J., Kolb D., Rentsch D. (2004). Senescence-related gene expression profiles of rosette leaves of *Arabidopsis thaliana*: Leaf age versus plant age. Plant Biol **6**: 178–183.

Zhai D., Zhang L.-Y., Li L.-Z., Xu Z.-G., Liu X.-L., Shang G.-D., Zhao B., Gao J., Wang F.-X., Wang J.-W. (2024). Reciprocal conversion between annual and

polycarpic perennial flowering behavior in the *Brassicaceae*. Cell **187**: 1–19.

Zhang S., Huang G., Zhang Y., Lv X., Wan K., Liang J., Feng Y., Dao J., Wu S., Zhang L., et al (2023). Sustained productivity and agronomic potential of perennial rice. Nat Sustain **6**: 28–38.

Zhao J., Favero D.S., Peng H., Neff M.M. (2013). *Arabidopsis thaliana* AHL family modulates hypocotyl growth redundantly by interacting with each other via the PPC/DUF296 domain. PNAS **110**: E4688–E4697.

Zhao J., Favero D.S., Qiu J., Roalson E.H., Neff M.M. (2014). Insights into the evolution and diversification of the AT-hook Motif Nuclear Localized gene family in land plants. BMC Plant Biol **14**: 1–19.

Zhou J., Wang X., Lee J.Y., Lee J.Y. (2013). Cell-to-Cell Movement of Two Interacting AT-Hook Factors in Arabidopsis Root Vascular Tissue Patterning. Plant Cell **25**: 187–201.

Zhou M., Yang J. (2023). Delaying or promoting? Manipulation of leaf senescence to improve crop yield and quality. Planta **258**: 1–10.

Zhu Y., Klasfeld S., Jeong C.W., Jin R., Goto K., Yamaguchi N., Wagner D. (2020). TERMINAL FLOWER 1-FD complex target genes and competition with FLOWERING LOCUS T. Nat Commun **11**: 1–12.

Zhu Y., Wagner D. (2020). Plant inflorescence architecture: The formation, activity, and fate of axillary meristems. CSH Perspectives in Biology **12**: a034652.

Zwack P.J., Robinson B.R., Risley M.G., Rashotte A.M. (2013). Cytokinin Response Factor 6 negatively regulates leaf senescence and is induced in response to cytokinin and numerous abiotic stresses. Plant Cell Phys **54**: 971–981.

Chapter 2

Insights into polycarpic plant development through natural variation in the aerial rosette phenotype in *Arabidopsis thaliana*

Thalia Luden[1], Marieke Koekkoek[1], Remko Offringa[1]

[1] Plant Developmental Genetics, Institute of Biology Leiden, Leiden University, Sylviusweg 72, 2333 BE Leiden, the Netherlands

Abstract

The model plant *Arabidopsis thaliana* (Arabidopsis) is considered to be a monocarpic species based on commonly used early flowering ecotypes (e.g. Col-0 and Ler). For these ecotypes flowering is initiated once, followed by seed set, senescence and death of the whole plant. Polycarpic plants, on the other hand, can flower multiple times in their life cycle and maintain vegetative development during and between each flowering event. The precise mechanism with which vegetative development is regulated and restarted in polycarpic plants remains elusive. Investigating polycarpic traits, such as the formation of vegetative aerial rosettes (ARs) from inflorescence axillary meristems in Arabidopsis can improve the understanding of polycarpic development. In this study, we characterized 12 Arabidopsis ecotypes displaying polycarpic features with the formation of ARs as the main indicative phenotype. By comparing the natural variation in expression of genes known to be involved in the AR phenotype to phenotypic data, we showed that expression of *SUPPRESSOR of OVEREXPRESSION of CONSTANS 1* (*SOC1*) and *FLOWERING LOCUS C* (*FLC*) are the strongest predictors of the AR phenotype in Arabidopsis, confirming earlier findings on the role of these genes in the polycarpic life history strategy of *Arabis alpina*. In addition, we show that *AT-HOOK MOTIF NUCLEAR LOCALIZED 20* (*AHL20*) expression correlates with the AR phenotype, indicating its potential role in the polycarpic life history strategy. Finally, we show that *FLC* silencing by vernalization is sufficient to repress AR production, indicating that *FLC* acts upstream of other genes involved in AR production. Together, our data show that variation in gene expression can reliably predict phenotypic variation. This shows that correlating natural variation in polycarpic traits with natural variation in gene expression can help identify new genes involved in polycarpic development.

Keywords: life history strategy, monocarpy, polycarpy, aerial rosettes, natural variation, vernalization, *FLC, SOC1, AHL15, AHL20, SPL15*

Introduction

Flowering plants generally follow one of two life history strategies: monocarpy or polycarpy. The monocarpic life cycle includes only a single flowering period, eventually leading to a general arrest of all vegetative development and to the plant's death following seed set. During monocarpic flowering, the plant's axillary meristems (AMs) either transition to the inflorescence fate or remain dormant (Thomas, 2013). Polycarpic plants, on the other hand, can initiate flowering repeatedly and maintain vegetative development between flowering cycles (Thomas, 2013; Kiefer et al., 2019). This renewed vegetative development requires the maintenance of vegetative meristems during flowering (Amasino, 2009; Vayssières et al., 2020). Monocarps and polycarps thus regulate axillary meristem identity differently, and this difference can be clearly seen when comparing the two *Brassicaceae* species *Arabidopsis thaliana* (Arabidopsis) and *Arabis alpina.* Unlike Arabidopsis, which is considered to be monocarpic, the polycarp *A. alpina* maintains vegetative identity in part of its AMs during flowering (Ponraj and Theres, 2020; Vayssières et al., 2020). The *A. alpina* gene *PERPETUAL FLOWERING 1 (PEP1)* is a homolog of the Arabidopsis gene *FLOWERING LOCUS C (FLC),* and has been identified as a regulator of polycarpy in this species. It was shown that a renewed expression of the floral repressor *PEP1* in *A. alpina* after vernalization is sufficient to maintain a vegetative identity in axillary buds of flowering plants (Kiefer et al., 2017; Hyun et al., 2019; Tilmes et al., 2019). Therefore, FLC/PEP1 is not only important in coordinating the timing of flowering in vernalization-dependent plants, but is also involved in renewing vegetative development in *Brassicaceae* species.

In Arabidopsis, the protein FRIGIDA (FRI) acts upstream of *FLC* to promote its expression. Vernalization results in degradation of FRI and activates several other mechanisms that together cause silencing of *FLC* expression (Hu et al., 2014). The commonly studied ecotypes Col-0 and Ler carry a *fri* loss-of-function allele that causes a permanent loss of *FLC* expression, resulting in rapid flowering cycles. In contrast, most Arabidopsis ecotypes contain a functional *FRI* allele and consequently flower late when not vernalized (Johanson et al., 2000; Zhang and Jiménez-Gómez, 2020). Unlike the temporary silencing of *PEP1* in *A. alpina*, vernalization permanently silences the expression of *FLC* in Arabidopsis and in *A. alpina's* monocarpic relative *Arabis montbretiana* (Kiefer et al., 2017). The phenotype of Arabidopsis ecotype Landsberg erecta (Ler) plants overexpressing *FLC* also illustrates this: in addition to a severely delayed flowering time, these plants also produce rosette leaves from the inflorescence AMs in structures called aerial rosettes (ARs) (Wang et al., 2007).

Together, these data indicate that re-initiation of *FLC* expression in polycarpic plants is a key process allowing renewed vegetative- and therefore polycarpic development.

Since polycarpic species retain vegetative identity in some AMs, studying factors that regulate AM identity can reveal new regulators of polycarpy. Most AMs on the inflorescences of Arabidopsis ecotype Colombia-0 (Col-0) plants develop into a secondary- or tertiary inflorescence branch, indicating that they are in an inflorescence meristem (IM) state. However, some ecotypes and mutants are capable of producing ARs from these AMs, implying a more vegetative state in these AMs. The status of an inflorescence AM can therefore be deduced from the type of tissue it produces, and the production of ARs in Arabidopsis indicates a form of ectopic vegetative development. In addition to *FLC* overexpression, several other mutants with ARs have been identified, which has shed light on other potential regulators of polycarpic development. For example, loss-of-function of both MADS-box genes *SUPPRESSOR of OVEREXPRESSION of CONSTANS 1* (*SOC1*) and *FRUITFULL* (*FUL*) causes delayed flowering and ectopic vegetative growth in the form of ARs (Melzer et al., 2008). Individually, loss-of-function of *soc1* causes a strong delay in flowering time and increased bract formation in inflorescences, whereas the *ful* mutation reduces fruit size and inflorescence determinacy and only shows a mild increase in flowering time (Melzer et al., 2008; Dorca-Fornell et al., 2011; Balanzà et al., 2014). SOC1 and FUL interact *in vivo* to regulate expression of their target genes, and the *soc1 ful* double mutant shows a strongly delayed flowering time, enhanced vegetative growth, longer life span, and multiple flowering cycles, indicating that these genes repress vegetative development and polycarpic growth (Melzer et al., 2008). In addition, knockout of several members of the adult-phase *SQUAMOSA PROMOTER-LIKE (SPL)* transcription factor gene family also delays the juvenile-to-adult transition known as vegetative phase change (VPC) and causes delayed flowering and AR production. This is similar to phenotypes observed in lines overexpressing the juvenile-phase microRNA *miR156* that regulates mRNA abundance of several *SPL* genes (Wu and Poethig, 2006; Schwarz et al., 2008). The similarity in phenotypes between the *soc1 ful*, *spl,* and *p35S:MIR156* mutants can be partially explained by the fact that SOC1 and SPL15 co-regulate the expression of some genes (Hyun et al., 2016). In addition, *SOC1* and *SPL15* are repressed by FLC (Deng et al., 2011), and SPL15 is required for vernalization-induced flowering in *A. alpina*, as only plants that are vernalized after a certain age can initiate flowering when returned to ambient temperatures (Hyun et al., 2019).

Recently, we identified the *AT-HOOK MOTIF NUCLEAR LOCALISED 15 (AHL15)* gene as another key switch between mono- and polycarpic life history strategy in Arabidopsis. Plants overexpressing *AHL15* show a similar AR-producing phenotype as the aforementioned *soc1 ful* or *spl* mutants or the *MIR156* overexpression lines (Karami et al., 2020; Rahimi et al., 2022). Moreover, *ahl15* loss-of-function almost completely abolishes the polycarpic AR-phenotype of the *soc1 ful* mutant, and ChIP-qPCR and EMSA experiments showed that SOC1 and FUL bind regions up- and downstream of the *AHL15* gene (Karami et al., 2020). In addition, we observed reciprocal negative feedback between *AHL15* and *SPL* genes (Rahimi et al., 2022). These results indicate that AHL15 delays AM maturation, thereby maintaining their vegetative state by repressing components of the ageing pathway. However, in wild-type Arabidopsis, *AHL15* expression is repressed by the SOC1/FUL-triggered flowering and SPL-mediated ageing pathways, resulting in a monocarpic life history strategy. Interestingly, *AHL15* and its close homologs *AHL19* and *AHL20* are upregulated after flowering in the polycarpic *Arabidopsis lyrata* but not in Arabidopsis, indicating that these genes could be involved in the polycarpic life history strategy of this species (Karami et al., 2020).

In this study, we identified and analysed 12 Arabidopsis ecotypes that show the AR phenotype and other polycarpic traits, and compared their development to Col-0. All selected ecotypes show delayed flowering, but neither this nor the AR phenotype correlate with a prolonged juvenile phase. We show that FLC is responsible for the AR phenotype of these ecotypes, but is not the sole factor explaining AR production. We provide further evidence that expression of *SOC1* and *SPL15* is negatively correlated to the production of ARs in different genetic backgrounds, and that in addition to *FLC*, expression of the *AHL15* homolog *AHL20* positively correlates with AR production. Moreover, co-expression analyses imply that expression of *FLC* and *AHL15* and of *SOC1* and *AHL20* are linked, which reveals potential new interactions within regulatory pathways. In conclusion, our data shows that variation in gene expression can be reliably linked to variations in polycarpic traits in wild-type Arabidopsis plants.

Results

Phenotypes of AR-producing ecotypes

In this study, we used an unbiased approach to look at which key regulators determine natural variation in polycarpic traits in Arabidopsis, with the AR phenotype as key trait. Because most research on the AR phenotype has been

based either on studying Arabidopsis mutants or on the description of a single ecotype, we set out to study the AR phenotype in non-mutant conditions in a larger set of ecotypes. To do this, we searched for ecotypes producing ARs based on their phenotypic description in the NASC database, and selected twelve ecotypes based on their phenotype and availability. These twelve ecotypes originate from different environments and a large geographical range in terms of latitude and longitude, ensuring diversity in genetic background as well as environmental adaptations (Supplementary figure 1).

To compare the phenotypes of the AR ecotypes in an unbiased manner, we scored a number of polycarpy-related phenotypes at five weeks after bolting for each ecotype. First, the total number of ARs on all inflorescences was counted at five weeks after bolting for each ecotype and compared to the total number of inflorescence AMs (IAMs) to calculate the percentage ARs (Figure 1A, B). The latter number was used to rank the ecotypes according to their AR production phenotype. The ecotypes were left to continue growing in the same climate room for up to six months to monitor the phenotype at later stages (Supplementary figure 2).The percentage of IAMs producing ARs differed strongly between ecotypes, with Es-0 producing ARs in over 40% of the inflorescence AMs, while other ecotypes like Tha-1, Mv-0 and Gifu-2 only produced very few ARs at this time point (Figure 1A, B). The timing of ARs emergence also differed between ecotypes: in some, like Es-0, Kas-2, and Had-1B, ARs could be observed as early as three weeks after bolting, whereas in other ecotypes such as Mv-0 and Gifu-2 no ARs were produced until after the five-week time point (Supplementary figures 2 and 3E-M). During pilot experiments, we observed that the first (lowest) IAM on the primary inflorescence was usually the first to produce an AR, which also developed the most rosette-like leaves of all ARs on the inflorescence. We counted the number of leaves produced from this IAM on the first node (Figure 1C), to test if this could be an early indicator for the overall AR production, as measured by the percentage of IAMs forming ARs (Figure 1A). Although the ranking between the two methods did not match perfectly, Es-0 came out as the ecotype with the strongest AR phenotype in both methods, and ecotypes that produced few ARs (such as Tha-1, Do-0, and Hh-0) still had a higher number of leaves at the first IAM than Col-0 (Figure 1C). At six months after sowing, all ecotypes except Col-0, which had completely senesced by this time, produced ARs in varying quantities and continued to grow, producing more ARs (Supplementary Figure 2). This indicated that in these AR-producing ecotypes, like in polycarpic species, not all IAMs become reproductive upon flowering and that as a result flowering does not trigger

whole-plant senescence.

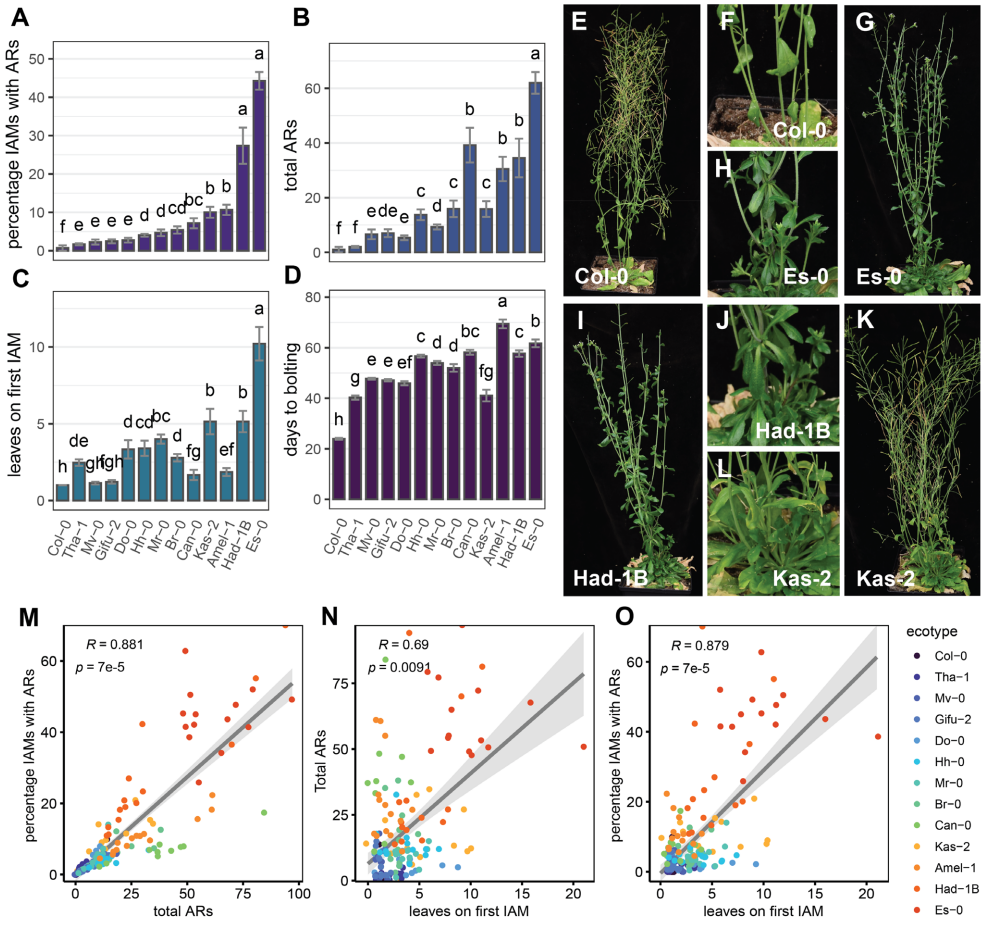

Figure 1: Phenotypes of AR-producing Arabidopsis ecotypes grown in lovng day conditions at five weeks after bolting. **A**: The percentage of inflorescence axillary meristems (IAMs) bearing three of more leaves. **B**: The total number of IAMs bearing three or more leaves. **C:** The number of leaves on the first AM of the primary inflorescence. **D:** Number of days from the start of seed germination to the first visible bolt. For each ecotype in figures **A-D**, 10-15 plants were analyzed and groups were compared with the Kruskall-Wallis test. Letters above bars indicate significance groups; different letters indicate significant differences between measurements. **E-L:** Phenotype of three of the AR-producing ecotypes compared to Col-0 at five weeks after bolting. All pots are 11 cm wide. **M:** Correlation of the total number of ARs with the percentage of IAMs bearing ARs. **N:** Correlation of the total number of ARs with the number of leaves produced by the first IAM. **O:** Correlation between the percentage of IAMs bearing ARs and the number of leaves produced by the first IAM. Correlation analyses in **M-O** were performed using Pearson's correlation, data are based on 10-15 plants per ecotype with a total of 172 plants.

The bolting time varied among ecotypes, but was significantly delayed for all ecotypes compared to Col-0 (Figure 1D). In order to exclude the possibility

that the AR phenotype was caused by delayed vegetative phase change (VPC), we counted the number of leaves lacking abaxial trichomes as a measure of juvenility (Supplementary figure 4A). We did not compare the length : width ratio of leaves between ecotypes, as the leaf shape varied strongly between ecotypes, making it an unreliable VPC marker. For some ecotypes, such as Es-0, both a delayed bolting time and a prolonged juvenile phase were observed, but generally there was no clear correlation between length of the juvenile phase and bolting time or the total number of ARs (Supplementary figure 4B, C). In fact, in several AR ecotypes VPC occurred significantly earlier than in Col-0.

Linear regression analysis (Pearson's correlation, n = 172) showed that the percentage of ARs strongly correlated with the total number of ARs (Figure 1M). Both the total number of ARs and the percentage of ARs also correlated positively with the number of leaves on the first IAM (Figure 1N and 1O). This shows that the number of leaves on the first IAM could be a sufficiently accurate measure to assess the AR trait in a more high-throughput manner than by counting all the IAMs with and without ARs. Finally, bolting time correlated significantly with all other polycarpic phenotypes (Supplementary figure 5), suggesting that at least in Arabidopsis, polycarpy coincides with late flowering.

Expression of polycarpy-related genes in AR-producing ecotypes

In previous research, ARs have been observed in different mutant or overexpression lines in which the floral transition was affected. The mutated or overexpressed genes are known to act in a regulatory network with the vernalization-repressed gene *FLC*, which represses the expression of *SOC1* and *SPL* genes (Figure 2A). SOC1 inhibits AR formation by repressing the expression of *AHL15* (Karami et al., 2020), and *AHL15* and several *SPL* genes interact in a reciprocal negative feedback loop (Rahimi et al., 2022). To understand whether the AR phenotype in AR ecotypes is caused by differential expression of one or more of the genes in this network, we performed RT-qPCR on RNA isolated from plant tissues at three different phases of development, i.e. in juvenile plants, in the rosette base at bolting (RBB), and in the IAMs at five weeks after bolting.

AHL15 expression was similar for all ecotypes at the juvenile stage, and generally increased in the RBB for AR ecotypes but not Col-0, and decreased again in the IAMs (Supplementary figure 6A-C, G). *AHL20* expression followed a similar pattern, and was strongly enhanced in the RBB for most AR ecotypes compared to Col-0 (Supplementary figure 6D-F, H). *AHL19* could barely be detected in all ecotypes during the juvenile stage nor in the RBB, and was

therefore excluded from the analysis. The expression of *FLC* was higher in all AR ecotypes compared to Col-0 at all stages (Supplementary figure 6G-H). This enhanced *FLC* expression explains the delayed bolting time of the ecotypes, and could also explain the observed AR phenotype.

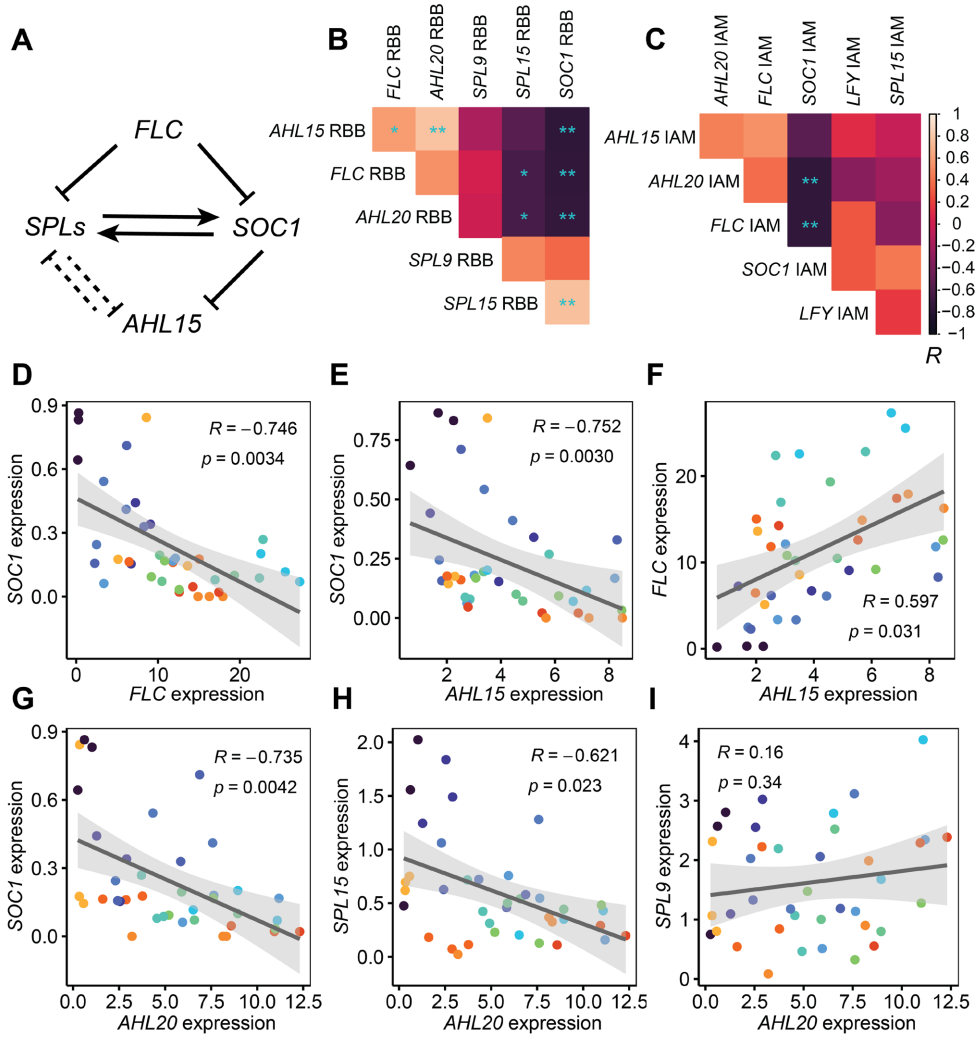

Figure 2: Correlations between expression of genes in AR ecotypes. **A:** Interaction network between *FLC*, *SOC1*, *SPL* and *AHL15* genes based on literature. **B:** Heatmap showing Pearson's correlation between genes expressed in the rosette base at bolting (RBB). **C:** Heatmap showing Pearson's correlation between genes expressed in the inflorescence axillary meristem (IAM) at five weeks after bolting. Blue stars indicate statistically significant correlations (*: p<0.05, **: p<0.01, ***: p<0.001), and tile colors are scaled to the Pearson's R coefficient. **D-I:** Examples of individual Pearson's correlations between genes expressed in the RBB. For each correlation analysis, 36 samples from 13 ecotypes were included.

In contrast, the expression of *SOC1* in the RBB was significantly lower than in Col-0 for most AR ecotypes, and its expression increased in the IAMs where the differences between ecotypes were less pronounced (Supplementary figure 7A-C). *SPL9* expression was similar for all ecotypes in the RBB (Supplementary figure 7E), while *SPL15* expression appeared reduced in most AR ecotypes in both the RBB and IAMs, but not significantly (Supplementary figure 7C, D).

In order to establish whether the AR-producing IAMs were in a vegetative or reproductive state, we studied the expression of the floral meristem identity gene *LEAFY (LFY)* (Weigel and Nilsson, 1995). Surprisingly, *LFY* expression in the IAMs was similar to Col-0 in most ecotypes (Supplementary figure 7F). This indicates that the IAMs maintain a floral identity despite producing vegetative structures, which is illustrated by the fact that from some ARs, a secondary or tertiary inflorescence can still emerge (Figure 1H-K, Supplementary figure 3E-M).

In summary, *FLC* and *SOC1* expression showed a clear difference in expression between the AR ecotypes and Col-0. However, due to the high variation between biological triplicates it was difficult to conclude on the role of *AHL* and *SPL* genes in the AR phenotype. We therefore decided to perform a more global analysis of the interaction between the genes that were measured in the RBB and IAM tissues.

With the expression data from the RBB and IAM tissues, we investigated the interaction between genes by linear regression (Pearson's correlation, Figure 2, Supplementary table 1). By adding the biological replicates of each ecotype in the analysis individually, we reduced the weight of "genotype" as a factor in the analysis. As expected*, FLC* and *SOC1* showed a significant negative correlation in both tissues (Figure 2B-D). *SOC1* expression also correlated negatively with *AHL15* in the RBB (Figure 2B, 2E), confirming earlier reports that *AHL15* expression is repressed by SOC1 (Karami et al., 2020). Interestingly, *SOC1* and *AHL20* expression also negatively correlated in the RBB and the IAMs (Figure 2B, C, G), indicating that both *AHL15* and *AHL20* might play similar roles downstream of SOC1. In line with this, *AHL15* and *AHL20* expression showed a significant positive correlation in the RBB (Figure 2B). *FLC* expression correlated positively with *AHL15* but not with *AHL20* expression, and negatively with *SPL15* expression in the RBB (Figure 2B, F). Finally, we tested whether there was a correlation between the expression of the *AHL* and *SPL* genes in this experiment. Surprisingly, a significant negative correlation could be seen between expression of *SPL15* and *AHL20,* but not *AHL15* in the RBB (Figure 2B, H)*. SPL9* and *LFY* expression did not correlate positively or negatively to the

expression of any of the genes tested (Figure 2B, C, I).

Together, the expression patterns of these *TF* genes in different ecotypes and the correlations found between these genes confirm gene interaction networks identified in earlier studies based on mutant screens in the Col-0 or Ler background (Figure 2A). Our results show that by comparing expression data collected from a panel of ecotypes, the same interactions can be observed, but also unknown interactions between genes are revealed (e.g. between *SOC1*, *SPL15* and *AHL20*).

Expression of *FLC, AHL20* and *SOC1* predicts AR production

Because the ecotypes showed variation in phenotype as well as in gene expression, we investigated whether gene expression correlated with the observed phenotypes and whether it could be a good predictor of the phenotype. The average gene expression in the IAMs (collected directly after phenotyping at five weeks after bolting) and expression in the RBB (collected in an independent experiment in the same growth chamber) were both compared to the average bolting time and the AR traits measured at five weeks after bolting (Figure 3, Supplementary table 1).

AHL15, AHL20, and FLC have each been shown to delay flowering time in Col-0 (Gu et al., 2013; Karami et al., 2020; Tayengwa et al., 2020). From our data, there is a clear positive correlation between bolting time and *AHL15*, *AHL20*, and *FLC* expression, indicating that these genes play similar roles in our panel of ecotypes (Figure 3A). We also observed a strong negative correlation between bolting time and *SOC1* expression in both tissues (Figure 3A), again showing that expression data can predict interactions between genes and their associated phenotypes.

Next, we looked at the interaction between gene expression and the AR phenotype. As expected, we could see a significant negative correlation between *SOC1* expression in both tissues and the total number of ARs (Figure 3A, D). The total number of ARs was also negatively influenced by *SPL15* expression in the RBB, but surprisingly not in IAMs (Figure 3A). *FLC* expression in the IAMs correlated positively with all three indicators of AR production (Figure 3A-C). Surprisingly, we also observed a significant positive correlation between *AHL20* expression and the total number of ARs, but not for *AHL15* (Figure 3A, E). This suggests that AHL20 might play a similar, if not more important role than AHL15 in AR production downstream of SOC1 in the tested AR ecotypes.

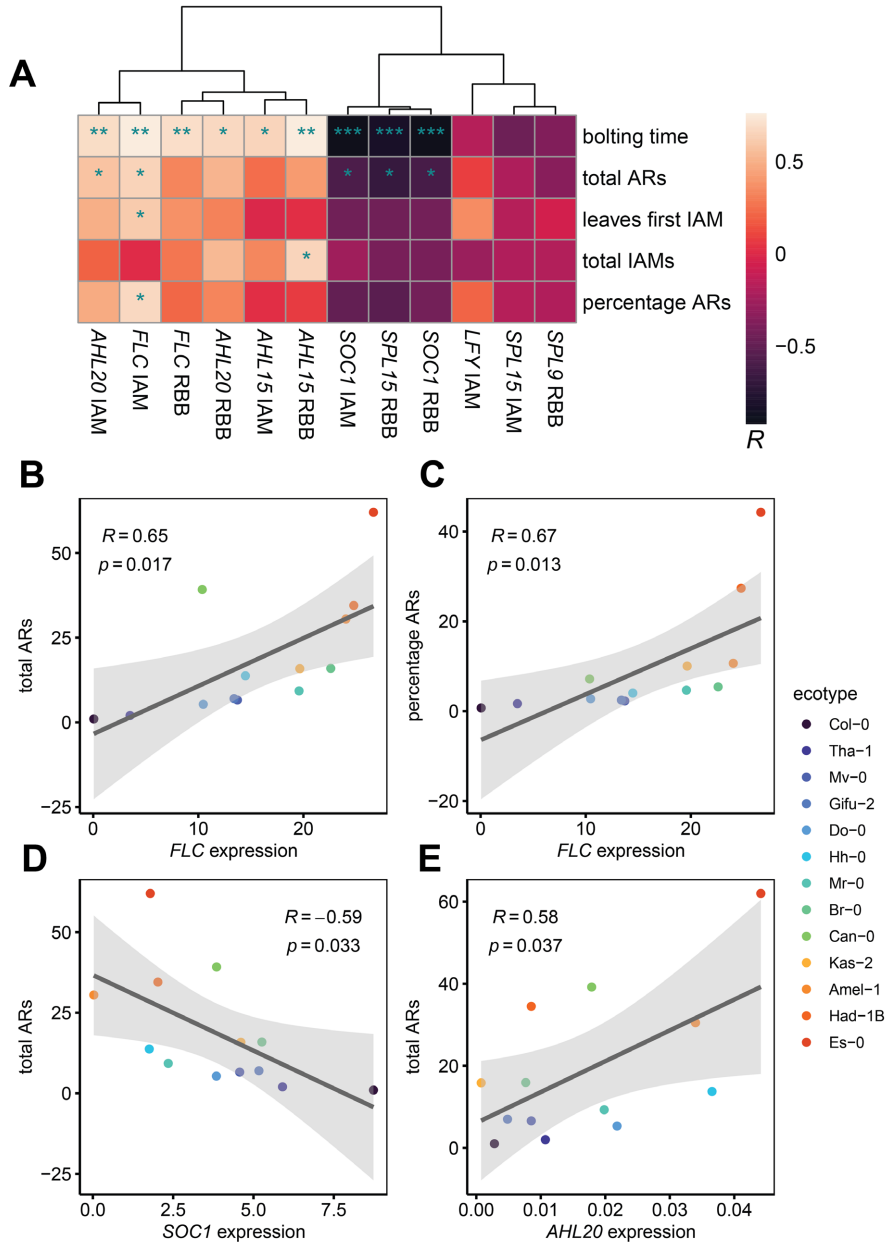

Principal component analysis of phenotypic- and gene expression data reveals SOC1 as the major driver of diversity

Because the expression of multiple genes correlates significantly with the AR phenotype, we performed a principal component analysis (PCA) to identify the gene that most strongly influences the variation between ecotypes. We

Figure 3 (left page): Correlations between expression of genes and the AR phenotype at five weeks after bolting. **A:** Heatmap showing Pearson's correlation analysis between phenotypic data and expression of genes in the rosette base at bolting (RBB) or in the inflorescence axillary meristem (IAM) at five weeks after bolting. Blue stars indicate statistically significant correlations (*: p<0.05, **: p<0.01, ***: p<0.001), and tile colors are according to the indicated Pearson's R coefficient color scale. **B-C:** Pearson's correlation analysis of *FLC* expression in the IAMs with the total number of ARs (**B**) or the percentage of ARs (**C**). **D-E:** Pearson's correlation analysis of the total number of ARs and the expression of *SOC1* (**D**) or *AHL20* in the IAMs (**E**). Mean values of gene expression of 2-3 biological replicates consisting of material from three plants each and phenotypic traits of 10-15 plants per ecotype were used for the analysis.

compared average gene expression at both stages (in the RBB and in IAMs) between all ecotypes, and found that the strongest driver of variation between ecotypes is the expression of *SOC1* in both the RBB and IAM, followed by expression of *AHL15* and *FLC* in the RBB (Figure 4, Supplementary table 2A). This is represented by their respective contribution to the first principal component (PC1) in the PCA, which is highest for *SOC1* expression in the RBB followed by *SOC1* expression in the IAM (Supplementary table 2A). In addition, *SOC1* expression showed the strongest (negative) correlation with the AR phenotype of all genes (Figure 3A, D) and the importance of *SOC1* for the AR phenotype is further confirmed by its strong contribution to PC1. Furthermore, this PCA shows that the expression of genes in the RBB varies more strongly between ecotypes and has a stronger influence on variation between ecotypes. This could indicate that gene expression during the bolting phase might be more indicative of the later shoot phenotype than gene expression at later developmental stages. The observed correlation of the AR phenotype with *SPL15* expression in the RBB, but not in IAMs further supports this (Figure 3A).

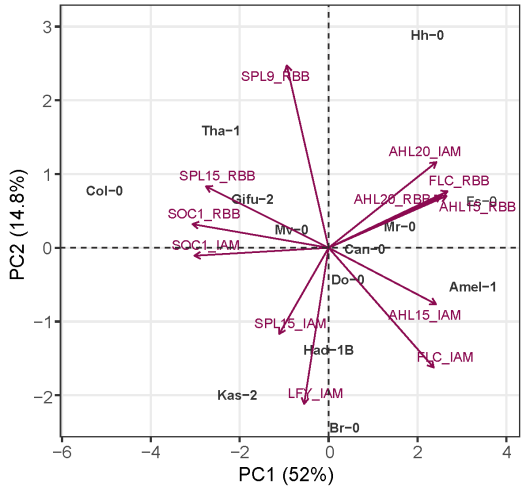

Figure 4: Principal component analysis of variation between ecotypes based on gene expression in rosette before bolting (RBB) or inflorescence axillary meristems (IAM) tissue. The length and direction of the arrows (in purple) indicate the weight with which the variable contributes to the first two principal components. Ecotype names (in black) are plotted based on the first two principal components. Mean values for gene expression of 2-3 biological replicates consisting of material from three plants each were used for the analysis.

FLC is required for aerial rosette production

Because of the significant positive correlation between *FLC* expression and AR production, we tested whether the ecotypes would still produce ARs when *FLC* was no longer expressed. In order to do this, we measured the same phenotypic traits in plants that had been subjected to a five-week seed vernalization treatment, which should be sufficient time for silencing of *FLC* in most ecotypes (Duncan et al., 2015).

Vernalization treatment strongly accelerated bolting time in all ecotypes, except for Had-1B and Mr-0, which flowered only slightly earlier than in non-vernalized control conditions (Figure 5A). At five weeks after bolting, the phenotype of vernalized plants was markedly different from their non-vernalized counterparts (Figure 5D-H, Figure 1E-K, Supplementary figures 3, 9). First, most vernalized ecotypes no longer produced ARs at five weeks after bolting, except Had-1B and Mr-0, which were also the latest to bolt (Figure 5A, B). Second, in many cases the leaf- and inflorescence morphology of vernalized plants was markedly different compared to their non-vernalized counterparts. This was especially obvious in ecotypes Es-0, Kas-2 and Amel-1 (Figure 5D, E, H). Non-vernalized Es-0 plants, for example, had dark-green leaves with a firm texture and prominent trichomes in control conditions, whereas the colour and texture of the leaves became lighter and less rigid following vernalization.

In order to confirm whether the absence of ARs was indeed a result of decreased *FLC* expression, the expression of *FLC* was analysed in the IAMs of the two ecotypes still producing ARs (Had-1B and Mr-0) as well as three ecotypes producing the highest percentage of IAMs (Es-0, Amel-1, Kas-2) (Figure 5C). *FLC* expression was significantly reduced in Kas-2, Amel-1 and Es-0, while its expression remained high in Had-1B and Mr-0. The continued expression of *FLC* in the latter two ecotypes explains the late bolting time and continued production of ARs, and suggests that the vernalization period was too short for full *FLC* repression in these ecotypes. The absence of ARs and the repressed expression of *FLC* in the three other vernalized AR ecotypes, along with the strong and significant positive correlation between *FLC* expression and AR production in non-vernalized plants show that *FLC* is the main determinant of AR production in these ecotypes. *FLC* is likely to act upstream of *SOC1, SPL15,* and *AHL20*, whose expression was shown to correlate with the total number of ARs in this study.

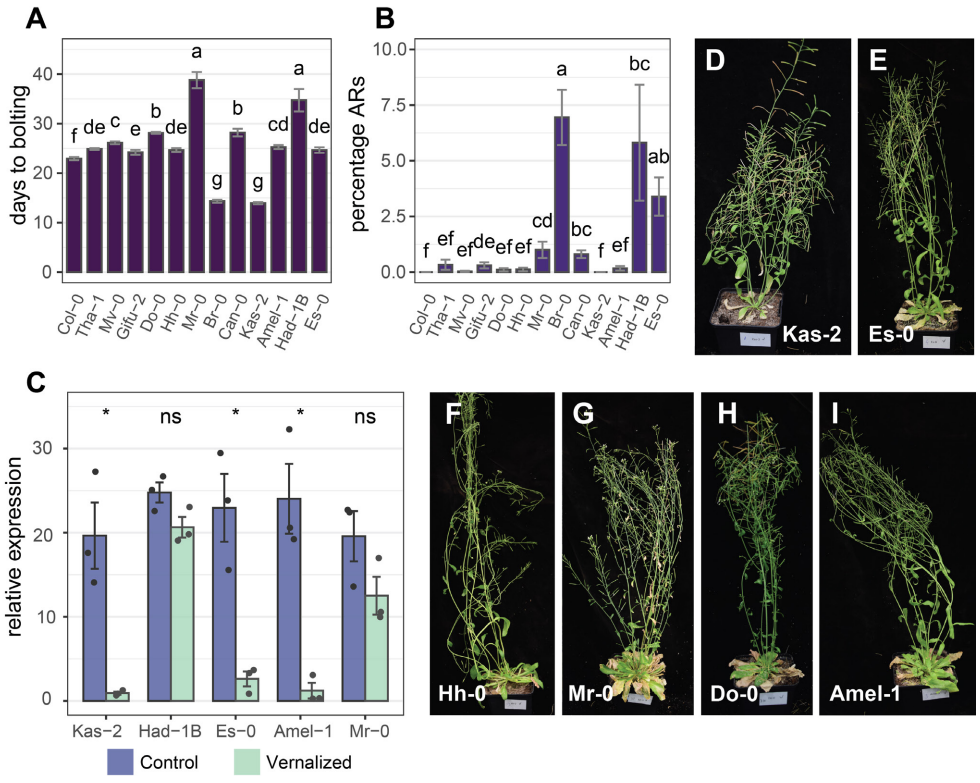

Figure 5: Phenotypes of vernalized AR ecotypes at five weeks after bolting. **A:** Days between the end of seed vernalization and the first visible bolt. **B:** The percentage of IAMs bearing three or more rosette leaves. For each ecotype in **A** and **B**, 15 plants were analyzed, and groups were compared with the Kruskall-Wallis test. Statistically significant differences are indicated with different letters above the bars. **C:** Expression of *FLC* in IAMs at five weeks after bolting in non-vernalized (blue) and vernalized plants (turquoise). Each measurement is based on three biological repeats, and differences between non-vernalized and vernalized were compared using a Student's *t*-test. Asterisk indicates a significant difference ($p < 0.05$) ; ns = not significant. **D-H**: phenotypes of vernalized plants of the indicated ecotypes at five weeks after bolting. All pots are 9 cm wide.

Discussion

In Arabidopsis, the AR phenotype can be observed in mutants in which the flowering pathway is affected or repressed (Wang et al., 2007; Melzer et al., 2008; Xu et al., 2016; Karami et al., 2020). In this research, we have studied multiple Arabidopsis accessions that naturally produce ARs and investigated the relationship between the AR phenotype and the expression of genes that have previously been shown to affect AR production. Our results show that the floral repressor *FLC* is the major determinant of AR production in this panel of accessions, and that silencing *FLC* expression by vernalization is sufficient to

repress the AR phenotype. In addition, we show that the expression of *SOC1* in both early- and late stages of flowering is negatively associated with the AR phenotype. Our findings confirm earlier results that show that knockout of *soc1* in combination with *ful,* or overexpression of *FLC* results in an AR-producing phenotype, similar to that seen in the strongest AR ecotypes such as Es-0. This shows that gene function can be deduced by correlating gene expression to phenotypic traits when studying a panel of phenotypically diverse genotypes, avoiding the need for using transgenic- or mutagenized lines. In addition, we have shown that this method can identify interactions between genes based on their expression, as can be seen for the negative correlation between the expression of *SOC1* and its repressor *FLC*.

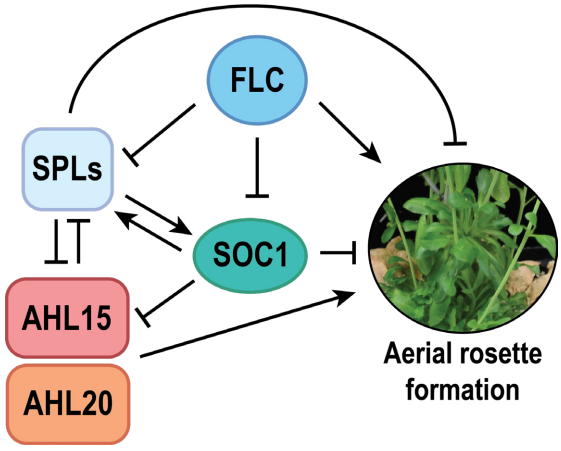

Figure 6: Genetic regulation of aerial rosette formation. SOC1 and SPL15 repress the formation of ARs, whereas FLC, AHL15, and AHL20 promote the formation of ARs. FLC represses expression of *SOC1* and *SPL15*, and its expression correlates positively with *AHL15* expression. SOC1 represses expression of *AHL15* and *AHL20*, and promotes *SPL15* expression and *vice versa*.

AHL20 as a new player in AR production

Our data show that expression of the *AT-HOOK MOTIF NUCLEAR LOCALISED* family gene *AHL20* in the IAMs positively correlates with AR formation, and that it is likely repressed by SOC1, identifying a previously unknown function for this gene (Figure 6). Surprisingly, despite previous evidence that *AHL15* is required for the AR phenotype in the *soc1ful* mutant and is directly repressed by SOC1 in the IAMs (Karami et al., 2020), the expression of *AHL15* in the IAMs did not show a significant correlation with the AR phenotype. RNA-seq data shows that both *AHL15* and *AHL20* are upregulated in the stem of the *soc1ful* mutant, indicating that *AHL20* could be another direct target of SOC1 (Davin et al., 2016). However, ChIP-seq on the shoot apices of short day (SD)-grown *gSOC1:GFP* plants showed significant enrichment at the *AHL15* locus, but not the *AHL20* locus (Immink et al., 2012), which suggests that *AHL20* is

not directly repressed by SOC1, or possibly that SOC1 targets differ between SD and (in our case) LD-grown plants and between shoot apices and stem tissue. The RBB samples were enriched in stem tissue, and we found a strongly enhanced *AHL20* expression in the AR ecotypes compared to Col-0 in these samples. It is therefore possible that *AHL20* has an expanded function during the floral transition or in stem tissue in the AR ecotypes, or is targeted by SOC1 specifically in this tissue type.

Interestingly, *AHL20* expression in the IAMs was much lower than that of *AHL15,* but was a better predictor of AR production. Previous studies on *AHL* genes have revealed a high level of functional redundancy (Zhao et al., 2013; Karami et al., 2020; Rahimi et al., 2022), and it is likely that *AHL20* and *AHL15* play very similar roles in promoting vegetative development of AMs. Considering the number of genes associated with the AR phenotype in Arabidopsis, it is likely that in addition to *AHL15* and *AHL20*, the production of ARs is controlled by other factors that act downstream of FLC, SOC1, and SPL15, such as the NAC TF ANAC087 (Vargas-Hernández et al., 2022), and RADICAL-INDUCED CELL DEATH 1 (RCD1) and SIMILAR TO RCD-ONE1 (SRO1) (Teotia and Lamb, 2009). *AHL* genes might therefore also play a more nuanced role in wild-type plants than when overexpressed, a situation where the high dose of AHLs might override the balanced regulation of AM outgrowth. Taken together, our data clearly show that FLC and AHL20 promote AR formation whereas SPL15 and especially SOC1 repress AR formation (Figure 6).

FLC is a major determinant of AR production

Previous research has shown that an altered *FLC* expression resulting from changes in its upstream regulator AERIAL ROSETTE 1 (ART1)/HUA2 was responsible for the AR phenotype in the Arabidopsis ecotype Sy-0 (Wang et al., 2007). Unfortunately, the authors did not investigate whether the AR phenotype persisted after vernalization, which would indicate whether any other factors are responsible for AR formation in this ecotype. Here, we show that *FLC* plays a similar role in ecotypes retrieved from geographically diverse locations, indicating that this mechanism is conserved.

FLC has been shown to be required for the polycarpic life history strategy in *Arabis alpina* by protecting AMs from transitioning into an inflorescence- or floral identity (Hyun et al., 2019; Kiefer et al., 2019). *A. alpina* starts flowering when *FLC* /*PEP1* expression is temporarily repressed by vernalization, but re-initiates vegetative growth due to a reset of *FLC/PEP1* expression. Our data show that FLC can play a similar role in the monocarpic Arabidopsis in

the absence of vernalization, and causes a significant increase in life span when its expression remains high during flowering. It has been shown that *FLC* expression is regulated differently between monocarps like *Arabis montbretiana* and Arabidopsis compared to the polycarpic *A. alpina*, and that this is a result of sequence variation in the regulatory elements of the *FLC* locus (Kiefer et al., 2017). A recent study has shown that similar differences in *FLC* regulation are key to the differences in the life history strategy of two other *Brassicaceae* genera (Zhai et al., 2024). These studies make it clear that FLC is a major player in the polycarpic life history strategy. However, the role of FLC in this process may be unique to the *Brassicaceae*, as it has been shown that the vernalization response is conferred by *Terminal Flower 1*-like genes in the *Rosaceae* (Kurokura et al., 2013). In addition, many polycarpic species grow in climates in which they are never exposed to vernalizing conditions. It would therefore be interesting to investigate how polycarpic development is regulated in (tropical) polycarpic species that do not experience winter cold in order to better understand the evolution of polycarpy.

SOC1 and *SPL15* have been shown to act downstream of FLC (Deng et al. 2011), and our data show that *AHL20* most likely acts downstream of SOC1 (Figure 6). It is therefore likely that FLC induces the AR phenotype by regulating the expression of these and potential other genes directly and indirectly. FLC expression alone is unlikely to be sufficient to initiate the AR phenotype, as the AR phenotype is relatively rare in Arabidopsis ecotypes, despite the fact that many ecotypes are vernalization-dependent and therefore also express *FLC* (Zhang and Jiménez-Gómez 2020). This is most likely due to differences in *FLC* expression levels similar to what we have observed in our panel of ecotypes. However, since the initiation of AR production was relatively slow in some of the ecotypes described here, it is also possible that many more vernalization-dependent ecotypes are capable of producing ARs, but have never been described as such due to the late emergence of this trait. The differences in the number of ARs and the number of leaves on the first node also shows that there is variation in the intensity of the AR phenotype, which could depend on differences in downstream target regulation. Most genome-wide association studies (GWAS) have studied pre-flowering traits or traits that can be observed soon after flowering, while longevity and life span has never been studied in much depth (Togninalli et al. 2018; Atwell et al. 2010). Studying the AR phenotype and overall life span in a larger panel of ecotypes could therefore help identify potential novel regulators of AM outgrowth and polycarpy.

Gene expression at bolting determines the inflorescence phenotype

The expression of *SOC1* and *SPL15* in RBB tissue, and *SOC1* in IAMs show a significant negative correlation with the total number of ARs. In addition, PCA shows that *SOC1* expression in both RBB and IAM tissue is the strongest driver of variation between the ecotypes in this study. These results confirm earlier studies that have shown that the FLC-repressed gene *SOC1* acts as a repressor of AR formation, as the *soc1ful* mutations in the Col-0 background produce ARs (Melzer et al. 2008; Karami et al. 2020). Similarly, the expression of *SPL15* in the RBB is negatively correlated to both *FLC* expression and the AR phenotype, and has previously been shown to repress AR formation in the Col-0 background (Rahimi et al. 2022). Our results show that these genes fulfil similar roles in geographically diverse ecotypes in repressing the outgrowth of IAMs into ARs. Although the AR phenotype often appeared only several weeks after flowering, the intensity of this phenotype in some cases correlated more strongly with gene expression in the RBB compared to expression in the IAMs (Figure 3). This observation is further supported by the PCA, which showed that five out of six of the main contributors to the first principle component were expressed during the bolting stage (Figure 4). These results suggest that the inflorescence architecture is likely to be determined before outgrowth of the inflorescence stem and rosette branches, and that gene expression at this stage can predict the inflorescence architecture.

Arabidopsis ecotypes as a tool for studying polycarpy

In this study, we have described ecotypes that display a range of polycarpic traits that include a longer life span and delayed bolting time, and most importantly the production of ARs. The renewed vegetative growth in the form of ARs on the inflorescence stems of these ecotypes resembles that of polycarpic species, showing that polycarpic traits can arise in monocarpic species. Studying polycarpic traits in species that are generally considered monocarpic can help shed light on how meristematic fate is regulated in plants with different life history strategies, and on how these differences in life history strategy have evolved. The fast life cycle and expansive genetic toolkit associated with Arabidopsis make this species a useful tool for studying such phenotypes, as even slow-flowering ecotypes, such as those described in this study, still have a relatively quicker development than other, polycarpic, species. As the formation of ARs and other post-bolting traits have been poorly covered in GWAS, focusing mainly on the plant's life span (Atwell et al. 2010),

the mechanisms driving post-bolting shoot development and longevity remain elusive. With this panel of ecotypes we show that significant variation exists even within a relatively rare trait such as AR formation, and that this trait could be an interesting subject for future GWAS. To our knowledge, this study is the first in which AR traits have been investigated in a quantitative manner, and our results show that instead of the total number and percentage of ARs, which can only be scored relatively late during development, the number of leaves on the first inflorescence node can be used as a much earlier phenotype to compare polycarpic development between ecotypes.

Methods

Plant material and growth conditions

The Arabidopsis ecotypes Amel-1 (N76434), Br-0 (N76455), Can-0 (N76109), Do-0 (N76474), Es-0 (N76484), Gifu-2 (N76494), Had-1B (N76509), Hh-0 (N76512), Kas-2 (N78905), Mv-0 (N76556), Mr-0 (N78474), Tha-1 (N76611) were acquired from the Nottingham Arabidopsis Stock Centre (NASC; www.arabidopsis.info). The Col-0 ecotype was used as a non-AR producing control.

Seeds were sown on soil (90% turf soil with 10% sand) and stratified on damp soil for 5 days at 4°C for the control conditions, or kept at 4°C in the dark for 5 weeks for seed vernalization. After stratification or seed vernalization, pots were transferred to a climate chamber and seeds were germinated under long day (16h photoperiod) at 21°C and 65% relative humidity. One week after sowing, individual seedlings were transferred to large individual pots.

The number of juvenile leaves (without abaxial trichomes) was counted after 4 weeks of growth in unvernalized plants. Bolting time was recorded as the day on which the inflorescence stem was first visible, corresponding to a bolt of approximately 1 cm. The number of aerial rosettes, inflorescence axillary meristems (IAMs), and leaves on the first AM on the primary inflorescence (first IAM) were counted at five weeks (35 days) after the bolting date in vernalized and unvernalized plants.

RNA isolation and RT-qPCR

For juvenile plants, five 14 day-old seedlings were pooled in 2 ml Eppendorf tubes with a metal bead, snap-frozen in liquid nitrogen and pulverized in the Qiagen Tissuelyser (Qiagen, Hilden, Germany). For bolting plants, the above-ground rosette of 3 plants showing a 1 cm bolt was harvested, leaves and

the emerging inflorescence were removed, and the rosette cores were snap frozen in liquid nitrogen and ground with a mortar and pestle. IAMs (from the central inflorescence and rosette branches) were harvested at 5 weeks after bolting and material of three plants was pooled in a 2 ml Eppendorf tube with a metal bead, snap frozen in liquid nitrogen, and pulverized using the Qiagen Tissuelyser.

RNA was isolated using the RNeasy Plant mini kit (Qiagen, Hilden, Germany). For qPCR analysis, 1 µg of RNA was aliquoted to a fresh tube and treated with DNAse I for 30 minutes to remove any remaining DNA, and used for cDNA synthesis with the RevertAid First Strand Kit (ThermoFisher, Vilnius, Lithuania) according to the supplied protocol. RT-qPCR was performed using TB green ex-taq II (Takara Bio Europe, Saint-Germain-en-Laye, France) in the quantstudio 5 qPCR machine (Invitrogen). Primers used for RT-qPCR are listed in Supplementary table 3 and were synthesized by Sigma Aldrich (Haverhill, United Kingdom).

Data analysis and statistics

All data analysis was performed using R version 4.2.1. (R Core Team, 2023), plots were made with ggplot2 version 3.3.6 (Wickham, 2016) and ggpubr version 0.4.0 (Kassambara, 2023a). Statistical analysis was performed using the packages rstatix version 0.7.0 (Kassambara, 2023b) and agricolae version 1.3.5 (de Mendiburu, 2023). The package psych version 2.3.6 (William Revelle, 2023) was used to calculate Pearson correlation matrices, and heatmaps were plotted with corrplot version 0.92 (Wei and Simko, 2021).

Means between ecotypes were compared using non-parametric tests (Kruskall-Wallis) and significance groups were determined accordingly. Correlations between phenotypes were done by comparing the phenotypic data (bolting time, total number of ARs, total number of IAMs, percentage ARs, and the number of leaves on the first inflorescence IAM) from each individual plant (n = 195). For comparisons to gene expression and the number of juvenile leaves, the mean values of each phenotype or relative expression per genotype were used (n = 13), as the observations from gene expression studies could not be linked to an individual plant, and the number of juvenile leaves was phenotyped in a destructive manner.

For principal component analysis, the average values of phenotypic- or expression data per ecotype were used and the calculations and plots were made in R using the packages FactoMineR version 2.8 (Lê et al., 2008) and factoextra version 1.0.7 (Kassambara and Mundt, 2020).

Acknowledgements

We thank Jan Vink, Ward de Winter and Mariel Lavrijsen for technical support and Kiki Spaninks, Jelmer van Lieshout, and Jihed Chouaref for help with phenotyping. This work was supported the graduate school green top sectors grant (grant nr. GSGT.2019.024) from the Dutch Research Council (NWO) to TL.

Author contributions

TL and RO conceived and designed the study. Phenotyping of the juvenile phase and gene expression studies in juvenile and RBB tissue were done by TL and MK. Phenotyping of AR traits, gene expression studies in IAM tissue, and data analysis were performed by TL. TL and RO interpreted the data and wrote the manuscript.

Literature

Amasino R. (2009). Floral induction and monocarpic versus polycarpic life histories. Genome Biol **10**: 228.

Atwell S., Huang Y.S., Vilhjálmsson B.J., Willems G., Horton M., Li Y., Meng D., Platt A., Tarone A.M., Hu T.T., et al (2010). Genome-wide association study of 107 phenotypes in *Arabidopsis thaliana* inbred lines. Nature 2010 465:7298 **465**: 627–631.

Balanzà V., Martínez-Fernández I., Ferrándiz C. (2014). Sequential action of FRUITFULL as a modulator of the activity of the floral regulators SVP and SOC1. J EXP BOT **65**: 1193–1203.

Davin N., Edger P.P., Hefer C.A., Mizrachi E., Schuetz M., Smets E., Myburg A.A., Douglas C.J., Schranz M.E., Lens F. (2016). Functional network analysis of genes differentially expressed during xylogenesis in *soc1ful* woody *Arabidopsis plants*. The Plant Journal **86**: 376–390.

Deng W., Ying H., Helliwell C.A., Taylor J.M., Peacock W.J., Dennis E.S. (2011). FLOWERING LOCUS C (FLC) regulates development pathways throughout the life cycle of Arabidopsis. PNAS **108**: 6680–6685.

Dorca-Fornell C., Gregis V., Grandi V., Coupland G., Colombo L., Kater M.M. (2011). The Arabidopsis *SOC1*-like genes *AGL42, AGL71* and *AGL72* promote flowering in the shoot apical and axillary meristems. Plant J **67**: 1006–1017.

Duncan S., Holm S., Questa J., Irwin J., Grant A., Dean C. (2015). Seasonal shift in timing of vernalization as an adaptation to extreme winter. Elife **4**: e06620.

Gu X., Le C., Wang Y., Li Z., Jiang D., Wang Y., He Y. (2013). Arabidopsis *FLC* clade members form flowering-repressor complexes coordinating responses to endogenous and environmental cues. Nat Commun **4**: 1–10.

Hu X., Kong X., Wang C., Ma L., Zhao J., Wei J., Zhang X., Loake G.J., Zhang T., Huang J., et al (2014). Proteasome-mediated degradation of FRIGIDA modulates glowering time in Arabidopsis during vernalization. Plant Cell **26**: 4763–4781.

Hyun Y., Richter R., Vincent C., Martinez-Gallegos R., Porri A., Coupland G. (2016). Multi-layered regulation of *SPL15* and cooperation with SOC1 integrate endogenous flowering pathways at the Arabidopsis shoot meristem. Dev Cell **37**: 254–266.

Hyun Y., Vincent C., Tilmes V., Bergonzi S., Kiefer C., Richter R., Martinez-Gallegos R., Severing E., Coupland G. (2019). A regulatory circuit conferring varied flowering response to cold in annual and perennial plants. Science (1979) **363**: 409–412.

Immink R.G.H., Posé D., Ferrario S., Ott F., Kaufmann K., Valentim F.L., de Folter S., van der Wal F., van Dijk A.D.J., Schmid M., et al (2012). Characterization of SOC1's central role in flowering by the identification of its upstream and downstream regulators. Plant Physiol **160**: 433–449.

Johanson U., West J., Lister C., Michaels S., Amasino R., Dean C. (2000). Molecular analysis of *FRIGIDA*, a major determinant of natural variation in Arabidopsis flowering time. Science (1979) **290**: 344–347.

Karami O., Rahimi A., Khan M., Bemer M., Hazarika R.R., Mak P., Compier M.,

van Noort V., Offringa R. (2020). A suppressor of axillary meristem maturation promotes longevity in flowering plants. Nat Plants **6**: 368–376.

Kassambara A. (2023a). ggpubr: "ggplot2" Based Publication Ready Plots.

Kassambara A. (2023b). rstatix: Pipe-Friendly Framework for Basic Statistical Tests.

Kassambara A., Mundt F. (2020). factoextra: Extract and Visualize the Results of Multivariate Data Analyses.

Kiefer C., Bergonzi S., Brand L., Wötzel S., Koch M.A. (2019). Contrasting life history traits in monocarpic versus polycarpic plants from a molecular-evolutionary point of view. Annu Plant Rev **2**: 479–504.

Kiefer C., Severing E., Karl R., Bergonzi S., Koch M., Tresch A., Coupland G. (2017). Divergence of annual and perennial species in the *Brassicaceae* and the contribution of cis-acting variation at *FLC* orthologues. Mol Ecol **26**: 3437–3457.

Kurokura T., Mimida N., Battey N.H., Hytönen T. (2013). The regulation of seasonal flowering in the *Rosaceae*. J EXP BOT **64**: 4131–4141.

Lê S., Josse J., Husson F. (2008). {FactoMineR}: A Package for Multivariate Analysis. J Stat Softw **25**: 1–18.

Melzer S., Lens F., Gennen J., Vanneste S., Rohde A., Beeckman T. (2008). Flowering-time genes modulate meristem determinacy and growth form in *Arabidopsis thaliana*. Nat Genet **40**: 1489–1492.

de Mendiburu F. (2023). agricolae: Statistical Procedures for Agricultural Research.

Ponraj U., Theres K. (2020). Keep a distance to be different: axillary buds initiating at a distance from the shoot apical meristem are crucial for the perennial lifestyle of *Arabis alpina*. New Phytol **227**: 116–131.

R Core Team (2023). R: A Language and Environment for Statistical Computing.

Rahimi A., Karami O., Balazadeh S., Offringa R. (2022). miR156 -independent repression of the ageing pathway by longevity-promoting AHL proteins in Arabidopsis. New Phytol **235**: 2424–2438.

Schwarz S., Grande A. V., Bujdoso N., Saedler H., Huijser P. (2008). The microRNA regulated *SBP*-box genes *SPL9* and *SPL15* control shoot maturation in Arabidopsis. Plant Mol Biol **67**: 183–195.

Tayengwa R., Sharma Koirala P., Pierce C.F., Werner B.E., Neff M.M. (2020). Overexpression of *AtAHL20* causes delayed flowering in Arabidopsis via repression of *FT* expression. BMC Plant Biol **20**: 559.

Teotia S., Lamb R.S. (2009). The paralogous genes *RADICAL-INDUCED CELL DEATH1* and *SIMILAR TO RCD ONE1* have partially redundant functions during Arabidopsis development. Plant Physiol **151**: 180–198.

Thomas H. (2013). Senescence, ageing and death of the whole plant. New Phytol **197**: 696–711.

Tilmes V., Mateos J.L., Madrid E., Vincent C., Severing E., Carrera E., López-Díaz I., Coupland G. (2019). Gibberellins act downstream of *Arabis alpina* PERPETUAL FLOWERING1 to accelerate floral induction during vernalization. Plant Physiol **180**: 1549–1563.

Togninalli M., Seren Ü., Meng D., Fitz J., Nordborg M., Weigel D., Borgwardt

K., Korte A., Grimm D.G. (2018). The AraGWAS Catalog: a curated and standardized *Arabidopsis thaliana* GWAS catalog. Nucleic Acids Res **46**: D1150–D1156.

Vargas-Hernández B.Y., Núñez-Muñoz L., Calderón-Pérez B., Xoconostle-Cázares B., Ruiz-Medrano R. (2022). The NAC transcription factor ANAC087 induces aerial rosette development and leaf senescence in Arabidopsis. Front Plant Sci **13**: 117.

Vayssières A., Mishra P., Roggen A., Neumann U., Ljung K., Albani M.C. (2020). Vernalization shapes shoot architecture and ensures the maintenance of dormant buds in the perennial *Arabis alpina*. New Phytol **227**: 99–115.

Wang Q., Sajja U., Rosloski S., Humphrey T., Kim M.C., Bomblies K., Weigel D., Grbic V. (2007). HUA2 caused natural variation in shoot morphology of *A. thaliana*. Current Biology **17**: 1513–1519.

Wei T., Simko V. (2021). R package "corrplot": Visualization of a Correlation Matrix.

Weigel D., Nilsson O. (1995). A developmental switch sufficient for flower initiation in diverse plants. Nature **377**: 495–500.

Wickham H. (2016). ggplot2: Elegant Graphics for Data Analysis.

William Revelle (2023). psych: Procedures for Psychological, Psychometric, and Personality Research.

Wu G., Poethig R.S. (2006). Temporal regulation of shoot development in *Arabidopsis thaliana* by miR156 and its target *SPL3*. Development **133**: 3539–3547.

Xu M., Hu T., Zhao J., Park M.-Y., Earley K.W., Wu G., Yang L., Poethig R.S. (2016). Developmental functions of miR156-Regulated *SQUAMOSA PROMOTER BINDING PROTEIN-LIKE (SPL)* genes in *Arabidopsis thaliana*. PLOS Genet **12**: e1006263.

Zhai D., Zhang L.-Y., Li L.-Z., Xu Z.-G., Liu X.-L., Shang G.-D., Zhao B., Gao J., Wang F.-X., Wang J.-W. (2024). Reciprocal conversion between annual and polycarpic perennial flowering behavior in the *Brassicaceae*. Cell **187**: 1–19.

Zhang L., Jiménez-Gómez J.M. (2020). Functional analysis of *FRIGIDA* using naturally occurring variation in *Arabidopsis thaliana*. The Plant Journal **103**: 154–165.

Zhao J., Favero D.S., Peng H., Neff M.M. (2013). *Arabidopsis thaliana* AHL family modulates hypocotyl growth redundantly by interacting with each other via the PPC/DUF296 domain. PNAS **110**: E4688–E4697.

Supplementary figures

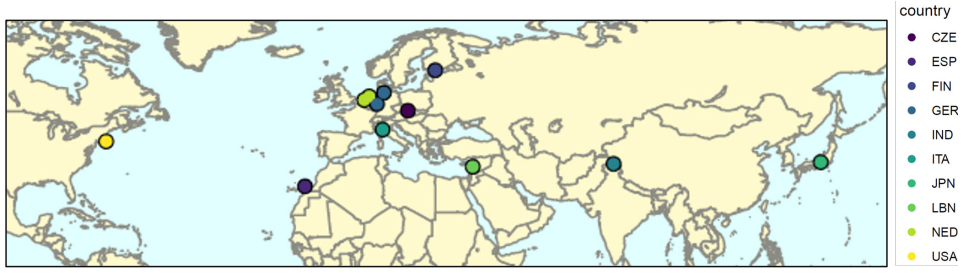

Name	Country	NASC ID
Amel-1	NED	N76434
Br-0	CZE	N76455
Do-0	GER	N76474
Es-0	FIN	N76484
Gifu-2	JPN	N76494
Had-1b	LBN	N76509
Hh-0	GER	N76512
Kas-2	IND	N78905
Mr-0	ITA	N78474
Mv-0	USA	N76556
Tha-1	NED	N76611
Can-0	ESP	N28130

Supplementary Figure 1: Geographical origin of the 12 AR ecotypes. Seeds were retrieved from the Nottingham Arabidopsis Stock Centre (NASC).

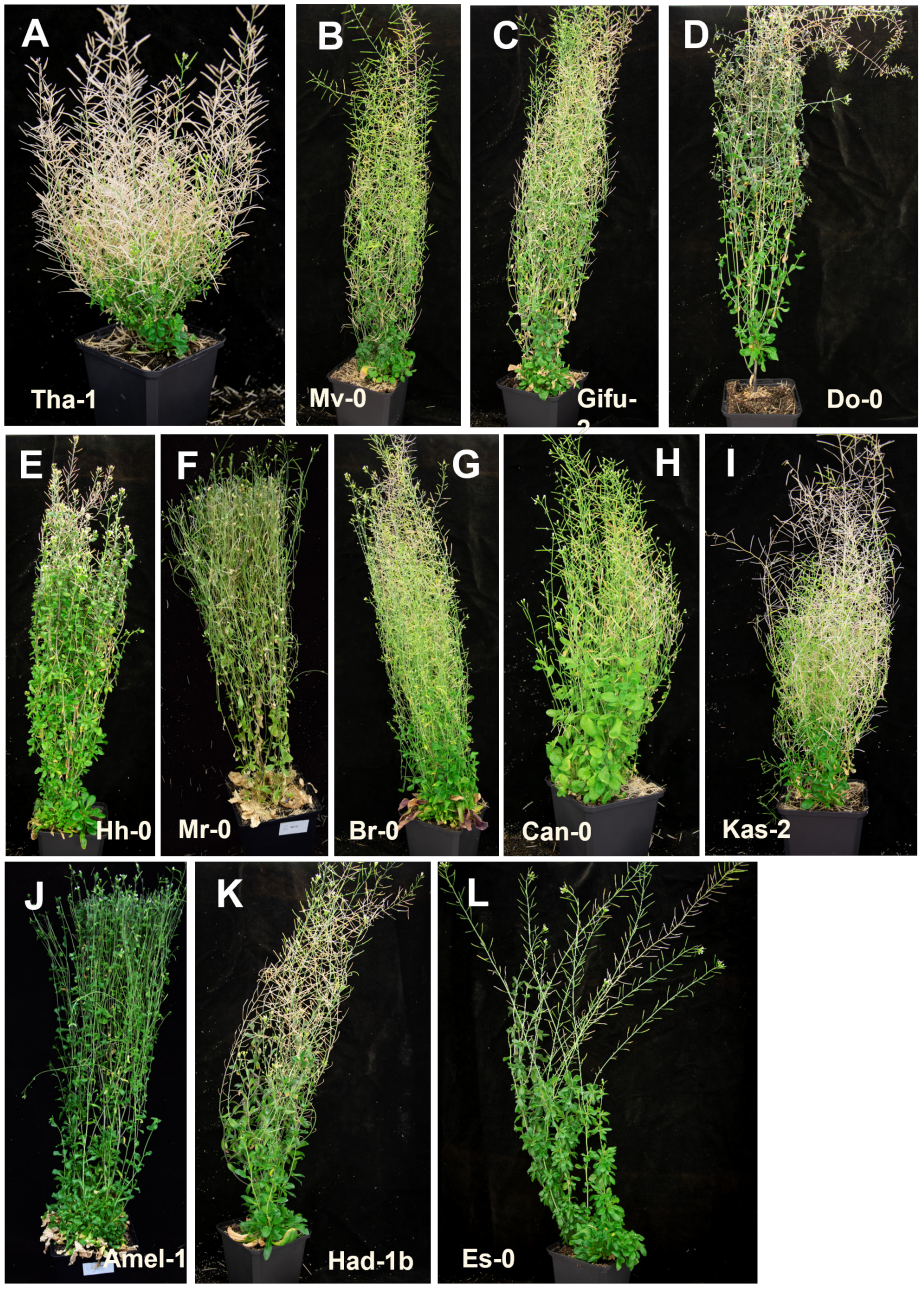

Supplementary figure 2: Phenotypes of 6-month old AR ecotypes grown in long day conditions. The ecotypes are arranged according to the percentage of IAMs forming ARs. Col-0 (not included) had completely senesced at this time point. All pots are 11 cm wide.

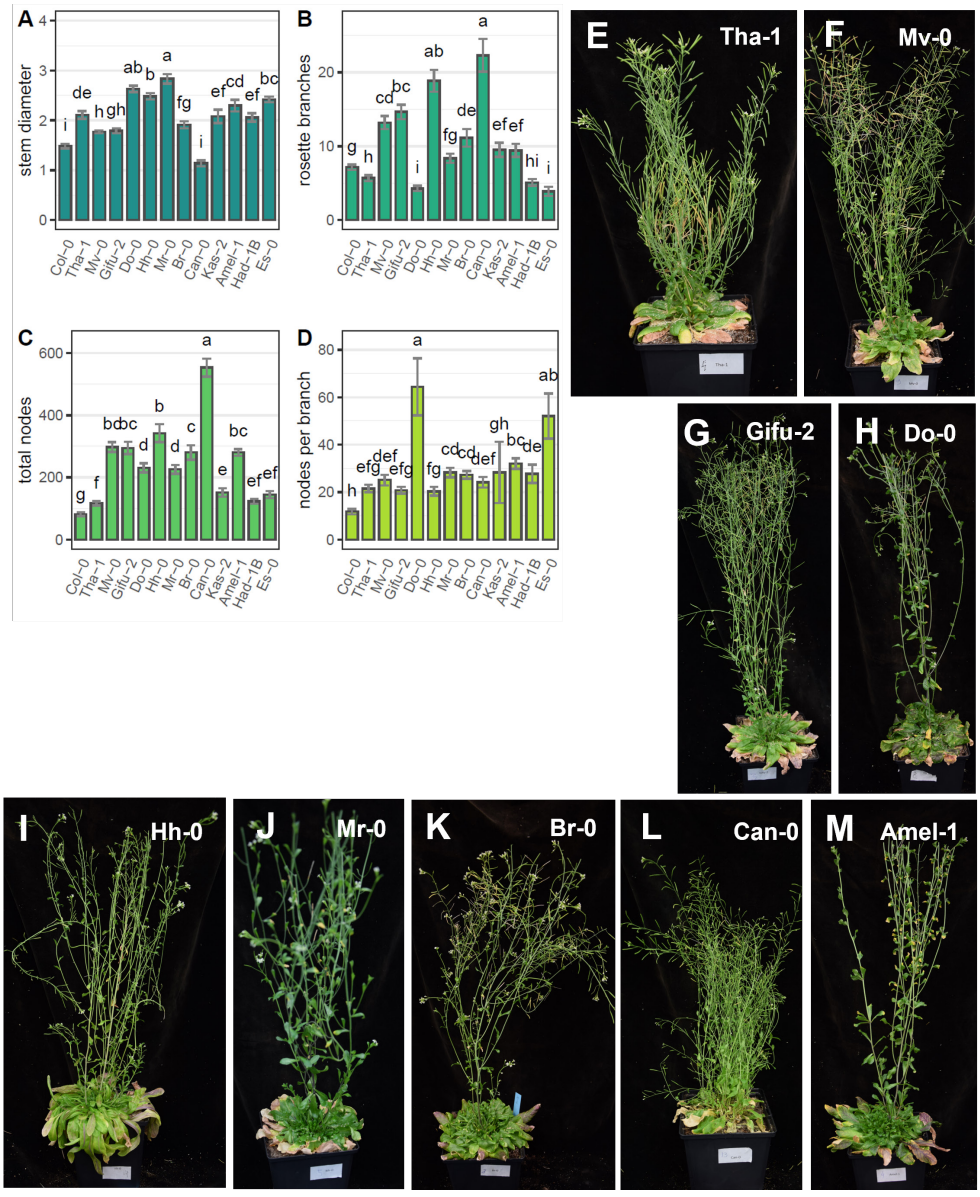

Supplementary figure 3: Phenotypes of AR ecotypes at five weeks after bolting. **A**: the stem diameter below the first node in mm. **B**: the number of rosette branches. **C**: the total number of influencerence axillary mersitems (IAMs). **D**: the number of inflorescence nodes/IAMs per rosette branch (total number of nodes divided by the number of rosette branches). Phenotypes in **A-D** were all measured at five weeks after bolting and were based on measurements in 10-15 plants per ecotype. Measurements were compared between ecotypes with the Kruskall-Wallis test, and significantly different groups are indicated by Chapter 2 different letters. **E-M**: Inflorescence phenotypes of 9 AR ecotypes at five weeks after bolting. All pots have a width of 11 cm.

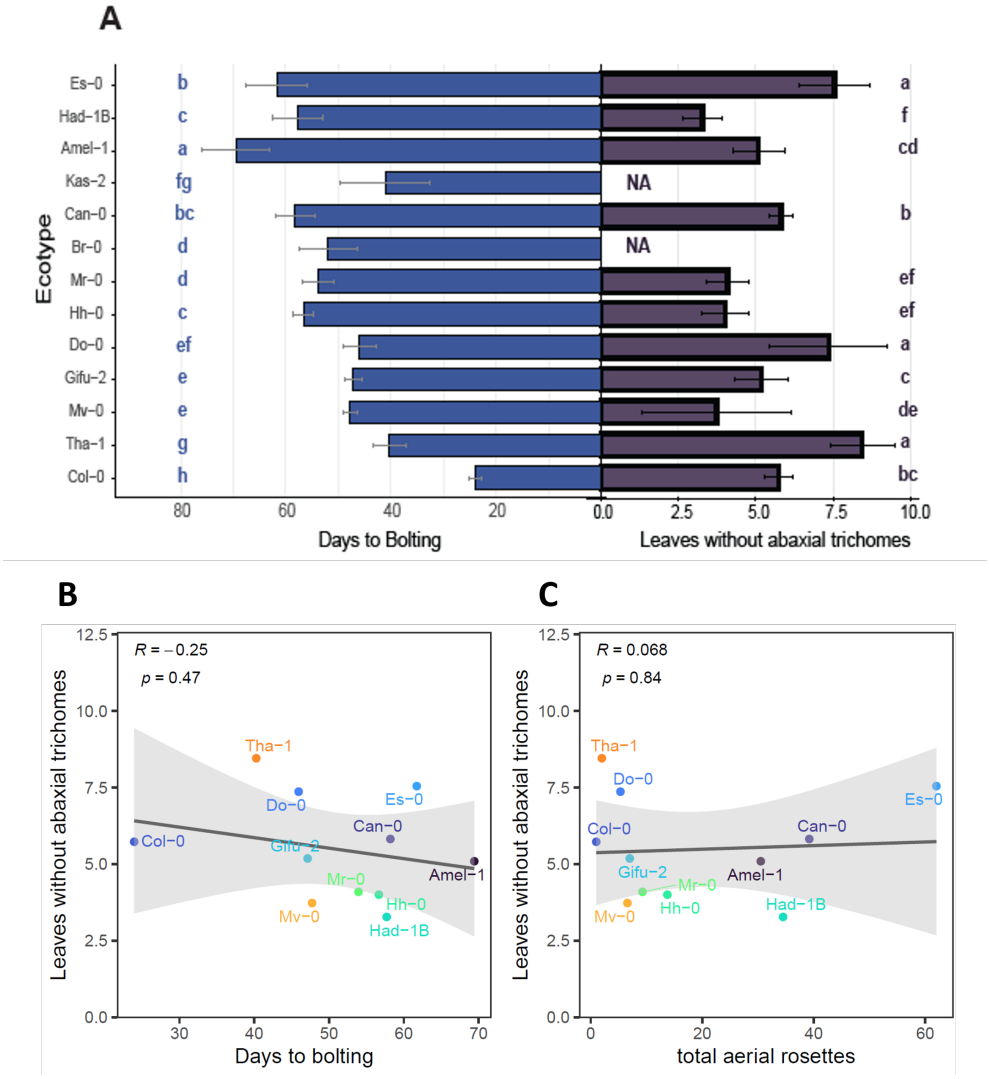

Supplementary figure 4: Juvenile leaves (leaves without abaxial trichomes) in AR ecotypes. **A**: days to bolting and the number of juvenile leaves. Ecotypes Br-0 and Kas-2 do not produce abaxial trichomes on juvenile or adult leaves, and could therefore not be phenotyped for this trait. Measurements were compared between ecotypes with the Kruskall-Wallis test; letters indicate significance groups and error bars show the standard error of the mean. **B-C:** Pearson's correlation between bolting time and juvenile leaf number (**B**) and the total number of aerial rosettes and juvenile leaf number (**C**) showing that bolting time and aerial rosette number do not correlate with the number of juvenile leaves. Measurements in A are based on 10-15 plants each, and average values for each value were entered in the correlation analysis.

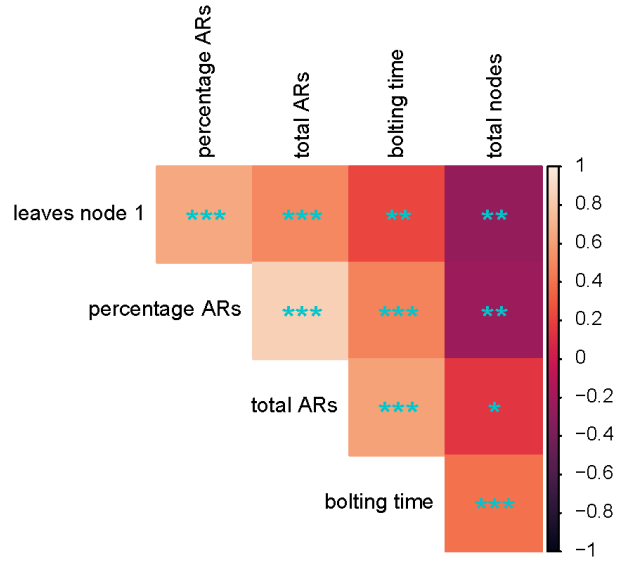

Supplementary figure 5: Heatmap showing Pearson's correlation analysis between phenotypes at five weeks after bolting. Average values for each phenotype were entered in the analyses and were each based on 10-15 plants per ecotype. Blue stars indicate significance levels (*: p<0.05, **: p<0.01, ***: p<0.01) and colors are scaled to Pearson's R.

Supplementary figure 6 (right): Expression of *AHL15, AHL20*, and *FLC* at different developmental stages (juvenile (JUV), rosette base at bolting (RBB), inflorescence axillary meristem (IAM) at five weeks after bolting). **A-C**: Expression of *AHL15* in JUV (**A**), RBB (**B**), and in the IAM (**C**). **D-F**: Expression of *AHL20* in JUV (**D**), RBB (**E**), and in the IAM (**F**). **G**: Comparison of expression of *AHL15* in JUV, RBB, and IAM tissue. **H**: Comparison of expression of *AHL20* in JUV, RBB, and IAM tissue. **I-K**: Expression of *FLC* in JUV (**I**), RBB (**J**), and IAM tissue (**K**). Expression was measured in three samples per ecotype, and each sample consisted of tissue collected from three plants. Differences in expression were calculated between the ecotypes and Col-0 by student's t-test, stars indicate significant differences (*: p<0.05, **: p<0.01) and error bars represent the standard error of the mean.

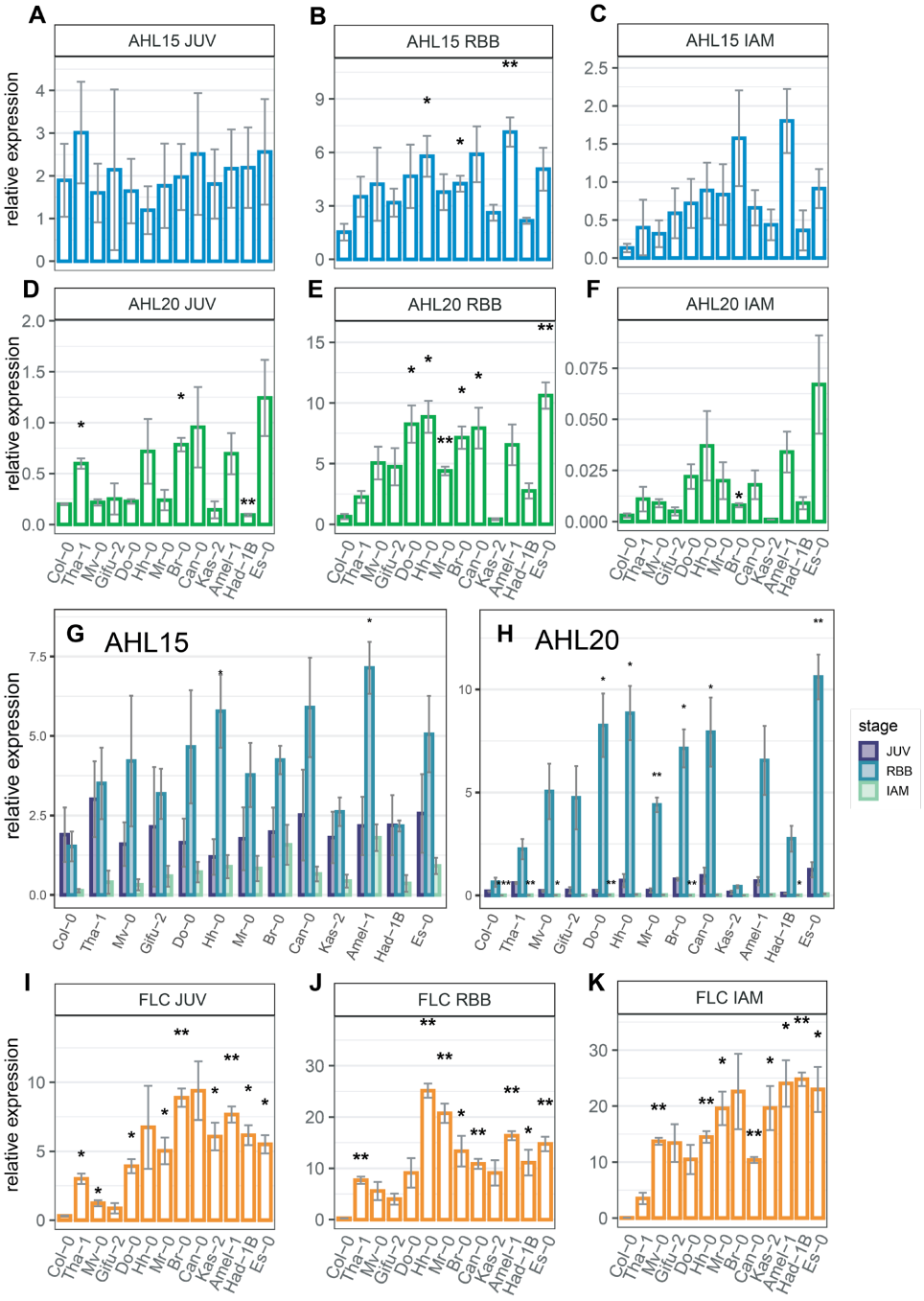
A
AHL15 JUV
B
AHL15 RBB
C
AHL15 IAM
D
AHL20 JUV
E
AHL20 RBB
F
AHL20 IAM
G
AHL15
H
AHL20
I
FLC JUV
J
FLC RBB
K
FLC IAM
relative expression
stage
JUV
RBB
IAM
Col-0
Tha-1
Mv-0
Gifu-2
Do-0
Hh-0
Mr-0
Br-0
Can-0
Kas-2
Amel-1
Had-1B
Es-0

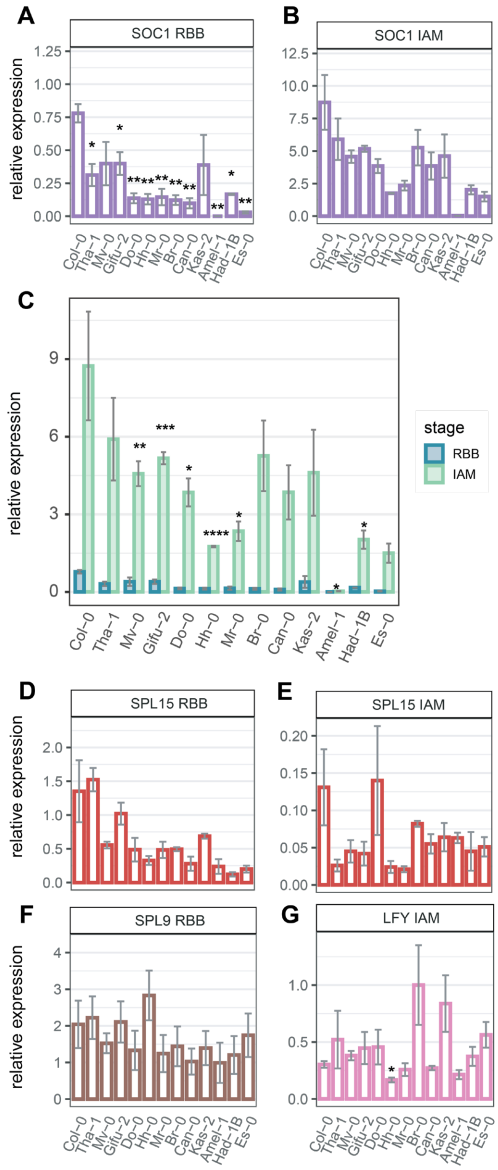

Supplementary figure 7: Expression of *SOC1, SPL15, SPL9* and *LFY* at different developmental stages (Rosette base at bolting (RBB), inflorescence axillary meristem at five weeks after bolting (IAM)). **A-C**: Expression of *SOC1* in the RBB (**A**) or in the IAM (**B**) or both RBB and IAM (**C**). **D-E**: Expression of *SPL15* in the RBB (**D**) or the IAM (**E**). **F**: Expression of *SPL9* in the RBB. **G**: Expression of *LFY* in the IAM. Expression was measured in three samples per ecotype, and each consisted sample of tissue collected from three plants. Differences in expression were calculated between the ecotypes and Col-0 by t-test, stars indicate significant differences (*: p<0.05, **: p<0.01, ***: p<0.001), and error bars show the standard error of the mean.

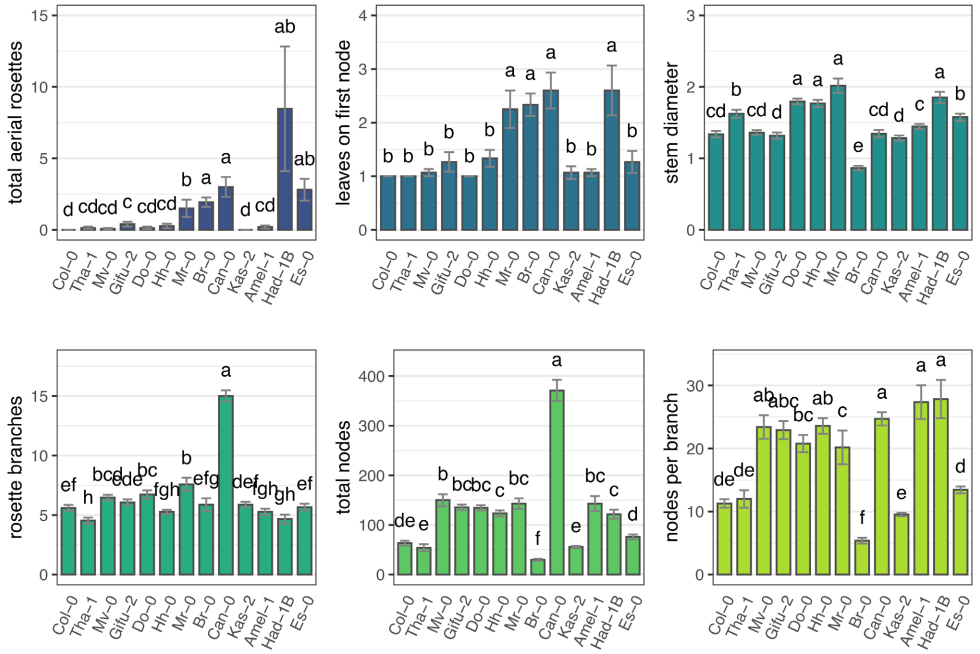

Supplementary figure 8: Phenotypic analysis of vernalized plants at five weeks after bolting. **A**: The total number of inflorescence nodes bearing three or more cauline leaves (ARs). **B**: The number of leaves on the first inflorescence node. **C**: The diameter of the central stem beneath the first inflorescence node in mm. **D**: The number of rosette branches. **E**: The total number of inflorescence nodes/AMs. **F**: The number of inflorescence nodes per branch, calculated by dividing the total number of nodes by the total number of rosette branches. For each phenotypic trait, 10-15 plants per ecotype were measured. Measurements between ecotypes were compared by Kruskall-Wallis test. Significantly different groups are indicated by different letters and error bars show the standard error of the mean.

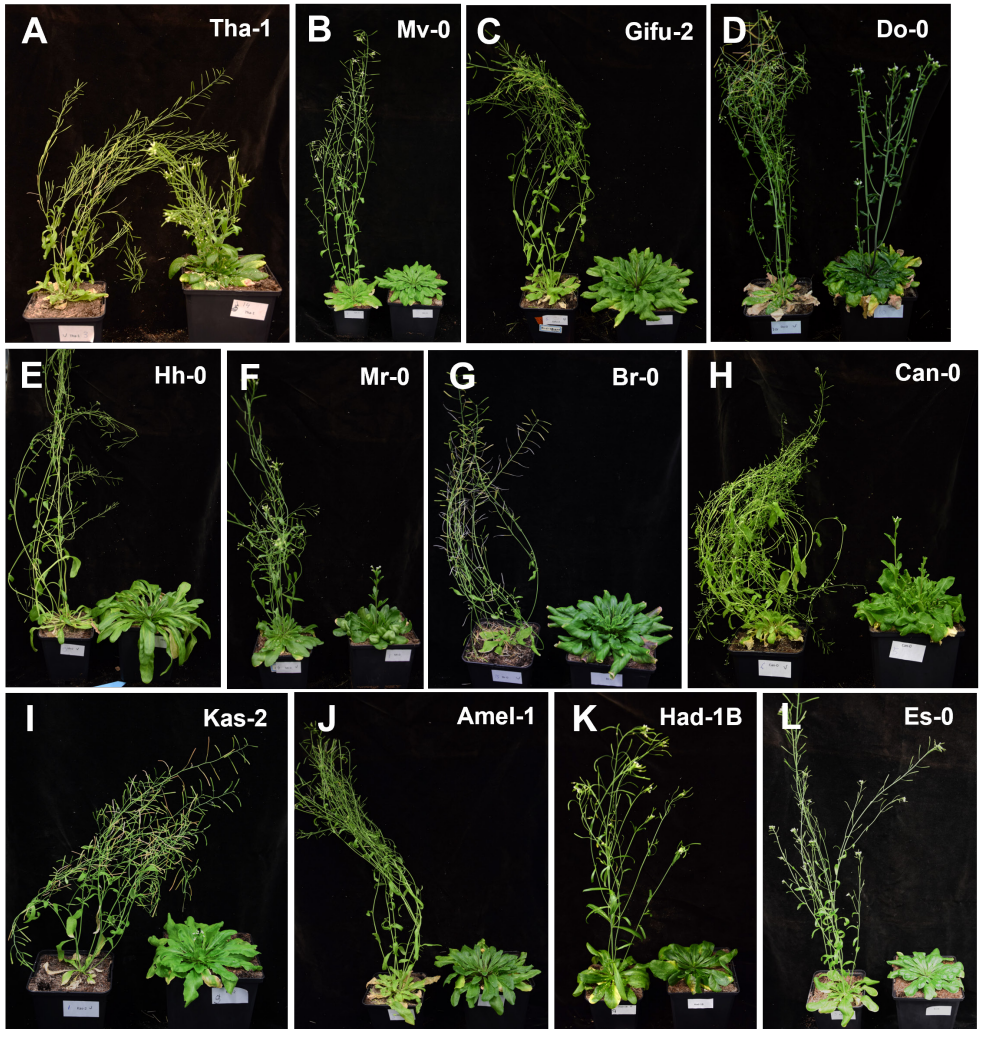

Supplementary figure 9: Phenotypes of vernalized AR ecotypes at five weeks after bolting (left) and non-vernalized plants of the same ecotype at the same age (right). Ecotypes are arranged by ascending percentage of ARs at five weeks after bolting in non-vernalized conditions. Pots of vernalized plants (left) are 9 cm wide and pots of non-vernalized plants (right) are 11 cm wide.

Supplementary data

Supplementary table 1: Pearson's correlation coefficients between phenotypic and gene expression data in non-vernalized ecotypes. Significant negative correlations are indicated in blue and significant positive correlations are given in red.

variable 1	variable 2	*R*	R^2	*p*
bolting time	SOC1 IAM	**-0.92**	0.85	0.000007
bolting time	SOC1 RBB	**-0.91**	0.83	0.000016
total ARs	percentage ARs	**0.88**	0.78	0.000070
leaves node 1	percentage ARs	**0.88**	0.77	0.000074
SOC1 IAM	SOC1 RBB	**0.85**	0.72	0.000239
bolting time	SPL15 RBB	**-0.83**	0.69	0.000455
SOC1 IAM	SPL15 RBB	**0.82**	0.67	0.000625
AHL20 IAM	AHL20 RBB	**0.80**	0.63	0.001137
AHL15 RBB	AHL20 RBB	**0.79**	0.62	0.001457
FLC IAM	SPL15 RBB	**-0.78**	0.60	0.001762
SOC1 IAM	FLC RBB	**-0.77**	0.60	0.001868
AHL20 IAM	AHL15 RBB	**0.77**	0.59	0.002249
SPL15 RBB	SOC1 RBB	**0.77**	0.59	0.002306
bolting time	FLC IAM	**0.76**	0.58	0.002574
bolting time	AHL15 RBB	**0.76**	0.57	0.002719
AHL15 RBB	SOC1 RBB	**-0.75**	0.57	0.003011
FLC IAM	SOC1 IAM	**-0.75**	0.56	0.003215
FLC RBB	SOC1 RBB	**-0.75**	0.56	0.003396
AHL20 IAM	SOC1 IAM	**-0.74**	0.55	0.003754
AHL20 RBB	SOC1 RBB	**-0.73**	0.54	0.004234
AHL20 IAM	FLC RBB	**0.71**	0.50	0.006837
AHL20 IAM	SOC1 RBB	**-0.70**	0.49	0.007409
AHL15 IAM	AHL15 RBB	**0.70**	0.49	0.007524
bolting time	FLC RBB	**0.70**	0.48	0.008220
bolting time	total ARs	**0.69**	0.48	0.008656
bolting time	AHL20 IAM	**0.69**	0.48	0.009014
total ARs	leaves node 1	**0.69**	0.48	0.009055
total ARs	SPL15 RBB	**-0.68**	0.47	0.010245
FLC IAM	SOC1 RBB	**-0.67**	0.45	0.011443
AHL15 IAM	SOC1 RBB	**-0.67**	0.45	0.011969
bolting time	AHL20 RBB	**0.67**	0.45	0.012265
SOC1 IAM	AHL15 RBB	**-0.67**	0.45	0.012596
percentage ARs	FLC IAM	**0.67**	0.45	0.012694
bolting time	AHL15 IAM	**0.65**	0.43	0.015347
total nodes	AHL15 RBB	**0.65**	0.42	0.015788
total ARs	FLC IAM	**0.65**	0.42	0.016543
FLC RBB	SPL15 RBB	**-0.62**	0.39	0.022478
AHL20 RBB	SPL15 RBB	**-0.62**	0.39	0.023480
leaves node 1	FLC IAM	**0.61**	0.37	0.026699
total ARs	SOC1 RBB	**-0.61**	0.37	0.027645
AHL15 RBB	FLC RBB	**0.60**	0.36	0.031237
total ARs	SOC1 IAM	**-0.59**	0.35	0.032747
total ARs	AHL20 IAM	**0.58**	0.34	0.036836
AHL15 IAM	FLC RBB	**0.57**	0.32	0.042782

AHL20 IAM	SPL15 RBB	**-0.56**	0.31	0.047552
SOC1 IAM	AHL20 RBB	-0.55	0.30	0.050741
AHL15 RBB	SPL15 RBB	-0.55	0.30	0.051516
FLC IAM	FLC RBB	0.54	0.29	0.056104
FLC RBB	AHL20 RBB	0.54	0.29	0.058275
AHL15 IAM	FLC IAM	0.54	0.29	0.058622
AHL15 IAM	SOC1 IAM	-0.54	0.29	0.058622
total nodes	AHL20 RBB	0.54	0.29	0.059483
percentage ARs	SPL15 RBB	-0.53	0.28	0.061831
total ARs	AHL20 RBB	0.52	0.27	0.066967
AHL15 IAM	AHL20 RBB	0.51	0.26	0.073259
leaves node 1	AHL20 IAM	0.49	0.24	0.085683
percentage ARs	SOC1 IAM	-0.49	0.24	0.085863
bolting time	percentage ARs	0.49	0.24	0.088578
SPL9 RBB	SPL15 RBB	0.49	0.24	0.090275
SPL15 IAM	FLC RBB	-0.48	0.23	0.095469
percentage ARs	AHL20 IAM	0.48	0.23	0.096703
AHL15 IAM	AHL20 IAM	0.47	0.22	0.109286
bolting time	SPL15 IAM	-0.46	0.21	0.115731
bolting time	total nodes	0.46	0.21	0.117051
AHL15 IAM	SPL15 RBB	-0.45	0.20	0.120279
leaves node 1	SOC1 IAM	-0.44	0.19	0.132496
SOC1 IAM	SPL15 IAM	0.44	0.19	0.134263
leaves node 1	SPL15 RBB	-0.44	0.19	0.136517
percentage ARs	SOC1 RBB	-0.43	0.19	0.140733
FLC IAM	SPL9 RBB	-0.43	0.19	0.141592
leaves node 1	SOC1 RBB	-0.43	0.18	0.143615
total nodes	SPL15 RBB	-0.41	0.17	0.166515
total ARs	AHL15 RBB	0.41	0.17	0.167474
total nodes	SOC1 RBB	-0.40	0.16	0.172873
AHL20 IAM	FLC IAM	0.39	0.15	0.188801
leaves node 1	FLC RBB	0.37	0.14	0.210644
leaves node 1	total nodes	-0.37	0.14	0.212089
bolting time	SPL9 RBB	-0.37	0.14	0.214437
FLC IAM	AHL20 RBB	0.36	0.13	0.229296
SPL9 RBB	SOC1 RBB	0.36	0.13	0.230107
leaves node 1	LFY IAM	0.36	0.13	0.233347
total ARs	SPL9 RBB	-0.35	0.12	0.245555
bolting time	leaves node 1	0.34	0.12	0.251103
total nodes	AHL15 IAM	0.33	0.11	0.265257
percentage ARs	AHL20 RBB	0.33	0.11	0.270420
total ARs	FLC RBB	0.33	0.11	0.272554
SPL15 IAM	SOC1 RBB	0.33	0.11	0.274754
leaves node 1	AHL20 RBB	0.32	0.10	0.288613
FLC IAM	SPL15 IAM	-0.32	0.10	0.289916
AHL20 IAM	LFY IAM	-0.31	0.10	0.295563
FLC IAM	AHL15 RBB	0.30	0.09	0.319850
SOC1 IAM	SPL9 RBB	0.30	0.09	0.320981
FLC IAM	LFY IAM	0.29	0.08	0.337974
SOC1 IAM	LFY IAM	0.29	0.08	0.343096

AHL15 IAM	SPL9 RBB	-0.28	0.08	0.346542
total nodes	LFY IAM	-0.28	0.08	0.353776
total nodes	FLC RBB	0.27	0.07	0.365457
total nodes	percentage ARs	-0.27	0.07	0.367042
LFY IAM	AHL15 RBB	-0.27	0.07	0.378106
total nodes	SOC1 IAM	-0.25	0.06	0.406558
total ARs	AHL15 IAM	0.24	0.06	0.423353
percentage ARs	FLC RBB	0.22	0.05	0.467809
percentage ARs	LFY IAM	0.21	0.04	0.496996
SPL15 IAM	SPL9 RBB	-0.20	0.04	0.507845
total nodes	AHL20 IAM	0.20	0.04	0.510321
total ARs	SPL15 IAM	-0.20	0.04	0.510530
LFY IAM	FLC RBB	-0.20	0.04	0.510959
AHL20 IAM	SPL15 IAM	-0.20	0.04	0.511028
total nodes	SPL15 IAM	-0.20	0.04	0.518925
percentage ARs	SPL9 RBB	-0.20	0.04	0.522352
SPL15 IAM	AHL15 RBB	-0.19	0.04	0.533598
total nodes	SPL9 RBB	-0.19	0.03	0.543956
LFY IAM	SPL15 IAM	0.17	0.03	0.570269
bolting time	LFY IAM	-0.17	0.03	0.573146
percentage ARs	SPL15 IAM	-0.17	0.03	0.580095
leaves node 1	SPL15 IAM	-0.17	0.03	0.583464
total ARs	total nodes	0.16	0.03	0.600188
AHL15 RBB	SPL9 RBB	-0.16	0.03	0.600703
SPL15 IAM	SPL15 RBB	0.15	0.02	0.618937
AHL15 IAM	LFY IAM	0.12	0.01	0.701505
LFY IAM	SPL9 RBB	-0.10	0.01	0.750270
LFY IAM	SPL15 RBB	0.10	0.01	0.753373
AHL20 IAM	SPL9 RBB	0.08	0.01	0.792394
total ARs	LFY IAM	0.08	0.01	0.796683
percentage ARs	AHL15 RBB	0.08	0.01	0.804599
LFY IAM	AHL20 RBB	-0.07	0.00	0.822797
SPL15 IAM	AHL20 RBB	-0.05	0.00	0.860349
leaves node 1	SPL9 RBB	-0.05	0.00	0.873601
FLC RBB	SPL9 RBB	0.04	0.00	0.901335
AHL15 IAM	SPL15 IAM	-0.03	0.00	0.916355
percentage ARs	AHL15 IAM	0.03	0.00	0.931908
leaves node 1	AHL15 RBB	0.02	0.00	0.947784
leaves node 1	AHL15 IAM	-0.01	0.00	0.977059
total nodes	FLC IAM	0.01	0.00	0.977901
AHL20 RBB	SPL9 RBB	-0.01	0.00	0.982716
LFY IAM	SOC1 RBB	0.00	0.00	0.995843

Supplementary table 2A: contributions of phenotype- and gene expression variables to the principal component analysis shown in Figure 4.

Variable	Dim.1	Dim.2	Dim.3	Dim.4	Dim.5
SOC1_RBB	14.11	0.54	0.00	0.29	0.45
SOC1_IAM	13.72	0.06	4.30	3.14	0.65
SPL15_RBB	11.46	3.66	0.33	6.48	11.76
FLC_RBB	10.77	3.10	4.50	2.27	0.86
AHL15_RBB	10.60	2.61	8.78	0.17	18.04
AHL20_RBB	9.65	2.59	16.33	1.41	5.01
AHL20_IAM	8.85	7.14	4.46	0.65	20.90
AHL15_IAM	8.80	3.10	4.82	7.91	28.47
FLC_IAM	8.41	13.93	10.33	1.24	4.16
SPL15_IAM	1.86	7.21	45.87	3.02	4.02
SPL9_RBB	1.33	32.35	0.07	24.78	3.10
LFY_IAM	0.46	23.71	0.21	48.63	2.61

Supplementary table 2B: Contributions of the individual ecotypes to the principal component analysis shown in Figure 4.

Ecotype	Dim.1	Dim.2	Dim.3	Dim.4	Dim.5
Col-0	38.26	1.77	9.27	3.60	0.75
Amel-1	18.18	1.16	1.64	5.46	25.52
Es-0	12.50	1.03	2.65	5.28	39.03
Tha-1	8.89	9.06	1.49	8.66	9.58
Hh-0	7.54	39.71	0.92	4.53	0.24
Gifu-2	4.62	1.15	0.81	2.11	0.43
Kas-2	4.07	14.89	8.07	2.83	0.89
Mr-0	2.21	0.09	14.22	2.59	2.33
Mv-0	1.47	0.05	0.66	3.60	0.16
Can-0	1.40	0.07	3.01	12.94	3.15
Br-0	0.75	22.92	3.71	34.81	3.69
Had-1B	0.07	6.67	22.16	9.88	11.28
Do-0	0.04	1.44	31.38	3.70	2.94

Supplementary table 3: RT-qPCR primers used to measure gene expression in this study.

name*	sequence (5' to 3')	function
PP2A-3-Q-fw	ACGTGGCCAAAATGATGCAA	reference gene for RT-qPCR
PP2A-3-Q-rev	TCATGTTCTCCACAACCGCT	reference gene for RT-qPCR
AHL15-Q-fw	CTGAGCGGTAGTGGTTTGGT	RT-qPCR of AHL15
AHL15-Q-rev	AGGAGAGCCAGACGTAGGAA	RT-qPCR of AHL15
AHL20-Q-fw	GGCGGCTCAAGACAGATTCA	RT-qPCR of AHL20
AHL20-Q-rev	AGTAAGGTGGTCTTGCGTGG	RT-qPCR of AHL20
AHL19 Q-fw	CTCTAACGCGACTTACGAGAGATT	RT-qPCR of AHL19
AHL19 Q-rev	ATATTATACACCGGAAGTCCTTGGT	RT-qPCR of AHL19
FLC Q-fw	TGACTAGAGCCAAGAAGACCG	RT-qPCR of FLC
FLC Q-rev	AGTCACCGGAAGATTGTCGG	RT-qPCR of FLC
SOC1 Q-fw	AGCTGCAGAAAACGAGAAGC	RT-qPCR of SOC1
SOC1 Q-rev	TGAAGAACAAGGTAACCCAATG	RT-qPCR of SOC1
LFY-Q-fw	TCATTTGCTACTCTCCGCCG	RT-qPCR of LFY
LFY-Q-rev	CGGTTCCTCAGATAACCCTGT	RT-qPCR of LFY
SPL9-Q-fw	AATTGGCGACTCAAACTGTG	RT-qPCR of SPL9
SPL9-Q-rev	CTGAAGAAGCTCGCCATGTA	RT-qPCR of SPL9
SPL15-Q-fw	TGAATGTTTTATCACATGGAAGCTC	RT-qPCR of SPL15
SPL15-Q-rev	TCATCGAGTCGAAACCAGAAGATG	RT-qPCR of SPL15

* fw: forward, rev: reverse

Chapter 3

GreenLeafVI: An ImageJ plugin for high-throughput analysis of leaf chlorophyll content

Thalia Luden[1†], Jelmer van Lieshout[1†], Sarah Mehrem[3], Basten Snoek[3], Joost Willemse[2], Remko Offringa[1]

[1] Plant Developmental Genetics and [2] Cell Observatory, Institute of Biology Leiden, Leiden University, Sylviusweg 72, 2333 BE Leiden, The Netherlands

[3] Bioinformatics, Biodynamics and Biocomplexity, Utrecht University, Padualaan 8, 3584 CH Utrecht, The Netherlands

[†] These authors contributed equally to this work

Abstract

Leaf chlorophyll content is a strong predictor of plant health, and chlorophyll breakdown is a central process during leaf senescence. Chlorophyll quantification can be done in several ways, many of which are time-consuming or require specialized equipment. An alternative to this is the use of image-based chlorophyll estimation, which relies on the color values in RGB images that are used to calculate colorimetric visual indexes that indicate the leaf chlorophyll content. Image-based chlorophyll measurement is non-destructive and apart from a digital camera requires no specialized equipment. Here, we developed the ImageJ plugin GreenLeafVI that facilitates high-throughput image analysis for measuring leaf chlorophyll content. Our plugin offers the option to white-balance images to decrease variation between images, and has an optional background removal step. We show that this method can reliably quantify leaf chlorophyll content in a variety of plant species. In addition, we show that image-based chlorophyll quantification can replicate GWAS results based on traditional chlorophyll extraction methods, showing that this method is highly accurate.

Keywords: ImageJ, chlorophyll, leaf senescence, image-based chlorophyll quantification, high-throughput phenotyping

Introduction

Plant health can in many cases be deducted from the leaf chlorophyll (Chl) content, as several stressing factors can affect the photosynthetic capacity of plants. Chl content can be reduced by, for example, drought and salt stress, nutrient deficiency, pathogen infection, and other stressors (Hörtensteiner and Kräutler, 2011). Quantification of Chl is therefore an important tool to monitor plant health in a variety of conditions. Various methods for measuring Chl content can be applied, such as acetone-based Chl isolation followed by photospectrometry at 645 nm and 663 nm (Arnon, 1949), SPAD (Soil Plant Analysis Development) measurement (Yadava, 1986; Markwell et al., 1995; Konica Minolta Optics, 2009), Chl fluorescence measurement (Murchie and Lawson, 2013; Legendre et al., 2021), hyperspectral imaging (Zhang et al., 2022a; Taha et al., 2024), and image-based colorimetric visual index (CVI) estimations of Chl (Ali et al., 2012; Bresson et al., 2018; Guendouz et al., 2021). The acetone-based Chl extraction method directly measures the Chl content, and is one of the most accurate ways to quantify Chl. However, this method is labor-intensive and destructive, and requires specialized equipment to measure the OD_{645} and OD_{663}. Due to the destructive nature of this method, it is also poorly suited to monitor Chl content over a plant's development. Chl measurements with a SPAD meter are non-destructive, but SPAD measurements remain labor-intensive, as each measurement needs to be recorded manually, and SPAD values are strongly affected by the position on the leaf where the measurements are made. In addition, the SPAD meter can only be used on leaves above a certain size, which excludes the possibility to measure young or small leaves, or plants grown in tissue culture that need to remain in sterile conditions. Chl fluorescence measurements and hyperspectral imaging methods are non-destructive and can yield useful information, but require specialized equipment that can be expensive and are therefore not universally available to researchers. In addition, measuring Chl fluorescence makes use of the photo-saturation of Chl followed by a cool-down period, which makes this type of measurement relatively time-consuming. In contrast, image-based Chl quantification methods require only the use of a digital camera and uniform lighting, are non-destructive, and are highly adaptable to different environments and experimental setups. Because no specialized equipment is required, image-based Chl estimation can readily be applied in any environment and is almost universally available to all researchers. Moreover, digital images can be easily processed in batch, allowing high-throughput monitoring of Chl content in a variety of experimental setups (Prakash Yadav et al., 2010; Zhang et

al., 2018; Fernando Sánchez-Sastre et al., 2020; Guo et al., 2020; Özreçberoğlu and Kahramanoğlu, 2020; Guendouz et al., 2021; Zhang et al., 2022a; Taha et al., 2024).

Image-based Chl estimation relies on the relative pixel intensity in the Red, Green, and Blue channels of RGB images, from which Chl content can be deduced by using different mathematical models. Alternatively, values in the hue saturation value color-space (HSV) can be measured (Bresson et al., 2018). Various studies have shown the usefulness of RGB image analysis and their derived CVIs in estimating Chl content in different species, and strong correlations with total Chl content have been shown for many plant species. For example, Kawashima and Nakatani (1998) showed that the Chl content of wheat and rye leaves could be measured by using a video camera, and showed that the best predictor of Chl content was the normalized difference between the Red and Blue values (R-B)/(R+B), henceforth referred to as the Kawashima index. Other well-performing models that were tested by Kawashima and Nakatani include the normalized Red, Green, and Blue indexes (R/(R+G+B), G/(R+G+B), B/(R+G+B)), and the difference between red and blue divided by the sum of all channels ((R-B)/(R+G+B)). Ali et al. (2012) showed that the Kawashima index correlated strongly with SPAD-502 readings in tomato, and Taha et al. (2024) showed the same in hydroponically-grown lettuce. Similarly, Fernando Sánchez-Sastre et al. (2020) showed that the highest-scoring models tested by Kawashima and Nakatani (1998) also showed a strong correlation with Chl content in sugar beet leaves. On the other hand, Ibrahim et al. (2021) and Ali et al. (2012) found that the Green : Red ratio (G:R) correlated to Chl content in lettuce more strongly than the Kawashima index. Other researchers have used custom models to link the RGB color values to Chl content. For example, Prakash Yadav et al. (2010) showed that Chl content could be accurately measured in micro-propagated potato by using RGB images as well as by the hue, saturation, and intensity values derived from these images, and a similar approach was used in Sorghum by Zhang et al. (2022a). Other applications of the RGB color space have also been applied, for example by Govindasamy et al. (2017) who used RGB images to monitor the symbiosis efficiency between rhizobia and soybean plants, and Bu et al. (2024) who used RGB parameters to measure soybean pod freshness. Han et al. (2021) used aerial images to monitor the growth of *Hibiscus cannabinus* based on RGB-derived parameters, and Barraza-Moraga et al. (2022) applied RGB analysis to satellite images in order to estimate the Chl-A content of algae in lake Lanalhue in Chile. Overall, these examples show that analysis of RGB images can successfully be applied in plant research and

is a feasible method of Chl measurement.

The open-source software FIJI is a distribution of the image analysis program ImageJ, which is a commonly used and highly customizable tool for image analysis in the life sciences (Schindelin et al., 2012). FIJI offers possibilities to automate analysis steps via the use of macros or custom-made plugins. In order to enhance the throughput of RGB image analysis, we developed the FIJI plugin called Green Leaf Visual Index (GreenLeafVI) that can perform multiple steps of RGB analysis in batch mode for a large number of images. GreenLeafVI offers the option to normalize image brightness, segment images to reduce background noise, and calculate the RGB values of multiple objects per image along with various methods of leaf Chl content estimation for a large number of images, allowing for high-throughput analysis. The output data is stored in a tidyR-compatible format that can readily be used for further statistical analysis in R or other statistics software. We show that GreenLeafVI can be applied for measuring Chl content of different plant species, and can accurately reproduce GWAS results obtained by traditional Chl measurement methods in lettuce, validating its use for high-throughput phenotyping experiments.

Methods

Plant materials and growth conditions

Arabidopsis thaliana (Arabidopsis) ecotype Col-0 seeds were sown on humid soil (90% turf, 10 % sand) and stratified at 4 °C for three days, and subsequently transferred to a growth chamber with long day conditions (16h light / 8h dark) at 21 °C and 65 % relative humidity. Seedlings were repotted to individual pots after 7 days, and the fifth leaf of each plant was harvested at 23 days after the end of stratification. Leaves incubated for 0-5 days in the dark were used for senescence measurements to represent various stages of leaf senescence.

For testing the correlation between colorimetric measurements and chlorophyll content, *Lactuca sativa* (lettuce) cv. Cobham green seeds were sterilized in 50% bleach solution and stratified in distilled water for 4 days at 4 °C. Subsequently, seeds were sown on moist soil (90% turf, 10 % sand) and transferred to a growth chamber with long day conditions (16h light / 8h dark) at 21 °C and 70 % relative humidity. The fourth leaf was harvested ten days after emergence, and 30 mm Ø leaf disks were taken and incubated on demineralized water with 1% agarose in the dark for up to 5 days. Leaves subjected to different dark incubation periods were used for senescence measurements to represent a range of senescence stages. For the GWAS experiment, lettuce seeds of 184

cultivars were treated as described above, and leaf disks of the fourth leaf were taken at 10 days after emergence and used directly for imaging and chlorophyll extraction.

Nicotiana benthamiana (tobacco) seeds were sown on moist soil (90% turf, 10 % sand) in a growth chamber with long day conditions (16h light / 8h dark) at 21 °C and 70 % relative humidity. After seven days, seedlings were repotted to individual pots. After three weeks, mature leaves were detached and incubated in large petri dishes on demineralized water with 1% agarose in the dark for up to seven days.

Solanum lycopersicum (tomato) cv. Moneymaker seeds were sterilized in bleach and germinated on solid MS medium, and transferred to soil after three weeks. Plants were grown in long days conditions (16h light/8h dark) at a 24 °C day / 18 °C night temperature regime. Leaves were harvested from flowering plants and incubated in large petri dishes on demineralized water with 1% agarose in the dark for up to seven days, with harvesting points between 0-7 days of dark incubation.

Senescence induction, imaging, and chlorophyll isolation

Arabidopsis leaves were floated on 5 mM MES buffer (pH 5.6) in 5 cm petri dishes sealed with parafilm, wrapped in aluminium foil, and kept at 21 °C for up to five days. Lettuce, tomato, and tobacco leaves were harvested at various ages and placed in petri dishes with demineralized water with 0.5% agarose, sealed with parafilm, wrapped in aluminium foil, and stored at 21 °C for up to 7 days. Leaves were imaged at different time points between 0 and 7 days of dark incubation and leaf disks were collected for chlorophyll extraction after imaging. All images were taken with a Nikon DC3000 DSLR camera under uniform white light. Plant leaves were placed on a homogenous white or black background along with a white square that served as a reference for image brightness.

Chlorophyll extraction was performed according to the protocol of Arnon et al. (1949). Briefly, 5 mm diameter round leaf disks were taken after imaging (2 for Arabidopsis, 3 for other species) and placed in a 96-well deepwell plate along with a metal bead and stored at -80 °C until extraction. For extraction, the leaf tissue was pulverized and resuspended in 200 µL 25 mM sodium phosphate buffer (pH 7) and 800 µL 80% (v/v) acetone. Samples were then incubated at room temperature in the dark for 1 hour with gentle shaking and centrifuged for 10 minutes at 3000 *g*. 200 µL of the supernatant was then transferred to a 96-well transparent-bottom plate and the absorption (D) at 645nm and 663

nm was measured with a TECAN reader. The total chlorophyll content in mg/L was then calculated with the following formula: $Chl_{Total} = 20{,}2 \cdot D_{645} + 8{,}02 \cdot D_{663}$ as described by Arnon (1949), and the amount of Chl in one mL (the extraction volume for each sample) was divided over the total area of leaf tissue used for extraction.

Image analysis

All images were analyzed using the FIJI distribution of ImageJ (Schindelin et al., 2012), with the custom GreenLeafVI plugin that can perform white balancing, automatic selection of leaves and removal of background, and RGB pixel intensity measurements semi-automatically. The plugin is described in detail in Supplementary protocol 1, and Figure 1 shows a schematic overview of the steps performed by the plugin.

White balancing

In order to calibrate the image brightness and reduce inter-image variation, we normalized the pixel intensity to the white reference area included in each image (Figure 1). This was done by splitting the image into Red, Green, and Blue channels and automatic measurement of the mean pixel intensity in the white reference area. Next, the pixel adjustment factor for each of the channels was calculated by dividing the maximum brightness (255 for 8-bit images) by the mean pixel intensity of the white area (adjustment factor = 255/mean). The white reference was then set to an intensity of 255 in all three channels, and the pixels outside of the reference area were normalized based on the adjustment factor for each channel, and re-stacked into an RGB image with a "_whitebalanced" suffix for further analysis.

Segmentation of images to reduce background

In order to exclude measurements of non-leaf objects or areas in the background of the image, we included an optional segmentation step in the GreenLeafVI plugin (Figure 1). The segmentation step extracts leaf-like objects from the background by creating a mask covering the leaves based on HSV and minimum area parameters, and removes the background by setting the pixel intensity outside of masked areas to 0. The HSV values used to distinguish leaves from the background were calibrated manually for each species. The images were then saved extended by a "_segmented" suffix for further analysis.

RGB analysis and color-based methods of chlorophyll estimation

To measure the R, G, and B pixel intensities of individual objects in an image, a mask selecting individual objects was made like in the segmentation step. The original image was then split into Red, Green, and Blue channels and the minimum, maximum, median, and mean pixel intensity was measured in each object of the mask covering the leaves (Figure 1). The mean values of each leaf measured in the Red, Green, and Blue channels were used to calculate the different visual indexes: Green:Red ratio (GR_ratio), Red:Green ratio (RG_ratio), Kawashima index (Kawashima), Green Leaf Index (GLI), Normalized Difference Index (NDI), normalized Red (Red_norm), normalized Green (Green_norm), normalized Blue (Blue_norm), and the Woebbecke index (Woebbecke).

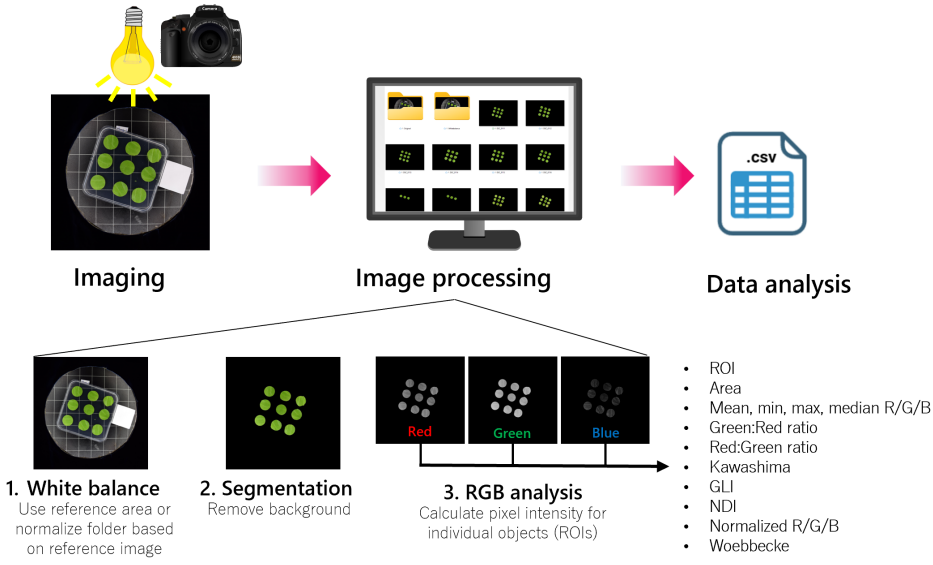

Figure 1: Workflow for high-throughput chlorophyll measurement with GreenLeafVI. Images are taken under homogeneous light with a white reference area. The images are then batch-processed for **1**) white-balancing based on the white reference area; **2)** segmentation to remove the background; and **3)** measurement of pixel intensity in the Red, Green, and Blue channels. The results of the RGB analysis are stored in a results.csv file which, in addition to the RGB values, also contains the region of interest (ROI) ROI, the area of the objects, and several colorimetric visual indeces (CVIs).

Data analysis

Correlation analyses

Data generated by the ImageJ plugin and from spectrophotometry results were analyzed in R (R Core Team, 2023). Pearson's correlation analysis between

the different colorimetric indexes and the total Chl content as mg Chl / cm^2 was performed with the R package psych (William Revelle, 2023), and plots were generated by using the ggplot2 (Wickham, 2016) and ggpubr packages (Kassambara, 2023).

GWAS analysis

SNP data was obtained from Dijkhuizen et al. (2024). Kinship was computed as the covariance matrix of SNPs using the cov() function in R. SNPs were filtered for a MAF > 0.05. For GWAS, we used R version 4.2.2 and the lme4QTL package (Ziyatdinov et al., 2018). GWAS was performed on the filtered SNP set using a linear mixed model (relmatLmer and matlm), with the kinship matrix included as a random effect. The Bonferroni method was used to correct for multiple testing, with the Bonferroni-corrected significance threshold being -log10(0.05/2,485,803) > 7.69. Manhattan plots were created using ggplot (Wickham, 2016). Quantile-Quantile (Q-Q) plots were created using the ggfastman R-package (Tremmel, 2021). The genome annotation and gene function prediction of the Salinas reference genome V8 were used for annotation of significantly associated loci (Reyes-Chin-Wo et al., 2017).

Results and discussion

Normalized Red and Green:Red ratio are accurate predictors of chlorophyll content in leaves

We designed the Green Leaf Visual Index (GreenLeafVI) plugin as a tool to easily phenotype the Chl content in different plant species. We therefore ran the three steps of the GreenLeafVI plugin (white balancing, segmentation, and RGB analysis) on four different plant species: *Arabidopsis thaliana* (Arabidopsis), *Nicotiana benthamiana* (tobacco), *Solanum lycopersicum* (tomato), and *Lactuca sativa* (lettuce). In addition, we extracted chlorophyll from each imaged leaf by a classical method in order to test how well the different CVIs measured by the GreenLeafVI plugin correlated to the actual Chl content. Our data show that several CVIs show a strong correlation with the total Chl content for these different plant species. Figures 2A-D show the correlation between the total Chl content in $mg \cdot cm^{-2}$ and the best scoring CVI for each of the four species (Pearson's correlation). Our results show that the CVI-based prediction of Chl is most accurate for lettuce, and that the Green : Red ratio (G:R) and Normalized Difference Index (NDI) are the most robust Chl predictors for this species (Figure 2D, Table 1). For Arabidopsis, tobacco, and tomato the normalized Red

value (Rn; R/(R+G+B)) best predicted Chl content, although the G:R and NDI correlated significantly with the Chl content as well (Figure 2A-C, Table 1).

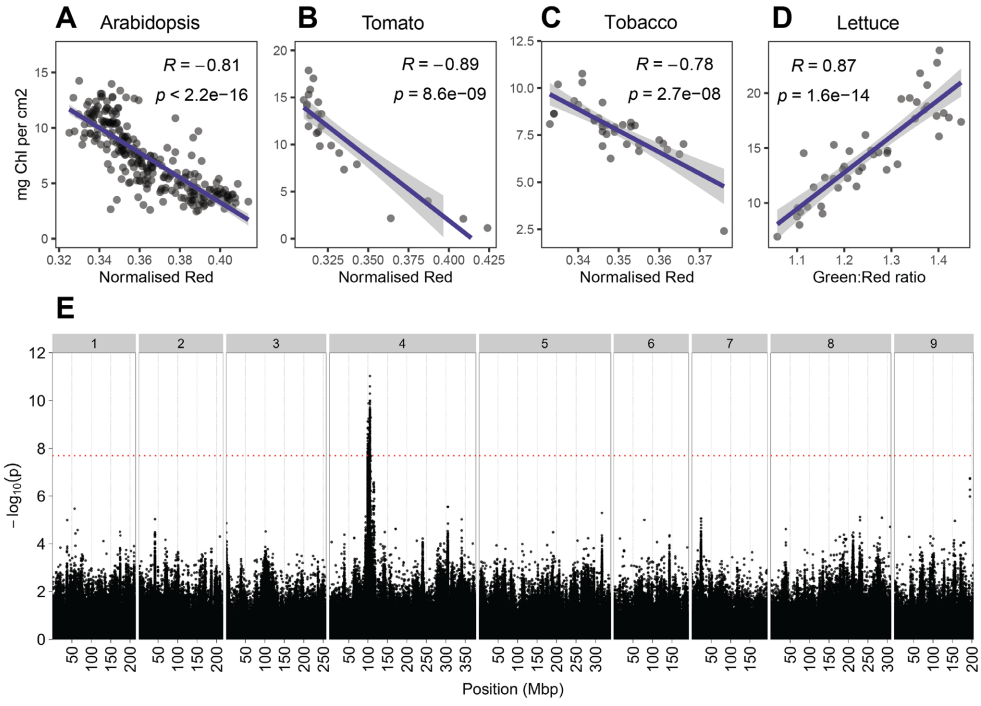

Figure 2: Application of CVIs for measuring chlorophyll content in different species. **A-D**: correlations between total Chl content as mg Chl/cm2 and the best-scoring CVI for each species. **A**: Arabidopsis, **B**: tomato and **C**: tobacco each show the strongest correlation between mg Chl·cm^{-2} and the normalized Red value (Rn). **D**: In lettuce, mg Chl·cm^{-2} correlates best with the Green : Red ratio (G:R). **E**: Manhattan plot of the GWAS on the Green : Red ratio measured on the fourth leaf of 184 lettuce cultivars. Genomic position, indicated in mega base pairs, is shown on the x-axis, chromosome numbers are indicated on top. Significance as – log10(p) is shown on the y-axis. The Bonferroni threshold of -log10(p) > 7.69 is indicated by the red horizontal line.

Table 1: Correlations of various CVIs with the chlorophyll content in mg Chl/cm2 (Pearson's correlation). In the formula column, R, G, and B stand for average Red, Green, and Blue pixel intensity values.

		Arabidopsis		Tomato		Tobacco		Lettuce	
Index	***Formula***	***R***	***p value***	***R***	***p value***	***R***	***p value***	***R***	***p value***
Green:Red ratio	G/R	0.73	7.35E-46	0.87	4.55E-08	0.62	6.09E-05	**0.87**	**1.61E-14**
Kawashima Index	(R-B)/(R+B)	-0.42	9.63E-13	-0.76	2.00E-05	-0.05	0.7600	0.46	0.0016
Normalized Red (Rn)	R/(R+G+B)	**-0.79**	**6.16E-60**	**-0.89**	**8.62E-09**	**-0.78**	**2.72E-08**	-0.82	5.92E-12
Normalized Green (Gn)	G/(R+G+B)	0.49	2.08E-17	0.71	0.0001	0.48	0.0034	0.81	3.11E-11
Normalized Difference Index (NDI)	(Rn-Gn)/(Rn+Gn+0.01)	-0.72	2.09E-45	-0.87	4.45E-08	-0.62	4.98E-05	**-0.87**	**1.37E-14**
Green Leaf Index (GLI)	(2G-R-B)/(2G+R+B)	0.48	2.43E-17	0.71	9.10E-05	0.47	0.0034	0.81	2.60E-11
Woebbecke Index	(G-B)/(R-G)	-0.11	0.0794	0.24	0.2667	0.74	2.50E-07	0.78	6.00E-10

Surprisingly, the correlation between the Chl content and the Kawashima index was not as strong as in earlier reports, and was outperformed by G:R, NDI, and Rn in all four species. This could be because the pixel intensity in the green channel is not used to calculate the Kawashima Index, despite the fact that Chl appears green in colour. Each of the best-performing indexes included green pixel intensity in their formulas. However, greenness alone is not sufficient to accurately predict Chl content, as the normalized Green value (Gn; G/(R+G+B)) showed only a moderate correlation with the Chl content. In addition, the Woebbecke Index correlated very poorly with the total Chl content per cm^2. This is because the Woebbecke Index formula does not handle yellow colours well, resulting in extremely negative values for yellowing leaves due to high R and low G values. Although the Woebbecke Index might be suitable to compare greenness among healthy, non-senescent plants, it is unsuitable for quantifying Chl in senescent leaves and using other, more consistent indexes such as Rn or G:R is advisable. Because we used leaves at various stages of senescence (non-senescent up to completely senesced) in our experiments, our data are representative for an array of conditions. Previous research may have focused on measurement of Chl content in healthy, young plants only, and have omitted using senescent or otherwise yellow leaves in the calibration of the index, which could explain why some indexes perform less well than in previous studies. In conclusion, our data shows that several visual indexes perform well in predicting Chl content, and that the Rn, G:R, and NDI indexes are all reliable, with the most reliable one depending on the species.

In order to test whether visual indexes are sufficiently accurate to identify phenotypic differences between genotypes, we ran a Genome-Wide Association Study (GWAS) on leaf Chl content in lettuce and applied the plugin in a high-throughput manner to analyse 446 images at once. We then compared our method to a previous study that used chlorophyll extraction to identify loci controlling leaf Chl content in lettuce (Zhang et al., 2022b). We used a panel of 184 lettuce genotypes and imaged the fourth leaf at 10 days after emergence. We then used an extensive SNP dataset to run a GWAS on G:R (the best-performing CVI for lettuce) as a measure of Chl content. From this GWAS, a significant peak on chromosome 4 was identified (figure 2E), which corresponded to the peak found by Zhang et al. (2022b) in their GWAS on extracted Chl data. This peak is associated with the lettuce *Golden-Like (LsGLK)* gene, which is an important regulator of chloroplast development. The similarity in outcomes between the two GWASs shows that our G:R data can reproduce the association between the Chl content phenotype and the

SNP located near the *LsGLK* gene, indicating that G:R is not only an accurate measure of Chl content, but is also a reliable method to identify a phenotypic vs genotypic association. In addition, digital images can be re-examined at a later time and may provide additional information next to Chl content, whereas this information is lost when using destructive methods of Chl quantification. Since making digital images and automated image processing is less labor-intensive and less costly than large-scale Chl extraction, we propose that this method be used in future applications.

Author contributions

TL, JvL, and RO designed the experiments. TL and JvL performed Chl extraction experiments, and JvL performed lettuce phenotyping for GWAS. Correlation analyses were done by TL, and SLM and BS performed GWAS analysis. JvL, TL, and JW wrote the ImageJ scripts. TL wrote the manuscript with input from all other authors.

Acknowledgements

We thank Jan Vink, Ward de Winter and Mariel Lavrijsen for technical support and Marion Larue, Karin Verkerk, and Kim Roos for help with phenotyping. This work was supported the graduate school green top sectors grant (grant nr. GSGT.2019.024) from the Dutch Research Council (NWO) to TL.

Literature

Ali M.M., Al-Ani A., Eamus D., Tan D.K.Y. (2012). A new image processing based technique to determine chlorophyll in plants. J Agric & Environ Sci **12**: 1323–1328.

Arnon D.I. (1949). Copper enzymes in isolated chloroplasts. Polyphenoloxidase in *Beta Vulgaris*. Plant Physiol **24**: 1–15.

Barraza-Moraga F., Alcayaga H., Pizarro A., Félez-Bernal J., Urrutia R. (2022). Estimation of chlorophyll-a concentrations in Lanalhue lake using Sentinel-2 MSI satellite images. Remote Sens **14**: 5647.

Bresson J., Bieker S., Riester L., Doll J., Zentgraf U. (2018). A guideline for leaf senescence analyses: from quantification to physiological and molecular investigations. J Exp Bot **69**: 769–786.

Bu Y., Hu J., Chen C., Bai S., Chen Z., Hu T., Zhang G., Liu N., Cai C., Li Y., et al (2024). ResNet incorporating the fusion data of RGB & hyperspectral images improves classification accuracy of vegetable soybean freshness. Sci Rep **14**: 1–13.

Dijkhuizen R.F., Eijnatten A.L. van, Mehrem S.L., Bergh E.S. van den, Lieshout J. van, Spaninks K., Kaandorp S., Offringa R., Proveniers M., Ackerveken G. van den, et al (2024). From aerial drone to QTL: Leveraging next-generation phenotyping to reveal the genetics of color and height in field-grown *Lactuca sativa*. bioRxiv 2024.11.07.622452.

Fernando Sánchez-Sastre L., S Alte da Veiga N.M., Miguel Ruiz-Potosme N., Carrión-Prieto P., Luis Marcos-Robles J., Manuel Navas-Gracia L., Martín-Ramos P. (2020). Assessment of RGB vegetation indices to estimate chlorophyll content in sugar beet leaves in the final cultivation stage. AgriEngineering **2**: 128–149.

Govindasamy V., George P., Aher L., Ramesh S. V., Thangasamy A., Anandan S., Kumar Raina S., Kumar M., Rane J., Annapurna K., et al (2017). Comparative conventional and phenomics approaches to assess symbiotic effectiveness of *Bradyrhizobia* strains in soybean (Glycine max L. Merrill) to drought. Sci Rep. doi: 10.1038/s41598-017-06441-3

Guendouz A., Bendada H., Benniou R. (2021). A comparative study of chlorophyll content estimation in barley (*Hordeum vulgare L.*) genotypes based on RGB (Red, Green, Blue) image analysis. Agric Sci Digest **42**: 68–71.

Guo Y., Yin G., Sun H., Wang H., Chen S., Senthilnath J., Wang J., Fu Y. (2020). Scaling effects on chlorophyll content estimations with RGB camera mounted on a UAV platform using machine-learning methods. Sensors **20**: 5130.

Han G.D., Jang G.J., Kim J., Kim D.W., Rodrogues R., Kim S.H., Kim H.J., Chung Y.S. (2021). RGB images-based vegetative index for phenotyping kenaf (*Hibiscus cannabinus L.*). PLoS One **16**: e0256978.

Hörtensteiner S., Kräutler B. (2011). Chlorophyll breakdown in higher plants. BBA **1807**: 977–988.

Ibrahim N.U.A., Aziz A., Jamaludin S., Harith D. (2021). Development of smartphone-based imaging techniques for the estimation of chlorophyll content in lettuce leaves. Food Res **5**: 33–38.

Kassambara A. (2023). ggpubr: "ggplot2" Based Publication Ready Plots.

Kawashima S., Nakatani M. (1998). An algorithm for estimating chlorophyll content in leaves using a video camera. Ann Bot **81**: 49–54.

Konica Minolta Optics I. (2009). A lightweight handheld meter for measuring the chlorophyll content of leaves without causing damage to plants. SPAD-502Plus.

Legendre R., Basinger N.T., van Iersel M.W. (2021). Low-cost chlorophyll fluorescence imaging for stress detection. Sensors **21**: 1–17.

Markwell J., Osterman J.C., Mitchell J.L. (1995). Calibration of the Minolta SPAD-502 leaf chlorophyll meter. Photosynth Res **46**: 467–472.

Murchie E.H., Lawson T. (2013). Chlorophyll fluorescence analysis: a guide to good practice and understanding some new applications. J Exp Bot **64**: 3983–3998.

Özreçberoglu N., Kahramanoglu I. (2020). Mathematical models for the estimation of leaf chlorophyll content based on RGB colours of contact imaging with smartphones: A pomegranate example. Folia Hortic **32**: 57–67.

Prakash Yadav S., Ibaraki Y., Dutta Gupta S. (2010). Estimation of the chlorophyll content of micropropagated potato plants using RGB based image analysis. Plant Cell Tiss Organ Cult **100**: 183–188.

R Core Team (2023). R: A Language and Environment for Statistical Computing.

Reyes-Chin-Wo S., Wang Z., Yang X., Kozik A., Arikit S., Song C., Xia L., Froenicke L., Lavelle D.O., Truco M.J., et al (2017). Genome assembly with in vitro proximity ligation data and whole-genome triplication in lettuce. Nature Communications 2017 8:1 **8**: 1–11.

Schindelin J., Arganda-Carreras I., Frise E., Kaynig V., Longair M., Pietzsch T., Preibisch S., Rueden C., Saalfeld S., Schmid B., et al (2012). Fiji: an open-source platform for biological-image analysis. Nat Meth **9**: 676–682.

Taha M.F., Mao H., Wang Y., ElManawy A.I., Elmasry G., Wu L., Memon M.S., Niu Z., Huang T., Qiu Z. (2024). High-Throughput analysis of leaf chlorophyll content in aquaponically grown lettuce using hyperspectral reflectance and RGB images. Plants **13**: 392.

Tremmel R. (2021). ggfastman 1.2.0. https://github.com/roman-tremmel/ggfastman,

Wickham H. (2016). ggplot2: Elegant Graphics for Data Analysis.

William Revelle (2023). psych: Procedures for Psychological, Psychometric, and Personality Research. https://cran.r-project.org/package=psych

Yadava U.L. (1986). A Rapid and Nondestructive Method to Determine Chlorophyll in Intact Leaves. HortScience **21**: 1449–1450.

Zhang H., Ge Y., Xie X., Atefi A., Wijewardane N.K., Thapa S. (2022a). High

throughput analysis of leaf chlorophyll content in sorghum using RGB, hyperspectral, and fluorescence imaging and sensor fusion. Plant Methods **18**: 1–17.

Zhang J., Li M., Sun Z., Liu H., Sun H., Yang W. (2018). Chlorophyll content detection of field maize using RGB-NIR camera. IFAC PapersOnLine **51**: 700–705.

Zhang L., Qian J., Han Y., Jia Y., Kuang H., Chen J. (2022b). Alternative splicing triggered by the insertion of a *CACTA* transposon attenuates *LsGLK* and leads to the development of pale-green leaves in lettuce. Plant J **109**: 182–195.

Ziyatdinov A., Vázquez-Santiago M., Brunel H., Martinez-Perez A., Aschard H., Soria J.M. (2018). lme4qtl: Linear mixed models with flexible covariance structure for genetic studies of related individuals. BMC Bioinformatics **19**: 1–5.

Supplementary Figures

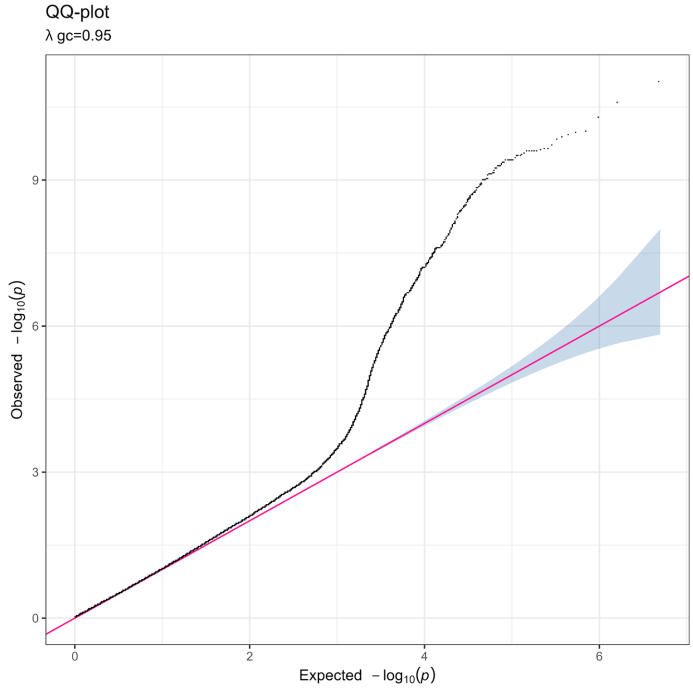

Supplementary figure 1: Quantile-Quantile plot for Green : Red ratio on the fourth leaf of 184 lettuce cultivars.

Supplementary protocol

Imaging setup and white balancing

The main limitation to image-based measurement is the variation in brightness and contrast between images. In order to calibrate the image brightness to reduce inter-image variation, we included an optional white-balancing step in the GreenLeafVI plugin (figure 1). The white-balancing step requires that a white reference area be photographed under the same conditions as the images to be analysed. This ensures that all images are white balanced to the same reference, reducing the variation in brightness between images that can arise from differential lighting or exposure settings during the imaging process. For this purpose, we recommend including a small white reference square or circle of a known size (e.g. 4 cm^2) in each of the images. This will serve as a reference for both the white balancing and for setting the image scale (via Analyze > set scale), which is useful for measuring the leaf area in addition to its Chl content. Alternatively, a single white reference area could be photographed at the start or end of the series of images to calibrate the entire set, assuming that lighting and exposure conditions are constant throughout the process.

When running the white balancing step, the user can select an input- and output folder and can select whether the images should be calibrated individually or batch-calibrated based on a single white reference image. Individual white balancing requires the user to select the reference area in each of the images and is therefore more time-consuming than the batch calibration, but is also more accurate and suitable for comparing images where the lighting, exposure, and focal distances are not constant. After the user has chosen whether to process images individually or in batch, the image is split into Red, Green, and Blue channels and the mean pixel intensity in the each channel is automatically calculated in the selected white area. Next, the pixel adjustment factor for each of the channels is calculated by dividing the maximum brightness of 8-bit images (255) by the mean pixel intensity of the white area (adj_factor = 255/mean). The white reference is then set to an intensity of 255 in all three channels, and the pixels outside of the reference area are then normalized based on the adjustment factor. Finally, the image is re-stacked to an 8-bit RGB image and saved in a folder selected by the user, and the image is saved under its original name with addition of a "_whitebalanced" suffix.

For optimal reproducibility between images, we recommend imaging under

constant lighting with a uniform background that shows sufficient contrast to the leaves that will be imaged such as a black, white, light blue, or orange background. In addition, variation between images can be further reduced by using the same focal distance between the camera and the leaves or plants that will be imaged throughout the process. If multiple objects are to be measured in one image, it is important that these do not overlap if a separate measurement of each object is desired.

Segmentation of images to reduce background

In order to exclude measurements of non-leaf objects or areas in the background of the image, we included an optional segmentation step in the GreenLeafVI plugin (figure 1). This process uses the difference in colour between the leaves and the background to extract only leaf-like objects. Because of this, the segmentation performs better when a background with an even colour that has sufficient contrast to the leaves is used during imaging, such as black, white, light blue, or orange. In order to run the segmentation process, the user needs to select an input- and output folder, and can adjust the settings for minimum object area, as well as minimum- and maximum values in the hue saturation value colour space (HSV). While the settings included in our plugin should perform well for any leaf-like object, we recommend that users customize these settings to the object of their interest to optimise segmentation performance. When the segmentation step is performed, a mask is created based on the HSV and minimum area inputs, and used to remove the background which is set to 0. The images are then saved in a folder selected by the user under their original name extended by a "_segmented" suffix.

RGB analysis and colour-based methods of chlorophyll estimation

The main feature of the GreenLeafVI plugin is the measurement of pixel intensity of individual objects (leaves) in the Red, Green, and Blue channels and the calculation of various colorimetric visual indexes (CVIs) from these data (figure 1C). The RedGreenBlue measurement can be run on all images saved in a single folder at once (we analyzed up to 446 images at a time), and the results are saved as a .csv file in the same folder. Images that can be used as input are preferably white-balanced and segmented, but the measurements can be run on unprocessed images as well, although this may result in poor identification of individual objects.

To measure the R, G, and B pixel intensities of individual objects in an image, a mask is made that selects individual objects in a similar manner as

in the segmentation step. It then splits the original image into Red, Green, and Blue channels and overlays the mask on each of the channels. The minimum, maximum, median, and mean pixel intensity of each object of the mask is then measured for each of the channels, and written to the results file. The mean values of the Red, Green, and Blue channels are used to calculate the different visual indexes that are used to estimate Chl content: Green:Red ratio (GR_ratio), Red:Green ratio (RG_ratio), Kawashima index (Kawashima), Green Leaf Index (GLI), Normalized Difference Index (NDI), normalized Red (Red_norm), normalized Green (Green_norm), normalized Blue (Blue_norm), and the Woebbecke index (Woebbecke). The results file also contains a column with the image name, the region of interest (ROI), which refers to individual objects in the image, their area, and an x- and y- coordinate that can be used to retrace to which object a measurement refers.

Since ImageJ scans for objects in a left-to-right and top-to-bottom order, the top left object will be the first to be detected and the bottom-right the last. This can be taken into account when preparing multiple leaves in one image, for example by making sure that the objects are ordered top-to-bottom or by arranging the objects in a diagonal from left to right (figure 1). Alternatively, each leaf or plant can be imaged individually. For high-throughput purposes, we advise creating a metadata file that links the image name to the content of the image, which can then be merged with the results file for further analysis.

Chapter 4

The plant longevity gene *AHL15* inhibits leaf senescence by repressing *ORESARA1* and cytokinin degradation

Thalia Luden[1], Petra Amakorová[3], Ondřej Novák[3], Salma Balazadeh[2], Remko Offringa[1]

[1] Plant Developmental Genetics and [2] Plant Stress Biology, Institute of Biology Leiden, Leiden University, Sylviusweg 72, 2333 BE Leiden, the Netherlands
[3] Laboratory of Growth Regulators, Faculty of Science, Palacký University and Institute of Experimental Botany, The Czech Academy of Sciences, CZ-77900 Olomouc, Czech Republic

Abstract

The *Arabidopsis thaliana* (Arabidopsis) *AT-HOOK MOTIF NULCEAR LOCALIZED15 (AHL15)* gene is associated with various longevity phenotypes and extends the life span of plants when overexpressed. Here, we show that, in addition to previously described longevity phenotypes, constitutive overexpression of *AHL15* in Arabidopsis delays leaf senescence, whereas *ahl15* loss-of-function accelerates this process. Dexamethasone-induced nuclear localization of AHL15-GR during dark-triggered senescence results in a stay-green phenotype and represses the expression of several early senescence-associated genes. Among these, the *ORESARA1* (*ORE1*) locus is directly bound by AHL15, implying a direct repressive effect of AHL15 on senescence. In addition, we show that AHL15 acts by directly repressing the expression of several *CYTOKININ OXIDASE* (*CKX*) genes involved in cytokinin inactivation, resulting in a delayed degradation of cytokinins during dark-induced senescence. Cytokinins are known to inhibit senescence, and together with the downregulation of *ORE1* expression, this explains the repressive effect of *AHL15* on senescence.

Keywords: AHL15, leaf senescence, ORESARA1, Cytokinin, CKX

Introduction

Leaf senescence is the process during which the photosynthetic machinery of leaves is catabolized and recycled for use in other parts of the plant (Lim et al., 2007a; Schippers et al., 2015; Guo et al., 2021). It is the final developmental stage of leaves, and its progression is tightly controlled by various transcription factors (TFs) among which the NAC-family TFs ORESARA1 (ORE1) and NAC-LIKE, ACTIVATED BY AP3/PI (NAP) (Guo and Gan, 2006; Kim et al., 2009; Qiu et al., 2015). Loss-of-function of *ore1*, *nap,* or other positive regulators of senescence results in a stay-green phenotype (Guo and Gan, 2006; Kim et al., 2009), and ORE1 regulates the transcription of numerous genes in the senescence pathway (Balazadeh et al., 2010). Upon initiation of senescence, genes involved in chlorophyll degradation (also called chlorophyll catabolic genes) are upregulated by ORE1, NAP, and other TFs in the senescence pathway, and together the resulting enzymes degrade chlorophyll (Chl) into smaller molecules that can be exported to other tissues in the plant, resulting in the characteristic yellowing of senescent leaves (Qiu et al., 2015; Yang et al., 2015; Woo et al., 2019). The relocation of nutrients from older leaves to other parts of the plant can help regulate the availability and distribution of nutrients, and thereby increases a plant's chance of survival in times of nutrient scarcity (Schippers et al., 2015). However, when senescence negatively impacts the overall quality of a crop, such as in leafy vegetables or in ornamental plants, delayed senescence can be a desirable trait. Therefore, achieving improved control of leaf senescence is essential for enhancing crop quality.

Senescence can be induced by various factors, including leaf age, dark incubation, nutrient shortage, and the application of hormones such as ethylene, jasmonic acid (JA), abscisic acid (ABA), salicylic acid (SA), or strigolactones (SL) (Woo et al., 2019). Ethylene induces a signaling cascade that activates the TF ETHYLENE INSENSITIVE 3 (EIN3), which in turn promotes transcription of *ORE1* and *NAP* (Li et al., 2013; Kim et al., 2014), and dark incubation induces transcription of both *ORE1* and *EIN3* via PHYTOCHROME INTERACTING FACTOR4 (PIF4) and PIF5 (Song et al., 2014). In monocarpic plants, flowering also triggers leaf senescence, allowing the relocation of nutrients from leaves to seeds and thereby enhancing the offspring's chances of survival (Thomas, 2013). For example, in *Arabidopsis thaliana* (Arabidopsis), the whole plant senesces within a few weeks after flowering. This process is controlled by several TFs, among which MYB2 and FRUITFULL (FUL), and coincides with reduced production of the hormone cytokinin (CK) (Guo and Gan, 2011; Balanzà et al., 2018).

In contrast to most other plant hormones that induce senescence, CKs inhibit leaf senescence: exogenous CK application significantly delays leaf senescence (Richmond et al., 1957; Gan and Amasino, 1995). The senescence-inhibiting activity of CK is mediated by the CK receptor ARABIDOPSIS HISTIDINE KINASE 3 (AHK3), which phosphorylates ARABIDOPSIS RESPONSE REGULATOR 2 (ARR2) upon CK perception (Kim et al., 2006). ARR2 then promotes expression of *CYTOKININ RESPONSE FACTOR 6* (*CRF6*), a TF that negatively regulates leaf senescence via an unknown mechanism (Zwack et al., 2013). Loss-of-function mutants of *ahk3* show accelerated senescence phenotypes and the senescence-inhibiting effect of CK treatment is reduced in these plants as a result of their weakened ability to transduce CK signals (Kim et al., 2006). A similar phenotype can be seen in *crf6* mutants (Zwack et al., 2013).

CKs are synthesized predominantly by enzymes of the ISOPENTENYL TRANSFERASE (IPT) and LONELY GUY (LOG) families. IPT-family enzymes are responsible for adding a prenyl group to N^6 of ATP or ADP (Kakimoto, 2001; Takei et al., 2001). Additional enzymes such as CYP735A are involved in making changes to this prenyl group, thereby producing precursors to different CK variants (Argueso and Kieber, 2024). Biological activation of these CK precursors relies on the removal of the riboside group by LOG-family enzymes, which are highly redundant and of which LOG7 and LOG8 appear to be the most important in Arabidopsis (Kuroha et al., 2009; Tokunaga et al., 2012). CK degradation is predominantly accomplished by enzymes of the CYTOKININ OXIDASE/DEHYDROGENASE (CKX) class. CKX enzymes irreversibly cleave off the N^6 side chains from active CKs, thereby inactivating them permanently (Galuszka et al., 2000; Schmülling et al., 2003). Knockout of the rice *ckx11* gene causes a delay in leaf senescence, indicating that reduced CK degradation negatively affects senescence (Zhang et al., 2021a). On the other hand, overexpression of *LOG4* delays leaf senescence in Arabidopsis (Kuroha et al., 2009), and expression of the *Agrobacterium tumefaciens IPT* gene under the senescence-specific *SAG12* promoter delays leaf senescence in several crops (Gan and Amasino, 1995; Jordi et al., 2000; McCabe et al., 2001). Thus, leaf senescence can be regulated by controlling the expression of the CK biosynthesis genes of the *IPT* and *LOG* families and by regulating the expression of the CK-degrading *CKX* genes.

While CK plays an important role in senescence, the regulatory mechanisms that control CK-mediated inhibition of senescence remain elusive. So far, only two TFs that regulate CK levels during senescence have been identified: MYB2 and NAP. In wild type plants, *IPT* expression in the leaf is silenced by MYB2, whose expression increases with progressing age (Guo and Gan, 2011). It

was shown that *MYB2* expression in Arabidopsis and the legume *Caragana intermedia* can be repressed by proteins of the S40 family, and overexpression of *S40*-family genes results in enhanced CK levels and a stay-green phenotype (Yang et al., 2022). The expression of *CRF6* also decreases in older leaves through an unknown mechanism (Zwack et al., 2013). At the same time, *CKX3* expression is induced by the senescence-promoting TF NAP, resulting in enhanced CK degradation (Hu et al., 2021). The repression of *CKX* expression by NAP was observed in Arabidopsis and in Chinese cabbage, indicating that this pathway is conserved (Hu et al., 2021; Li et al., 2023). These results show a clear link between CK and age-induced senescence, but additional regulatory mechanisms that control the expression of CK biosynthesis- and degrading genes during the senescence process remain to be identified.

Previously, we identified the Arabidopsis gene *AT-HOOK MOTIF NUCLEAR LOCALIZED15* (*AHL15*) as a regulator of plant longevity: overexpression of *AHL15* in Arabidopsis resulted in an increased life span and flowering time and an enhanced vegetative development of axillary meristems, branching and secondary growth, whereas *ahl15* loss-of-function or perturbed *ahl* function reduced all these aspects (Karami et al., 2020; Rahimi et al., 2022b). CK levels were increased in stems of *AHL15* overexpressing plants, explaining the enhanced secondary growth and branching phenotypes in these plants (Rahimi et al., 2022b). In Arabidopsis, the *AHL* gene family is comprised of 29 members that are subdivided into two clades (clade A and B) (Zhao et al., 2014). Previous research has demonstrated that members of the clade A *AHL* subfamily, which includes *AHL15*, exhibit a high level of functional redundancy (Yun et al., 2012; Zhao et al., 2013; Karami et al., 2020). Lim et al. (2007b) showed that overexpression of the clade A member *AHL27* represses leaf senescence, whereas recently, the clade B member *AHL9* has been identified as a promoter of leaf senescence, suggesting that clade A and B AHLs may operate antagonistically (Lim et al., 2007b; Zhou et al., 2022).

Here, we show that similar to *AHL27,* overexpression of *AHL15* delays leaf senescence, while loss-of-function *ahl15* mutants exhibit early senescence. Our results show that the expression of several senescence marker genes is repressed when AHL15 activity is induced and that AHL15 directly binds to the *ORESARA1* locus, indicating that AHL15 directly inhibits the senescence developmental program. Additionally, we found that AHL15 binds upstream of the *CKX2*, *CKX3*, and *CKX5* genes, and that induction of AHL15 activity leads to nearly complete silencing of their expression. This silencing coincides with a slower decrease in CK levels during dark-induced senescence. Together,

our data reveal that AHL15 delays the senescence program through parallel pathways: By repressing expression of *ORE1* and by repressing *CKX* expression and subsequent CK degradation.

Results

AHL15 overexpression delays the onset of leaf senescence

Given that overexpression of *AHL15* extends overall plant longevity and because delayed senescence has previously been reported for *AHL27* overexpressing lines (Lim et al., 2007b), we tested whether a similar late-senescence phenotype could also be observed in *p35S:3xFLAG-AHL15* plants (hereafter referred to as *AHL15* OX). At 42 days after germination, the older leaves of Col-0 (wild type) and *ahl15* knockout plants started to senesce, whereas leaves of the same age in *3xFLAG-AHL15* overexpressing lines stayed green, indicating that senescence may indeed be delayed by *AHL15* overexpression (Figure 1A). To monitor this in more detail, we harvested fifth leaves of different plants at 21, 24, 27, 30, 34, and 36 days of emergence and used images of these leaves to measure the chlorophyll content through a recently developed colorimetric assay (Figure 1B). This assay measures the pixel intensity value in Red, Green, and Blue channels of digital images, which can be used to calculate the normalized Red value (Rn; Red/(Red+Green+Blue)). Previously, we have shown that this correlates well with the total Chl content of leaves (this thesis chapter 3). The progression of senescence in the fifth leaf was also delayed in *AHL15* OX plants, whereas its onset was not affected in *ahl15* loss-of-function plants (Figure 1). Next, we tested whether this delayed senescence was also visible upon senescence induction by dark incubation. In *AHL15* OX plants, dark-induced senescence of the fifth leaf was significantly delayed compared to wild type, which was reflected by both the Rn value and the total Chl content (Figure 2). In addition, *ahl15* loss-of-function plants showed a mild but significant reduction in Rn value and total Chl content compared to Col-0, supporting our finding that *AHL15* inhibits leaf senescence.

Overexpression of *AHL15* and other clade-A *AHLs* generally delays flowering time and vegetative phase change (Karami et al., 2020; Rahimi et al., 2022a). To evaluate the effects of *AHL15* overexpression on the senescence phenotype independently of other developmental processes, we used a dexamethasone (DEX)-inducible *p35S:AHL15-GR* line in which the AHL15-GR fusion protein translocates to the nucleus upon DEX treatment (Karami et al., 2020). To induce AHL15 activity in this line simultaneously with the senescence process, we

added 10 µM DEX to the MES buffer on which leaves were floated during the dark incubation period. DEX-treated *p35S:AHL15-GR* leaves showed a similar delayed senescence phenotype as *AHL15* OX leaves, whereas mock-treated

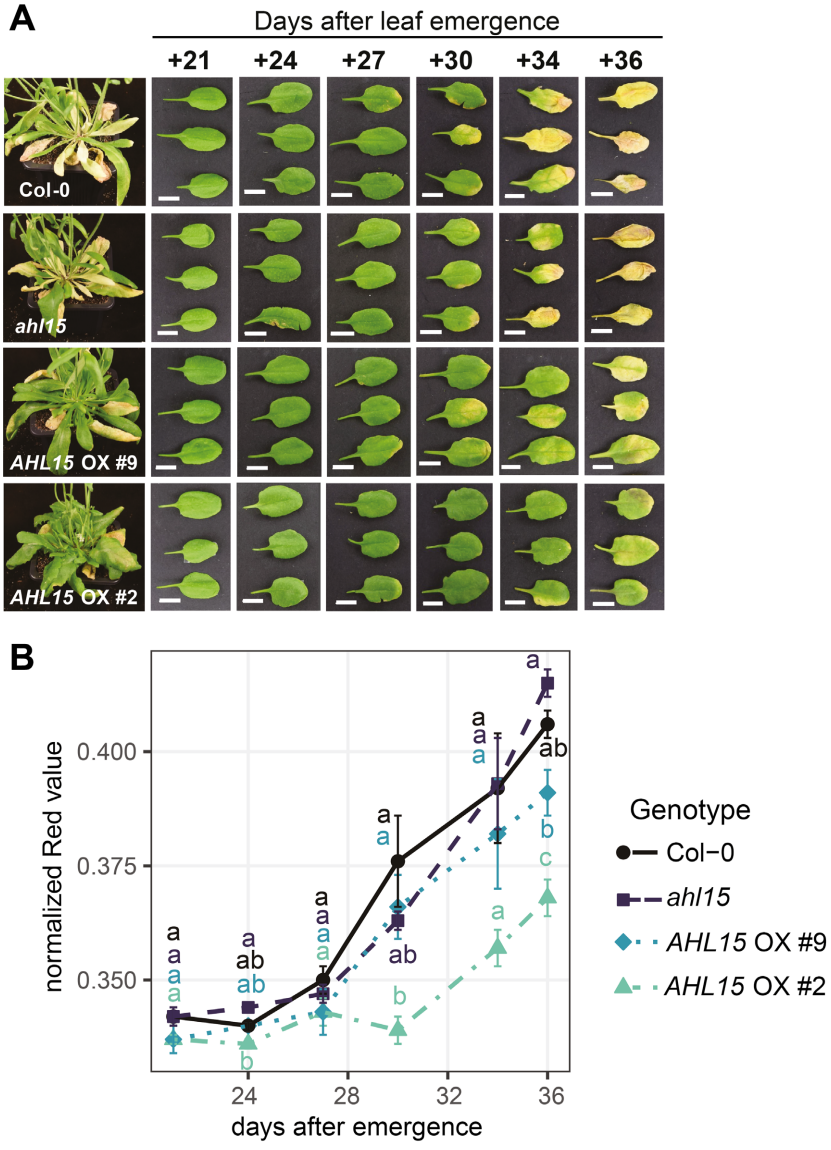

Figure 1: Progression of senescence in the fifth leaf of wild-type (Col-0), *ahl15*, and *AHL15 OX* (*p35S:3xFLAG-AHL15*) plants. **A**: images of 42 day-old plants grown at long day conditions (left) and the fifth leaf at progressing days after emergence (right). White bars represent 1 cm. Plants were grown in 5 cm wide pots. **B**:The chlorophyll content was quantified based on the images in **A** as the normalized Red value (Rn), with four leaves per time point. Groups were compared at each time point by Kruskall-Wallis test, and letters indicate significance groups; groups with the same letter do not differ significantly from one another (n = 4; $p<0.05$).

p35S:AHL15-GR leaves senesced like wild-type leaves (Figure 3A-C).

We next investigated the effect of DEX-induced AHL15-GR nuclear localization on the expression of senescence-associated genes after increasing periods of dark incubation. Based on the Rn value and total Chl content of leaves incubated in the dark over a five-day period, significant differences between DEX-induced and non-induced leaves (DEX-treated vs mock-treated *p35S:AHL15-GR,* or DEX-treated Col-0) became evident after three days of dark incubation. This indicates that senescence had been initiated at this

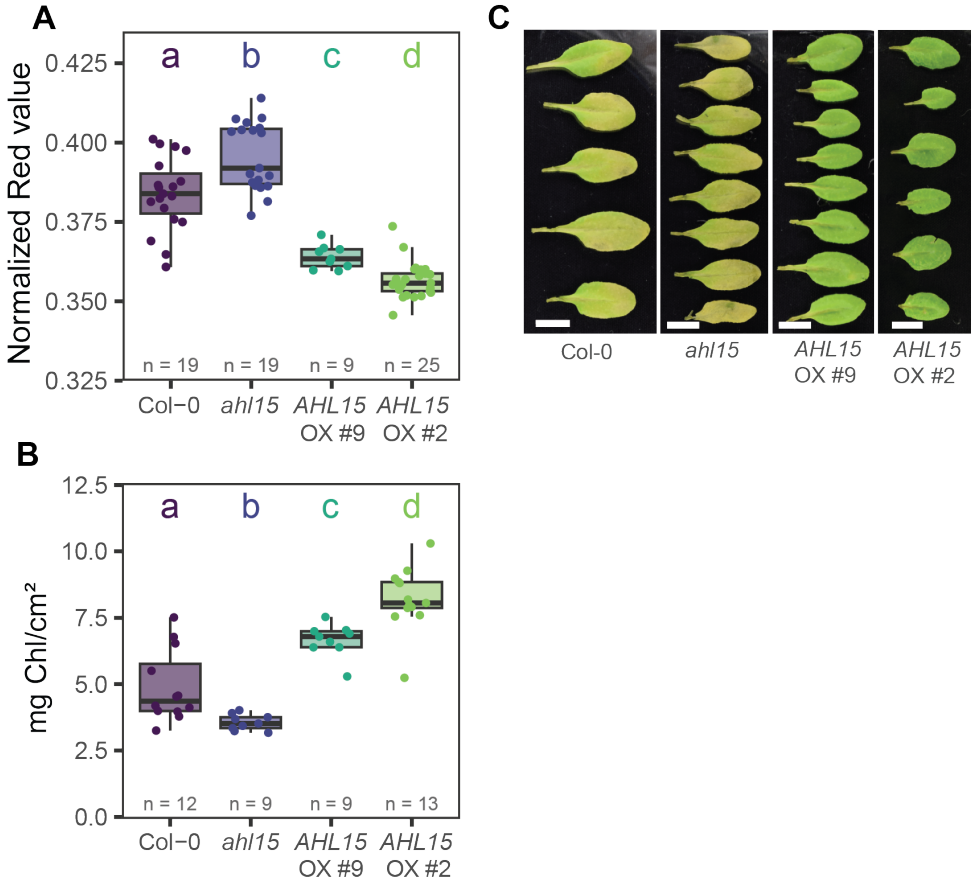

Figure 2: Dark-induced *s*enescence is delayed in leaves detached from *AHL15* OX (*p35S:3x-FLAG-AHL15*) plants and accelerated in ahl15 loss-of-function plants. **A-C**: The fifth leaf of 23 day-old plants was floated on 5 mM MES buffer for five days in the dark to induce the senescence process. Leaves were imaged for chlorophyll quantification as the normalized Red value (Rn) (**A**). Chlorophyll was extracted and quantified by spectrophotometer (**B**). Representative images of leaves of each genotype (**C**). Differences between genotypes in **A** and **B** were compared by a Kruskal-Wallis test, and significance groups are indicated by letters (n=9-25; $p < 0.05$). White bars in **C** represent 1 cm.

time point in non-induced leaves (Figure 3A-C). To determine whether AHL15 inhibits senescence at its onset or at a later stage, we measured the expression of *SENESCENCE-ASSOCIATED GENE (SAG) SAG13* and *SAG12,* which are associated with early- and late senescence, respectively (Lohman et al., 1994). RNA was isolated from leaves right before dark incubation and DEX treatment (day 0), and after three or five days of dark incubation with and without DEX treatment. A clear and significant difference in the expression of the early senescence marker *SAG13* as well as the late senescence marker *SAG12* was visible between DEX- and mock-treated plants (Figure 3D-E), whereas no difference was seen in the expression of *SEN1,* whose expression is induced by darkness (Oh et al., 1996; Chung et al., 1997; Supplementary figure 1). These results indicate that overexpression of *AHL15* affects the onset of senescence at an early stage but does not interfere with the response to darkness.

AHL15 directly represses the expression of *ORESARA1* and several *CKX* genes

ChIP-seq was performed using *AHL15* OX (*p35S:3xFLAG-AHL15*) plants to identify direct targets of AHL15 (this thesis chapter 5). This showed that AHL15 binds up- and downstream of many genes, among which the *SQUAMOSA PROMOTER BINDING PROTEIN-LIKE 9* (*SPL9*) gene, whose expression was previously shown to be suppressed by AHL15 (Rahimi et al., 2022a). Significant peaks were present at 600 bp upstream and 1 kb downstream of the senescence regulator *ORESARA1* (*ORE1*), which could explain the delayed senescence phenotype observed in *AHL15* overexpressing plants (Figure 4A). We next measured the expression of *ORE1* after senescence induction of DEX- or mock-treated leaves and saw that its expression was strongly repressed in DEX-treated leaves, implying a direct repression of this gene by AHL15 (Figure 4B).

In addition, we identified the *CKX* genes *2*, *3*, and *5* (Figure 4A) and several CK biosynthesis genes (*IPT7, LOG1, LOG7, LOG8;* Supplementary figure 2A) among the significant ChIP-seq peaks. Because of the previous finding that AHL15 promotes wood formation by enhancing CK levels (Rahimi et al., 2022b), and because CKs are known to have an inhibitory effect on leaf senescence (Kim et al., 2006; Guo and Gan, 2011; Hu et al., 2021; Yang et al., 2022), we hypothesized that the delayed senescence phenotype of *AHL15* overexpressing plants could in part be a result of increased CK levels. To test whether AHL15 directly regulates the expression of these genes, we measured the expression of each of these genes at 0, 3, or 5 days after senescence induction in DEX- or mock-treated

p35S:AHL15-GR leaves. The expression of *LOG8* and the three *CKX* genes in mock-treated leaves followed a similar pattern as the senescence markers *SAG13* and *SAG12*, and were all increased after 3 and 5 days of dark incubation (Figure 4B, Supplementary figure 2B). In contrast, the expression of *IPT7* and *LOG1* in mock-treated leaves was lower than at day 0, and the expression of *LOG7* was not affected (Supplementary figure 2B). Interestingly, the expression of the *CKX* genes was significantly lower in DEX-treated leaves compared

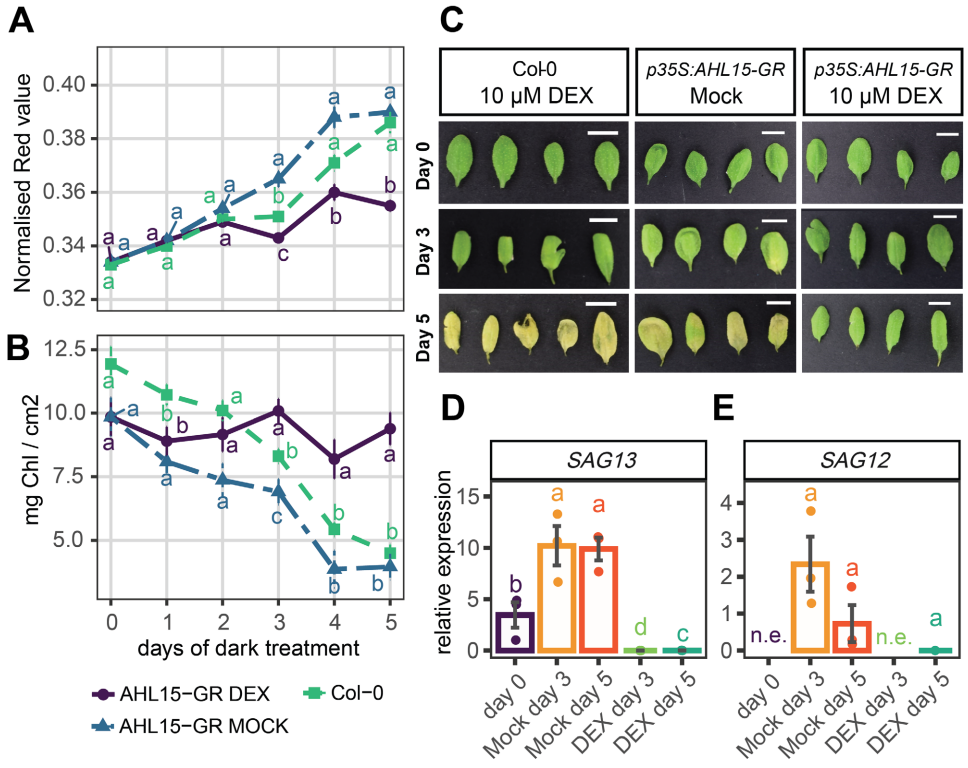

Figure 3: DEX-induced nuclear localization of AHL15-GR inhibits leaf senescence. **A-B**: quantification of chlorophyll in Col-0 and *p35S:AHL15-GR* leaves with and without DEX treatment over five days of dark incubation. The fifth leaf was taken from 23 day-old plants and incubated in the dark on 5 mM MES buffer with or without 10 µM DEX for the indicated number of days. Image-based calculation of the normalized Red value (**A**) or direct chlorophyll extraction (**B**) was used to quantify leaf chlorophyll content of eight leaves per time point (n = 8). **C**: representative images of leaves from each group before and after three or five days of dark incubation. White bars represent 1 cm. **D** and **E**: expression of senescence-associated genes (SAG) in DEX-or Mock-treated leaves. Gene expression was measured by RT-qPCR on RNA extracted from three samples per time point and condition (n=3), with each sample consisting of the fifth leaf of three individual plants. *SAG12* expression could not be detected (n.d.) at day 0 and in DEX-treated leaves at day 3. Expression was normalized to *ACTIN2*. Letters indicate significance groups calculated with the Kruskall-Wallis test ($p < 0.05$).

to the mock treatment, implying that these genes are directly repressed by AHL15 (Figure 4B). The repression of *IPT7* expression upon dark incubation was delayed in DEX-treated leaves, whereas the expression of *LOG1* and *LOG8* was repressed in comparison to mock-treated leaves and *LOG7* expression was unaffected (Supplementary figure 2B). These data suggest that unlike in stem tissue (Rahimi et al., 2022b), AHL15 does not promote CK biosynthesis during leaf senescence, but rather inhibits its degradation by repressing the expression of *CKX* genes.

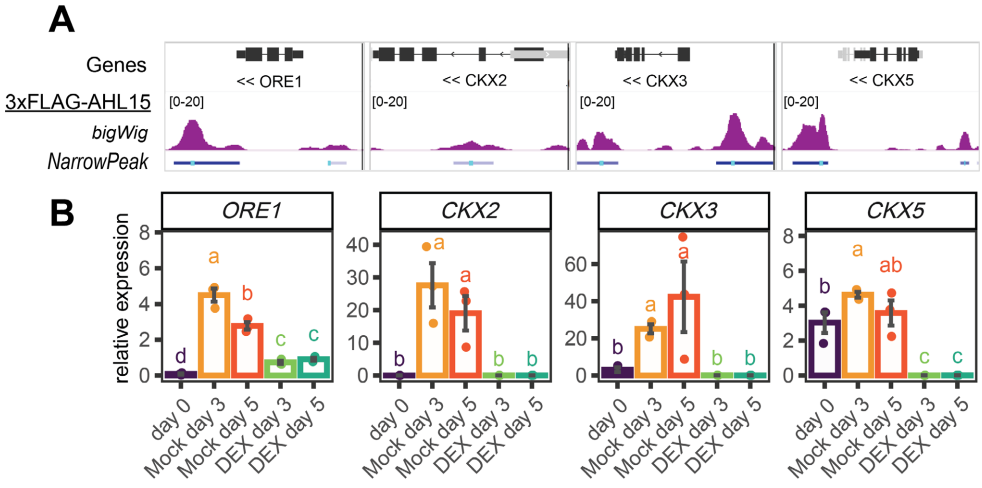

Figure 4: AHL15 directly regulates *ORE1* and *CKX* genes when overexpressed. **A**: ChIP peaks of AHL15 1 kb downstream and 600bp upstream of *ORE1*, in the second intron of *CKX2*, 1.9 kb upstream and directly downstream of *CKX3*, and at 2.3 kb upstream and 2 kb downstream of *CKX5*. ChIP was performed on the whole rosette of 31 days old *AHL15* OX (*p35S:3xFLAG-AHL15*) plants using an anti-flag antibody to pull down AHL15-bound DNA. The figure shows read alignment in purple (bigwig track), and the location of significant peaks in blue (narrowpeak track); a light blue bar indicates the peak summit. Significant peaks can be seen at the loci of *ORE1*, *CKX2, 3*, and *5*. Similar results were obtained in three biological replicates. **B**: The expression of *ORE1*, *CKX2, 3* and *5* is repressed by AHL15 in dark-incubated leaves. Leaves of 23 days old plants were floated on 5 mM MES buffer with or without 10 μM DEX for the indicated number of days in the dark. RNA used for RT-qPCR was extracted from three samples per time point and condition (n=3), with each sample consisting of the fifth leaf of three individual plants. Expression levels are relative to that of *ACTIN2*. Letters indicate significance groups as calculated by the Kruskall-Wallis test ($p < 0.05$).

Cytokinin levels are increased in *AHL15* overexpressing plants

The repression of *CKX* genes by AHL15 suggests that the inactivation of CKs is delayed in *AHL15*-overexpressing leaves, resulting in increased CK levels that repress the onset of senescence. To test whether this was the case, we measured the levels of a wide range of CKs in dark-induced *AHL15-GR* leaves

with and without DEX treatment before and during senescence (Figure 5, Supplementary figures 3-8). These measurements showed that total CK levels drop upon senescence induction in both DEX- and mock-treated leaves but that this decrease in CK levels is less pronounced in DEX-treated leaves (Figure 5A). This trend was especially clear for the isopentenyladenine (iP)-glucosides (Figure 5B, Supplementary figure 4), implying that they may be especially sensitive to degradation by CKX enzymes during the senescence process. Previous research has shown that both iP and iP-9-glucoside (IP9G) , but not iP-7-glucoside (iP7G) can inhibit senescence in Arabidopsis cotyledons (Hallmark and Rashotte, 2020). Although iP in its base form was not present at detectable levels in any of the samples, the elevated levels of iP9G in DEX-treated samples may partially explain the delayed senescence phenotype. In addition, the levels of trans-Zeatin base and trans-Zeatin Riboside (tZ and tZR) were reduced in all dark-incubated samples, but their concentration remained significantly higher in DEX-treated leaves (Figure 5C, D). Of all CK types, tZ-base and tZR have been shown to be among the most potent inhibitors of senescence (Hönig et al., 2018; Pokorná et al., 2020), and their elevated concentration in DEX- versus mock-treated leaves could therefore play an important role in senescence inhibition in DEX-treated leaves.

In addition to tZ and iP, we profiled the levels of cis-zeatine (cZ) and dihydrozeatin (DHZ) during the senescence process (Supplementary figure 6 and 7). Interestingly, cZ-base and cZG levels increased upon dark induction and were especially high after five days of DEX treatment (Supplementary figure 6). cZ has a weak effect on leaf senescence, and its function in the plant remains largely unknown (Gajdošová et al., 2011). Previous research has shown that DHZ levels drop during the senescence process in tobacco leaves (Hönig et al., 2018), and we observed a similar trend in our experiment. While DHZ-base levels were undetectable, we found that DHZ derivatives were present at reduced levels in all samples and that these levels did not differ significantly between treatments, indicating that this form of CK is not affected by AHL15 and its downstream targets (Supplementary figure 7). Finally, we observed an overall increase in CK bases in DEX-treated samples compared to untreated and mock-treated samples (Supplementary figure 3), suggesting that other CK bases may be of importance in the AHL15-mediated delay of senescence.

Taken together, our results indicate that AHL15 can repress senescence in different ways: by directly repressing *ORE1* expression, and by repressing *CKX* expression and thereby delaying inactivation of CKs in leaves. The latter process results in elevated CK levels in *AHL15*-overexpressing leaves,

ultimately contributing to the delay in leaf senescence (Figure 6).

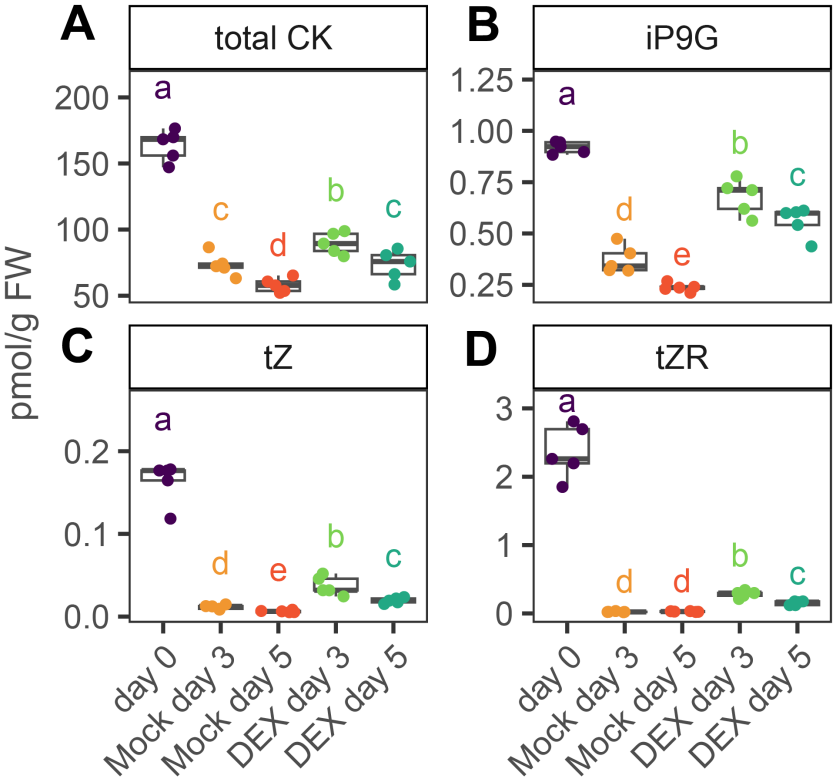

Figure 5: The effect of AHL15 induction on CK levels in dark-incubated leaves. **A**: Total CK; **B**: isopentenyladenine-9-glucoside; **C**: trans-zeatin base; **D**: trans-zeatin riboside. The fifth leaf was collected from 23-day old plants and floated on 5 mM MES with or without 10 µM DEX and stored in the dark for the indicated number of days. Material of three leaves was pooled for each sample, and five samples were measured for each condition (n = 5). Groups were compared using the Kruskall-Wallis test, and letters indicate significance groups ($p < 0.05$).

Discussion

AHL15 has previously been shown to delay several developmental processes, including vegetative phase change, flowering time, and axillary meristem maturation (Karami et al., 2020; Rahimi et al., 2022a). Our data show that in addition to these processes, AHL15 delays leaf senescence by directly repressing expression of *ORE1* encoding a key senescence regulator and by inhibiting CK degradation by repressing *CKX* expression. These two processes are likely to act in parallel and together explain the strong stay-green phenotype observed in *AHL15* overexpressing plants (Figure 6). Moreover, our data suggest that

AHL15 acts predominantly by repressing gene expression, as was the case for *ORE1* and three *CKX* genes.

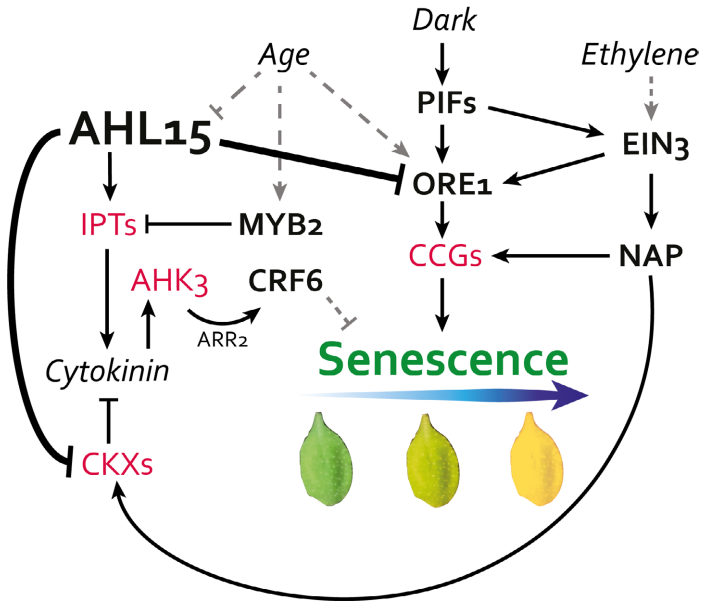

Figure 6: Model of AHL15-mediated repression of senescence. AHL15 represses ORESARA1 (ORE1), which is an important positive regulator of senescence. ORE1 can be induced by dark incubation via the PHYTOCHROME INTERACTING FACTORS (PIFs), by ethylene via ETHYLENE INSENSITIVE 3 (EIN3), or by age. ORE1 activates many downstream targets among which chlorophyll catabolic genes (CCGs) that ultimately lead to chlorophyll catabolism that causes the characteristic yellowing of senescent leaves. NAC-LIKE, ACTIVATED BY AP3/PI (NAP) acts in parallel to ORE1 and activates expression of CCGs as well as the CYTOKININ OXIDASE/DEHYDROGENASE (CKX) genes which can irreversibly inactivate cytokinins (CKs). CKs inhibit leaf senescence via ARABIDOPSIS HISTIDINE KINASE 3 (AHK3), which represses leaf senescence via CYTOKININ RESPONSE FACTOR 6 (CRF6). CKs are produced by ISOPENTENYL TRANSFERASE (IPT) enzymes, which are transcriptionally repressed by MYB2 in ageing plants. AHL15 represses *CKX* expression, and promotes expression of *IPT7*. Lower CKX levels result in slower breakdown of CKs, resulting in higher CK levels and delayed senescence. TFs are indicated with bold letters, enzymes are indicated in red, and hormones and external abiotic factors are written in italics.

ORE1 acts as a key transcriptional regulator of senescence, and its expression is induced by several senescence-promoting environmental cues. Ethylene promotes the expression of *ORE1* and *NAP* via EIN3 (Li et al., 2013; Kim et al., 2014), ABA promotes *ORE1* expression via the TF ACTIVATING FACTOR1 (ATAF1) (Garapati et al., 2015), and dark incubation leads to enhanced *ORE1* transcription via the PIF TFs (Song et al., 2014). It was also shown that *ORE1* expression is post-transcriptionally silenced in young leaves by miR164, and that this silencing is relieved with progressing age (Kim et al., 2009; Li et al.,

2013). Here, we have identified AHL15 as a novel repressor of *ORE1* expression, suggesting that AHL15 can antagonize the ethylene- and dark-induced senescence processes mediated by ORE1. In addition, *AHL15* is strongly expressed in juvenile plants and developing leaves, and is gradually silenced over developmental age (Rahimi et al., 2022a). It is therefore possible that AHL15 can act as an additional age-dependent repressor of *ORE1* expression in parallel to miR164 (Figure 6).

CK has long been known to inhibit leaf senescence, but relatively little is known about its position in the senescence pathway. Application or overproduction of CK can block the onset of leaf senescence (Richmond et al., 1957; Gan and Amasino, 1995; Kim et al., 2006; Argueso and Kieber, 2024), and it has been shown that CK degradation is promoted during the senescence process by NAP-mediated upregulation of *CKX* expression (Hu et al., 2021; Li et al., 2023). MYB2 was shown to lower CK production in an age-dependent manner by repressing the expression of several *IPT* genes, which are the rate-limiting enzymes in the CK biosynthesis pathway (Guo and Gan, 2011). Our data show that AHL15 acts antagonistically to NAP in *CKX* transcriptional regulation, and represses senescence via inhibition of CK degradation. In addition, we found that *IPT7* expression decreased in response to dark-induced senescence, and that this process was delayed after activation of AHL15-GR by DEX treatment. Taken together, our results indicate that AHL15 acts as a positive regulator of CK in the senescence pathway, and thereby acts antagonistically to NAP and MYB2 in this process (Figure 6).

Our experiments show that the expression of the CK biosynthesis genes *LOG1* and *IPT7* is downregulated upon senescence induction by dark treatment. On the other hand, we observed an increased expression of *LOG8* after senescence induction, and that *LOG7* expression is stable throughout the senescence process. In addition, the levels of cZ in its base form and most of its derivatives were increased in senescent leaves. Together, these data show that CK biosynthesis is not completely repressed but partially maintained during the senescence developmental program. Our data also confirm the previously reported induction of *CKX* expression during senescence. This indicates that CK levels are regulated both by biosynthesis and by degradation during the senescence process, and suggests a role for some CK variants in the senescence process. Finally, our data show that inhibition of CK breakdown by direct silencing of *CKX* genes partially explains the delayed senescence phenotype of *AHL15* overexpressing plants. Previously, it was shown that expression of *LOG4*, *IPT3* and *IPT7* was decreased in *ahl15* knockout plants, resulting in lower

CK levels and a decrease in radial xylem width (Rahimi et al., 2022b). Here, we observed delayed downregulation of *IPT7* in dark-incubated leaves following DEX-induced nuclear localization of AHL15-GR, indicating that AHL15 targets are partially shared between stem and leaf tissue.

Our data show that the senescence phenotype of *ahl15* leaves is relatively mild. This suggests that AHL15 plays a minor role in senescence in wild-type plants, or that its function is compensated for by other AHLs when it is absent in *ahl15* knockout plants. *AHL* genes have been shown to be highly functionally redundant, and developmental phenotypes are observed only in higher-order *ahl* mutants (Xiao et al., 2009; Zhao et al., 2013; Karami et al., 2020; Rahimi et al., 2022a). It is therefore possible that higher-order *ahl* mutants show a more clear acceleration of leaf senescence than the *ahl15* single mutant, and that knockout of clade-A *ahl* genes that are expressed in adult leaves will have a more pronounced phenotype. In addition, *AHL15* is expressed primarily in juvenile tissues of wild-type plants, and no GUS activity was seen in expanded or adult leaves when expressed under the *AHL15* promoter (Rahimi et al., 2022a). It is therefore likely that leaves of *ahl15* and wild-type plants do not significantly differ from each other because *AHL15* is not expressed in fully grown wild-type leaves, explaining the similarity in senescence phenotype between the two genotypes.

The functional redundancy between AHL proteins also implies that overexpression of other clade-A *AHLs* could have similar effects as AHL15 on the expression of *ORE1* and *CKX* genes and the overall CK levels in the plant, and that the repression of CK degradation is a general effect of high AHL dosage. Overexpression of at least one other clade-A *AHL, AHL27,* has been shown to inhibit senescence (Lim et al., 2007b), indicating that like flowering time, the senescence-inhibiting phenotype could be induced by multiple AHLs in this clade. It would therefore be interesting to see whether overexpression of other clade-A *AHLs* has a similar senescence phenotype as *AHL15* and *AHL27*, and whether this coincides with a higher CK level in the leaves. Arabidopsis contains 15 clade A *AHLs*, and the genomes of most crop species contain a similar or higher number of *AHL* genes (Zhao et al., 2014; Zhao et al., 2020; Machaj and Grzebelus, 2021; Zhang et al., 2021b; Wang et al., 2023). Breeding efforts to improve longevity and shelf life could focus on enhancing expression of clade-A *AHLs,* which, due to their functional overlap and large number, could provide convenient breeding targets.

Methods

Plant material and growth conditions

Seeds were sown on damp soil (90% turf soil with 10% sand) and stratified for three days at 4 °C before transfer to a climate chamber set at 21°C with long day (16h photoperiod) and 65% relative humidity. Seedlings were transferred to individual pots at one week after sowing and plants were watered weekly.
The *p35S:AHL15-GR* overexpression and *ahl15* loss-of-function lines were described previously (Karami et al., 2020). *p35S:3xFLAG-AHL15* overexpression lines were generated by replacing the *AHL15-GR* construct in the *p35S:AHL15-GR* vector made by Karami et al. (2020) with a synthetic *3xFLAG-AHL15* construct, which was transformed to *Agrobacterium tumefaciens* strain AGL1 by electroporation (Dulk-Ras and Hooykaas, 1995). Transgenic *p35S:AHL15* Arabidopsis Col-0 lines were obtained by the floral dip method (Clough and Bent, 1998) and by subsequently selecting T1 and T2 plants on ½ MS medium supplemented with 15 mg/L phosphinotricin. Single locus transgenic lines, showing a 3:1 segregation ratio of resistant : susceptible plants in the T2 generation, were selected and T3 seeds from homozygous T2 plants were subsequently used for senescence experiments.

For dark-induced senescence assays, fifth leaves were detached from the plants at 23 days after the start of germination and floated on 5 mM MES buffer (pH 5.6) in 5 cm ø Petri dishes, with a maximum of 10 leaves per dish. Petri dishes were sealed with parafilm, wrapped in aluminium foil, and stored in a cardboard box which was placed in the growth chamber to ensure a constant temperature at 20 °C. For the hormone treatments, a 10 mM dexamethasone (ThermoFisher, Vilnius, Lithuania) stock solution dissolved in DMSO was diluted 1000-fold in 5 mM MES buffer. For mock treatment, DMSO was diluted 1000-fold in 5 mM MES buffer.

Senescence measurements

For colorimetric measurements, the leaves were imaged on a dark background with a white reference card under uniform lighting with a Nikon DC3000 camera, with the following settings: ISO 160, exposure time 1/160 s. Image analysis was done in ImageJ with a self-made plugin (this thesis chapter 3). The analysis consisted of the following steps: white balancing of images based on a white reference sheet included in each picture; removal of background, conversion to an RGB image stack, automatic selection of individual leaves,

and measurement of pixel intensity for each leaf in each of the red, green, and blue channels. The mean red, green, and blue values for each leaf were used to calculate the Green: Red ratio and the normalized red value (Rn; Red/(Red+Green+Blue)).

After imaging for colorimetric measurements, two 5 mm ø leaf disks were taken from each leaf and stored at -80 °C. Aceton extraction was done following the method described by Arnon (1949). Briefly, frozen leaf material was pulverized with a metal bead and dissolved in 200 µL 25 mM sodium phosphate buffer (pH 7) and 800 µL 80% acetone. Samples were then incubated at room temperature for 1 hour with gentle shaking, and centrifuged for 10 minutes at 2500x*g*. 200 µL supernatant was then transferred to a clear-bottomed 96-well plate and the absorption (D) at 645 and 663 nm was measured with a TECAN Spark plate reader (Männedorf, Switzerland). The total chlorophyll content in mg/L was then calculated with the following formula: $Chl_{Total} = 20{,}2*D_{645} + 8{,}02*D_{663}$, as described by (Arnon, 1949), and then corrected for the total area of leaf tissue used for Chl extraction. Spectrophotometry results and colorimetric results from ImageJ were processed in R (R Core Team, 2023). Plots were generated using ggplot2 (Wickham, 2016) and ggpubr (Kassambara, 2023), and genotypes or treatments were compared with the Kruskal-Wallis test by using the package Agricolae (de Mendiburu, 2023).

RNA isolation and RT-qPCR

After imaging for colorimetric measurements, leaves were cut in half, of which one half was used for RNA extraction, while the other half of each leaf was used for chlorophyll extraction. For each RNA extraction, material of three plants was pooled and snap-frozen in liquid nitrogen, and tissue was pulverized with a metal bead using the Qiagen Tissuelyser. RNA was isolated with Trizol© reagent (ThermoFisher, Vilnius, Lithuania) by following the standard protocol for Trizol-based RNA extraction, with an additional ethanol wash step at the RNA precipitation stage. Next, 1 µg of RNA was aliquoted to a new tube and treated with DNAse I (ThermoFisher, Vilnius, Lithuania) at 37 °C for 30 minutes and used for cDNA synthesis with the RevertAid First Strand Kit (ThermoFisher, Vilnius, Lithuania) according to the kit's instructions. RT-qPCR was performed with TB green ex-Taq II (Takara Bio Europe, Saint-Germain-en-Laye, France) on the Quantstudio 5 Real-Time PCR machine (Applied Biosystems, Foster City, USA) in a reaction volume of 5 µL. Primers used for RT-qPCR can be found in Supplementary Table 1 and were synthesized by Sigma Aldrich (Haverhill, UK). Gene expression was normalized to *ACTIN2* expression by using the 2^-ΔΔCT

method (Livak and Schmittgen, 2001), and groups were compared with the Kruskall-Wallis test in R as described above.

Chromatin Immunoprecipitation

The ChIP protocol used here was adapted from the protocols by Kaufmann et al. (2010) and Chouaref et al. (2018). For each ChIP, 1 g shoot tissue of 31 day-old *p35S:3xFLAG-AHL15* plants was harvested and fixated for 10 minutes on ice and under vacuum in 1% formaldehyde in ice-cold MC buffer (10 mM sodium phosphate buffer pH 7, 50 mM NaCl, 0.1 M sucrose). The fixation reaction was stopped by addition of glycine to a concentration of 114 mM. Next, samples were washed with ice-cold MC buffer, dried thoroughly, flash-frozen and stored at -80 °C. For nuclei isolation, fixated tissue was ground to a very fine powder in liquid nitrogen using a mortar and pestle and resuspended in 15 mL M1 buffer (10 mM sodium phosphate buffer pH 7, 0.1 M NaCl, 1 M 2-methyl 2,4-pentanediol, 10 mM β-mercaptoethanol) in a 50 mL tube, which was gently shaken at 4 °C for 30 minutes. Suspensions were successively filtered through a 100 µM and 70 µM nylon mesh, both of which were washed with an additional 5 mL M1 buffer to extract additional nuclei. The filtered suspension was then centrifuged for 20 minutes at 1000x*g* at 4°C, and pellets were resuspended in 20 mL M2 buffer (10 mM sodium phosphate buffer pH 7, 0.1 M NaCl, 1 M 2-methyl 2,4-pentanediol, 10 mM β-mercaptoethanol, 10 mM $MgCl_2$, 0.5% Triton X-100). After 30 minutes of gentle shaking at 4 °C, the suspension was centrifuged for 10 minutes at 1000x*g* at 4 °C, the supernatant was discarded, and the pellet was resuspended again in 5 mL M2 buffer. After 10 minutes of gentle shaking followed by 10 minutes centrifugation at 1000x*g* at 4 °C, the pellet was resuspended in 1 mL sonication buffer (10 mM sodium phosphate buffer pH 7, 0.1 M NaCl, 0.5% Sarkosyl, 10 mM EDTA) and aliquoted to 300 µL in 1.5 mL protein lobind tubes (Eppendorf, Germany). Samples were then sonicated for 5 rounds of 10 cycles of 30 seconds ON / 30 seconds OFF on HIGH in a Bioruptor sonicator (Diagenode, Serain, Belgium) to a fragment size of ~300 bp. After sonication, tubes of the same replicate were pooled and centrifuged for 10 minutes at 12000x*g* at 4 °C, and supernatant was transferred to a new protein lobind tube and stored at -20 °C overnight.

For the immunoprecipitation, 50 µg chromatin was used per IP (ca 250 µL sonicated material), and 3.5 volumes IP buffer (50mM HEPES pH7.5, 150 mM NaCl, 5 mM $MgCl_2$, 10 µM $ZnSO_4$, 1% Triton X-100, 0.05% SDS) and 25 µL protein G dynabeads (ThermoFischer, Vilnius, Lithuania) conjugated to mouse monoclonal Anti-FLAG M2 antibodies (F1804; Sigma-Aldrich, Darmstadt,

Germany) were added and rotated at 4 °C overnight. After this, beads were washed once in 1 mL each of the following buffers: IP buffer, high salt buffer (500 mM NaCl, 0.1% SDS, 1% Triton X-100, 2 mM EDTA, 20 mM Tris-HCl pH 8), LiCl buffer (10 mM Tris-HCl pH 8, 1 mM EDTA, 1% NP-40, 1% sodium deoxycholate, 0.25 M LiCl), and twice in TE buffer (10 mM Tris-HCl pH 8, 1 mM EDTA), and then resuspended in 50 µL TE buffer. Samples were decrosslinked overnight at 65 °C in nine volumes of decrosslinking buffer (50 mM Tris-HCl pH 8, 10 mM EDTA pH 8, 250 mM NaCl, 1 % (w/v) SDS). DNA was isolated with the phenol : chloroform method, resuspended in water and treated with RNAse A (ThermoFischer, Vilnius, Lithuania) for 30 minutes at 37 °C, and then stored at -20 °C until further use.

ChIPped DNA was sequenced at Macrogen (Amsterdam, NL) with 20M 150 bp paired-end reads. ChIP-seq analysis was done using the nextflow ChIP-seq pipeline (Ewels et al., 2020), and the TAIR10 version of the Arabidopsis genome was used for read mapping. Reads were annotated in R using the ChIPSeeker package (Yu et al., 2015; Wang et al., 2022).

Cytokinin measurements

Quantification of cytokinin metabolites was performed on biological replicates according to the method described by Svağinová et al. (2012) including modifications described by Antoniadi et al. (2015). Samples (10 mg fresh weight) were homogenized and extracted in 1 ml of modified Bieleski buffer (60% methanol, 10% formic acid and 30% water) together with a cocktail of stable isotope-labeled internal standards (0.2 pmol of CK bases, ribosides, N-glucosides, and 0.5 pmol of CK O-glucosides, nucleotides per sample added). The extracts were applied onto an Oasis MCX column (30 mg/1 ml, Waters) conditioned with 1 ml each of 100% methanol and water, equilibrated sequentially with 1ml of 50% (v/v) nitric acid, 1 ml of water, and 1 ml of 1M formic acid, and washed with 1 ml of 1M formic acid and 1 ml 100% methanol. Analytes were then eluted by two-step elution using 1 ml of 0.35M ammonium hydroxide aqueous solution and 2 ml of 0.35M NH4OH in 60% (v/v) MeOH solution. The eluates were then evaporated to dryness in vacuo and stored at -20°C. Cytokinin levels were determined by an ultra-high performance liquid chromatography-electrospray tandem mass spectrometry (UHPLC-MS/MS) using stable isotope-labelled internal standards as a reference (Rittenberg and Foster, 1940). Separation was performed on an Acquity UPLC® i-Class System (Waters, Milford, MA, USA) equipped with an Acquity UPLC BEH Shield RP18 column (150x2.1 mm, 1.7 µm; Waters), and the effluent was introduced into the

electrospray ion source of a triple quadrupole mass spectrometer Xevo™ TQ-S MS (Waters). Five independent biological replicates each consisting of material from the fifth leaf of three plants were performed, including two technical replicates of each.

Acknowledgements

We thank Jan Vink, Altay Temel, Ward de Winter and Mariel Lavrijsen for technical support and Marion Larue and Jelmer van Lieshout for help with setting up the project. This work was supported the graduate school green top sectors grant (grant nr. GSGT.2019.024) from the Dutch Research Council (NWO) to TL.

Literature

Antoniadi I., Placková L., Simonovik B., Doležal K., Turnbull C., Ljung K., Novák O. (2015). Cell-type-specific cytokinin distribution within the Arabidopsis primary root apex. Plant Cell **27**: 1955–1967.

Argueso C.T., Kieber J.J. (2024). Cytokinin: From autoclaved DNA to two-component signaling. Plant Cell 1–22.

Balanzà V., Martínez-Fernández I., Sato S., Yanofsky M.F., Kaufmann K., Angenent G.C., Bemer M., Ferrándiz C. (2018). Genetic control of meristem arrest and life span in Arabidopsis by a FRUITFULL-APETALA2 pathway. Nat Commun **9**: 565.

Balazadeh S., Siddiqui H., Allu A.D., Matallana-Ramirez L.P., Caldana C., Mehrnia M., Zanor M.I., Köhler B., Mueller-Roeber B. (2010). A gene regulatory network controlled by the NAC transcription factor ANAC092/AtNAC2/ORE1 during salt-promoted senescence. Plant J **62**: 250–264.

Chouaref J., de Boer E., Fransz P., Stam M. (2018). Protocol for Chromatin Immunoprecipitation of meiotic-stage-specific tomato anthers. Curr Protoc Plant Biol **3**: e20074.

Chung B.-C., Lee S.Y., Oh S.A., Rhew T.H., Nam H.G., Lee C.-H. (1997). The promoter activity of *sen1*, a senescence-associated gene of Arabidopsis, is repressed by sugars. J Plant Phys **151**: 339–345.

Clough S.J., Bent A.F. (1998). Floral dip: a simplified method for *Agrobacterium*-mediated transformation of *Arabidopsis thaliana*. Plant J **16**: 735–743.

Dulk-Ras A. den, Hooykaas P.J.J. (1995). Electroporation of *Agrobacterium tumefaciens*. Plant Cell Electroporation And Electrofusion Protocols. Humana Press, New Jersey, pp 63–72

Ewels P.A., Peltzer A., Fillinger S., Patel H., Alneberg J., Wilm A., Garcia M.U., Di Tommaso P., Nahnsen S. (2020). The nf-core framework for community-curated bioinformatics pipelines. Nat Biotech **38**: 276–278.

Gajdošová S., Spíchal L., Kamínek M., Hoyerová K., Novák O., Dobrev P.I., Galuszka P., Klíma P., Gaudinová A., Žižková E., et al (2011). Distribution, biological activities, metabolism, and the conceivable function of cis-zeatin-type cytokinins in plants. J EXP BOT **62**: 2827–2840.

Galuszka P., Frébort I., Šebela M., Pec P. (2000). Degradation of cytokinins by cytokinin oxidases in plants. Plant Growth Regul **32**: 315–327.

Gan S., Amasino R.M. (1995). Inhibition of leaf senescence by autoregulated production of cytokinin. Science (1979) **270**: 1986–1988.

Garapati P., Xue G.P., Munné-Bosch S., Balazadeh S. (2015). Transcription factor ATAF1 in Arabidopsis promotes senescence by direct regulation of key chloroplast maintenance and senescence transcriptional cascades. Plant Physiol **168**: 1122–1139.

Guo Y., Gan S. (2006). AtNAP, a NAC family transcription factor, has an important role

in leaf senescence. Plant J **46**: 601–612.

Guo Y., Gan S. (2011). *AtMYB2* regulates whole plant senescence by inhibiting cytokinin-mediated branching at late stages of development in Arabidopsis. Plant Physiol **156**: 1612–1619.

Guo Y., Ren G., Zhang K., Li Z., Miao Y., Guo H. (2021). Leaf senescence: progression, regulation, and application. Mol Hortic **1**: 1–25.

Hallmark H.T., Rashotte A.M. (2020). Cytokinin isopentenyladenine and its glucoside isopentenyladenine-9G delay leaf senescence through activation of cytokinin-associated genes. Plant Direct **4**: e00292.

Hönig M., Plíhalová L., Husicková A., Nisler J., Doležal K. (2018). Role of cytokinins in senescence, antioxidant defence and photosynthesis. Int J Mol Sci. doi: 10.3390/IJMS19124045

Hu Y., Liu B., Ren H., Chen L., Watkins C.B., Gan S.S. (2021). The leaf senescence-promoting transcription factor AtNAP activates its direct target gene *CYTOKININ OXIDASE 3* to facilitate senescence processes by degrading cytokinins. Mol Hortic **1**: 1–12.

Jordi W., Schapendonk A., Davelaar E., Stoopen G.M., Pot C.S., De Visser R., Van Rhijn J.A., Gan S., Amasino R.M. (2000). Increased cytokinin levels in transgenic *PSAG12–IPT* tobacco plants have large direct and indirect effects on leaf senescence, photosynthesis and N partitioning. Plant Cell Environ **23**: 279–289.

Kakimoto T. (2001). Identification of plant cytokinin biosynthetic enzymes as dimethylallyl diphosphate: ATP/ADP isopentenyltransferases. Plant Cell Phys **42**: 677–685.

Karami O., Rahimi A., Khan M., Bemer M., Hazarika R.R., Mak P., Compier M., van Noort V., Offringa R. (2020). A suppressor of axillary meristem maturation promotes longevity in flowering plants. Nat Plants **6**: 368–376.

Kassambara A. (2023). ggpubr: "ggplot2" Based Publication Ready Plots.

Kaufmann K., Muiño J.M., Østerås M., Farinelli L., Krajewski P., Angenent G.C. (2010). Chromatin immunoprecipitation (ChIP) of plant transcription factors followed by sequencing (ChIP-SEQ) or hybridization to whole genome arrays (ChIP-CHIP). Nat Protoc **5**: 457–472.

Kim H.J., Hong S.H., Kim Y.W., Lee I.H., Jun J.H., Phee B.K., Rupak T., Jeong H., Lee Y., Hong B.S., et al (2014). Gene regulatory cascade of senescence-associated NAC transcription factors activated by ETHYLENE-INSENSITIVE2-mediated leaf senescence signalling in Arabidopsis. J EXP BOT **65**: 4023–4036.

Kim H.J., Ryu H., Hong S.H., Woo H.R., Lim P.O., Lee I.C., Sheen J., Nam H.G., Hwang I. (2006). Cytokinin-mediated control of leaf longevity by AHK3 through phosphorylation of ARR2 in Arabidopsis. PNAS **103**: 814–819.

Kim J.H., Woo H.R., Kim J., Lim P.O., Lee In Chul, Choi S.H., Hwang D., Hong G.N. (2009). Trifurcate feed-forward regulation of age-dependent cell death

involving miR164 in Arabidopsis. Science (1979) **323**: 1053–1057.

Kuroha T., Tokunaga H., Kojima M., Ueda N., Ishida T., Nagawa S., Fukuda H., Sugimoto K., Sakakibara H. (2009). Functional analyses of LONELY GUY cytokinin-activating enzymes reveal the importance of the direct activation pathway in Arabidopsis. Plant Cell **21**: 3152–3169.

Li F., Shan Y., Wang H., Jiang G., Ding X., Liang H., Wang C., Kong X., Xie L., Jiang Y. (2023). A NAC transcriptional factor BrNAC029 is involved in cytokinin-delayed leaf senescence in postharvest Chinese flowering cabbage. Food Chem **404**: 134657.

Li Z., Peng J., Wen X., Guo H. (2013). *ETHYLENE-INSENSITIVE3* is a senescence-associated gene that accelerates age-dependent leaf aenescence by directly repressing *miR164* transcription in Arabidopsis. Plant Cell **25**: 3311.

Lim P.O., Kim H.J., Nam H.G. (2007a). Leaf Senescence. Annu Rev Plant Biol **58**: 115–136.

Lim P.O., Kim Y., Breeze E., Koo J.C., Woo H.R., Ryu J.S., Park D.H., Beynon J., Tabrett A., Buchanan-Wollaston V., et al (2007b). Overexpression of a chromatin architecture-controlling AT-hook protein extends leaf longevity and increases the post-harvest storage life of plants. Plant J **52**: 1140–1153.

Livak K.J., Schmittgen T.D. (2001). Analysis of Relative Gene Expression Data Using Real-Time Quantitative PCR and the 2^-ΔΔCT Method. Methods **25**: 402–408.

Lohman K.N., Gan S., John M.C., Amasino R.M. (1994). Molecular analysis of natural leaf senescence in *Arabidopsis thaliana*. Physiol Plant **92**: 322–328.

Machaj G., Grzebelus D. (2021). Characteristics of the *AT-hook motif containing nuclear localized (AHL)* genes in carrot provides insight into their role in plant growth and storage root development. Genes (Basel) **12**: 764.

McCabe M.S., Garratt L.C., Schepers F., Jordi W.J.R.M., Stoopen G.M., Davelaar E., Van Rhijn J.H.A., Power J.B., Davey M.R. (2001). Effects of PSAG12-IPT gene expression on development and senescence in transgenic lettuce. Plant Physiol **127**: 505–516.

de Mendiburu F. (2023). agricolae: Statistical Procedures for Agricultural Research.

Oh S.A., Lee S.Y., Chung I.K., Lee C.-H., Nam H.G. (1996). A senescence-associated gene of *Arabidopsis thaliana* is distinctively regulated during natural and artificially induced leaf senescence. Plant Mol Biol **30**: 739–754.

Pokorná E., Hluska T., Galuszka P., Hallmark H.T., Dobrev P.I., Drábková L.Z., Filipi T., Holubová K., Plíhal O., Rashotte A.M., et al (2021). Cytokinin N-glucosides: occurrence, metabolism and biological activities in plants. Biomolecules **11**: 24.

Qiu K., Li Z., Yang Z., Chen J., Wu S., Zhu X., Gao S., Gao J., Ren G., Kuai B., et al (2015). EIN3 and ORE1 accelerate degreening during ethylene-mediated leaf senescence by directly activating chlorophyll catabolic genes in Arabidopsis. PLoS Genet **11**: e1005399.

R Core Team (2023). R: A Language and Environment for Statistical Computing.

Rahimi A., Karami O., Balazadeh S., Offringa R. (2022a). miR156 -independent repression of the ageing pathway by longevity-promoting AHL proteins in Arabidopsis. New Phytol **235**: 2424–2438.

Rahimi A., Karami O., Lestari A.D., de Werk T., Amakorová P., Shi D., Novák O., Greb T., Offringa R. (2022b). Control of cambium initiation and activity in Arabidopsis by the transcriptional regulator AHL15. Curr Biol **32**: 1764–1775.

Richmond A.E., Lang A., Okumura F.S., Mag B. (1957). Effect of kinetin on protein content and survival of detached *Xanthium* leaves. Science (1979) **125**: 650–651.

Rittenberg D., Foster G.L. (1940). A NEW PROCEDURE FOR QUANTITATIVE ANALYSIS BY ISOTOPE DILUTION, WITH APPLICATION TO THE DETERMINATION OF AMINO ACIDS AND FATTY ACIDS. J Biol Chem **133**: 737–744.

Schippers J.H.M., Schmidt R., Wagstaff C., Jing H.C. (2015). Living to die and dying to live: The survival strategy behind leaf senescence. Plant Physiol **169**: 914–930.

Schmülling T., Werner T., Riefler M., Krupková E., Bartrina y Manns I. (2003). Structure and function of cytokinin oxidase/dehydrogenase genes of maize, rice, Arabidopsis and other species. J Plant Res **116**: 241–252.

Song Y., Yang C., Gao S., Zhang W., Li L., Kuai B. (2014). Age-triggered and dark-induced leaf senescence require the bHLH transcription factors PIF3, 4, and 5. Mol Plant **7**: 1776–1787.

Svacinová J., Novák O., Placková L., Lenobel R., Holík J., Strnad M., Doležal K. (2012). A new approach for cytokinin isolation from Arabidopsis tissues using miniaturized purification: pipette tip solid-phase extraction. doi: 10.1186/1746-4811-8-17

Takei K., Sakakibara H., Sugiyama T. (2001). Identification of genes encoding adenylateisopentenyltransferase, a cytokinin biosynthesis enzyme, in *Arabidopsis thaliana*. J Biol Chem **276**: 26405–26410.

Thomas H. (2013). Senescence, ageing and death of the whole plant. New Phytol **197**: 696–711.

Tokunaga H., Kojima M., Kuroha T., Ishida T., Sugimoto K., Kiba T., Sakakibara H. (2012). Arabidopsis *lonely guy (LOG)* multiple mutants reveal a central role of the LOG-dependent pathway in cytokinin activation. Plant J **69**: 355–365.

Wang L., Li T., Liu N., Liu X. (2023). Identification of tomato *AHL* gene families and functional analysis their roles in fruit development and abiotic stress response. Plant Physiol Biochem **202**: 107931.

Wang Q., Li M., Wu T., Zhan L., Li L., Chen M., Xie W., Xie Z., Hu E., Xu S., et al (2022). Exploring Epigenomic Datasets by ChIPseeker. Curr protoc **2**: e585.

Wickham H. (2016). ggplot2: Elegant Graphics for Data Analysis.

Woo H.R., Kim H.J., Lim P.O., Nam H.G. (2019). Leaf Senescence: Systems and

dynamics aspects. Annu Rev Plant Biol **70**: 347–376.

Xiao C., Chen F., Yu X., Lin C., Fu Y.F. (2009). Over-expression of an AT-hook gene, *AHL22*, delays flowering and inhibits the elongation of the hypocotyl in *Arabidopsis thaliana*. Plant Mol Biol **71**: 39–50.

Yang J., Worley E., Udvardi M. (2015). A NAP-AAO3 tegulatory module promotes chlorophyll degradation via ABA biosynthesis in Arabidopsis leaves. Plant Cell **26**: 4862–4874.

Yang T., Zhang M., Yang Q., Liu K., Cui J., Chen J., Ren Y., Shao Y., Wang R., Li G. (2022). The S40 family members delay leaf senescence by promoting cytokinin synthesis. Plant Physiol Biochem **191**: 99–109.

Yu G., Wang L.G., He Q.Y. (2015). ChIPseeker: an R/Bioconductor package for ChIP peak annotation, comparison and visualization. Bioinformatics **31**: 2382–2383.

Yun J., Kim Y.-S., Jung J.-H., Seo P.J., Park C.-M. (2012). The AT-hook motif-containing protein AHL22 regulates flowering initiation by modifying *FLOWERING LOCUS T* chromatin in Arabidopsis. J Biol Chem **287**: 15307–15316.

Zhang W., Peng K., Cui F., Wang D., Zhao J., Zhang Y., Yu N., Wang Y., Zeng D., Wang Y., et al (2021a). Cytokinin oxidase/dehydrogenase OsCKX11 coordinates source and sink relationship in rice by simultaneous regulation of leaf senescence and grain number. Plant Biotechnol J **19**: 335–350.

Zhang W.M., Fang D., Cheng X.Z., Cao J., Tan X.L. (2021b). Insights into the molecular evolution of *AT-Hook Motif nuclear Localization* genes in *Brassica napus*. Front Plant Sci. doi: 10.3389/fpls.2021.714305

Zhao J., Favero D.S., Peng H., Neff M.M. (2013). *Arabidopsis thaliana AHL* family modulates hypocotyl growth redundantly by interacting with each other via the PPC/DUF296 domain. PNAS **110**: E4688–E4697.

Zhao J., Favero D.S., Qiu J., Roalson E.H., Neff M.M. (2014). Insights into the evolution and diversification of the *AT-hook Motif Nuclear Localized* gene family in land plants. BMC Plant Biol **14**: 1–19.

Zhao L., Lü Y., Chen W., Yao J., Li Y., Li Q., Pan J., Fang S., Sun J., Zhang Y. (2020). Genome-wide identification and analyses of the *AHL* gene family in cotton (*Gossypium*). BMC Genomics. doi: 10.1186/s12864-019-6406-6

Zhou Y., Zhang X., Chen J., Guo X., Wang H., Zhen W., Zhang J., Hu Z., Zhang X., Botella J.R., et al (2022). Overexpression of *AHL9* accelerates leaf senescence in *Arabidopsis thaliana*. BMC Plant Biol **22**: 1–12.

Zwack P.J., Robinson B.R., Risley M.G., Rashotte A.M. (2013). Cytokinin Response Factor 6 negatively regulates leaf senescence and is induced in response to cytokinin and numerous abiotic stresses. Plant Cell Phys **54**: 971–981.

Supplementary figures

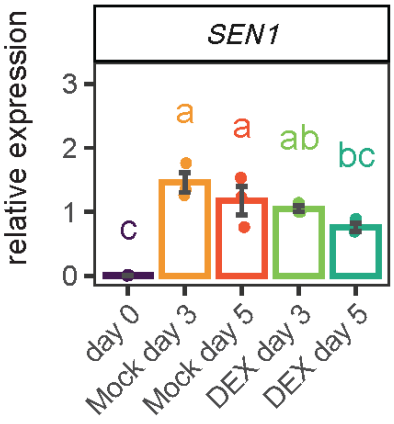

Supplementary figure 1. Expression of *SEN1* relative to *ACTIN2* in dark-incubated leaves with or without 10 µM DEX treatment. Expression was measured in three biological replicates (n=3) each composed of leaf material of three plants each. The Kruskall-Wallis test was used to compare conditions, and significance groups are indicated by different letters ($p < 0.05$).

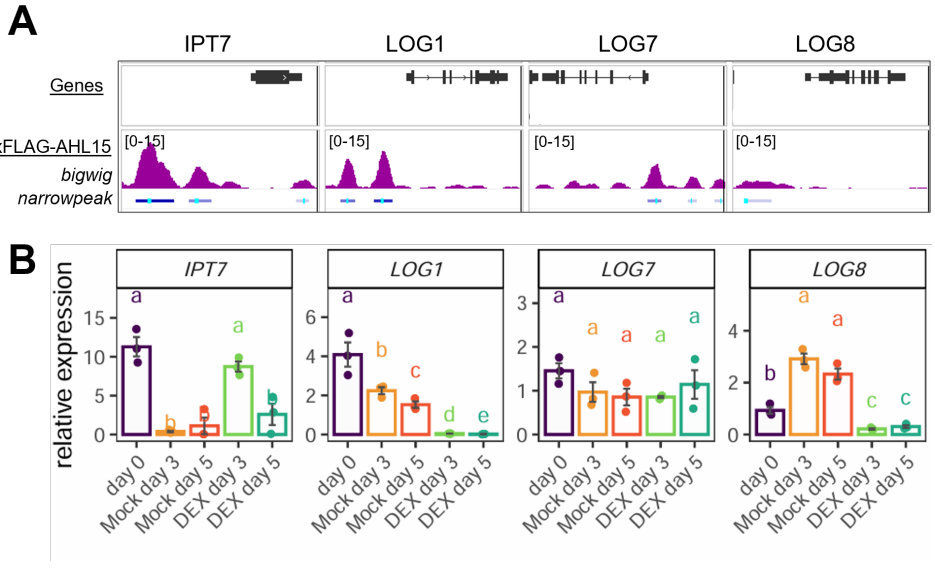

Supplementary figure 2. A: AHL15 binding to cytokinin biosynthesis genes *IPT7, LvvOG1, LOG7,* and *LOG8* in 31 day-old *AHL15* OX (*p35S:3xFLAG-AHL15*) plants using an anti-flag antibody to pull down AHL15-bound DNA. Signfiicant peaks were found at 1.4 kb and 3 kb upstream and in the 3' UTR of *IPT7,* at 1 kb and 2.1 kb upstream of *LOG1,* directly upstream of *LOG7,* and at 1.6 kb upstream of *LOG8.* The figure shows read alignment in purple (bigwig track), and the location of significant peaks in blue (narrowpeak track); a light blue bar indicates the peak summit. **B:** Expression of *IPT7, LOG1,LOG7,* and *LOG8* in the fifth leaf of 23-day old *35S:AHL15-GR* plants during dark-induced senescence with or without AHL15-GR induction by 10 µM DEX treatment. Expression was measured in three biological replicates (n=3) each composed of leaf material of three plants each. The Kruskall-Wallis test was used to compare conditions, and significance groups are indicated by different letters ($p < 0.05$).

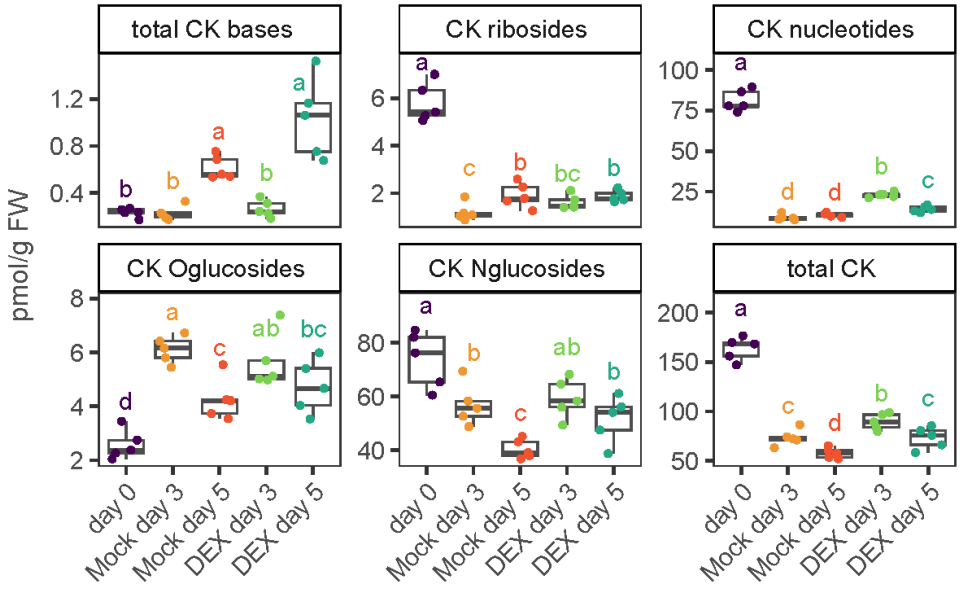

Supplementary figure 3. Effect of AHL15-GR induction on CK levels in dark-incubated leaves. The fifth leaf was collected from 23 days old plants and floated on 5 mM MES with or without 10 µM DEX and stored in the dark for the indicated number of days. Material of three leaves was pooled for each sample, and five samples were measured for each condition (n = 5). Groups were compared using the Kruskall-Wallis test, and letters indicate significance groups ($p < 0.05$).

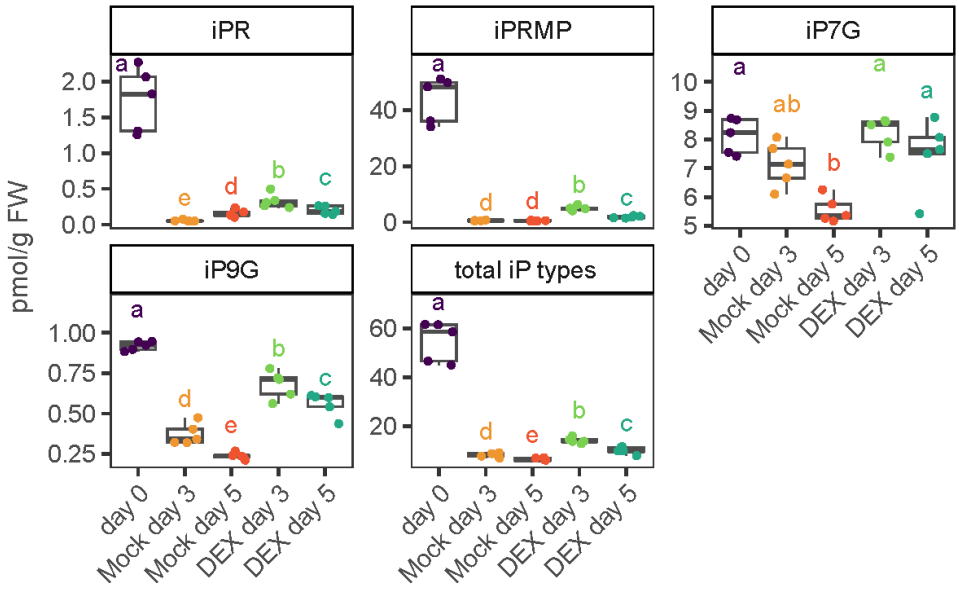

Supplementary figure 4. Effect of AHL15-GR induction on iP-derivatives in dark-incubated leaves. The fifth leaf was collected from 23 days old plants and floated on 5 mM MES with or without 10 μM DEX and stored in the dark for the indicated number of days. Material of three leaves was pooled for each sample, and five samples were measured for each condition (n = 5). Groups were compared using the Kruskall-Wallis test, and letters indicate significance groups ($p < 0.05$). iP base was not present at detectable levels.

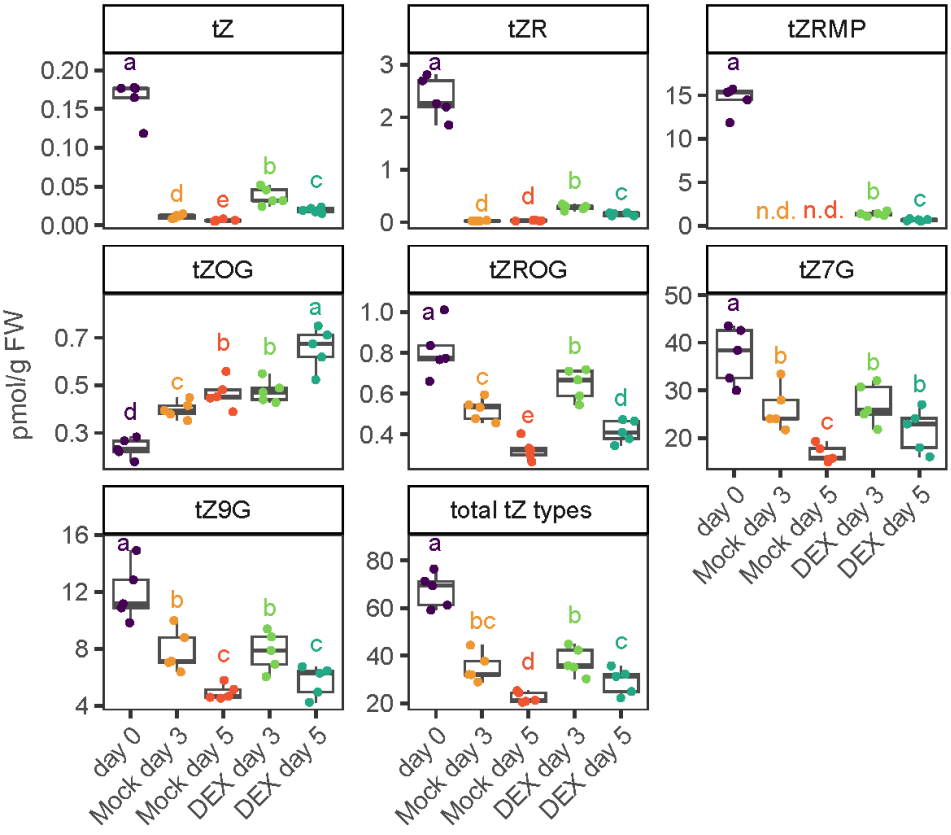

Supplementary figure 5. Effect of AHL15-GR induction on tZ and its derivatives in dark-incubated leaves. The fifth leaf was collected from 23 days old plants and floated on 5 mM MES with or without 10 µM DEX and stored in the dark for the indicated number of days. Material of three leaves was pooled for each sample, and five samples were measured for each condition (n = 5). Groups were compared using the Kruskall-Wallis test, and letters indicate significance groups ($p < 0.05$).

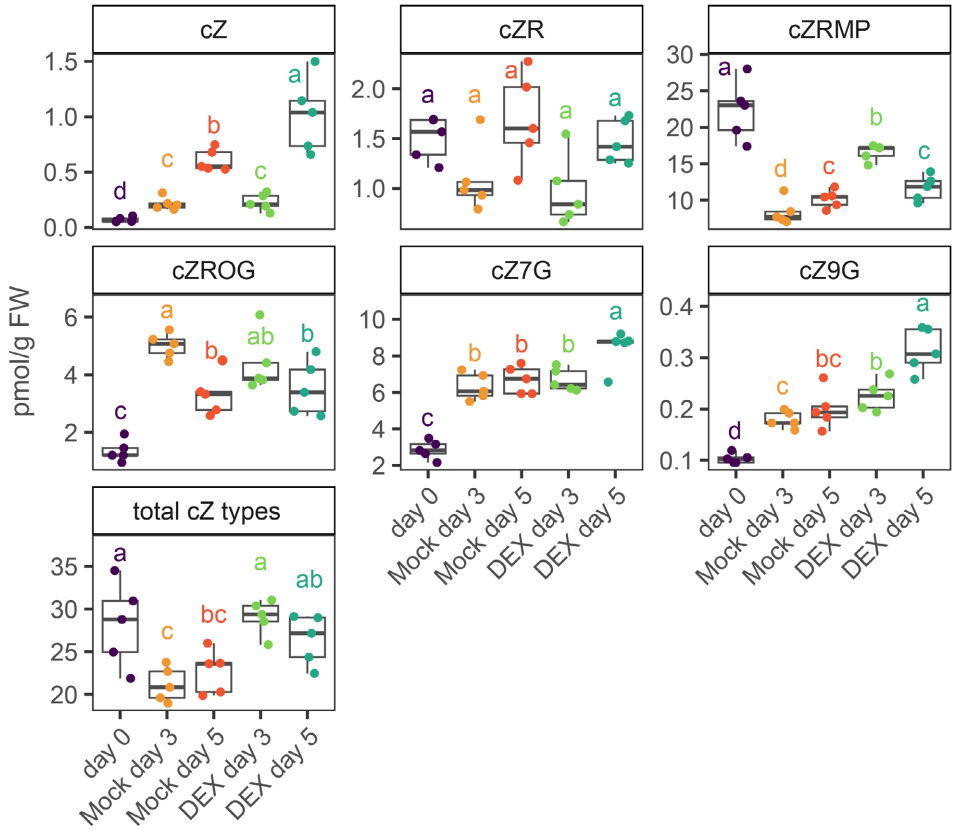

Supplementary figure 6. Effect of AHL15-GR induction on cZ and its derivatives in dark-incubated leaves. The fifth leaf was collected from 23 days old plants and floated on 5 mM MES with or without 10 μM DEX and stored in the dark for the indicated number of days. Material of three leaves was pooled for each sample, and five samples were measured for each condition (n = 5). Groups were compared using the Kruskall-Wallis test, and letters indicate significance groups ($p < 0.05$).

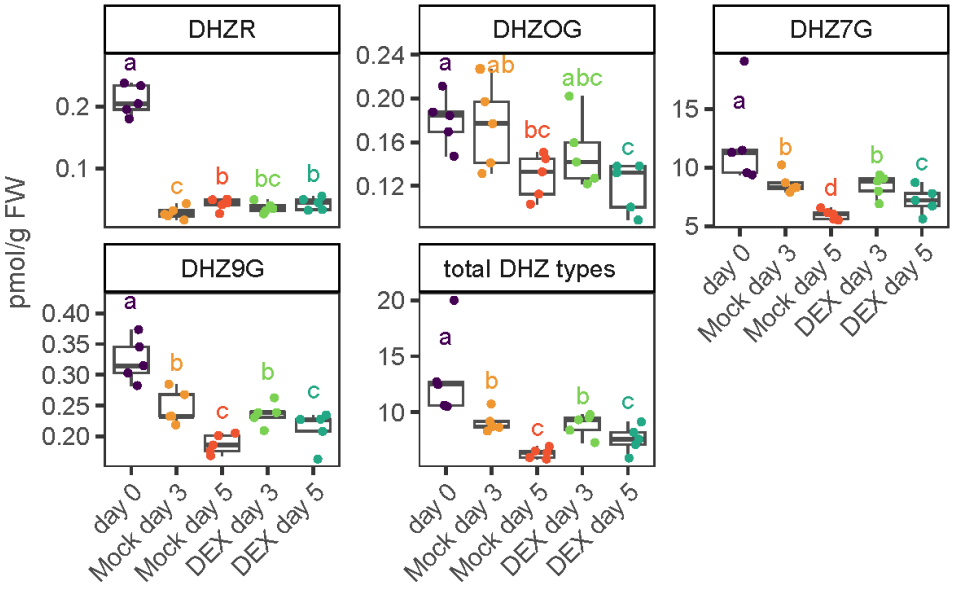

Supplementary figure 7. Effect of AHL15-GR induction on DHZ derivatives in dark-incubated leaves. The fifth leaf was collected from 23 days old plants and floated on 5 mM MES with or without 10 µM DEX and stored in the dark for the indicated number of days. Material of three leaves was pooled for each sample, and five samples were measured for each condition (n = 5). Groups were compared using the Kruskall-Wallis test, and letters indicate significance groups ($p < 0.05$). DHZ base was not present at detectable levels in these samples.

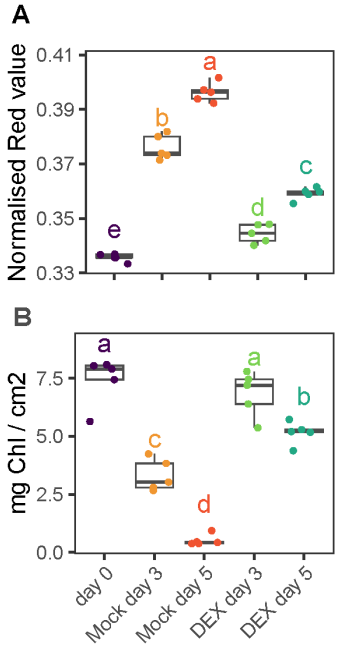

Supplementary figure 8. Quantification of senescence in leaves used for CK measurements. **A:** Normalized Red values (Rn) based on RGB images of leaves just before collecting material for CK measurements. **B:** Total chlorophyll content determined by acetone-based chlorophyll extraction in leaf disks taken from the same samples as used for CK measurements. For each condition, five samples were measured (n = 5), each consisting of material from the fifth leaf harvested from three individual plants. Groups were compared with the Kruskall-Wallis test, and letters indicate significance groups ($p < 0.05$).

Supplementary data

name	sequence (5' to 3')	function
ACTIN2-q-fw	TTCCTCAGCACATTCCAGCAGAT	reference gene for RT-qPCR
ACTIN2-q-rev	AACGATTCCTGGACCTGCCTCATC	reference gene for RT-qPCR
ORE1-q-fw	CTTACCATGGAAGGCTAAGATGGG	RT-qPCR of ORE1
ORE1-q-rev	TTCCAATAACCGGCTTCTGTCG	RT-qPCR of ORE1
SAG12-q-fw	ACCGGGACATCCTCATAACCTG	RT-qPCR of SAG12
SAG12-q-rev	ACAAAGGCGAAGACGCTACTTG	RT-qPCR of SAG12
SAG13-q-fw	AGGGAGCATCGTGCTCATATCC	RT-qPCR of SAG13
SAG13-q-rev	CCAGCTGATTCATGGCTCCTTTG	RT-qPCR of SAG13
SEN1-q-fw	GTTGTCGTTGCTTTCCTCCATC	RT-qPCR of SEN1
SEN1-q-rev	GTCATCGGCTATTTCTCCACCT	RT-qPCR of SEN1
CKX2-q-fw	GAGGTTTGGGTCAATTTGGA	RT-qPCR of CKX2
CKX2-q-rev	AGAGCATCCGAAACCATTTG	RT-qPCR of CKX2
CKX3-q-fw	TCTCAATACACAGTCAACGAGGA	RT-qPCR of CKX3
CKX3-q-rev	TCGTACATAAACCCTCTTACATGG	RT-qPCR of CKX3
CKX5-q-fw	CCATGGTCCTCAAATTAGTAACG	RT-qPCR of CKX5
CKX5-q-rev	TCTGAGCATCTCATCACCTCTC	RT-qPCR of CKX5
LOG1-q-fw	TTTTGTGGAAGTAGTGCTGGTAATA	RT-qPCR of LOG1
LOG1-q-ref	AAATCAAACCCATTAAACCAAT	RT-qPCR of LOG1
LOG2-q-fw	ACACTAAACCGGTGGGACTATTGAA	RT-qPCR of LOG2
LOG2-q-rev	GGAGCGTTTGGAGCCGAGAC	RT-qPCR of LOG2
LOG7-q-fw	CGCTGTTAACGTTTATTGATAAGGC	RT-qPCR of LOG7
LOG7-q-rev	TTATCTCATCAAACTCCGGTTCA	RT-qPCR of LOG7
LOG8-q-fw	GTTTATGGAGGAGGAAGTGTTGGAT	RT-qPCR of LOG8
LOG8-q-rev	TCACCAGATATCTCAATTGGCAT	RT-qPCR of LOG8
IPT7-q-fw	ACCTAACGGCCACCCAGTAT	RT-qPCR of IPT7
IPT7-q-rev	CGGAGTAATTCGCTTTTGGA	RT-qPCR of IPT7
	* fw: forward, rev: reverse	

Supplementary table 1: Primers used for RT-qPCR in this study.

Chapter 5

AHL15 modulates gene expression independently of chromatin accessibility and histone modifications

Thalia Luden[1], Jihed Chouaref[2], Remko Offringa[1]

[1] Plant Developmental Genetics, Institute of Biology Leiden, Leiden University, Sylviusweg 72, 2333 BE Leiden, the Netherlands

[2] Annogen, Science Park 406, 1098 XH Amsterdam, the Netherlands

Abstract

In recent years, members of the *AT-HOOK MOTIF NUCLEAR LOCALIZED (AHL)* gene family have been shown to play important roles in plant development. One member of this family, *AHL15*, enhances plant longevity when overexpressed by strongly repressing several ageing-related developmental switches, but its direct target genes and the manner with which it regulates their expression remained unknow so far. In this study we identified the genome-wide DNA binding sites of AHL15, and show that AHL15 binds throughout the genome at AT-rich regions near the transcription start- and end sites in regions depleted of epigenetic marks without recognizing a specific sequence. We show that induction of AHL15 activity causes strong and rapid changes in transcription, with the majority of the differentially expressed genes being downregulated but without directly affecting chromatin accessibility, resulting in developmental defects. In addition, AHL15 binding to regions near the transcription start and end sites was enhanced at genes that were differentially expressed upon AHL15 induction, and was especially strong near the transcription start site of upregulated genes and near the transcription end site of downregulated genes. Finally, we show that AHL15 shares binding sites with the chromatin architectural protein GH1-HMGA2/HON5, which was previously shown to alter transcription by disrupting gene loop formation. Together, our findings suggest that AHL15 affects the expression of its target genes by regulating the 3D organization of chromatin.

Keywords: AHL15, aging, AT-hook proteins, chromatin architecture, gene looping

Introduction

In recent years, research on the plant-specific AT-HOOK MOTIF NUCLEAR LOCALIZED (AHL) protein family has shown that members of this plant-specific gene family have diverse roles in developmental processes, such as hypocotyl elongation, root architecture, somatic embryogenesis, vegetative phase change, flowering time, and longevity (Street et al., 2008; Zhou et al., 2013; Karami et al., 2020; Karami et al., 2021; Rahimi et al., 2022a). The *AHL* family is conserved in all land plants, with the size of the family varying between ten genes in *Physcomitrella patens* (moss), 29 in *Arabidopsis thaliana* (Arabidopsis), 20-26 in *Oryza sativa* (rice) and 47 in carrot (Kim et al., 2011; Zhao et al., 2014; Machaj and Grzebelus, 2021; Kumar et al., 2023). Despite the considerable size of this gene family, research on AHLs has emerged only in recent years, and much remains to be discovered about their function in development and gene regulation.

AHL proteins bind to the minor groove of AT-rich DNA via their AT-hook domain, which can also be found in other DNA-binding proteins such as the High-Mobility Group A (HMGA) family (Klosterman and Hadwiger, 2002; Fujimoto et al., 2004). The AHL family is subdivided into two clades (A and B) based on the structure and number of AT-hook domains: clade A members have a single, type A AT-hook domain, whereas clade B members have a type B AT-hook domain that is sometimes accompanied by a second AT-hook domain of the A type (Zhao et al., 2013; Zhao et al., 2014). In the nucleus, AHL proteins are thought to form heterotrimeric complexes and to jointly recruit other nuclear proteins via their PPC (Plant and Prokaryote Conserved) domains (Zhao et al., 2013). While single *ahl* mutants often show very mild phenotypes, such as a slightly accelerated flowering time (Karami et al., 2020; Rahimi et al., 2022a), more striking phenotypic defects can be observed when one of the characteristic AHL domains are mutated. Removal of the AT-hook domain *(ΔAT-hook)* causes loss of DNA binding, whereas deletion of a six amino acid sequence in the PPC domain *(ΔG)* or interference with the PPC domain function by fusion of the ǧ-glucuronidase (GUS) reporter protein reduces the capacity to recruit other nuclear proteins (Lin et al., 2007; Zhao et al., 2013; Karami et al., 2021). Such mutant AHL proteins have a strong dominant-negative effect on AHL function, as was shown by the inhibitory effect of *AHL15-ΔG* or *AHL15-GUS* on zygotic or somatic embryogenesis when expressed in a heterozygous *ahl15* +/- background (Karami et al., 2021), or by the *sob3-6* mutant which expresses a *ΔAT-hook* allele of *AHL29* and shows a significantly longer hypocotyl than either wild-type or *ahl29* knockout plants (Zhao et al., 2013). The phenotype of

these dominant-negative mutants and the high level of redundancy between *AHLs* indicates that the absence of an AHL protein can be compensated for by other AHLs, but that the incorporation of a defective AHL protein disrupts the function of the trimeric complex.

Due to the high redundancy between *AHL* genes, most research has been focused on *AHL* overexpression phenotypes, which are generally similar for different *AHLs*. For example, overexpression of *AHL29/SOB3, AHL27/ESCAROLA/ORE7* and *AHL22* each suppress hypocotyl elongation (Street et al., 2008; Xiao et al., 2009), and overexpression of *AHL15, 19, 20, 22, 27,* or *29* each significantly delays flowering time and promotes plant longevity (Street et al., 2008; Yun et al., 2012; Karami et al., 2020; Tayengwa et al., 2020). The delayed flowering phenotype is caused at least in part by the repression of *FT* expression, suggesting that AHLs can suppress gene expression (Yun et al., 2012; Tayengwa et al., 2020).

Previous studies have shown that *AHL* overexpression affects the chromatin status: Lim et al. (2007) showed that *AHL27* overexpression results in a reduction of chromatin condensation, and Karami et al. (2021) showed that the number of nuclear foci is reduced when *AHL15* is overexpressed and that overexpression of *AHL15* interferes with the proper segregation of sister chromatids specifically during the somatic embryogenesis process, resulting in polyploid embryos. Various studies have shown that acetylation of HISTON 3 (H3Ac) is reduced at specific loci in plants that constitutively overexpress *AHL* genes, whereas its methylation at lysine 9 (H3K9me2) is increased at AHL-bound loci in such plants, suggesting that AHLs promote deposition of repressive epigenetic marks (Ng et al., 2009; Yun et al., 2012; Xu et al., 2013; Xiong et al., 2020). AHLs have been shown to interact with a range of chromatin-modifying proteins, among which several histone deacetylases (HDA) and subunits of the SWR1 complex that exchanges H2A for H2A.Z (Yun et al., 2012; Xu et al., 2013; Lee and Seo, 2017; Xu et al., 2024). A recent study has shown that AHL22 also associates with the transcriptional repressors FRS7 and FRS12 at the matrix attachment regions (MARs) that anchor DNA to the nuclear matrix, and that it recruits the histone deacetylase HDA15 to the DNA (Xu et al., 2024). In addition, RNA-seq datasets show that overexpression of *AHL* proteins causes differential expression of many genes, of which the majority is downregulated (Favero et al., 2020; Karami et al., 2022; Xu et al., 2024). Overall, it is clear that *AHL* overexpression results in differential gene expression, affects chromatin structure, and has a profound effect on plant development. However, the specific mechanisms recruiting AHLs to their target DNA, the direct effect of AHLs on histone modifications,

and the effects of AHLs on chromatin architecture on a global scale remain unclear.

The clade A AHL protein AHL15 has been shown to delay and even reverse developmental phase transitions when overexpressed, thereby extending plant longevity (Karami et al., 2020; Karami et al., 2021; Rahimi et al., 2022a; Rahimi et al., 2022b). Despite the variety of processes in which AHL15 has been shown to play a role, no direct targets of this protein have been identified as of yet. Here, we identified the DNA binding sites of AHL15 in native- and overexpression conditions and investigated the effect of AHL15 on gene expression, chromatin accessibility, and its colocalization with several chromatin modifications. We show that a large set of loci is only bound by AHL15 upon overexpression, and that this coincides predominantly with downregulation of genes. In addition, we show that AHL15 does not affect chromatin accessibility and that it preferentially binds at the boundaries of most epigenetic marks. Finally, we show that AHL15 binding sites largely overlap with those bound by GH1-GMGA2, an AT-hook protein shown to regulate chromatin architecture and gene loop formation (Zhao et al., 2021), implying that AHL15 could play a similar role.

Results

AHL15 binds near the TSS and TES of genes

To identify how AHL15 regulates juvenile plant development, we performed ChIP-seq experiments using a 3xFLAG-tagged AHL15 protein. Because wild-type and *AHL15* overexpressing plants show significant phenotypic differences, we expressed the 3xFLAG-AHL15 fusion protein both in native *(pAHL15:3xFLAG-AHL15* in *ahl15)* and overexpression (*p35S:3xFLAG-AHL15* in Col-0) conditions and pulled down AHL15-bound DNA from both lines (Figure 1A). In wild-type Arabidopsis, *AHL15* is expressed only in juvenile plants and its expression decreases significantly past the seedling stage (Rahimi et al., 2022a). We therefore performed ChIP on 10 day-old seedlings in which the *AHL15* promoter is still strongly active to identify the native DNA binding sites of AHL15. In contrast, *p35S:3xFLAG-AHL15* plants showed a severe delay in flowering time, and overexpression targets were identified in 31 day-old *p35S:3xFLAG-AHL15* plants, which had not yet started to flower at this stage in order to map overexpression-specific targets of AHL15 (Supplementary figure 1).

Our ChIP-seq data show that AHL15 binds DNA abundantly in both native and overexpression conditions (Figure 1A). Under native conditions, we

identified 2425 significant peaks that are shared between both replicates, and an additional 3481 significant peaks in the second replicate, which had a higher sequencing depth (Supplementary data 1). In the overexpression conditions, we identified over 14,000 significant peaks per replicate, of which 10,056 were shared between all three replicates, indicating that AHL15 binds DNA more

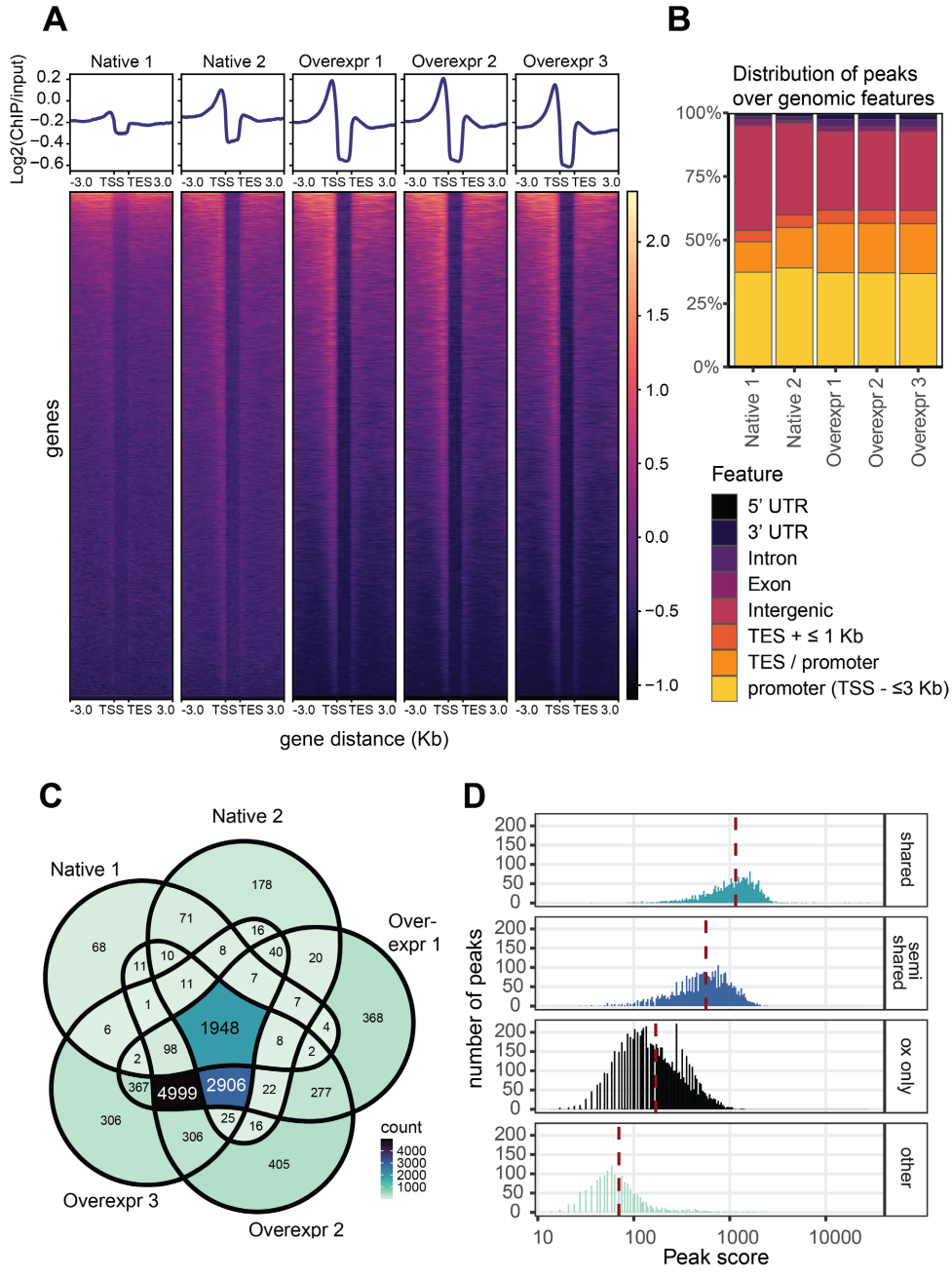

broadly when overexpressed than in wild-type conditions, and that some DNA binding sites are unique to the overexpression condition (Supplementary data 1). Next, we mapped the AHL15 peaks over all genes in the Arabidopsis genome, which showed that AHL15 predominantly binds within 1 kb upstream of the transcription start site (TSS) of genes, and to a lesser extent near the transcription end site (TES) and is depleted over gene bodies (Figure 1A, B). The peak of AHL15 occupancy in these regions was more pronounced in *AHL15* overexpression samples compared to the native condition, showing that AHL15 has a preference for the proximal promoter of genes regardless of whether these are genuine native targets or not. Annotation of the significant AHL15 ChIP-seq peaks over genomic features confirmed that the majority of AHL15 binding sites are located in promoters (up to 3 kb upstream of the TSS) or in intergenic regions (more than 3 kb upstream of the TSS or more than 1 kb downstream of the TES; Figure 1B). In addition, a substantial percentage of AHL15 peaks was located in within 1 kb downstream of the TES or in regions where the promoter and TES of two genes overlapped (TES/promoter; Figure 1B). In overexpression conditions, the share of AHL15 peaks mapping to intergenic regions reduced in favour of promoter- and TES regions, illustrating the increased enrichment of AHL15 near the TSS and TES regions that can be seen in Figure 1A.

To understand what loci are native targets of AHL15 and what loci are unique to the overexpression condition, we compared the significant ChIP

Figure 1 (left page): ChIP-seq of 3xFLAG-AHL15 in native and overexpression conditions. **A:** Heatmap and profile plots of AHL15 ChIP-seq peaks scaled over genes showing that AHL15 is enriched near the TSS and TES, and depleted over gene bodies. Shoots of ten day-old *pAHL15:3x-FLAG-AHL15* were used for ChIP in the native condition, and 31 day-old *p35S:3xFLAG-AHL15* shoots were used for the overexpression condition. Profile plots show the log2 of ChIP reads over input reads. **B:** Annotation of 3xFLAG-AHL15 ChIP-seq peaks in **A** over genomic features of the Araport11 annotation of the Arabidopsis genome. Intergenic: regions that are located more than 3 kb downstream of the TSS or more than 1 kb upstream of the TES and are depleted of genes. TES: region up to 1 kb upstream of the TES. Promoter: region up to 3 kb downstream of the TSS. TES / promoter: regions where promoters overlap with the TES region of neighbouring genes. Intergenic regions are regions not covered by any of the other features. **C:** Venn diagram showing the overlap in peak annotations between the five ChIP-seq samples in **A**. 1948 peaks were identified in all five datasets (*shared*), 2906 peaks were shared between the three overexpression conditions and the second native ChIP (*semi-shared*), and 4999 peaks were identified in all three overexpression (OX) conditions (*OX only*). **D:** Histogram of the peak score of significant ChIP-seq peaks in *p35S:3x-FLAG-AHL15* sample 2 (OX 2). Peaks identified in all five conditions have the highest peak score, followed by semi-shared peaks. OX-only peaks have a lower peak score than shared or semi-shared peaks, and peaks shared in less than 3 conditions have the lowest overall peak score. Reads were aligned with Bowtie2 and peak calling was performed with MACS2.

peaks and identified a set of 1948 loci that are shared between all five ChIP-seq datasets ("shared"; Figure 1C). This set includes the promoters of genes such as *CYTOKININ OXIDASE3 (CKX3), WUSCHEL-RELATED HOMEOBOX 4 (WOX4),* and *TWIN SISTER OF FT (TSF)* (Supplementary data 1). In addition, 2906 peaks were shared between the second replicate of the native ChIP and the three overexpression ChIPs ("semi-shared"), which included promoters of *SQUAMOSA PROMOTER BINDING-LIKE 9 (SPL9)* and *BRANCHED 1 (BRC1)*. We identified 4999 peaks that were common among all three overexpression datasets ("overexpression-only"), that among many others annotated to the promoters of *FLOWERING LOCUST (FT), SWEET10,* and *FLOWERING LOCUS C (FLC)* (Supplementary data 1). When comparing the distribution of peak scores in each category, it was clear that peaks that are shared by all datasets had a higher average peak score than those that are found only in overexpression datasets, indicating that AHL15 binds its native targets more strongly than its ectopic targets (Figure 1D). Thus, these data show that AHL15 can associate with DNA outside of its genuine native binding sites when overexpressed, but that the affinity for these regions is lower than for its native targets.

AHL15 non-specifically binds AT-rich DNA sequences

Because AHLs are known to bind AT-rich DNA and AHL15 binds a large number of promoter regions in both the native and overexpression conditions, we asked whether AHL15 recognizes or binds a specific DNA motif. To this end, we used the motif enrichment analysis tool HOMER (Heinz et al., 2010) to identify enriched motifs in the different datasets: shared, semi-shared, and overexpression-only AHL15 peaks as well as the total of significant peaks of the second overexpression replicate (Figure 2A, Supplementary figures 2-4, Supplementary data 2). Although several AT-rich motifs were found to be significantly enriched in the different datasets, closer inspection showed that the frequency at which these motifs occurred within AHL15 peaks was in most cases less than 1%, making it unlikely to represent a true binding site (Figure 2A, Supplementary figures 2-4). We argued that a true DNA binding motif would be present in a large portion of the AHL15 peaks (targets) and would be rare in other regions of the genome (background). In other words, the motif should have a high target : background ratio and be present in a high percentage of targets. We plotted the target : background ratio (Figure 2B) and the Log2 of the percentage of targets (Figure 2C) values for all significantly enriched *de novo* motifs identified by HOMER for the shared AHL15 peaks. These plots show that most motifs had a high target : background ratio, but

A Enriched motifs of shared peaks

Rank	Motif	P-value	log P-pvalue	% of Targets	% of Background
1		1e-23	-5.488e+01	0.96%	0.01%
2		1e-19	-4.594e+01	0.96%	0.01%
3		1e-15	-3.519e+01	0.67%	0.01%
4		1e-12	-2.937e+01	0.89%	0.04%
5		1e-12	-2.876e+01	0.52%	0.01%
6		1e-12	-2.876e+01	0.52%	0.00%
7		1e-12	-2.876e+01	0.52%	0.01%
8		1e-12	-2.876e+01	0.52%	0.01%

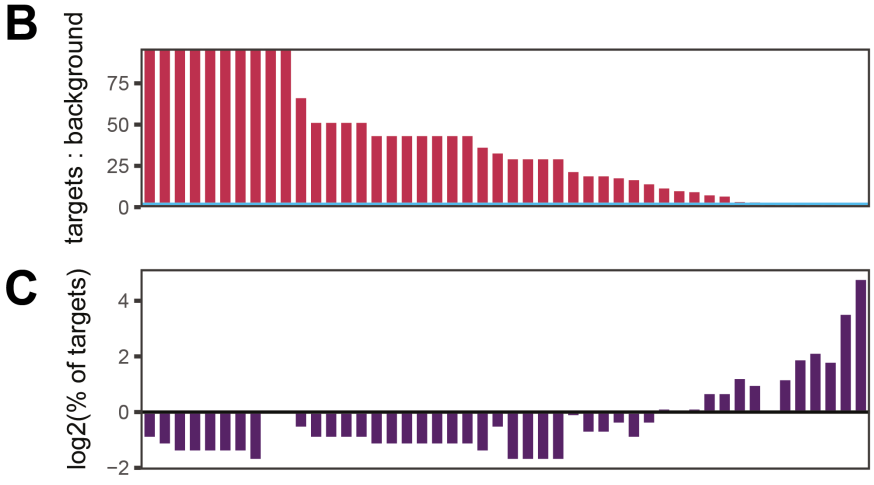

Figure 2: AHL15 binds to AT-rich DNA but does not have a specific DNA binding motif. **A:** Table of the top 8 enriched motifs identified by HOMER2 within the set of shared peaks. **B:** The number of times each motif (48 in total) is identified by HOMER2 in shared AHL15 peaks divided by its number over the entire genome (expressed as %: 100% means the motif is almost only present in AHL15 peaks). **C:** The frequency with which each motif identified by HOMER2 occurs in shared AHL15 peaks, expressed as the Log2 value of the % of shared AHL15 targets containing the specific motif (occurrence of more than 1% gives a positive value, 1% gives a value of 0, and less than 1% results in a negative value). Motifs in figures **B** and **C** are arranged by descending target : background value.

that their occurrence in AHL15 peaks in all such cases was less than 1%. On the other hand, motifs that are present in more than 1% of AHL15 peaks had a low target : background ratio, meaning that these motifs are also common in non-AHL15 bound regions. Similar results were found for each of the AHL15 peak datasets (semi-shared, overexpression-only, and all AHL15 ox rep2 peaks), and no motifs were shared between the four different datasets (Supplementary figures 2-4). Previous research has shown that AHL proteins preferentially bind to AT-rich DNA, and *in vitro* motif discovery experiments suggested several AT-rich sequences as binding sites for AHL proteins (Fujimoto et al., 2004; Franco-Zorrilla et al., 2014). Together, this indicates that AHL15 does not recognize a specific DNA motif but identifies its AT-rich target DNA based on other traits.

Gene expression is predominantly repressed by AHL15

The large number of binding sites we identified in the native and overexpression conditions, as well as the strong phenotypic changes caused by *AHL15* overexpression suggest that AHL15 may regulate the expression of many genes.

To determine which genes are affected by *AHL15* overexpression and may underly the developmental phenotypes associated with *AHL15* overexpression, we used the *p35S:AHL15-GR* line. In this line, a fusion protein of AHL15 and a glucocorticoid receptor (AHL15-GR) is overexpressed, and translocates from the cytosol to the nucleus upon treatment with the steroid hormone dexamethasone (DEX) (Karami et al., 2020). We drenched ten day-old wild type (Col-0) or *p35S:AHL15-GR* seedlings with 20 µM DEX or a mock solution for 15 minutes and harvested seedlings eight hours later for mRNA sequencing. Principal component analysis (PCA) of the RNA-seq data showed that the DEX-

Figure 3 (right page): Genes upregulated by AHL15 show enhanced AHL15 binding at the TSS. **A:** Volcano plot showing differentially expressed genes in 10 day-old *p35S:AHL15-GR* seedlings after 8 hours treatment with DEX compared to the three control conditions (*p35S:AHL15-GR* seedlings treated with mock solution and Col-0 seedlings treated with either DEX or mock solution). Blue dots indicate genes that are significantly more than 2-fold downregulated, red dots indicate genes that are significantly more than 2 fold upregulated, light grey dots show genes that are significantly differentially expressed with a fold change of less than 2, and dark grey dots represent genes whose expression was not significantly altered. **B-D:** Venn diagrams showing overlap of differentially expressed genes with shared ChIP-seq peaks (**B**), semi-shared peaks (**C**), or overexpression-only peaks (**D**). **E:** Table showing a selection of genes shared between ChIP-seq and RNA-seq datasets identified in **B-D**. **F:** Profile plots of AHL15 ChIP-seq peaks over AHL15-bound differentially expressed genes vs all genes. AHL15 enrichment is stronger near the TSS of AHL15-bound differentially expressed genes and especially upregulated genes compared to the average of all genes. Near the TES, AHL15 enrichment is highest for downregulated AHL15-bound genes.

treated *p35S:AHL15-GR* samples grouped at one end, whereas the mock- or DEX-treated Col-0 or the mock-treated *p35S:AHL15-GR* samples grouped at the other end of the PCA plot, showing that DEX treatment had a minimal effect on gene expression in wild type plants compared to *p35S:AHL15-GR* plants (Supplementary figure 5).

Induction of AHL15-GR activity by DEX treatment resulted in a large number of differentially expressed genes, with 1658 genes downregulated over 2-fold and 497 genes upregulated over 2-fold, showing that similar to other *AHL* genes, *AHL15* overexpression causes a net downregulation of gene expression

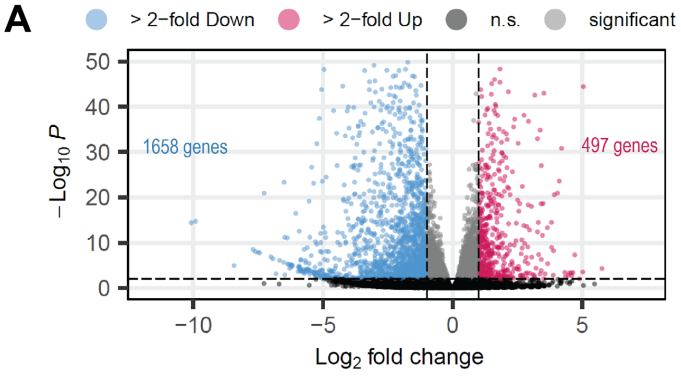

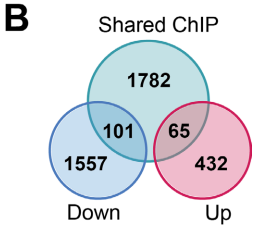

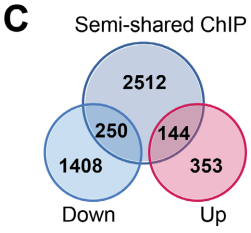

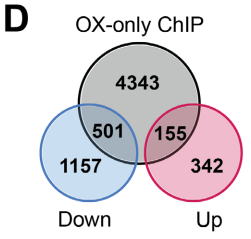

E

	shared		semi-shared		OX only	
	gene	log2FC	gene	log2FC	gene	log2FC
up	TCP16	4.2	JAZ4	2.9	AHP1	2.9
	AHL2	2.8	ANAC042	1.7	HB20	1.7
	GA2OX3	1.3	CLV3	1.3	SMZ	1.3
down	SWEET1	-2.28	BRC1	-1.5	CRC	-2.9
	GA2OX8	-3.1	UFO	-2.20	WOX4	-3.0
	TSF	-3.4	SAUR16	-3.0	BRC2	-4.6
	CKX3	-3.5	FUS3	-3.8	FT	-6.2

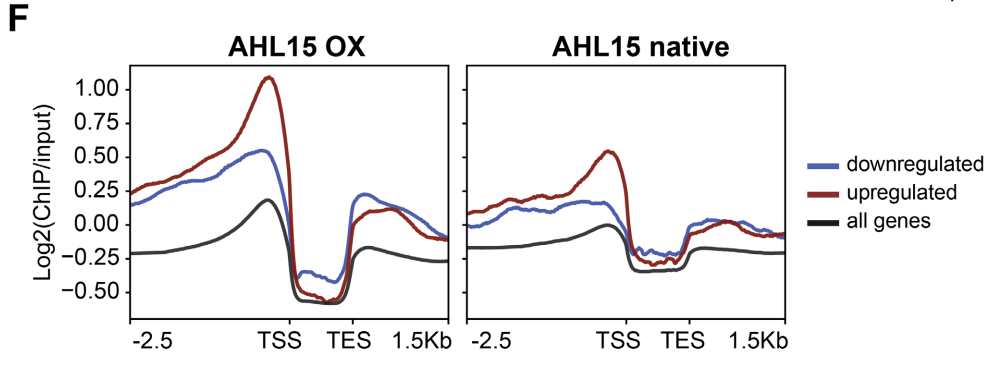

(Figure 3A, Supplementary data 3). Of these, 101 downregulated and 65 upregulated genes were also native targets of AHL15, and 501 downregulated and 155 upregulated genes were overexpression-only targets of AHL15 (Figure 3B-D, Supplementary data 4). A selection of differentially expressed genes that are targeted by AHL15 in native and overexpression conditions is shown in Figure 3E, and includes the flowering-promoting genes *TSF* and *FT* as native and overexpression-only targets, respectively, as well as the meristem maintenance genes *WOX4* and *CLAVATA3* (Fletcher et al., 1999; Ji et al., 2010).

Knowing which genes are differentially expressed upon DEX treatment, we investigated the enrichment of AHL15 ChIP-seq peaks over the differentially expressed genes. To do this, we plotted the average enrichment score of native and overexpression AHL15 ChIP-seq datasets over AHL15-bound upregulated, AHL15-bound downregulated, or all genes. This revealed that AHL15 enrichment was stronger around the TSS and TES of both up- and downregulated genes that were also bound by AHL15 compared to all genes (Figure 3F). Although the majority of differentially expressed genes was downregulated by DEX treatment, and downregulated genes represent a larger fraction of AHL15 DNA binding sites, we observed that AHL15 binding was highest around the TSS of upregulated genes, whereas AHL15 enrichment near the TES was highest for downregulated AHL-bound genes. This suggests that strong AHL15 presence near the TSS of genes may lead to their upregulation, whereas strong AHL15 presence near both the TSS and the TES leads to their downregulation.

Chromatin accessibility is not directly affected by AHL15 induction

Previous research has shown that overexpression of *AHL15* or *AHL27* results in visible changes in chromatin structure (Lim et al., 2007; Karami et al., 2021). , and our ChIP-seq data also show that AHL15 binds to AT-rich DNA with limited sequence specificity throughout the genome. This suggests that AHL15 might alter chromatin accessibility globally. We therefore asked whether the large changes in gene expression we observed upon DEX-induction of AHL15-GR could be a result of altered chromatin accessibility. To test this, we performed ATAC-seq on *p35S:AHL15-GR* seedlings harvested at 30 minutes, 1 hour, and 8 hours after DEX or mock treatment. Surprisingly, we did not observe clear changes in chromatin accessibility at any of the time points: PCA showed that differences between replicates of the same condition were similar or larger than the differences between time points (Figure 4A). For example, ATAC-seq peaks at and around the *FT* locus were similar for all time points, despite a strong downregulation of this gene upon DEX induction (Figure

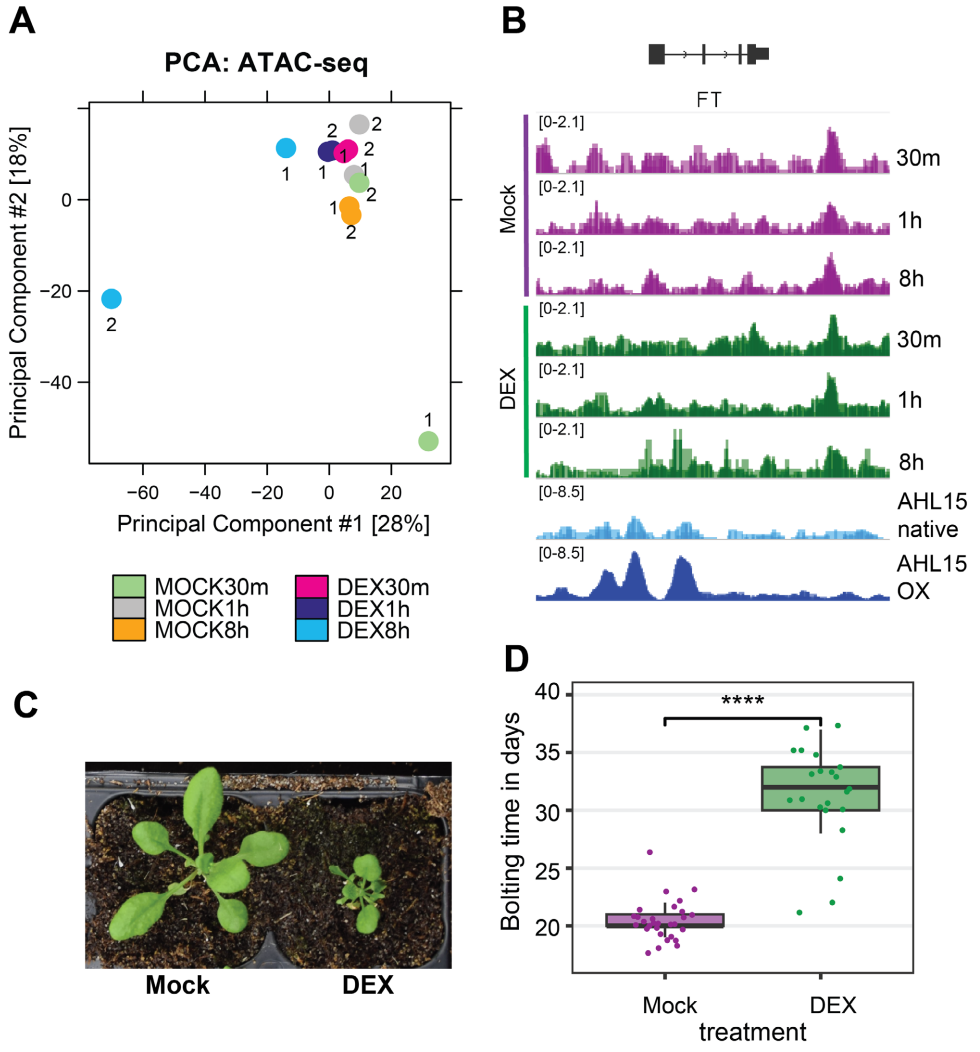

Figure 4: AHL15 delays development but does not affect chromatin accessibility. ATAC-seq of 10 day-old *p35S:AHL15-GR* seedlings that were mock- or DEX treated for 30 minutes, 1 hour or 8 hours. **A:** Principle component analysis of ATAC-seq samples, showing that most samples cluster together and that differences between replicates of the same condition are similar or larger than differences between conditions. **B:** ATAC-seq profiles and AHL15 ChIP-seq profiles at the *FT* locus, a gene that was strongly repressed 8 hours after DEX treatment. Each track shows the overlay of bigwig files from two (ATAC-seq and AHL15 native) or three (AHL15 OX) biological replicates. **C:** Phenotype of mock-treated and DEX-treated *p35S:AHL15-GR* plants at two weeks after DEX treatment (24 day-old plants). Mock-treated plants develop normally and start bolting at this time, whereas DEX-treated plants show an arrested leaf expansion, small stature, and delayed floral transition. **D:** AHL15-GR activation by DEX treatment strongly delays flowering time. Seedlings were transferred to soil two days after DEX treatment and monitored for flowering time (n = 25) and show a significant delay in flowering time (Wilcoxon test, $p = 3.71 \cdot 10^{-9}$). Plants were grown in long day conditions (16 hours light : 8 hours dark).

4B). In addition, we did not detect any differentially accessible regions when comparing DEX- and mock treated samples at the 30m and 1h time points, and identified only 10 regions with differential accessibility for the 8h time point that did not correspond to differentially expressed genes (Supplementary data 5). Although we did not observe clear changes in chromatin accessibility at 8 hours after DEX treatment, the DEX-treated seedlings showed clear phenotypic changes compared to mock-treated seedlings, which resembled the phenotype of *p35S:AHL15* plants (Figure 4C-D; Supplementary figure 1). In addition to a delay in bolting time of about 10 days in DEX-treated plants, new leaves produced at the time of DEX treatment remained very small and did not develop to a full size, resulting in a severe reduction of the plant size. Together with the large number of differentially expressed genes upon DEX treatment, these severe phenotypic changes indicate that AHL15 activation by DEX induces developmental reprogramming. However, our ATAC-seq data indicate that AHL15 does not affect chromatin accessibility directly, and that altered chromatin accessibility cannot explain the differential gene expression patterns observed at the 8h time point and the subsequent developmental reprogramming.

AHL15 binds in regions with reduced epigenetic signatures

Because AHL15 does not have a measurable effect on chromatin accessibility as determined by ATAC-seq, we investigated whether AHL15 binding coincides with epigenetic markers. For this we used publicly available ChIP-seq data of several epigenetic markers in 10 day-old wild-type seedlings (Bourguet et al., 2021). We compared the distribution of these epigenetic markers as well as our ATAC accessibility data with that of AHL15 binding in the native and overexpression conditions by plotting the enrichment of these marks over all Arabidopsis genes (Figure 5). This revealed that AHL15 binding is enriched in regions where chromatin accessibility (based on ATAC seq) is relatively low, and that AHL15 presence is depleted in the highly accessible regions near the TSS and in the gene body (Figure 5A). Similarly, AHL15 showed opposite patterns of enrichment compared to the deposition of H1 (Figure 5B), H2A variants (Figure 5C), and H3K9me1, H3K9me2, and H3K27me1 (Figure 5D). This opposing pattern of enrichment is clearly illustrated when inspecting the sequencing data at individual loci, showing that AHL15 peaks occur at regions where most or all other marks are depleted (Figure 5E). For example, the *TCP16* gene is upregulated in DEX-treated *p35S:AHL15-GR* seedlings, and AHL15 shows clear peaks flanking this gene in both native- and overexpression conditions (Figure

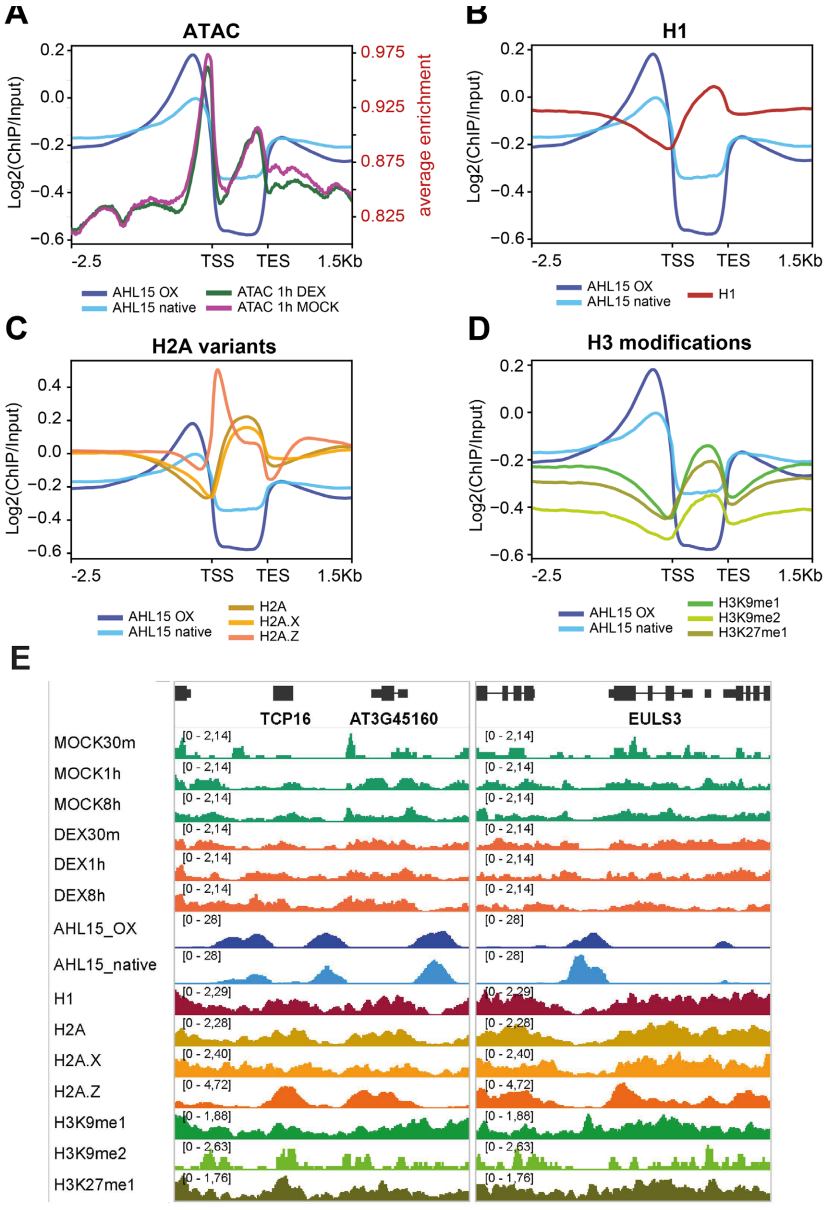

Figure 5: AHL15 binds in regions with reduced accessibility that are depleted of epigenetic marks. **A-D:** ChIP-seq profiles of *pAHL15:3xFLAG-AHL15* (AHL15 native) and *p35S:3xFLAG-AHL15* (AHL15 OX) scaled over all Arabidopsis genes and compared to the ATAC-seq profile of *p35S:AHL15-GR* plants treated with DEX or mock solution for 1 hour (**A**), or to the deposition of Histone 1 (H1) (**B**), Histone 2 variants H2A, H2A.X and H2A.Z (**C**), or the Histone 3 methylation marks H3K9me1, H3K9me2, and H3K27me1 (**D**). **E:** Alignment of the AHL15 native (AHL15_native) and overexpression (AHL15_OX) ChIP-seq profiles at the *TCP16* and *EULS3* loci with the averaged ATAC-seq profiles of ten day-old *p35S:AHL15-GR* seedlings that were mock- or DEX treated for 30 minutes, 1 hour or 8 hours and the epigenetic marks shown in **B-D**.

5E). At regions where AHL15 peaks are visible, a clear reduction in ATAC peaks and H2A.Z, and to a lesser extent H2A, H2A.X, H1, H3K9me1, H3K9me2, and H3K27me1 deposition can be seen. A similar pattern could be observed for all epigenetic marks except H3K9me1, and to a lesser extent H3K27me3, around the AHL15 peak near the *EULS3* locus, whose expression was unaffected by DEX treatment (Figure 5E). These patterns are also visible when plotting the enrichment of epigenetic marks around AHL15 ChIP-seq peaks. This analysis shows that chromatin accessibility (based on ATAC-seq) is reduced around the centre of AHL15 ChIP-seq peaks, and this reduction is most clear around strong AHL15 ChIP-seq peaks that were identified in both the native and overexpression condition and less pronounced around overexpression-only AHL15 peaks (Figure 6). H2A, H2A.X, H2A.Z, and H1 deposition is also depleted most strongly around shared AHL15 peaks (Figure 7), and H3K27me1 and H3K9me2 are both depleted around AHL15 peaks, but less strongly at shared AHL15 peaks than at overexpression-only peaks. Finally, H3K9me1 shows a slight enrichment at shared and semi-shared AHL15 peaks, illustrated by the peak seen at the *EULS3* locus (Figures 5E, 7E). Taken together, these analyses clearly show that AHL15 binds at regions that are depleted of most epigenetic marks, which could be explained in different ways. First, it is possible that AHL15 is repelled by the presence of specific marks such as H2A.Z, and therefore binds only in regions where these marks are absent. Alternatively, it is possible that AHL15 has a preference for regions with reduced chromatin accessibility, which would explain the opposing patterns of AHL15 binding and ATAC-seq peaks. A third possibility is that AHL15 binding results in the removal of the deposition of epigenetic marks, but the depletion of most histone modifications around overexpression-specific AHL15 peaks does not support this idea.

AHL15 binds genes at both ends and may be involved in gene looping

AHL15 binds predominantly near the TSS of genes and is also enriched near the TES (Figure 1[1]A, B, Figure 5E), indicating that its presence at both ends of genes may be inherent to its mechanism of transcriptional regulation. Like AHL proteins, members of the globular H1 domain containing high-mobility group A (GH1-HMGA) protein family have AT-hook DNA-binding domains that bind the minor groove of AT-rich DNA and can affect local chromatin structure (García-Heras et al., 2009; Ozturk et al., 2014; Charbonnel et al., 2018). It was shown that GH1-HMGA proteins bind at both the 5′ and 3′ end of the *FLC* locus and thereby disrupt the formation of a gene loop associated with active transcription, resulting in a reduced transcription of *FLC* and an accelerated flowering time

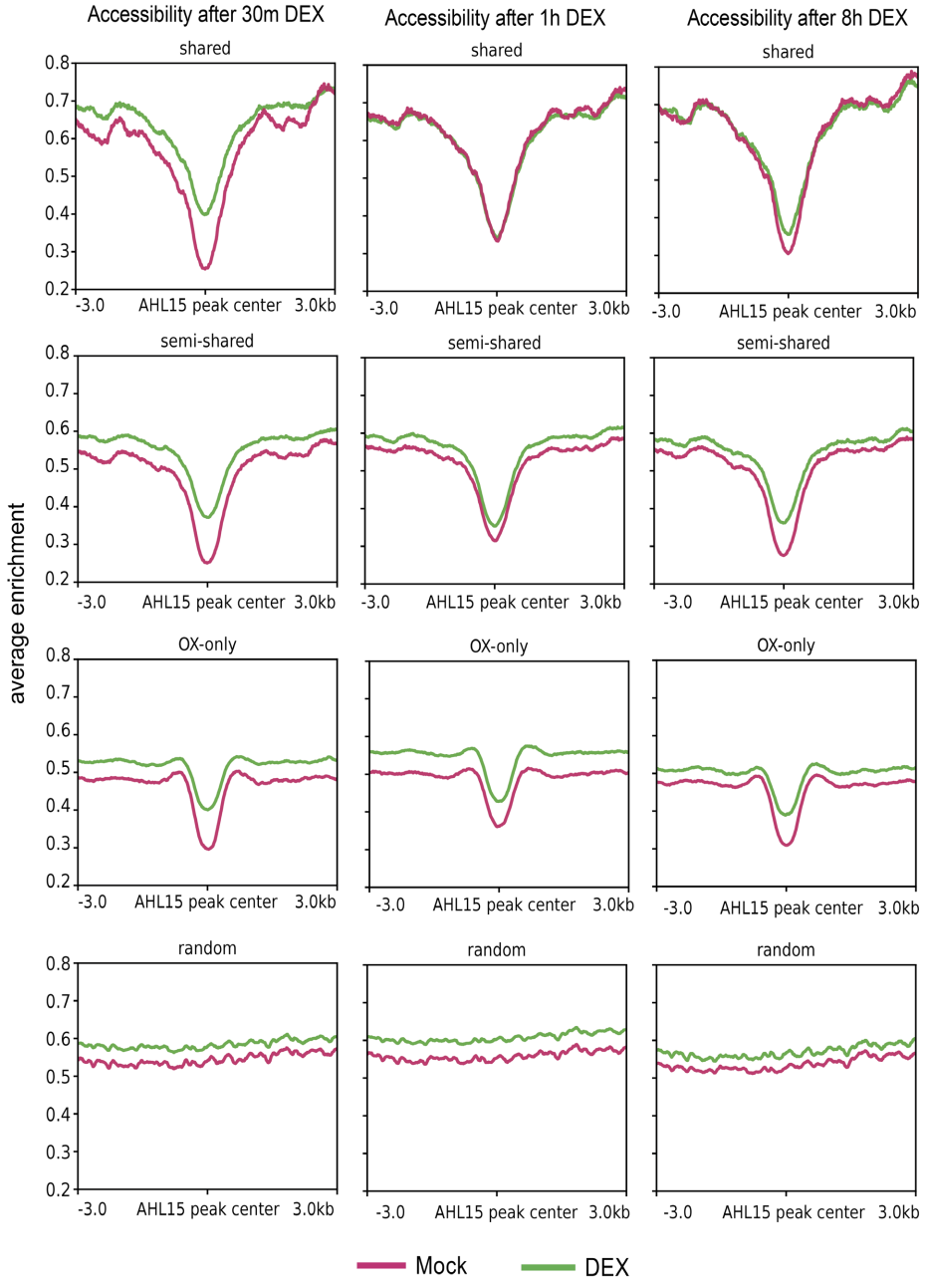

Figure 6: Chromatin accessibility is reduced around AHL15 binding sites. ATAC-seq reads from *p35S:AHL15-GR* plants treated with DEX or mock for 30 minutes, 1 hour or 8 hours were plotted over three classes of AHL15 ChIP-seq peaks presented in Figure 1C: shared (identified in native and overexpression conditions, n = 1948), semi-shared (identified in one native sample and in all overexpression samples, n = 2906), and OX-only (identified in all three overexpression samples, n = 4999). Random genomic coordinates with similar size distribution as the ChIP-seq peaks were used as a negative control (random, n = 15221 regions).

(Zhao et al., 2021). As AHL and GH1-HMGA proteins share the same type of DNA-binding domain, and because AHL15 peaks also flank genes at both ends, we compared our AHL15 ChIP-seq data to previously published ChIP-seq data of GH1-HMGA2/HON5. GH1-HMGA2/HON5 is enriched near the TSS and

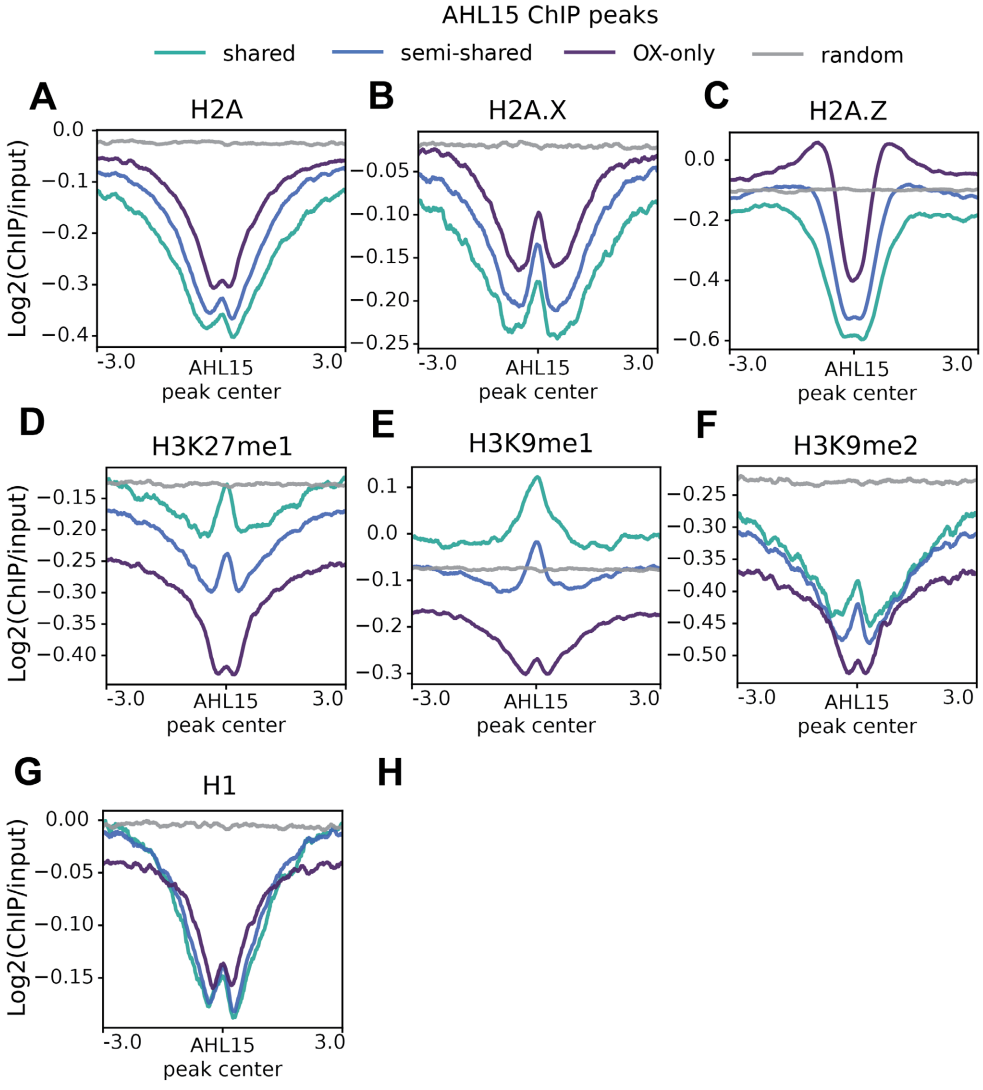

Figure 7: Epigenetic marks are depleted around AHL15 binding sites. **A-G:** ChIP-seq profiles for the epigenetic marks H2A (**A**), H2A.X (**B**), H2A.Z **(C),** H3K27me1 (**D**), H3K9me1 (**E**), H3K9me2 (**F**), and H1 (**G**) were plotted over three classes of AHL15 ChIP-seq peaks presented in Figure 1C: shared (identified in native and overexpression conditions, n = 1948), semi-shared (identified in one native sample and in all overexpression samples, n = 2906), and OX-only (identified in all three overexpression samples, n = 4999). Random genomic coordinates with similar size distribution as the ChIP-seq peaks were used as a negative control (random, n = 15221 regions).

TES of genes in a similar pattern as AHL15, indicating that both proteins may bind at the same position (Figure 8A). To test this, we plotted the enrichment of GH1-HMGA2/HON5 ChIP-seq reads over AHL15 peaks, and found that GH1-HMGA2/HON5 reads are strongly enriched at these positions (Figure 8B). GH1-HMGA2/HON5 binding is strongest at canonical AHL15 binding sites, as it was most enriched at shared AHL15 peaks and weaker at overexpression-only peaks. Comparison of AHL15 and GH1-HMGA2/HON5 enrichment at specific loci further confirmed that they bind at the same position: the GH1-HMGA2/HON55 peak near the TSS of *FLC* was also present in the AHL15 overexpression datasets, as well as a weaker peak near the *FLC* TES (Figure 8C). Similarly, both GH1-HMGA2/HON5 and AHL15 bind at both ends of the self-looping gene *RCD1,* which was also upregulated upon AHL15-GR activation by DEX (Figure 8C). Finally, we compared the AHL15 ChIP-seq data with 1766 previously identified self-looping genes, and found that AHL15 binding at self-looping genes is significantly enhanced in overexpression conditions compared to native conditions (Figure 8D). In addition, at least 91 AHL15-bound self-looping genes were also upregulated, and 77 AHL15-bound self-looping genes were downregulated upon DEX treatment (Figure 8E, Supplementary data 6). Taken together, these comparisons show that like GH1-HMGA proteins, AHL15 is likely to be involved in regulating gene loop formation and may affect the expression of its target genes in this way.

Discussion

Overexpression of various *AHL* genes, and in particular *AHL15,* has been shown to induce developmental reprogramming, causing a delay or even reversal of ageing-related developmental transitions such as vegetative phase change, the floral transition and leaf senescence (Lim et al., 2007; Street et al., 2008; Karami et al., 2020; Karami et al., 2021; Rahimi et al., 2022a; this thesis chapter 4). However, the mechanism causing these developmental changes remained unclear so far. Here, we mapped the genome-wide DNA binding sites of AHL15, and show that AHL15 binds throughout the genome at regions near the TSS and TES and is depleted in gene bodies. Our data show that when overexpressed, AHL15 is present at many ectopic binding sites, and also binds more strongly at its native targets. Despite the clear positional preference of AHL15 for regions upstream of the TSS and downstream of the TES, we did not identify a convincingly conserved binding motif, as the most frequently occurring motifs enriched in AHL15-bound regions also show high occurrence in the genomic background. This suggests that while they show a

clear preference for AT-rich DNA, AHL15 and likely other AHL proteins as well do not recognize specific DNA sequences, but are rather recruited to their AT-rich target sites in a different way.

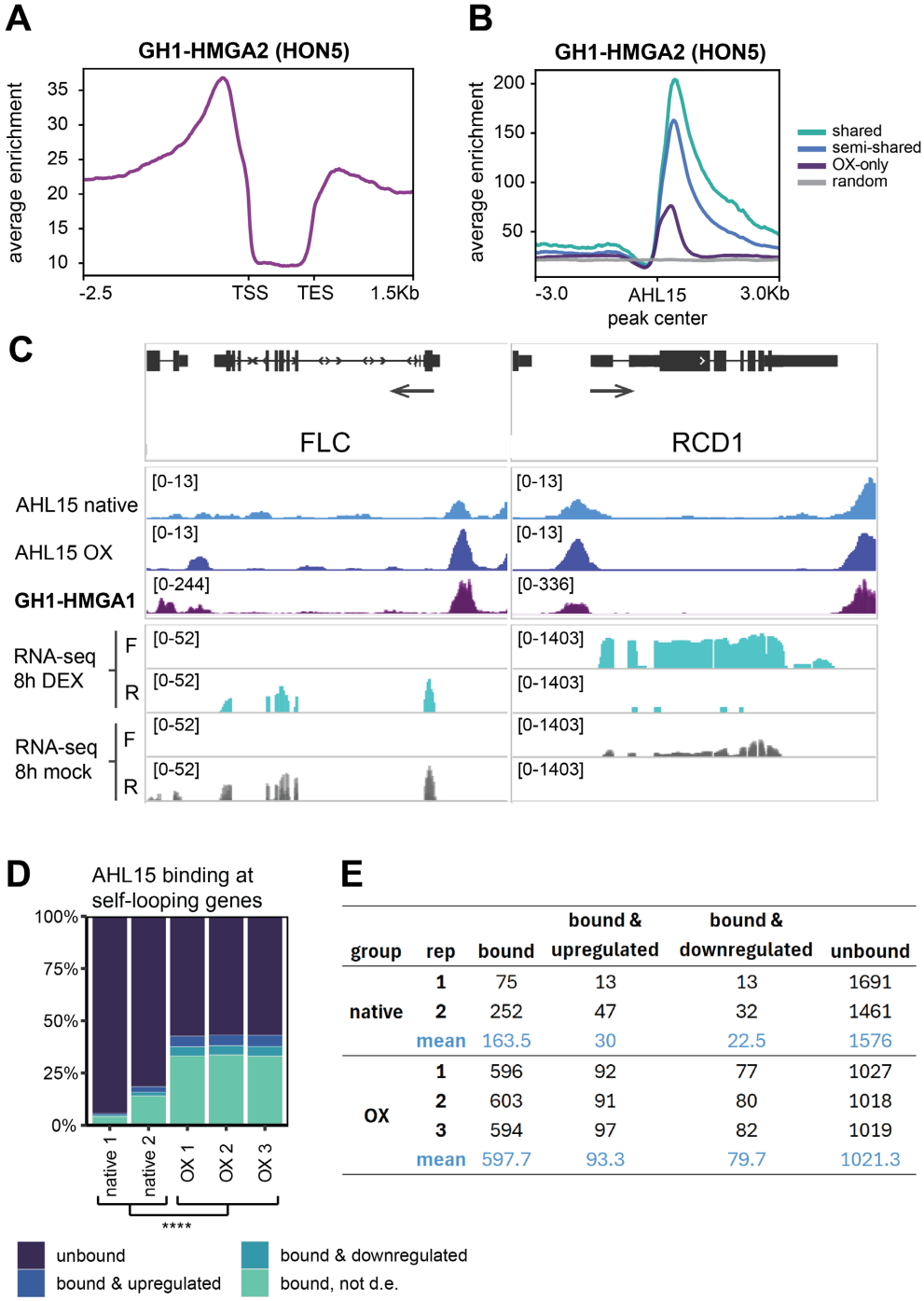

E

group	rep	bound	bound & upregulated	bound & downregulated	unbound
native	1	75	13	13	1691
	2	252	47	32	1461
	mean	163.5	30	22.5	1576
OX	1	596	92	77	1027
	2	603	91	80	1018
	3	594	97	82	1019
	mean	597.7	93.3	79.7	1021.3

Our experiments with the DEX-inducible *p35S:AHL15-GR* line show that *AHL15* overexpression causes strong transcriptional and phenotypic changes, with a majority of differentially expressed genes being downregulated. About one third of these differentially expressed genes was also bound by AHL15, indicating that AHL15 directly regulates the expression of a large number of genes. However, ATAC-seq in the same conditions showed that the changes in transcriptome induced by AHL15-GR activation do not coincide with changes in chromatin accessibility, suggesting that AHL15 regulates transcriptional activation or repression in an accessibility-independent manner. We also compared the positions of AHL15 peaks with ATAC-generated accessibility data, and saw that AHL15 binds regions with relatively low accessibility, just before the highly accessible region around the TSS. As AHL15-GR activation by DEX treatment did not cause changes in the ATAC-seq profile within 8 hours, it is likely that AHL15 binding does not reduce chromatin accessibility itself, but is rather recruited to regions with reduced accessibility. However, it remains unclear what attracts AHL15 or other AHL proteins to a specific locus.

We also investigated whether AHL15 peaks overlap with heterochromatin-associated epigenetic marks such as H1, H3K9me1, and H3K9me2, and observed a clear pattern in which AHL15 flanked most of these marks. AHL proteins were initially discovered as components of the nuclear matrix, and AHL1 was shown to localize at the boundary between heterochromatic regions and H3K4me-marked regions (Fujimoto et al., 2004). Our data show that AHL15 similarly flanks other epigenetic signatures, as we saw no overlap of AHL15 with any mark except a weak overlap with H3K9me1 deposition. It is likely

Figure 8 (left page): AHL15 binds at the same positions as the GH1-HMGA family protein HON5 and may be involved in gene looping. **A:** Profile plot of GH1-HMGA2/HON5 ChIP-seq reads scaled over Arabidopsis genes showing a similar enrichment pattern as AHL15. **B:** GH1-HMGA2/HON5 ChIP-seq reads are were plotted over three classes of AHL15 ChIP-seq peaks presented in Figure 1C shared (identified in native and overexpression conditions, n = 1948), semi-shared (identified in one native sample and in all overexpression samples, n = 2906), and OX-only (identified in all three overexpression samples, n = 4999). **C:** AHL15 and GH1-HMGA2/HON5 ChIP-seq peaks around the *FLC* and *RCD1* loci. ChIP-seq and RNA-seq tracks show an average of biological replicates of the same condition. RNA-seq tracks indicate mapped reads per strand; the *FLC* gene is located on the reverse strand (R) and *RCD1* is located on the forward (F) strand. **D:** AHL15 binding to self-looping genes increases when overexpressed. Percentages of self-looping genes that are not bound by AHL15, bound by AHL15 and are upregulated upon DEX treatment, bound by AHL15 and downregulated upon DEX treatment, and bound by AHL15 but not differentially expressed (d.e.) are shown for each AHL15 ChIP-seq sample. The number of self-looping genes that are bound by AHL15 increases significantly in overexpression samples compared to native samples (X^2 test, $p < 0.0001$). **E:** Table showing the number of self-looping genes in each category shown in **D.**

that AHL15 preferentially binds to regions devoid of epigenetic marks, but we cannot exclude the possibility that AHL15 induces removal of some histone variants or epigenetic modifications, for example that of H2A.Z or H1, which were both more depleted around shared (native and OX) AHL15 peaks than around OX-only peaks. Previous studies have shown that overexpression of different clade A *AHLs* results in increased H3K9me2 and decreased H3Ac deposition at the *FT* and *FLC* loci (Ng et al., 2009; Yun et al., 2012; Xu et al., 2013), but these findings are likely to represent indirect effects of enhanced *AHL* expression rather than direct effects of AHL binding to the loci that were investigated. Genome-wide profiling of epigenetic marks in DEX-induced and non-induced AHL15-GR plants should give conclusive evidence of the effect of AHL15, and by proxy other AHLs, on the deposition of epigenetic marks.

Interestingly, AHL15 peaks overlap with those of GH1-HMGA2/HON5, a protein that was previously shown to interfere with gene loop formation between the 5′ and 3′ ends of the *FLC* locus, thereby hindering *FLC* transcription (Zhao et al., 2021). The similarity in DNA-binding domains between AHL15 and GH1-HMGA2/HON5 explains their overlap in DNA binding sites, and suggests that AHL15 may play a similar role as GH1-HMGA2/HON5 in regulating loop formation. HMGA-family proteins contain four AT-hook domains, whereas clade A AHLs have a single AT-hook domain (Klosterman and Hadwiger, 2002; Zhao et al., 2014). AHLs are known to form complexes with themselves and with other AHLs (Zhao et al., 2013), resulting in a complex that contains three AT-hooks, and this property could be necessary to bind AT-rich DNA with sufficient strength to affect its 3D confirmation. This could explain the strong effect of dominant-negative AHL alleles on the phenotype: the absence of an AT-hook domain in ΔAT-hook variants likely reduces the affinity for DNA of the entire AHL complex they are part of, thereby reducing the potential of entire complexes to bind DNA and modify its architecture. On the other hand, AHL complexes that incorporate the ΔG variant can still bind DNA, but have a reduced ability to recruit interacting proteins that could be required to alter the chromatin architecture. In both cases, the reduced ability of AHL complexes to affect DNA structure likely interferes with the proper regulation of gene expression, explaining the strong phenotypes observed in dominant-negative mutants (Zhao et al., 2013; Karami et al., 2020; Karami et al., 2021). In addition, AHL complexes and HMGAs might compete for the same regions in the DNA and have an effect on gene loop formation via association with different interaction partners. Although the expression of *FLC* was not affected in DEX-treated seedlings, several other self-looping genes were differentially

expressed upon AHL15-GR activation. It would therefore be interesting to study whether these previously reported self-loops are altered upon AHL15-GR activation, whether AHL15 facilitates or disrupts these loops, and whether this results in altered transcription at these loci.

Previous research has shown that TFs that activate gene expression preferentially bind to regions near the TSS, whereas repressors are more likely to bind both near the TSS and near the TES (Franco-Zorrilla et al., 2014). In line with this, we observed that AHL15 enrichment was enhanced around the TSS of AHL15-bound upregulated genes, whereas enrichment near the TES was highest for AHL15-bound downregulated genes. This suggests that strong association of AHL15 with the TSS of genes relative to the TES enhances their expression and that a more equal distribution of AHL15 binding near the TSS and TES represses their expression. However, the effect of AHL15 binding at these regions on gene loop formation remains unclear.

Finally, our ATAC-seq data shows that AHL15 does not directly affect chromatin accessibility. This result is surprising, as earlier reports have shown that overexpression of *AHL15* or *AHL27* causes visible changes in the intensity of heterochromatin foci in the nucleus, suggesting a reduced chromatin compaction (Lim et al., 2007; Karami et al., 2021). It is possible that AHL15 induces chromatin opening on a slower time scale than measured here, but our finding that AHL15 may act similar to GH1-HMGA2/HON5 in the 3D organization of DNA could offer an alternative explanation for this phenomenon. GH1-HMGA2/HON5 was shown to disrupt chromatin looping on a local scale, but the authors did not investigate the effect of this protein on the global 3D structure of the DNA (Zhao et al., 2021). As chromatin architectural modifiers, it is likely that both GH1-HMGA and AHL proteins can affect chromatin looping on short-range as well as long-range scales. Here, we have shown that AHL15 binds in regions depleted in histone modifications and other epigenetic signatures, and similarly, AHL1 was shown to be present at the boundaries between H3K4me-marked euchromatin and DAPI-stained heterochromatin foci (Fujimoto et al., 2004). It is therefore possible that excessive AHL presence alters or disrupts these boundaries, causing changes in heterochromatin compartmentalization that result in the disappearance of heterochromatin foci that is observed in *AHL* overexpression lines (Lim et al., 2007; Karami et al., 2021).

Materials & methods

Plant material and growth conditions

The Arabidopsis *p35S:AHL15-GR* line and *ahl15* (SALK_040729) loss-of-function mutant have been described previously (Karami et al., 2020). *p35S:3xFLAG-AHL15* or *pAHL15:3xFLAG-AHL15* constructs were cloned into the binary vector pMDC32 (Karimi et al., 2007) and transformed to Arabidopsis by floral dip (Clough and Bent, 1998). Overexpression constructs were expressed in the Col-0 background and *pAHL15:3xFLAG-AHL15* was expressed in the *ahl15* loss-of-function mutant background, and only plants homozygous for the T-DNA insertion were used for experiments. Seeds were sterilized in 2% sodium hypochlorite for 2 minutes and washed with sterile milliQ water (mQ) before plating on ½ MS medium and then stratified for three days at 4 °C. For seedling experiments, plates were placed vertically in a growth chamber and grown for 10 days in long-day conditions (16h light/8h dark) at 21 °C. For overexpression ChIP, *p35S:3xFLAG-AHL15* seedlings were grown on ½ MS with 15 mg/L kanamycin for 10 days and then transferred to soil and grown in a growth chamber at 21 °C with long-day conditions for an additional 21 days prior to harvesting whole shoots for ChIP.

ChIP-seq

The ChIP protocol used was adapted from the protocols by Kaufmann et al. (2010) and Chouaref et al. (2018). For each ChIP, 1 g of shoot tissue from 31 day-old *35S:3xFLAG-AHL15* or 10 day-old *pAHL15:3xFLAG-AHL15* plants was harvested and fixated for 10 minutes on ice and under vacuum in 1% formaldehyde in ice-cold MC buffer (10 mM sodium phosphate buffer pH 7, 50 mM NaCl, 0.1 M sucrose). The fixation reaction was stopped by saturation with glycine, and samples were washed in ice-cold MC buffer, dried with tissue paper, and stored at -80 °C. For nuclei isolation, frozen fixated tissue was ground to a very fine powder in liquid nitrogen using a mortar and pestle, and was then resuspended in 15 mL M1 buffer (10 mM sodium phosphate buffer pH 7, 0.1 M NaCl, 1 M 2-methyl 2,4-pentanediol, 10 mM β-mercaptoethanol) and gently shaken at 4 °C for 30 minutes. Suspensions were subsequently filtered through respectively a 100 µM and a 70 µM nylon mesh, both of which were washed with an additional 5 mL M1 buffer to extract remaining nuclei. The filtered suspension was then centrifuged for 20 minutes at 1000x*g* at 4°C, and pellets were resuspended in 20 mL M2 buffer (10 mM sodium phosphate buffer

pH 7, 0.1 M NaCl, 1 M 2-methyl 2,4-pentanediol, 10 mM β-mercaptoethanol, 10 mM $MgCl_2$, 0.5% Triton X-100). After 30 minutes of gentle shaking at 4 °C, the suspension was centrifuged for 10 minutes at 1000x*g* at 4 °C, the supernatant was discarded and the pellet was resuspended again in 5 mL M2 buffer. After 10 minutes of gentle shaking followed by 10 minutes centrifugation at 1000x*g* at 4 °C, the pellet was resuspended in 1 mL sonication buffer (10 mM sodium phosphate buffer pH 7, 0.1 M NaCl, 0.5% Sarkosyl, 10 mM EDTA) and aliquoted to 300 µL in 1.5 mL protein lobind tubes (Eppendorf, Germany). Samples were then sonicated in a Bioruptor sonicator (Diagenode, Seraing, Belgium) on HIGH for 5 rounds of 10 cycles of 30 seconds ON / 30 seconds OFF to a fragment size of ~300 bp. After sonication, tubes of the same replicate were pooled and spun for 10 minutes at 12000x*g at* 4 °C, and the supernatant was transferred to a new tube and stored at -20 °C.

For the immunoprecipitation, 50 µg chromatin was used per IP (ca 250 µL sonicated material), and 3.5 volumes IP buffer (50 mM HEPES pH 7.5, 150 mM NaCl, 5 mM $MgCl_2$, 10 µM $ZnSO_4$, 1% Triton X-100, 0.05% SDS) and 25 µL protein G dynabeads (ThermoFischer, Lithuania) conjugated to mouse monoclonal Anti-FLAG M2 antibodies (F1804; Sigma-Aldrich, Darmstadt, Germany) were added and rotated at 4 °C overnight. After this, beads were washed once in 1 mL of each of the following buffers: IP buffer, high salt buffer (500 mM NaCl, 0.1% SDS, 1% Triton X-100, 2 mM EDTA, 20 mM Tris-HCl pH 8), LiCl buffer (10 mM Tris-HCl pH 8, 1 mM EDTA, 1% NP-40, 1% sodium deoxycholate, 0.25 M LiCl), and twice in TE buffer (10 mM Tris-HCl pH 8, 1 mM EDTA), and then resuspended in 50 µL TE buffer. Samples were decrosslinked overnight at 65 °C after adding 450 µL of decrosslinking buffer (50 mM Tris-HCl pH 8, 10 mM EDTA pH 8, 250 mM NaCl, 1 % (w/v) SDS). DNA was cleaned by phenol: chloroform extraction, ethanol precipitated, and resuspended in milliQ and treated with RNAse A (ThermoScientific, Vilnius, Lithuania) for 30 minutes at 37 °C, and then stored at -20 °C until sequencing. ChIP samples were sequenced with the Illumina Novaseq 6000 at Macrogen (Amsterdam, the Netherlands) with 20 million 150 bp paired-end reads.

RNA-seq

Ten day-old seedlings (Col-0 and *p35S:AHL15-GR*) were flooded at zeitgeber time 1 with 35 mL 20 µM DEX in milliQ or with a mock solution with an equivalent volume of DMSO for 15 minutes, after which the solution was siphoned off. The plates were returned to the growth chambers and five seedlings per replicate (n=3) of each condition (*p35S:AHL15-GR* + DEX, *p35S:AHL15-GR* + mock, Col-

0 + DEX, Col-0 + mock) were harvested (shoot only) after eight hours and snap-frozen in liquid nitrogen. The frozen plant material was pulverized with a metal bead in a Tissuelyser (Qiagen, Hilden, Germany) and RNA was isolated using Trizol© (ThermoFischer, Vilnius, Lithuania) with an additional ethanol wash step. For sequencing, 3 µg RNA was aliquoted and treated with DNAse-I (ThermoFischer, Vilnius, Lithuania) for 30 minutes at 37 °C. Library preparation and sequencing with the Illumina Novaseq 6000 (150 bp paired-end, 10 million reads) was done at Baseclear (Leiden, the Netherlands).

ATAC-seq

Seedlings were treated with DEX or mock solution as for RNA-seq. For each replicate, approximately 50 DEX- or mock-treated seedlings were harvested (shoot only) at 30 minutes, 1 hour, or 8 hours after treatment, dried, and snap-frozen in liquid nitrogen and stored at -80 °C. Nuclei isolation was done by chopping frozen seedlings on ice in 2 mL nuclei isolation buffer (INGR) and subsequent filtering through a 40 µM mesh according to the protocol by Wang et al. (2021). Nuclei were diluted 5-fold in nuclei isolation buffer and stained with propidium iodide. 55,000 nuclei were sorted per sample using the S3e Cell Sorter (Bio-Rad, Hercules, USA) with FSC = 365 and SSC = 299. Nuclei were subsequently pelleted and Tagmentation and library amplification was done using the Zymo-seq ATAC library kit (D5458, Zymo Research, Irvine, USA). Sequencing was done with the Illumina Novaseq 6000 (150 bp paired-end, 20 million reads) at Baseclear (Leiden, the Netherlands).

Bioinformatic analysis

ChIP-seq, RNA-seq, and ATAC-seq analyses were done with Nextflow using the NF core ChIP-seq, ATAC-seq, or RNA-seq pipelines (Ewels et al., 2020), and reads were mapped to the TAIR10 Arabidopsis genome annotation. The threshold for peak identification by MACS2 in the NF core pipeline was lowered to $p < 0.05$ for ATAC-seq samples due to a low library complexity in these samples. For ChIP, reads were annotated in R using the ChIPSeeker package (Yu et al., 2015; Wang et al., 2022), and differential expression analysis for RNA-seq and differential accessibility analysis for ATAC-seq was done using the DESeq2 package (Love et al., 2014). Differentially expressed genes were calculated by comparing the DEX-treated *p35S:AHL15-GR* condition with the three control conditions (*p35S:AHL15-GR* + mock, Col-0 + mock and Col-0 + DEX), as the difference between control conditions was sufficiently small to exclude a strong effect

of DEX on gene expression in Col-0 (Supplementary Figure 5). For ATAC-seq, mock- and DEX-treated samples at the same time point were compared.

Heatmaps of ChIP-seq reads were generated using deepTools (Ramírez et al., 2016). To annotate ChIP-seq peaks over genomic features, we used BEDTools (Quinlan and Hall, 2010) to categorize the TAIR10 genome into non-overlapping regions of the following categories: promoters (0-3 kb upstream of TSS), TES (0-1 kb downstream of TES), TES and promoter (regions where promoters and TES of adjacent genes overlapped), exon, intron, 5′ UTR, 3′ UTR, and intergenic (regions that are not covered by any of the other categories). Overlap between ChIP-seq and RNA-seq datasets was calculated in R, and ChIP-seq peaks shared between all AHL15 datasets, shared between 4/5 AHL15 datasets, or unique to the overexpression datasets were identified using R and exported as BED files for further comparisons. Additionally, the ChIP peak coordinates of one *AHL15* overexpression ChIP-seq dataset were shuffled over the Arabidopsis genome to generate a set of random peak coordinates as a control. Motif enrichment analyses and de novo motif finding were done using HOMER2 (Heinz et al., 2010).

For the analysis of ChIP-seq data of epigenetic marks, raw data of epigenetic markers in wild type plants generated by Bourguet et al. (2021) was downloaded from GEO and re-analyzed with the NF core ChIP-seq pipeline. For generating profile plots of the various epigenetic marks over Arabidopsis genes or the AHL15 peaks, bigwig files of individual replicates were first normalized to input using a log2 normalization method and subsequently averaged before calculation of the count matrices and profile plotting with deepTools.

Acknowledgements

We thank Jan Vink, Altay Temel, Ward de Winter and Mariel Lavrijsen for technical support and Alex Bos, Marjolein Crooijmans and Dennis Claessen for help with nuclear sorting for ATAC-seq. We thank Salma Balazadeh for sharing her ChIP-seq protocol and Maike Stam for her advice on the ATAC-seq experiment.

Literature

Bourguet P., Picard C.L., Yelagandula R., Pélissier T., Lorković Z.J., Feng S., Pouch-Pélissier M.N., Schmücker A., Jacobsen S.E., Berger F., et al (2021). The histone variant H2A.W and linker histone H1 co-regulate heterochromatin accessibility and DNA methylation. Nat Commun **12**: 1–12.

Charbonnel C., Rymarenko O., Ines O. Da, Benyahya F., White C.I., Butter F., Amiard S. (2018). The linker histone GH1-HMGA1 is involved in telomere stability and DNA damage repair. Plant Physiol **177**: 311–327.

Chouaref J., de Boer E., Fransz P., Stam M. (2018). Protocol for chromatin immunoprecipitation of meiotic-stage-specific tomato anthers. Curr Protoc Plant Biol **3**: e20074.

Clough S.J., Bent A.F. (1998). Floral dip: a simplified method for *Agrobacterium*-mediated transformation of *Arabidopsis thaliana*. Plant J **16**: 735–743.

Ewels P.A., Peltzer A., Fillinger S., Patel H., Alneberg J., Wilm A., Garcia M.U., Di Tommaso P., Nahnsen S. (2020). The nf-core framework for community-curated bioinformatics pipelines. Nat Biotech **38**: 276–278.

Favero D.S., Kawamura A., Shibata M., Takebayashi A., Jung J.H., Suzuki T., Jaeger K.E., Ishida T., Iwase A., Wigge P.A., et al (2020). AT-Hook transcription factors restrict petiole growth by antagonizing PIFs. Curr Biol **30**: 1454–1466.

Fletcher J.C., Brand U., Running M.P., Simon R., Meyerowitz E.M. (1999). Signaling of cell fate decisions by CLAVATA3 in Arabidopsis shoot meristems. Science (1979) **283**: 1911–1914.

Franco-Zorrilla J.M., López-Vidriero I., Carrasco J.L., Godoy M., Vera P., Solano R. (2014). DNA-binding specificities of plant transcription factors and their potential to define target genes. PNAS **111**: 2367–2372.

Fujimoto S., Matsunaga S., Yonemura M., Uchiyama S., Azuma T., Fukui K. (2004). Identification of a novel plant MAR DNA binding protein localized on chromosomal surfaces. Plant Mol Biol **56**: 225–239.

García-Heras F., Padmanabhan S., Murillo F.J., Elías-Arnanz M. (2009). Functional equivalence of HMGA- and histone H1-like domains in a bacterial transcriptional factor. PNAS **106**: 13546–13551.

Heinz S., Benner C., Spann N., Bertolino E., Lin Y.C., Laslo P., Cheng J.X., Murre C., Singh H., Glass C.K. (2010). Simple combinations of lineage-determining transcription factors prime cis-regulatory elements required for macrophage and B cell identities. Mol Cell **38**: 576–89.

Ji J., Strable J., Shimizu R., Koenig D., Sinha N., Scanlon M.J. (2010). WOX4 promotes procambial development. Plant Physiol **152**: 1346–1356.

Karami O., Henkel C., Offringa R. (2022). The effect of short-term activation of AHL15 on long-term plant developmental change and transcriptome profile. bioRxiv 2022.09.05.506087.

Karami O., Rahimi A., Khan M., Bemer M., Hazarika R.R., Mak P., Compier M., van Noort V., Offringa R. (2020). A suppressor of axillary meristem maturation promotes longevity in flowering plants. Nat Plants **6**: 368–376.

Karami O., Rahimi A., Mak P., Horstman A., Boutilier K., Compier M., van der Zaal B., Offringa R. (2021). An Arabidopsis AT-hook motif nuclear protein mediates somatic embryogenesis and coinciding genome duplication. Nat Commun **12**: 2508.

Karimi M., Depicker A., Hilson P. (2007). Recombinational Cloning with Plant Gateway Vectors. Plant Physiol **145**: 1144–1154.

Kaufmann K., Muiño J.M., Østerås M., Farinelli L., Krajewski P., Angenent G.C. (2010). Chromatin immunoprecipitation (ChIP) of plant transcription factors followed by sequencing (ChIP-SEQ) or hybridization to whole genome arrays (ChIP-CHIP). Nat Protoc **5**: 457–472.

Kim H.B., Oh C.J., Park Y.C., Lee Y., Choe S., An C.S., Choi S.B. (2011). Comprehensive analysis of *AHL* homologous genes encoding AT-hook motif nuclear localized protein in rice. BMB Rep **44**: 680–685.

Klosterman S.J., Hadwiger L.A. (2002). Plant HMG proteins bearing the AT-hook motif. Plant Science **162**: 855–866.

Kumar A., Singh S., Mishra A. (2023). Genome-wide identification and analyses of the AHL gene family in rice (*Oryza sativa*). 3 Biotech. doi: 10.1007/s13205-023-03666-0

Lee K., Seo P.J. (2017). Coordination of matrix attachment and ATP-dependent chromatin remodeling regulate auxin biosynthesis and Arabidopsis hypocotyl elongation. PLoS One **12**: 1–19.

Lim P.O., Kim Y., Breeze E., Koo J.C., Woo H.R., Ryu J.S., Park D.H., Beynon J., Tabrett A., Buchanan-Wollaston V., et al (2007). Overexpression of a chromatin architecture-controlling AT-hook protein extends leaf longevity and increases the post-harvest storage life of plants. Plant J **52**: 1140–1153.

Lin L., Nakano H., Nakamura S., Uchiyama S., Fujimoto S., Matsunaga S., Kobayashi Y., Ohkubo T., Fukui K. (2007). Crystal structure of *Pyrococcus horikoshii* PPC protein at 1.60 Å resolution. Proteins: Structure, Function, and Bioinformatics **67**: 505–507.

Love M.I., Huber W., Anders S. (2014). Moderated estimation of fold change and dispersion for RNA-seq data with DESeq2. Genome Biol **15**: 550.

Machaj G., Grzebelus D. (2021). Characteristics of the *at-hook motif containing nuclear localized (AHL)* genes in carrot provides insight into their role in plant growth and storage root development. Genes (Basel) **12**: 764.

Ng K.H., Yu H., Ito T. (2009). AGAMOUS controls GIANT KILLER, a multifunctional chromatin modifier in reproductive organ patterning and differentiation. PLoS Biol **7**: e1000251.

Ozturk N., Singh I., Mehta A., Braun T., Barreto G. (2014). HMGA proteins as

modulators of chromatin structure during transcriptional activation. Front Cell Dev Biol **2**: 1–9.

Quinlan A.R., Hall I.M. (2010). BEDTools: a flexible suite of utilities for comparing genomic features. Bioinformatics **26**: 841.

Rahimi A., Karami O., Balazadeh S., Offringa R. (2022a). miR156 -independent repression of the ageing pathway by longevity-promoting AHL proteins in Arabidopsis. New Phytol **235**: 2424–2438.

Rahimi A., Karami O., Lestari A.D., de Werk T., Amakorová P., Shi D., Novák O., Greb T., Offringa R. (2022b). Control of cambium initiation and activity in Arabidopsis by the transcriptional regulator AHL15. Curr Biol **32**: 1764–1775.

Ramírez F., Ryan D.P., Grüning B., Bhardwaj V., Kilpert F., Richter A.S., Heyne S., Dündar F., Manke T. (2016). deepTools2: a next generation web server for deep-sequencing data analysis. Nucleic Acids Res **44**: W160–W165.

Street I.H., Shah P.K., Smith A.M., Avery N., Neff M.M. (2008). The AT-hook-containing proteins SOB3/AHL29 and ESC/AHL27 are negative modulators of hypocotyl growth in Arabidopsis. Plant Journal **54**: 1–14.

Tayengwa R., Sharma Koirala P., Pierce C.F., Werner B.E., Neff M.M. (2020). Overexpression of *AtAHL20* causes delayed flowering in Arabidopsis via repression of *FT* expression. BMC Plant Biol **20**: 559.

Wang F.X., Shang G.D., Wu L.Y., Mai Y.X., Gao J., Xu Z.G., Wang J.W. (2021). Protocol for assaying chromatin accessibility using ATAC-seq in plants. STAR Protoc. doi: 10.1016/j.xpro.2020.100289

Wang Q., Li M., Wu T., Zhan L., Li L., Chen M., Xie W., Xie Z., Hu E., Xu S., et al (2022). Exploring Epigenomic Datasets by ChIPseeker. Curr protoc **2**: e585.

Xiao C., Chen F., Yu X., Lin C., Fu Y.F. (2009). Over-expression of an *AT-hook gene, AHL22*, delays flowering and inhibits the elongation of the hypocotyl in *Arabidopsis thaliana*. Plant Mol Biol **71**: 39–50.

Xiong S.X., Zeng Q.Y., Hou J.Q., Hou L.L., Zhu J., Yang M., Yang Z.N., Lou Y. (2020). The temporal regulation of TEK contributes to pollen wall exine patterning. PLoS Genet **16**: e1008807.

Xu L., Zheng S., Witzel K., Van De Slijke E., Baekelandt A., Mylle E., Van Damme D., Cheng J., De Jaeger G., Inzé D., et al (2024). Chromatin attachment to the nuclear matrix represses hypocotyl elongation in *Arabidopsis thaliana*. Nat Commun **15**: 1286.

Xu Y., Wang Y., Stroud H., Gu X., Sun B., Gan E.S., Ng K.H., Jacobsen S.E., He Y., Ito T. (2013). A matrix protein silences transposons and repeats through interaction with retinoblastoma-associated proteins. Curr Biol **23**: 345–350.

Yu G., Wang L.G., He Q.Y. (2015). ChIPseeker: an R/Bioconductor package for ChIP peak annotation, comparison and visualization. Bioinformatics **31**: 2382–2383.

Yun J., Kim Y.-S., Jung J.-H., Seo P.J., Park C.-M. (2012). The AT-hook motif-containing protein AHL22 regulates flowering initiation by modifying

FLOWERING LOCUS T chromatin in Arabidopsis. J Biol Chem **287**: 15307–15316.

Zhao B., Xi Y., Kim J., Sung S. (2021). Chromatin architectural proteins regulate flowering time by precluding gene looping. Sci Adv **7**: 3097–3108.

Zhao J., Favero D.S., Peng H., Neff M.M. (2013). *Arabidopsis thaliana AHL* family modulates hypocotyl growth redundantly by interacting with each other via the PPC/DUF296 domain. PNAS **110**: E4688–E4697.

Zhao J., Favero D.S., Qiu J., Roalson E.H., Neff M.M. (2014). Insights into the evolution and diversification of the *AT-hook Motif Nuclear Localized* gene family in land plants. BMC Plant Biol **14**: 1–19.

Zhou J., Wang X., Lee J.Y., Lee J.Y. (2013). Cell-to-cell movement of two interacting AT-Hook factors in Arabidopsis root vascular tissue patterning. Plant Cell **25**: 187–201.

Supplementary figures

Supplementary figure 1: Phenotype of 31 day-old *p35S:3xFLAG-AHL15* plants right before harvesting for ChIP. White arrowheads mark plants with particularly strong AHL15-induced delay of development. Plants were grown in LD (16h light / 8h dark), and the scale on the bottom of the image is in cm.

Supplementary figure 2 (right page): HOMER de novo motif finding results calculated based on all AHL15 peaks (shared, semi-shared, and overexpression-only). **A:** Table of the top 20 enriched motifs identified by HOMER2 within all AHL15 peaks. **B:** The number of times each motif (75 in total) is identified by HOMER2 in all AHL15 peaks divided by its number over the entire genome (expressed as %: 100% means the motif is almost only present in AHL15 peaks). **C:** The frequency with which each motif identified by HOMER2 occurs in all AHL15 peaks, expressed as the Log2 value of the % of shared AHL15 targets containing the specific motif (occurrence of more than 1% gives a positive value, 1% gives a value of 0, and less than 1% results in a negative value). Motifs in figures **B** and **C** are arranged by descending target : background value.

A

Total target sequences = 12083
Total background sequences = 40333
* - possible false positive

Rank	Motif	P-value	log P-pvalue	% of Targets	% of Background	STD(Bg STD)
1		1e-23	-5.519e+01	0.17%	0.01%	11.2bp (9.9bp)
2		1e-18	-4.155e+01	0.14%	0.01%	9.2bp (6.3bp)
3		1e-18	-4.155e+01	0.14%	0.01%	11.5bp (4.2bp)
4		1e-17	-4.087e+01	0.16%	0.01%	13.7bp (10.2bp)
5		1e-17	-3.948e+01	0.18%	0.02%	11.2bp (7.8bp)
6		1e-16	-3.828e+01	0.13%	0.01%	9.1bp (19.7bp)
7		1e-16	-3.789e+01	0.15%	0.01%	12.5bp (15.6bp)
8		1e-15	-3.573e+01	0.24%	0.03%	14.2bp (13.1bp)
9		1e-15	-3.506e+01	0.12%	0.01%	13.0bp (8.1bp)
10		1e-15	-3.506e+01	0.12%	0.01%	8.1bp (1.6bp)
11		1e-15	-3.496e+01	0.14%	0.01%	11.2bp (10.9bp)
12		1e-14	-3.322e+01	0.41%	0.11%	12.1bp (15.7bp)
13		1e-14	-3.269e+01	0.18%	0.02%	10.5bp (11.0bp)
14		1e-13	-3.192e+01	0.12%	0.01%	12.3bp (17.4bp)
15		1e-13	-3.177e+01	0.16%	0.02%	10.5bp (8.9bp)
16		1e-13	-3.173e+01	0.21%	0.03%	12.8bp (14.7bp)
17		1e-13	-3.170e+01	3.14%	2.08%	12.2bp (13.9bp)
18		1e-12	-2.779e+01	0.13%	0.01%	13.0bp (3.4bp)
19		1e-12	-2.778e+01	0.18%	0.03%	12.6bp (10.0bp)
20 *		1e-11	-2.663e+01	0.22%	0.04%	12.9bp (12.6bp)

B

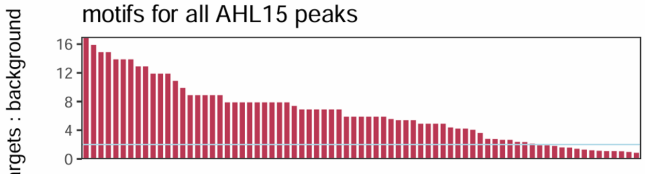

C

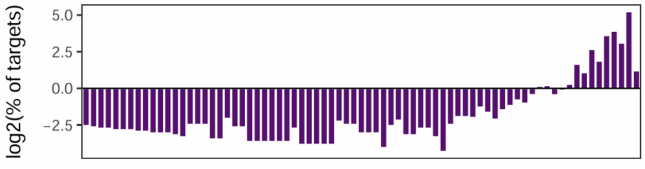

A

Total target sequences = 6522
Total background sequences = 40000
* - possible false positive

Rank	Motif	P-value	log P-pvalue	% of Targets	% of Background	STD(Bg STD)
1		1e-18	-4.268e+01	0.18%	0.00%	15.2bp (0.8bp)
2		1e-18	-4.248e+01	0.26%	0.01%	12.1bp (3.0bp)
3		1e-15	-3.572e+01	0.24%	0.01%	12.4bp (14.4bp)
4		1e-14	-3.451e+01	0.18%	0.01%	14.1bp (10.8bp)
5		1e-14	-3.404e+01	0.15%	0.00%	9.3bp (6.5bp)
6		1e-12	-2.985e+01	0.14%	0.00%	7.6bp (0.0bp)
7		1e-12	-2.871e+01	0.59%	0.14%	10.8bp (13.2bp)
8 *		1e-11	-2.605e+01	0.23%	0.02%	8.6bp (20.3bp)

B

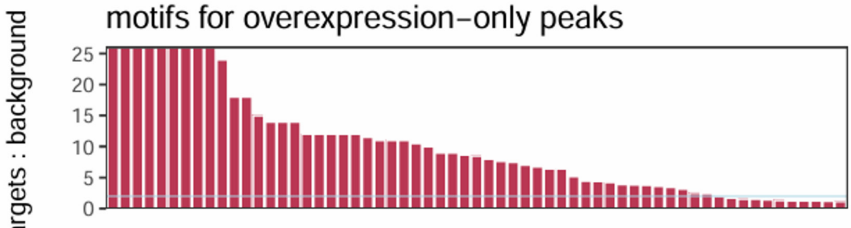

C

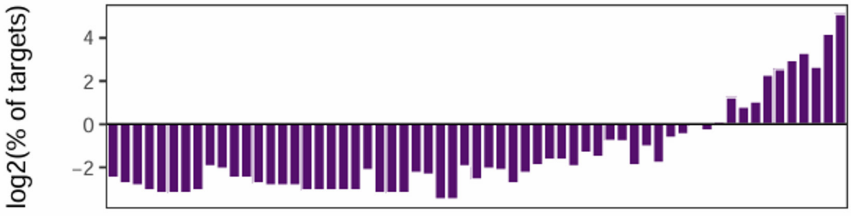

Supplementary figure 3: HOMER de novo motif finding results for overexpression-only peaks. **A:** Table of the top 8 enriched motifs identified by HOMER2 within the set of overexpression-only peaks. **B:** The number of times each motif (61 in total) is identified by HOMER2 in overexpression-only AHL15 peaks divided by its number over the entire genome (expressed as %: 100% means the motif is almost only present in AHL15 peaks). **C:** The frequency with which each motif identified by HOMER2 occurs in overexpression-only AHL15 peaks, expressed as the Log2 value of the % of shared AHL15 targets containing the specific motif (occurrence of more than 1% gives a positive value, 1% gives a value of 0, and less than 1% results in a negative value). Motifs in figures **B** and **C** are arranged by descending target : background value.

A

Total target sequences = 4000
Total background sequences = 51667
* - possible false positive

Rank	Motif	P-value	log P-pvalue	% of Targets	% of Background	STD(Bg STD)
1		1e-19	-4.398e+01	0.38%	0.01%	10.8bp (9.3bp)
2		1e-15	-3.683e+01	0.28%	0.01%	10.2bp (5.9bp)
3		1e-14	-3.269e+01	0.25%	0.01%	9.5bp (10.4bp)
4		1e-14	-3.263e+01	0.35%	0.02%	13.7bp (12.0bp)
5		1e-13	-3.124e+01	8.03%	5.18%	11.4bp (13.0bp)
6		1e-13	-3.017e+01	0.20%	0.00%	8.2bp (0.0bp)
7		1e-13	-3.017e+01	0.20%	0.00%	10.6bp (1.7bp)
8		1e-12	-2.937e+01	0.28%	0.01%	12.7bp (14.0bp)
9		1e-12	-2.872e+01	0.25%	0.01%	9.2bp (10.2bp)
10		1e-12	-2.864e+01	0.23%	0.01%	11.5bp (7.6bp)
11 *		1e-11	-2.592e+01	0.25%	0.01%	10.4bp (5.8bp)

B

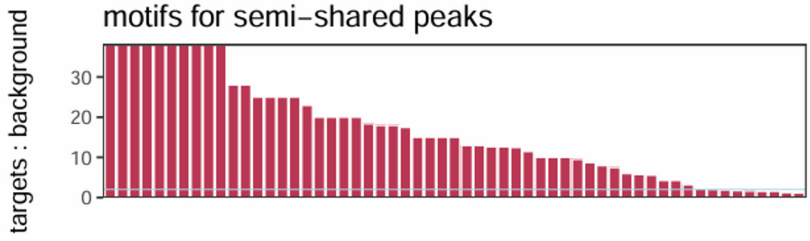

C

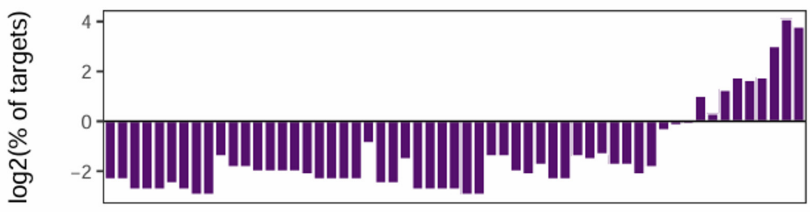

Supplementary figure 4: HOMER de novo motif finding results for semi-shared peaks. **A:** Table of the top 11 enriched motifs identified by HOMER2 within the set of semi-shared peaks. **B:** The number of times each motif (57 in total) is identified by HOMER2 in semi-shared AHL15 peaks divided by its number over the entire genome (expressed as %: 100% means the motif is almost only present in AHL15 peaks). **C:** The frequency with which each motif identified by HOMER2 occurs in semi-shared AHL15 peaks, expressed as the Log2 value of the % of shared AHL15 targets containing the specific motif (occurrence of more than 1% gives a positive value, 1% gives a value of 0, and less than 1% results in a negative value). Motifs in figures **B** and **C** are arranged by descending target : background value.

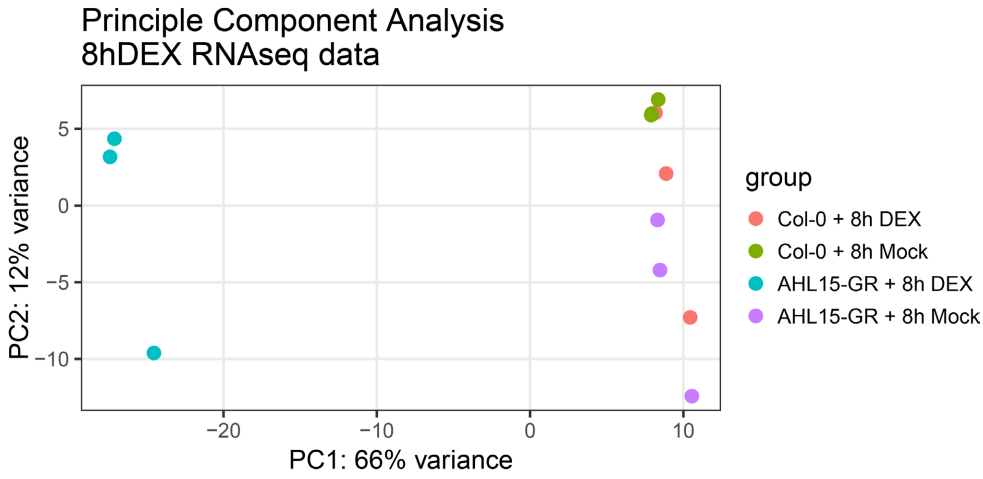

Supplementary figure 5: Principle component analysis of RNA-seq datasets. RNA-seq was performed on RNA isolated from 10 day-old wild-type (Col-0) or *p35S:AHL15-GR* seedlings that were drenched in 20 µM DEX or mock solution for 15 minutes, after which the DEX solution was removed and plants were left to recover. Per replicate (n=3) shoot tissue of five plants was harvested at 8 hours after drenching for RNA isolation and sequencing.

Summary

Plants undergo specific developmental phase changes during their lifetime, such as the transition from juvenile seedlings to adult plants during vegetative development or the change from the vegetative to reproductive phase. Developmental phase transitions are tightly controlled processes that are regulated by several elements including age, phytohormones and environmental cues such as light and temperature. Each of these factors can affect the expression and activity of transcription factors (TFs), nuclear proteins that bind DNA to regulate the expression of genes. Many TFs are expressed during a specific developmental window and either trigger or inhibit developmental phase transitions by promoting or repressing the transcription of their target genes. Other types of proteins can also have an effect on developmental phase transitions, for example by altering phytohormone levels, transmitting environmental cues, or by interacting with DNA directly and modifying its structure. This latter process can influence developmental phase changes when the epigenetic code or the 3D organization of DNA is altered in a way that interferes with the ability of TFs to regulate the expression of their target genes. The research described in this thesis continues on the initial identification of the AT-HOOK MOTIF NUCLEAR LOCALIZED 15 (AHL15) protein as a general suppressor of developmental phase transitions in *Arabidopsis thaliana* (Arabidopsis), and focuses on its role in two different developmental phase transitions and on its molecular function as a transcriptional regulator.

Chapter 1 reviews the current knowledge on how developmental phase transitions are regulated in the model plant Arabidopsis, with an emphasis on the role of TFs in this process. We describe the life cycle of Arabidopsis and focus on several developmental transitions during the vegetative- and flowering stage (Figure 1). Vegetative Arabidopsis plants undergo a juvenile-to-adult transition also called vegetative phase change (VPC), which mainly affects leaf morphology. VPC is inhibited by juvenile-stage factors such as AHL15 and the microRNA miR156, which are both expressed at high level in young plants and repress expression of TFs encoded by the *SQUAMOSA PROMOTER BINDING-LIKE* (*SPL*) gene family respectively pre- and post-transcriptionally. With developmental time, the repression of *SPL* genes decreases, resulting in VPC and an adult morphology. Adult plants undergo the floral transition, which is responsive to several cues. Long days promote the floral transition in Arabidopsis by activation of the floral promoter *FLOWERING LOCUS T* (*FT*), and prolonged cold exposure (vernalization) silences the floral repressor *FLOWERING LOCUS C* (*FLC*). FT and FLC promote- and repress the expression of several flowering genes, respectively, and the floral transition

is induced when promoting cues are stronger than repressive cues. This leads to the formation of an inflorescence, whose architecture is determined by a balanced spatial expression pattern of several promoters- and repressors of

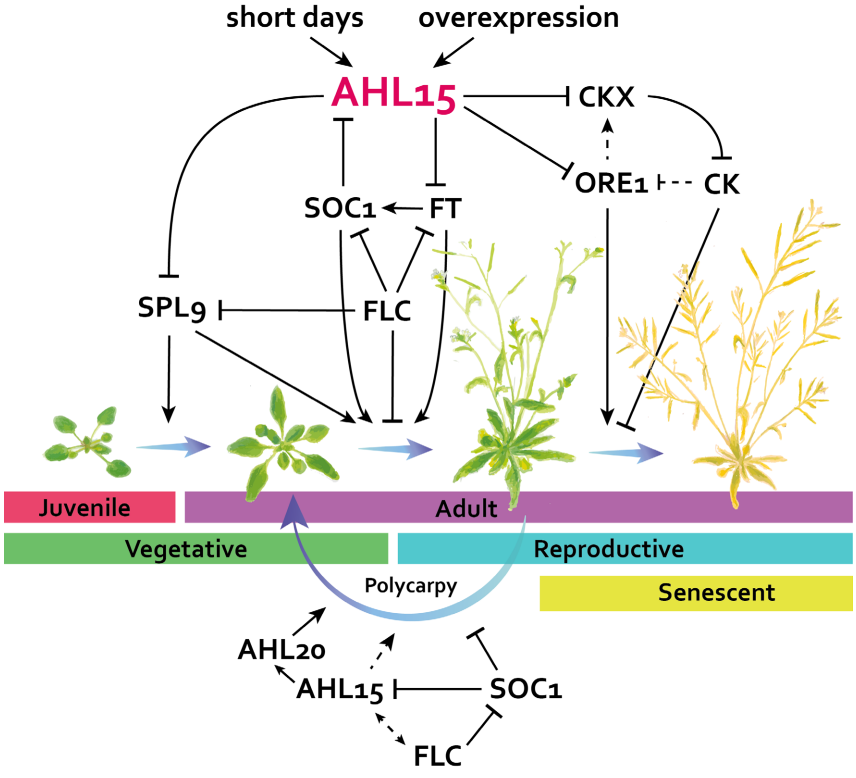

Figure 1: The effects of enhanced AHL15 expression on developmental phase transitions in monocarpic Arabidopsis. **Top:** AHL15 delays developmental phase transitions by repressing the expression of several genes when expressed at high levels. High AHL15 expression can be induced by short days or by overexpression in a transgenic plant. The juvenile-to-adult transition is promoted by SPL9, whose expression is repressed in AHL15 overexpression lines. Flowering is promoted by SOC1 and FT, which are both repressed by FLC. AHL15 inhibits flowering by repressing FT expression, and AHL15 expression during the flowering stage is repressed by SOC1. AHL15 also represses senescence via direct downregulation of ORE1 and CKX expression. ORE1 is a transcription factor that acts as a master regulator of senescence, and the senescence developmental program initiated by ORE1 induces transcription of CKX. CKX proteins inactivate cytokinins (CK), phytohormones that have an inhibitory effect on senescence. **Bottom:** Regulation of polycarpy by flowering time and AHL genes. FLC is a repressor of SOC1 and many other flowering-promoting genes, and helps to retain the vegetative state during the flowering stage. SOC1 levels show a strong negative correlation with polycarpic traits, indicating that it is a repressor of this phenotype. AHL15 is repressed by SOC1, and high AHL15 expression is associated with polycarpic traits. Its closest homolog AHL20 shows a significant correlation with polycarpic traits, suggesting that it is involved in polycarpic development. A positive correlation between AHL15 and FLC expression was also found, but the relation between these genes remains unclear.

flower development. Flowering also triggers senescence in rosette leaves, a process that helps relocate nutrients from old to young, developing tissues. Leaf senescence is regulated by several TFs of which *ETHYLENE INSENSITIVE 3* (*EIN3*), *ORESARA1* (*ORE1*) and *NAC-LIKE ACTIVATED BY AP3/PI* (*NAP*) act upstream of several genes involved in chlorophyll (Chl) catabolism as well other TFs that act further downstream in the senescence process. In addition, senescence is affected by phytohormones, of which ethylene is the best-known inducer of senescence whereas cytokinins (CKs) act as inhibitors. We also discuss the differences between plants that undergo complete senescence and death upon reproduction (monocarps) and plants that can resume their vegetative growth during- and after flowering and can flower again from these vegetative tissues (polycarps). We describe how FLC promotes polycarpic development in *Brassicaceae* species by repressing the floral transition in axillary meristems (AMs), and discuss the roles of *FRUITFULL* (*FUL*) and CKs in inflorescence arrest. At the end of **chapter 1**, we discuss what is currently known about the *AT-HOOK MOTIF NUCLEAR LOCALIZED* (*AHL*) gene family with a focus on *AHL15*, the gene on which the research in this thesis is focused, and describe its effects on plant development.

In **chapter 2**, we used a panel of Arabidopsis ecotypes that show the formation of aerial rosettes (ARs), a polycarpic trait that was observed in Arabidopsis lines overexpressing *AHL15*, to investigate the role of *AHL15* and several other genes in this phenotype. We quantified the AR phenotype and show that this phenotype is strongly variable and is positively correlated to the expression of *FLC* and *AHL20,* a close homolog of *AHL15.* We also show that the expression of *SUPPRESSOR OF OVEREXPRESSION OF CO 1* (*SOC1*), a floral promoter that represses expression of *AHL15*, shows a strong negative correlation with the AR phenotype, and that the adult-state promoting gene *SPL15* shows a similar, but weaker trend. Finally, we show that silencing of *FLC* expression by vernalization results in a complete loss of the AR phenotype, demonstrating that FLC is a master regulator of AR production in these ecotypes (Figure 1). Our results show that a panel of phenotypically diverse ecotypes can be used to determine gene-to-phenotype relations, and that natural variation in the presumedly monocarpic species Arabidopsis can be used to study polycarpic development.

One of the developmental phase transitions that is inhibited by AHL15 is leaf senescence, a process in which Chl is broken down and results in visible changes in leaf color from green to yellow. In order to study this process more efficiently, we developed a method to quantify the Chl content of leaves based

on their visual appearance. In **chapter 3**, we describe a method for rapid, non-destructive Chl quantification based on digital images of plant leaves. We developed a plugin for the imageJ software that automatically detects leaves, and measures the pixel intensity in the red, green, and blue channels (RGB) in 8-bit digital images. These values can then be used to calculate several colorimetric visual indexes, of which the normalized Red value (R/(R+G+B)) is the most strongly correlated to leaf Chl content as determined by the traditional, labor-intensive method of Chl extraction. We applied this new image-based quantification method on a large panel of lettuce genotypes to measure leaf Chl content for a genome-wide association study (GWAS). With the data obtained in this way, we identified a significant peak around a locus involved in chloroplast development that was previously identified in a GWAS using a traditional Chl quantification method. Together, our data show that image-based Chl quantification is a suitable and more efficient alternative to the labor-intensive extraction-based Chl quantification, and can be applied in high-throughput systems.

We applied the protocol developed in **chapter 3** to measure the effect of *AHL15* on leaf senescence, which is described in **chapter 4**. We show that overexpression of *AHL15* delays leaf senescence, resulting in a stay-green phenotype, which was apparent during the plants life cycle as well as in dark-induced senescence in detached leaves. Loss-of-function *ahl15* plants showed a slight but significant acceleration of senescence, indicating that AHL15 has a repressive effect on senescence. We also investigated which genes act downstream of AHL15 during this process, and show that AHL15 directly represses the expression of the master regulator of senescence *ORESARA1* (*ORE1*). In addition, we show that AHL15 represses the expression of CK degrading enzymes of the CYTOKININ OXIDASE/DEHYDROGENASE (CKX) family, resulting in a delayed decrease of CK levels during dark-induced senescence. Thus, AHL15 represses senescence via two parallel pathways: by repressing *ORE1* expression, and by inhibiting CK degradation (Figure 1).

Finally, in **chapter 5**, we investigated where in the genome AHL15 binds, and how it regulates gene expression. We show that AHL15 binds closely upstream of the transcription start site (TSS) or just downstream of the transcription end site (TES) of genes, and is depleted in gene bodies. We show that constitutive *AHL15* overexpression results in stronger binding at native AHL15 binding sites and at ectopic sites, where it binds with a lower affinity than at its genuine native targets. In addition, we show that induction of nuclear localization of the AHL15-GR fusion protein by dexamethasone (DEX) results in

large transcriptional changes, of which the majority of genes is downregulated. Downregulated genes include floral promoters such as *FT* (Figure 1), explaining the delayed flowering phenotype of *AHL15*-overexpressing plants. Interestingly, AHL15 binding was higher near the TSS and TES of differentially expressed genes compared to genes whose expression was unaffected by DEX treatment. AHL15 peaks were most strongly enriched near the TSS of upregulated genes, and downregulated genes had the strongest AHL15 enrichment near the TES, suggesting that the location of AHL15 binding near a gene affects its expression. We also investigated the effect of AHL15 on chromatin accessibility with ATAC-seq in DEX-induced *p35S:AHL15-GR* plants, and surprisingly found that AHL15-GR activation did not affect chromatin accessibility. Comparison of AHL15 DNA binding sites with ATAC-seq data that shows where chromatin is accessible also revealed that AHL15 binds at poorly accessible regions that flank regions with high accessibility. In addition, AHL15 ChIP-seq peaks did not overlap with several epigenetic marks, but were located at the boundaries of regions enriched in such marks. Together, this indicates that AHL15 and likely also other AHL family proteins have an affinity for regions with reduced accessibility and that are poorly covered by most epigenetic marks.. Finally, we show that AHL15 binds in the same regions as the high-mobility group A (HMGA) protein GH1-HMGA2/HON5, which has several AT-Hook DNA-binding domains. GH1-HMGA2/HON5 was previously shown to interfere with the formation of gene loops, which are necessary for efficient transcription of the gene they encompass. The overlap in DNA binding sites suggests that like GH1-HMGA2/HON5, AHL15 can affect the 3D organization of DNA which can influence gene expression, explaining why *AHL15* overexpression affects plant development so strongly.

In conclusion, our genome-wide analyses reveal that AHL15 acts as a transcriptional regulator that binds to DNA with little sequence specificity, but with a preference for regions depleted of epigenetic signatures and that this preference overlaps with that of another type of chromatin architecture-modifying protein class, suggesting that the large-scale changes in gene expression induced by AHL15 stem from changes in chromatin architecture. By combining this information with phenotypic and gene expression data, we show that AHL15 directly represses the expression of several TFs involved in developmental processes, and thereby inhibits developmental phase changes associated with ageing.

Samenvatting

Veroudering vindt plaats in alle organismen, en is een gevolg van het ondergaan van opeenvolgende stadia in de ontwikkeling. Planten ondergaan gedurende hun levensloop verschillende ontwikkelingsstadia, en de overgangen tussen opeenvolgende ontwikkelingsstadia worden ook wel fasetransities genoemd. Voorbeelden hiervan zijn de transitie van juveniele zaailingen naar volwassen planten tijdens de vegetatieve fase, en de transitie van volwassen vegetatieve planten naar een reproductieve staat. Deze fasetransities in de ontwikkeling zijn nauw gereguleerde processen die door verschillende factoren worden beïnvloed, waaronder leeftijd, fytohormonen en omgevingsfactoren zoals licht en temperatuur. Elk van deze factoren heeft invloed op de expressie en activiteit van kern-gelokaliseerde eiwitten genaamd transcriptiefactoren (TFs) die DNA kunnen binden en daarmee de expressie van genen reguleren.

Veel TFs komen tot expressie op een specifiek tijdstip in de ontwikkeling, en kunnen de fasetransitie tussen twee ontwikkelingsstadia bevorderen dan wel remmen door de transcriptie van hun targetgenen aan of uit te zetten. Andere eiwittypen kunnen ook effect hebben op fasetransities door bijvoorbeeld de concentratie van fytohormonen te veranderen, door het overbrengen/waarnemen van omgevingsfactoren of door de fysieke structuur van het DNA aan te passen via directe interactie daarmee. Dit laatste proces kan ontwikkelingstransities beïnvloeden wanneer de epigenetische code of de 3D-structuur van het DNA zodanig wordt veranderd dat het vermogen van TFs om de expressie van hun targetgenen te reguleren wordt gehinderd.

Het onderzoek in dit proefschrift is een vervolg op de eerdere ontdekking dat het AT-HOOK MOTIF NUCLEAR LOCALIZED 15 (AHL15) eiwit fungeert als algemene suppressor van fasetransities tussen ontwikkelingsstadia in de modelplant *Arabidopsis thaliana* (Arabidopsis). We focussen hierbij op de rol van AHL15 in twee specifieke fasetransities en op de functie van AHL15 als regulator van gentranscriptie.

Hoofdstuk 1 geeft een overzicht van de huidige kennis over hoe fasetransities tussen ontwikkelingsstadia worden gereguleerd in de modelplant Arabidopsis, met een nadruk op de functie van TFs in deze processen. We beschrijven de levenscyclus van Arabidopsis en een aantal specifieke fasetransities tijdens de vegetatieve en reproductieve stadia (Figuur 1). Tijdens de vegetatieve fase ondergaan Arabidopsisplanten een transitie tussen de juveniele en volwassen fase waarbij met name de bladmorfologie wordt beïnvloed, een proces dat ook wel vegetatieve faseverandering (VFV) wordt genoemd. VFV wordt onderdrukt door verschillende juveniele fase-specifieke factoren, waaronder AHL15 en het microRNA miR156, die beiden hoog tot expressie komen in

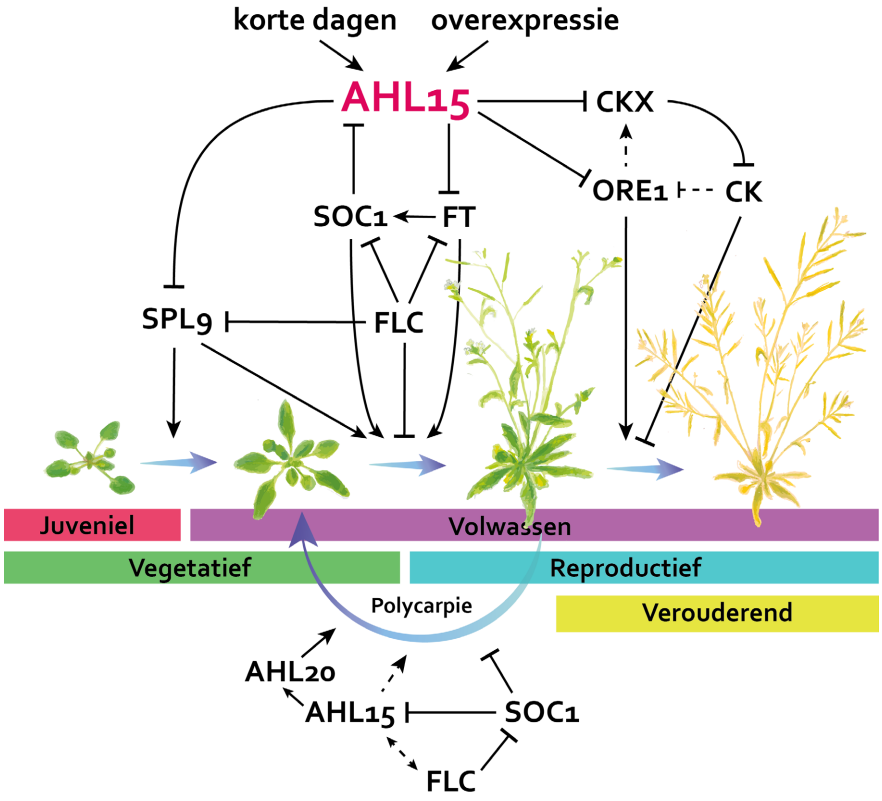

Figuur 1: De effecten van verhoogde *AHL15* expressie op de fasetransitites tussen ontwikkelingsstadia in de monocarpe soort Arabidopsis. **Boven:** AHL15 vertraagt de fasetransities tussen ontwikkelingsstadia door de expressie van verschillende genen te onderdrukken wanneer het hoog tot expressie wordt gebracht. *AHL15* komt sterk tot expressie wanneer de plant in korte dag condities wordt gegroeid, of in transgene planten met een overexpressieconstruct. De juveniel-naar-volwassen transitie wordt bevorderd door SPL9, waarvan de expressie wordt onderdrukt in plantenlijnen met sterke *AHL15* expressie. Bloei wordt bevorderd door SOC1 en FT, die beiden worden onderdrukt door FLC. AHL15 remt bloei door de expressie van *FT* te represseren, en *AHL15* expressie wordt tijdens de bloeifase door SOC1 onderdrukt. AHL15 remt ook de bladveroudering door de expressie van *ORE1* en *CKX* genen direct te remmen. ORE1 is een TF die als hoofdregulator van bladveroudering fungeert, en het bladverouderingsprogramma dat door ORE1 in gang wordt gezet induceert ook de expressie van *CKX* genen. CKX eiwitten inactiveren cytokinines (CKs), fytohormonen die de bladveroudering remmen. **Onder:** Regulatie van polycarpie door bloeigenen en *AHL* genen. FLC is een repressor van *SOC1* en veel andere bloei-stimulerende genen, en helpt in polycarpe soorten bij het behouden van de vegetatieve staat tijdens het bloeien. Het expressieniveau van *SOC1* correleert sterk negatief met polycarpe eigenschappen, wat aangeeft dat dit gen een repressor van dit fenotype is. *AHL15* wordt gerepresseerd door SOC1, en hoge expressie van *AHL15* is geassocieerd met polycarpe eigenschappen. Het aan *AHL15* nauw verwante gen *AHL20* laat een significant positieve correlatie zien met polycarpe eigenschappen, wat suggereert dat dit gen betrokken is bij polycarpe ontwikkeling. Daarnaast bestaat er een positieve correlatie tussen de expressie van *AHL15* en *FLC*, maar de interactie tussen deze twee genen is vooralsnog onduidelijk.

jonge planten. Deze factoren onderdrukken de expressie van leden van de *SQUAMOSA PROMOTER BINDING-LIKE* (*SPL*) TF genfamilie op respectievelijk pre- en post-transcriptionele wijze. *SPL* genen stimuleren de volwassen staat, en hun repressie neemt af naar mate de ontwikkeling van planten vordert, wat resulteert in VFV en een volwassen morfologie.

Volwassen planten ondergaan vervolgens de bloeitransitie, een faseverandering die gevoelig is voor verscheidene factoren. In Arabidopsis wordt de bloeitransitie gestimuleerd door groei in lange dagen via activatie van het bloei-inducerende mobiele *FLOWERING LOCUS T* (*FT*) eiwit. Daarnaast wordt de expressie van de bloeirepressor *FLOWERING LOCUS C (FLC)* gedempt wanneer de plant bloot wordt gesteld aan langdurige kou (vernalisatie). FT en FLC hebben respectievelijk een activerend- en remmend effect op de expressie van meerdere genen die betrokken zijn bij de bloei, en de bloeitransitie wordt in gang gezet wanneer de signalen die bloei stimuleren sterker zijn dan de remmende signalen. Dit leidt vervolgens tot formatie van een bloeiwijze, waarvan de vorm bepaald wordt door het ruimtelijke patroon waarop genen die de aanmaak van bloem-specifieke weefsels positief of negatief reguleren tot expressie komen.

Bloei activeert ook een proces van veroudering in de rozetbladeren van Arabidopsisplanten, wat helpt bij het herverdelen van nutriënten vanuit oudere bladeren naar jonge en nieuw ontwikkelende weefsels zoals de bloemen en zaden. Bladveroudering wordt gereguleerd door meerdere TFs, waaronder ETHYLENE INSENSITIVE 3 (EIN3), ORESARA1 (ORE1) en NAC-LIKE ACTIVATED BY AP3/PI (NAP). Deze TFs reguleren zowel de expressie van genen die betrokken zijn bij de afbraak van chlorofyl (Chl) als de expressie van andere TFs die andere processen in het bladverouderingsproces in gang zetten. Daarnaast wordt bladveroudering ook sterk beïnvloed door fytohormonen, waarbij ethyleen de meest bekende promotor van veroudering is en cytokinines (CKs) juist als remmers van dit proces optreden. We bespreken ook de verschillen tussen plantensoorten die na het bloeien een volledig verouderingsproces ondergaan en vervolgens sterven (monocarpen) en planten die tijdens en na het bloeien hun vegetatieve groei kunnen voortzetten en daardoor opnieuw kunnen bloeien (polycarpen). We beschrijven hoe FLC polycarpe ontwikkeling in *Brassicaceae* soorten promoot door de bloeitransitie te onderdrukken in de axillaire meristemen (AMs), en bespreken de rol van de TF FRUITFULL (FUL) en van CKs in het reguleren van de levensduur van de bloeiwijze. Aan het eind van **hoofdstuk 1** bespreken we de huidige kennis over de *AT-HOOK MOTIF NUCLEAR LOCALIZED* (*AHL*) genfamilie en benadrukken de rol van *AHL15* en

de effecten van dit gen op de ontwikkelingsbiologie van planten.

In hoofdstuk 2 hebben we gebruik gemaakt van een panel van Arabidopsis ecotypen die luchtrozetten vormen, een polycarpe eigenschap die ook in Arabidopsis lijnen waarin *AHL15* tot overexpressie is gebracht voorkomt, om de rol van *AHL15* en andere genen in dit fenotype te onderzoeken. Hiervoor kwantificeerden we het luchtrozet-fenotype en laten zien dat deze eigenschap zeer variabel is en een positieve correlatie vertoont met de expressie van *FLC* en van *AHL20,* een nauwe verwant van *AHL15.* We tonen ook aan dat de expressie van *SUPPRESSOR OF OVEREXPRESSION OF CO 1 (SOC1)*, een bloeistimulerende TF die de expressie van *AHL15* onderdrukt, sterk negatief correleert met het luchtrozet-fenotype en dat er een vergelijkbare maar zwakkere correlatie te zien is met de expressie van *SPL15*, een gen dat de volwassen fase promoot. Tot slot laten we zien dat repressie van *FLC* expressie door vernalisatie leidt tot een volledig verlies van het luchtrozet-fenotype, wat aantoont dat FLC de belangrijkste regulator van luchtrozetvorming is in deze ecotypen (Figuur 1). Onze resultaten tonen aan dat een panel van fenotypisch diverse ecotypen kan worden gebruikt om gen-naar-fenotype relaties te onderzoeken en dat natuurlijke variatie in Arabidopsis, een als monocarp beschouwde soort, kan worden gebruikt om polycarpe ontwikkeling te onderzoeken.

Eén van de fasetransities die door AHL15 wordt onderdrukt is bladveroudering, een proces waarbij Chl wordt afgebroken met een zichtbare verkleuring van het blad van groen naar geel als resultaat. Om dit proces op een efficiëntere manier te bestuderen ontwikkelden we een protocol waarbij bladkeur wordt gebruikt om de hoeveelheid Chl in bladeren te meten. In **hoofdstuk 3** beschrijven we een snelle, niet-destructieve methode om de hoeveelheid Chl in bladeren te meten met behulp van digitale foto's. We ontwikkelden hiervoor een plugin die in de ImageJ software kan worden gebruikt en waarmee bladeren automatisch worden gedetecteerd zodat de pixelintensiteit in de groene, rode en blauwe kanalen van 8-bits foto's kan worden gemeten. Deze waarden worden vervolgens gebruikt om verschillende visuele kleurindexen te berekenen, waarvan de genormaliseerde roodwaarde (R/(R+G+B)) de sterkste correlatie toont met een traditionele, arbeidsintensieve methode van Chl meting.

We pasten deze nieuwe meetmethode toe om de hoeveelheid Chl in de bladeren van een groot aantal genotypes van sla te bepalen voor een genoom-wijde associatie studie (GWAS). Met deze data identificeerden we een significante piek rond een locus waarvan in een eerdere GWAS waarbij gebruik werd gemaakt van een traditionele Chl meetmethode was aangetoond dat het betrokken is bij chloroplastontwikkeling. Dit resultaat demonstreert dat het

meten van Chl op basis van digitale foto's een geschikt en efficiënter alternatief vormt voor de arbeidsintensieve methode van Chl extractie, en dat het kan worden toegepast in systemen waarbij een hoge doorvoer gewenst is.

In **hoofdstuk 4** hebben we de methode die wordt beschreven in **hoofdstuk 3** toegepast om het effect van AHL15 op bladveroudering te meten. We tonen aan dat overexpressie van *AHL15* de bladveroudering vertraagt, zowel tijdens de natuurlijke levensloop van de plant als wanneer bladveroudering wordt geïnduceerd door incubatie in het donker. Planten waarbij het *ahl15* gen niet meer functioneert lieten een licht maar significante versnelling van bladveroudering zien, wat aangeeft dat AHL15 een remmend effect heeft op de bladveroudering. We onderzochten ook welke door AHL15 gereguleerde genen een rol spelen in dit proces, en vonden dat AHL15 de expressie van *ORE1,* een master-regulator van bladveroudering direct onderdrukt. Daarnaast tonen we aan dat de expressie van genen in de *CYTOKININ OXIDASE (CKX)* familie, die coderen voor enzymen die CKs afbreken, door AHL15 wordt onderdrukt, wat resulteert in een vertraagde afbraak van CK tijdens door donker geïnduceerde bladveroudering. AHL15 remt zo de bladveroudering op twee manieren: door het onderdrukken van *ORE1* en door het verhinderen van CK afbraak (Figuur 1).

Tot slot hebben we in **hoofdstuk 5** onderzocht waar in het genoom AHL15 bindt en hoe het genexpressie reguleert. We tonen aan dat AHL15 bij voorkeur bindt in de regio stroomopwaarts van de transcriptie start site (TSS) en net na de transcriptie eind site (TES) van genen, en dat het vrijwel afwezig is in de genen zelf. We laten ook zien dat AHL15 sterker aan het DNA bindt wanneer het tot overexpressie wordt gebracht. Daarnaast bindt AHL15 in deze condities ook nieuwe plaatsen in het DNA, maar met een lagere affiniteit dan bij de oorspronkelijke bindingsplaatsen. Vervolgens laten we zien dat in *p35S:AHL15-GR* planten waarin het AHL15-GR fusie-eiwit door behandeling met DEX naar de nucleus wordt getransporteerd het transcriptoom grote veranderingen ondergaat, waarbij het merendeel van de genen lager tot expressie komt. Één van de genen waarvan de expressie op deze manier wordt onderdrukt is *FT* (Figuur 1), wat de vertraagde bloei in *AHL15* overexpressielijnen verklaart. Interessant genoeg bleek de affiniteit waarmee AHL15 de TSS en TES van genen die anders tot expressie kwamen bindt hoger dan bij genen waarvan de expressie niet veranderde door behandeling met DEX. Pieken van AHL15 binding waren het sterkst verrijkt bij de TSS van omhoog-gereguleerde genen, terwijl genen die verlaagd tot expressie kwamen de sterkste AHL15 verrijking hadden bij de TES. Dit suggereert dat de expressie van een gen beïnvloed wordt door de locatie waar AHL15 ten opzichte van dit gen bindt.

We onderzochten ook het effect van AHL15 op de toegankelijkheid van het chromatine door ATAC-seq toe te passen op DEX behandelde planten, en vonden tot onze verrassing dat activatie van AHL15-GR hier geen invloed op heeft. Een vergelijking van de chromatinetoegankelijkheid (ATAC-seq) met de locatie van AHL15 bindingsplaatsen (ChIP-seq) liet zien dat AHL15 bij voorkeur bindt in regio's met verlaagde chromatine toegankelijkheid die zich tussen gebieden met hoge toegankelijkheid bevinden. Vervolgens maakten we gebruik van reeds gepubliceerde data over de positie van verschillende epigenetische markers om eenzelfde vergelijking te maken. Dit wees uit dat AHL15 vooral bindt in regio's net naast gebieden in het DNA met verhoogde epigenetische modificatie. Dit laat zien dat AHL15 en waarschijnlijk ook andere eiwitten uit de AHL familie een hoge affiniteit heeft voor regio's met verlaagde toegankelijkheid met weinig epigenetische modificaties.

Tot slot laten we zien dat AHL15 het DNA op vergelijkbare plekken bindt als het high-mobility group A (HMGA) eiwit GH1-HMGA2/HON5, dat meerdere DNA bindende AT-HOOK domeinen bevat. Eerder onderzoek heeft aangetoond dat GH1-HMGA2/HON5 de vorming van genlussen, die nodig zijn voor efficiënte transcriptie van een gen, verhindert. De overlap tussen de DNA bindingsplaatsen van AHL15 en GH1-HMGA2/HON5 suggereert dat AHL15 een vergelijkbare rol zou kunnen spelen in de 3D organisatie van het DNA, en daarmee genexpressie zou kunnen beïnvloeden, wat zou verklaren waarom *AHL15* overexpressie zo'n sterk effect heeft op de ontwikkeling van planten.

Samengevat onthullen onze genoom-wijde analyses dat AHL15 als een transcriptionele regulator werkt die DNA bindt met weinig voorkeur voor specifieke sequenties, maar met een hoge voorkeur voor regio's met minder epigenetische modificaties. Daarnaast laten we zien dat deze voorkeuren overlappen met die van een andere klasse van eiwitten die de chromatinestructuur kunnen aanpassen, wat suggereert dat de grootschalige veranderingen van genexpressie die door AHL15 het resultaat zijn van veranderingen in de chromatineconfirmatie. Door deze informatie te combineren met fenotypische- en genexpressie data laten we zien dat AHL15 de expressie van verscheidene TFs die betrokken zijn bij ontwikkelingsprocessen onderdrukt, en daarmee de fasetransities die gelinkt zijn met veroudering tegenhoudt. Dit onderzoek levert nieuwe inzichten op over hoe verouderingsprocessen worden gereguleerd in planten en mogelijke manieren waarop deze processen kunnen worden geremd of versneld.

Curriculum Vitae

Curriculum Vitae

Thalia Luden was born on July 8th 1993 in Amsterdam, the Netherlands. She attended gymnasium at het Amsterdams Lyceum and graduated in 2011, after which she started studying Biomedical Sciences at the University of Amsterdam. In 2012, she transferred to the Liberal Arts and Sciences program of Amsterdam University College, where she attended courses in in a variety of subjects including mathematics, geology, economics, and literature. In 2014, she returned to the University of Amsterdam to study Biology and obtained her BSc in Biology in 2016. During her BSc program, she spent one semester abroad at the university of Auckland in New Zealand, where she studied local plant diversity and evolution and biogeography of the Pacific. She finished her BSc with an internship in plant epigenetics under supervision of Dr. Maike Stam and PhD student Blaise Weber, during which she assisted in the validation of regulatory activity of predicted enhancer sequences in maize.

After obtaining her BSc degree, she worked as a teacher for the first-year BSc laboratory courses "van Molecuul tot Cel" and "Genetica en Evolutie" at the University of Amsterdam, where she helped introduce BSc students to the scientific method and molecular biology techniques. Later, she also worked as a teaching assistant in the course "Ecogenomics" taught by prof. Harro Bouwmeester, during which 3rd-year BSc students perform a GWAS on *Arabidopsis thaliana*, which was her first introduction to this species.

In 2017, she continued studying plant biology in the MSc program Biological Sciences at the University of Amsterdam in the track Green Life Sciences, which included two research internships and a literature review. For the first internship, she joined the plant development and genetics group of prof. Ronald Koes and Dr. Francesca Quatrocchio. Under supervision of PhD student Kai Ding she studied the effect of vacuolar pH on flower color by expressing a fluorescent protein-based pH reporter in Petunia petal protoplasts. Her second research internship was at the phytopathology department of the plant breeding company Enza Zaden under supervision of Dr. Manos Domazakis. Here, she studied chemically induced priming of disease resistance in several crop species. She concluded her MSc program by writing a review about the role of transposable elements in plant evolution and diversity under supervision of Dr. Maike Stam. During her MSc program, Thalia participated in the graduate program organized by the graduate school of experimental plant sciences (EPS), which invites talented MSc students to write and submit a proposal for a PhD research project. During this program she met prof. Remko Offringa, with whom she wrote a research proposal that she submitted and successfully

defended to the Dutch Research Council (NWO) in the autumn of 2019. In 2020, she started this proposed PhD research at the Plant Developmental Genetics group under supervision of prof. Remko Offringa.